

**University of Miskolc**



**MISKOLCI**  
**EGYETEM**  
UNIVERSITY OF MISKOLC

**Faculty of Mechanical Engineering**

**Institute of Energy Engineering and Chemical Machinery**

**Department of Fluid and Heat Engineering**

**Increase the efficiency of the hybrid photovoltaic thermal system**

**Mohammed Alktranee**

**PhD Dissertation**

**István Sályi Doctoral School**

**Main Topic Group: Fundamental Sciences in Mechanical Engineering**

**Topic Group: Transport Processes and Machines**

**Head of Doctoral School**

**Gabriella Vadaszne Bognar**

**Director of Science, Full Professor**

**Scientific Supervisor:**

**Peter Bencs**

**Associate professor**

**2023**

## **Acknowledgement**

Obtaining a PhD degree was a major turning point in my life, as it constituted a bright point in my professional life, which would not be achieved without the support and assistance of many people.

Firstly, I would like to thank my supervisor, Dr Peter Bencs, for accepting me as a PhD under his supervision, for his great support for the success of scientific research and attendance at various conferences, and for giving me intellectual freedom in my work.

Many thanks to my parents for their moral support and prayers for me. Big thanks to my wife and kids for enduring my absence from them and supporting me in all circumstances.

I would like to thank Mr Peter Bozzay for his help during the experiments, and many thanks to Dr Zoltan Nemeth for his help with laboratory work.

## Abstract

In recent years, the energy sector has raised many concerns about the sustainability of energy supplies in future, which constitutes a huge burden on governments worldwide and a great incentive to adopt alternative sources to bridge the shortfall in energy supplies. Renewable energy is considered the most important alternative energy source due to its high potential and reliable performance to compensate for the shortfall in energy supply. Solar energy systems are the most effective and widespread due to their various applications to supply clean electrical and thermal energy without emissions which can cause environmental effects. Hybrid Photovoltaic-Thermal (PVT) system is an effective solar energy system that simultaneously provides electrical and thermal energy. The mechanism work of the PVT system represents converting solar radiation to electrical energy by Photovoltaic (PV) cells and absorbing the excessive heat of the PV cells to improve their performance and convert it to thermal energy. However, improvements have been made to the PVT system to enhance its performance and maximize its production, but it's still some weaknesses in the methods used to improve performance and system efficiency. The previous studies about improving the efficiency of the PVT system have been reviewed by considering the techniques used. During the depth review of the literature, the gaps found in previous studies have been identified to be addressed during the PhD dissertation by new methods. This PhD dissertation presents a study of using active and passive cooling by new approaches to contribute to improving the PVT system performance. According to thermodynamics laws (the first and second), the energy and exergy of the PVT system have been analyzed to show the quantity and quality of the PVT system's performance.

Passive cooling consists of cotton wicks (CWs) immersed in water as (evaporative cooling). The CW has stacked as one piece attached to the PV module and supplied with water by gravity from top to bottom by the ends of CWs connected in plastic bottles. This cooling approach helped decrease the PV cell's temperature by 22.34% and increased the electrical power by 17.78%, then improved the electrical efficiency to 7.25%. Reducing the PV module temperature contributes to reduced exergy losses and entropy generation by 14% and 14.32%, respectively. The first cooling approach was developed by integrating with aluminium fins to increase the heat dissipation area and enhance the evaporative cooling as a second cooling approach. The new approaches were applied according to hot operation conditions and significantly improved the PV module performance during reduced temperature by 31.2% and increased electrical power by about 23.16 W and electrical efficiency to 8.6%. On another side, the quality of the PV module performance is enhanced by decreasing the exergy losses and entropy generation with achieving appropriate economic feasibility.

The active cooling approaches adopted mono and new hybrid nanofluids as cooling fluids circulated into tubes which a soldered absorber plate attached at the backside of the PV module. Thereby to prevent the formation of air gaps at the contact region between the backside of the PV module and absorber plate, thermal grease was used; then to reduce the heat convection losses, a new high-performance insulation layer was placed on the tubes. The nanomaterials have been synthesized in different morphologies at the laboratory to avoid the high purchase cost and for more purity of the nanomaterials produced. All manufactured nanomaterials ( $\text{WO}_3$ , CuO,  $\text{TiO}_2$ ,  $\text{Fe}_2\text{O}_3$ ,  $\text{TiO}_2\text{-CuO}$  and  $\text{TiO}_2\text{-Fe}_2\text{O}_3$ ) were subjected to different measurements such as crystal structure, morphological and thermophysical properties to investigate their effect on enhancing the thermal performance. The nanofluids have prepared at different volume concentrations (vol%) and used with the PVT system at different operation conditions, then compared the

performance of the PVT system with another previous study to show the effectiveness of the nanofluids used to improve the PVT system performance.

The results indicated that using some mono nanofluids such as  $\text{Fe}_2\text{O}_3$ / deionized (DI) water has a high performance by reducing the PV cells temperature by 29.64% and incrementing the electrical power by 76.69%, then incrementing the thermal and electrical efficiency to 12.1%, 43.3% at 0.3 vol% compared with reference PV module. This is attributed to the high thermal properties and surface area of  $\text{Fe}_2\text{O}_3$  nanorods dispersed in DI water and the configuration of the cooling system. Using  $\text{CuO}$ /DI water achieved better performance of the PVT system than another previous study by reducing the PV cell's temperature by 23.44% and incrementing electrical and thermal energy to 10.3% and 38.9% compared with the reference PV module. The  $\text{TiO}_2$  nanofluid was a less performance than the

mono nanofluids mentioned above through reduced the PV cells temperature by 14% and incremented the electrical and thermal efficiency to 8.44 and 34.6% compared with the reference PV module, which recorded electrical efficiency that was not excess of 5.3% due to rising their temperature up to 55 °C.

Improving the nanofluid performance is positively reflected in the PVT system performance; in this dissertation, a new hybrid nanofluid has been applied consisting of TiO<sub>2</sub> nanowires (NWs) loaded on the Fe<sub>2</sub>O<sub>3</sub> nanoparticles (NPs) and TiO<sub>2</sub> NWs loaded on CuO NPs which has been dispersed into DI ware at different vol%. Thereby, using a hybrid TiO<sub>2</sub>-Fe<sub>2</sub>O<sub>3</sub> nanofluid reduced the PV cell's temperature to 37%, then incremented both the electrical and thermal efficiencies of the PVT system to 12.62% and 48.2% at 0.3 vol%. Then the exergy losses and entropy generation were reduced by 47.3% and 70.47% compared with the reference PV module. In contrast, using TiO<sub>2</sub>-CuO nanofluid provides a performance no less important than the TiO<sub>2</sub>-Fe<sub>2</sub>O<sub>3</sub> nanofluid, dispersed 0.3 vol% of TiO<sub>2</sub>-CuO nanocomposite help reduce the PV cell temperature by 39.16%, then increment of electrical and thermal efficiency to 12.4% and 45.8%. The exergy losses have been reduced by 37.9% and entropy generation by 69.9%, which is attributed to enhancing the thermophysical properties of hybrid nanofluids which is reflected by enhancing the PVT system performance. Furthermore, increased volume concentrations of the nanomaterials in DI water directly enhanced the heat transfer coefficient, and the Nusselt number increased with an increased Reynold number.

On another side, increased volume concentrations cause an increase in the density of nanofluids, then a decrease in friction factor friction factors and an increased pressure drop. In chapter 7, numerical simulation was conducted on the PVT system to investigate the effect of mono and hybrid nanofluids on the energy and exergy of the PVT system. Experimental results validated the numerical simulation results to confirm the reliability of the simulation results. The simulation results show temperature distribution and heat transfer mechanism between the PVT system components that help to decrease the PV cell temperature. Thereby, improving the thermal parameters of nanofluids has a significant effect by incrementing the energy and exergy efficiencies of the PVT system. The numerical simulation results show logical convergence with experiment results with a deviation not exceeding 3.7%, which confirms the reliability of the simulation results. The economic analysis of the passive and active cooling approaches has achieved a good payback period, confirming the feasibility of the cooling approach applied.

# Contents

<b>Abstract</b> .....	I
<b>Content</b> .....	III
<b>Nomenclature</b> .....	VI
<b>1. Introduction</b> .....	1
1.1 Factors causing failure or damage of the PV modules .....	2
1.2 Hybrid photovoltaic thermal system .....	2
1.3 Cooling systems applied with the PVT system .....	4
1.3.1 Passive cooling system .....	4
1.3.2 Active cooling system .....	7
1.3.2.1 Cooling by conventional fluids .....	7
1.3.2.2 Cooling by nanofluids .....	9
1.4 Objectives of the dissertation .....	10
<b>2. Methodology</b> .....	12
2.1 Thermal analysis of heat transfer between the PVT system components .....	12
2.2 Energy balance equations for the PVT system .....	16
2.3 Energy and exergy analysis of PVT system .....	18
2.4 Synthesized of nanomaterials .....	20
2.4.1 Hybrid titanium oxide/iron oxide nanocomposite .....	20
2.4.2 Hybrid titanium oxide/copper oxide nanocomposite .....	21
2.5 Preparation of nanofluid .....	22
2.6 Thermophysical properties of nanofluids .....	24
2.6.1 Density and viscosity of nanofluid .....	24
2.6.2 Thermal conductivity and specific heat of nanofluid .....	25
<b>3. Factors affecting the PV module performance</b> .....	27
3.1 Simulation study of the photovoltaic module under different operation conditions .....	27
3.1.1 Operation conditions and governing equations .....	27
3.1.2 Results and discussion .....	29
3.2 Test the photovoltaic module under different conditions by using Matlab-Simulink .....	31
3.2.1 Mathematical modeling of PV module .....	31
3.2.2 Simulation of the mathematic module .....	33
3.2.3 Results and discussions .....	34
3.3 Conclusions .....	36
<b>4. Investigation of the effect of using nanofluids on the boiler system behaviour</b> .....	37
4.1 Data reduction .....	37
4.2 System description .....	37
4.3 Validation of experimental .....	38
4.4 Results and discussion .....	39
4.4.1 Effect the volume concentrations on friction factor and Reynolds number .....	39
4.4.2 Heat transfer coefficient and heat transfer rate .....	40
4.4.3 Nusselt number .....	41

4.5 Conclusions .....	42
5. Effect of passive and active cooling on the efficiency of the PV and PVT system .....	43
5.1 Effect of evaporative cooling on PV module performance .....	43
5.1.1 Cooling technique and instruments used .....	43
5.1.2 Results and discussion .....	45
5.1.2.1 Energy analysis of the PV modules with and without CWIW's .....	46
5.1.2.2 Exergy and entropy generation .....	48
5.2 Effect of Zirconium Oxide nanofluid on the behaviour of PVT System .....	50
5.2.1 Experimental setup and work procedure .....	50
5.2.2 Results and discussion .....	51
5.2.2.1 Energy analysis results .....	51
5.2.2.2 Exergy analysis results .....	54
5.2.3 New contributions results .....	56
<b>6. Effect of active cooling by nanofluids on the PVT system efficiency .....</b>	<b>58</b>
6.1 Instruments used with experiments .....	58
6.2 Effect of DI water on the PVT system efficiency .....	59
6.3 Effect of CuO nanofluid on the PVT system efficiency .....	61
6.4 Effect of TiO <sub>2</sub> nanofluid on the PVT system efficiency .....	63
6.5 Effect of Fe <sub>2</sub> O <sub>3</sub> nanofluid on the PVT system efficiency .....	65
6.6 Effect of hybrid TiO <sub>2</sub> /CuO nanofluid on the PVT system efficiency of the .....	66
6.6.1 Energy analysis results .....	66
6.6.2 Exergy analysis results .....	70
6.6.3 Economic analysis of the PVT system .....	72
6.7 Effect of hybrid TiO <sub>2</sub> -Fe <sub>2</sub> O <sub>3</sub> nanofluid on the PVT system efficiency .....	73
6.7.1 Energy analysis results .....	73
6.7.2 Exergy analysis results .....	75
6.8 New contributions results .....	77
<b>7. Numerical simulation of the PVT system by using different nanofluids .....</b>	<b>81</b>
7.1 The model geometry and assumptions .....	81
7.2 Boundary conditions and numerical procedure .....	82
7.3 Results and discussions .....	84
7.3.1 Temperature distribution on the proposed model .....	84
7.3.2 Energy evaluation of the PVT system .....	85
7.3.3 Exergy evaluation of the PVT system .....	89
7.4 New contributions results .....	90
<b>8. Contributions to the scientific knowledge .....</b>	<b>92</b>
8.1 Prediction of PV module thermal and electrical behaviour under different conditions .....	92
8.2 Effect of passive cooling approaches applied .....	93
8.3 Effect of active cooling approaches applied .....	94
8.4 Numerical simulation the effect of nanofluids on the PVT system performance .....	96

<b>Bibliography</b> .....	97
<b>References</b> .....	98
<b>Appendix A Synthesized of mono nanomaterials</b> .....	107
A.1 Tungsten trioxide (WO <sub>3</sub> NPs).....	107
A.2 Titanium oxide nanowires (TiO <sub>2</sub> NWs) .....	108
A.3 Copper oxide nanoparticles (CuO NPs) .....	109
A.3 Copper oxide nanoparticles (CuO NPs) .....	109
A.4 Iron oxide nanorods (Fe <sub>2</sub> O <sub>3</sub> ).....	110
A.5 Zirconium Oxide nanoparticles (ZrO <sub>2</sub> NPs)1 .....	110
<b>Appendix B Effect of passive and active cooling on the efficiency of the PVT system</b> .....	111
B.1 Effect of evaporative cooling on photovoltaic module performance .....	111
B.1.1 Cooling technique used.....	111
B.1.2 Results and discussion .....	113
B.1.2.1 Performance of PV module with CWIRAFs.....	113
B.1.2.2 Performance of the PVT system.....	115
B.1.2.3 Comparison of performance under different cooling techniques.....	117
B.1.2.4 Economic analysis for the passive cooling techniques .....	118
B.2 Energy and exergy assessment of PVT system using tungsten trioxide nanofluid .....	119
B.2.1 Results and discussions.....	119
B.2.1.1 Energy analysis .....	119
B.2.1.2 Exergy and entropy generation results .....	122
B.3 <b>New contributions results</b> .....	124

## Nomenclature

$A$	Area of the module [ $m^2$ ]	FF	Fill factor
$b$	width [m]	$Fe_2O_3$	Iron oxide nanorods
$C_p$	Specific heat [ $kJ/kg \cdot ^\circ C$ ]	in	Input
CuO	Copper Oxide	NP	Nanoparticles
$D$	Tube diameter [m]	nf	Nanofluid
$D_h$	Hydraulic diameter [m]	$np_s$	Nanoparticles
$f$	Friction factor	out	Output
$h$	Heat transfer coefficient [ $W/m^2 \cdot K$ ]	PV	Photovoltaic
$g$	gravity acceleration [ $N/kg$ ]	SEM	Scanning electron microscope
$S$	Solar radiation [ $W/m^2$ ]	TEM	Transmission Electron Microscopy
$I_{SC}$	Short circuit current	$TiO_2$	Titanium oxide
$I_{pv}$	Current [A]	STC	Stander test condition ( $25^\circ C$ , $1000 W/m^2$ )
$L$	Riser length [ $m^2$ ]	$V_{OC}$	Open circuit voltage
$K$	Thermal conductivity [ $W/m \cdot K$ ]	XRD	X-ray power diffraction
$\dot{m}$	Mass flow rate [L/min]	PVT	Photovoltaic-thermal
$n$	Number of tubes	$WO_3$	Tungsten trioxide
Nu	Nusselt number	$ZrO_2$	Zirconium Oxide
NW <sub>s</sub>	Nanowires	$\Delta P$	Pressure drops [Pa]
$P_{pv}$	Electrical power [W]	<b>Greek symbols</b>	
$P_{inc}$	The percentage improve electrical power [%]	$\eta_{th}$	Thermal efficiency [%]
$Q_u$	Thermal energy [W]	$\eta_{ov}$	Overall efficiency [%]
$R$	Thermal resistance [ $^\circ C/W$ ]	$\eta_{ele}$	Electrical efficiency [%]
$R_a$	Rayleigh number	$\beta$	Title angle [ $^\circ$ ]
Re	Reynold's number	$\sigma$	Boltzman constant = $5.67 \times 10^{-8}$ [ $W/m^2 K$ ]
$T$	Temperature [ $^\circ C$ ]	$\varepsilon$	Emissivity [ $W/m^2 k^4$ ]
$U_L$	The overall loss coefficient	$\eta_{el}$	Electrical efficiency [%]
$V_{pv}$	Voltage [V]	$\rho$	Density [ $Kg/m^3$ ]
$W$	Tube spacing [m]	$\mu$	Viscosity [ $Kg/m \cdot s$ ]
<b>Subscript</b>		$\dot{E}_x$	Exergy [J]
amb	Ambient	$\eta_{\dot{E}_x}$	Exergy efficiency [%]
bf	Base fluid	$\dot{S}_{gen}$	Entropy generation [ $W/^\circ C$ ]
CuO	Copper oxide	$\varphi$	Volume concentration [%]
DI	Deionized	$\delta$	Thickness [mm]
ele	Etricalcal		

# Chapter 1

## Introduction

In recent decades, the world has rapidly developed using renewable energy sources, reaching significant usage percentages in several countries, particularly for electricity supply [1]. Energy is the most important requirement of humankind that faces a great challenge in future with the increasing energy demand. Crude oil, natural gas and coal are conventional energy resources representing a significant portion of the energy supply for various industrial, domestic and agricultural sectors [2]. Many factors raise a concern about dependence on conventional sources, such as rapid growth, which increases the requirement exponentially energy demands, and the depletion of conventional energy sources, which may threaten the balance of energy demand in of future. Moreover, the fluctuation of supply costs, the negative influence of political issues between the oil exporting/importing countries and increasing greenhouse gas emissions [3,4]. Modern economies depend on long-term energy availability for future economic growth. The energy sector has manifested significant concerns due to the unavailability of sufficient energy resources and increasing conventional energy demands due to human activities. Although fossil fuels are a significant energy source for power generation, burning fossil fuels increases air pollution and greenhouse gas emissions. Fluctuating fossil fuel prices and significant environmental damages encourage renewable energy sources to be an alternative to conventional energy sources in various applications [5,6]. Sustainable energy source systems are one of the solutions to the mentioned problems that we have faced recently; renewable energy sources are sustainable energy characterized by being reliable, cost-effective, efficient for local usage and environment friendly [7]. Different type of renewable energy systems (i.e., solar energy, wind, biomass, hydroelectric, geothermal energy, ocean) has special advantages for certain applications. Advantages of renewable energy applications include lowering external conventional energy dependence, transformation losses, transmission, reduction of gas emission, etc. [8]. Solar energy is an abundant clean energy source, applicable in various fields and help reduces environmental impact. The solar energy system converts sunlight into heat or electricity energy, one of the important branches of renewable energy systems and a better alternative to environmental safety; its freely available energy is most sustainable in the future [9].

In future energy, the solar industry is the best option due to its availability, accessibility, cost-effectiveness, and efficiency compared to other renewable energies. The solar industry has rapidly developed worldwide due to the increased demand for energy, which became cost-effective because of the aggressive scientific research conducted to develop its performance [10]. Photovoltaic modules (PV) are one of the solar energy systems that convert incident solar radiation into electricity. About 20% of incident solar radiation is converted into electrical energy, and the resting is converted to heat [11]. The PV module consists of semiconductor materials that convert solar radiation (i.e. short-wavelength) to electricity energy [12]. The PV module consists of cells made of silicon; their efficiency depends on the incident solar radiation and the ambient temperature. Increasing the PV cell temperature causes loss of their properties and low conversion efficiency, and then the degradation of the PV module work [13]. The PV module's surface temperature is inversely proportional to the electrical power output of the PV module [14]. The reports indicated that a rise in the PV module temperature by 1 °C decreased the PV module efficiency by 0.45–0.50% [15].

Furthermore, increasing the PV cell temperature leads to drops in the output power, efficiency, durability and lifetime of the PV module affected [16]. Different methods are applied to improve

the efficiency of the PV module by reducing its temperatures. The literature survey in (subsections of chapter 1) covers the main problem and factors that affect the PV module performance and cooling approaches applied to PV modules that help to improve their performance. Thus, highlighting the important designs and cooling methods used to improve the performance of the PV modules to give a future view of the possibilities of cooling methods and identify weaknesses that could be improved to enhance solar systems performance.

### **1.1 Factors causing failure or damage of the PV modules**

Failure or degradation of PV modules is one of the key factors that should be addressed to reduce this phenomenon, thus increasing its performance and operational lifetime. The PV modules are working outdoors which exposed to different environmental stresses such as sunlight, temperature, moisture, cold, and mechanical loads, which cause degradation or decrease in their performance [17]. Solar radiation is a main environmental factor affecting the PV module's operation. The intensity of solar radiation, incidence angle, and spectral distribution depends on the season, latitude, azimuth angle, time of the day, tilt angle, surface reflection, air pollution and cloud cover [18]. The PV module productivity is proportional to incident solar radiation on the PV module surface, a specific part of incident solar radiation is converted to electrical power and a large part to heat which causes serious problems for PV modules [19]. The PV cells convert solar radiation into electricity. This process causes the heating up of the PV cells and then faster degradation of conversion efficiency [20]. The high solar radiance leads to overheating of the PV cells, thus reducing the conversion efficiency of PV cells and may cause the thermal stress of solar modules [21]. The intensity of solar radiation affects the PV module's short circuit current by the number of photons absorbed by the semiconductor material PV cells are made from [22]. A marginal change by open-circuit voltage with an increase in the intensity of solar radiation, while conversion efficiency is somewhat constant and is reduced with the rising of PV cells [23]. An increase in solar radiation with ambient temperature to a high-level cause reducing the output power of PV modules and a decline in their lifetime [24]. An increase in the ambient temperature causes an increase of PV cells, which lead to a significant decrease in open-circuit voltage when the PV module temperature is above 25 °C with a slight drop by short circuits current, then a reduction in power output. Rising temperature above 45 °C causes degradation of the PV module performance and causes local hotspots when the temperature reaches the extreme range. Therefore, the high irradiance and temperature lead to overheating of the PV module, which may cause a decrease in its performance due to degradation of cell work, a drop in conversion efficiency and then reduce the lifetime of the PV cell [25]. In this subsection, we have focused on the most effective factors on PV module performance, such as the intensity of solar radiation and rising ambient temperature and their effect on the performance of PV modules. The next subsections discuss the methods used to solve the problems of rising PV cells temperature, the type of cooling used and the improvements in applied cooling systems design.

### **1.2 Hybrid photovoltaic thermal system**

Solar energy is abundant energy on earth that is directly used to generate electricity by employing PV modules, including PV cells, made of semiconductor materials (silicon) which convert solar radiation directly into electrical energy in silent operation without emissions [26]. The band gap of thin film silicon allows typical crystalline silicon of PV cells can absorb sunlight in the range of 300–1100 nm [27]. PV cells work on absorbing photons that come from the sunlight, which are captured by the electron and produced in high electric potential then,

resulting in electric current. Nevertheless, not all photons generate electric current; the photons with high frequencies above threshold frequency produce heat, causing increased PV cell temperature. The rising of the PV cell's temperature above 25-27 °C causes a drop of electrical energy by 0.4-0.65% with a rise of one-degree celsius [28]. Rising PV cell temperature is an intrinsic problem that leads to a drop in the open-circuit voltage, damaging the PV panel or reducing its productivity [29]. Keeping PV cells close to optimum values of operating conditions is important to avoid hot spots, which significantly drop their efficiency.

Furthermore, increasing the PV cell temperature leads to drops in the output power, efficiency, durability and lifetime of the PV module affected [30]. Different methods are applied to improve the efficiency of the PV module by reducing its temperatures. The hybrid PVT system is one of the most effective solutions to reduce the excess heat of the PV module and use it to produce thermal energy. The PVT system is categorized into two types according to the cooling media used; air-based PVT and fluid-based PVT systems. Several experiments and studies have been conducted in developing PVT systems based on air or fluids. In this dissertation, we will be examined the PVT system using water and nanofluid-based for cooling the PVT system as active cooling and apply passive cooling to improve the PV module performance. The PVT system consists of a PV module combined with a heat exchanger attached at the backside of the PV module; air or fluids are used as a coolant media. Attaching heat exchanger, which consists of pipes with absorb plate at the backside of the PV module, contributes to reducing the temperature of the PV cells by heat transfer from the backside of the PV module to the absorbing plat then to fluid circulated into pipes by conduction and convection. Figure 1 is a cross-section of the PVT system showing the components of the system and the heat transfer mechanism.

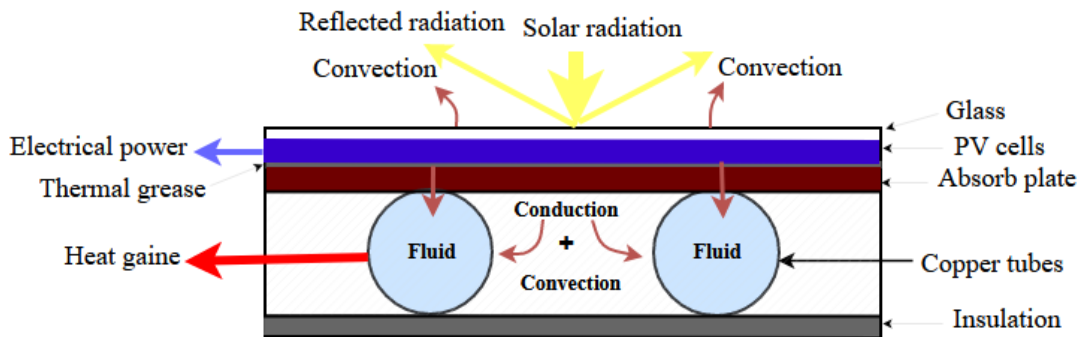


Figure 1. A schematic diagram of heat transfer mechanisms between PVT system components

The essential function of the absorbing plate is absorbing the heat of the PV cells from the back of the PV panel and then transferring the heat to copper pipes and the circulating working fluids. The absorber plate is usually made of copper and aluminium. Both materials have high thermal conductivity, are noncorrosive and stable at high temperatures. Different designs have used piping systems to achieve a high level of heat transfer. Aluminium sheets and copper pipes have been arranged as serpentine coils placed at the backside of the PV module. The serpentine coil helps to absorb as much heat as possible from the PV module due to an increase in the time of fluid residence in pipes [31]. Aluminium spiral pipes are a new design for cooling the PV module, which has been used to enhance the PV performance by water as a working fluid [32]. An experimental investigation was conducted using metal-oxide nanofluids to improve the PVT system; the PV module has equipped heat exchanger consisting of a thin copper sheet soldered on serpentine copper tubing [33]. Heat exchanger attached at backside of PV module, which consists of parallel tubes combined with a single pass air heater. The purpose of the cooling

system designed is to force the fluid to circulate in the copper tubes and the air in the duct independently to increase the heat dissipation area simultaneously[34]. Figure 2 below shows the different heat exchanger designs applied with the PVT system.

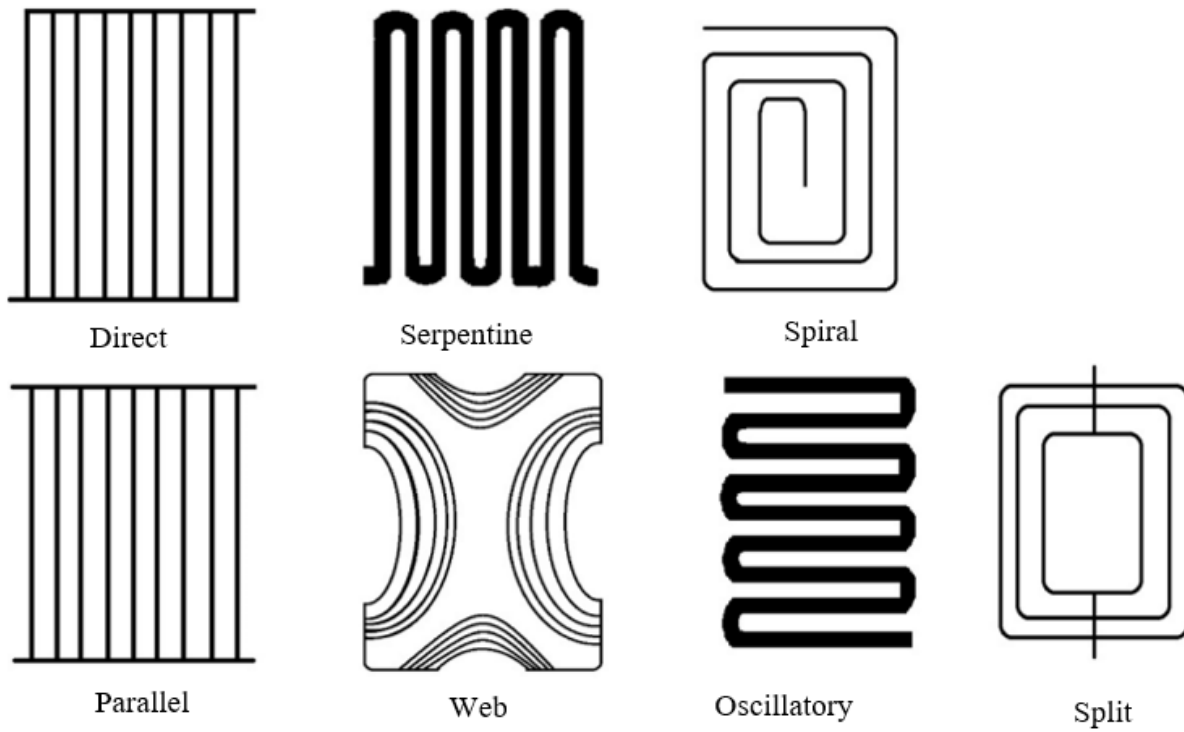


Figure 2. Types of heat exchangers used with PVT system

### 1.3 Cooling systems applied with the PVT system

#### 1.3.1 Passive cooling system

Different cooling techniques help reduce productivity loss and enhance PV module efficiency at high temperatures. Passive cooling techniques are commonly used to maintain PV module performance at high operating temperatures. Passive cooling does not necessarily require external power such pump or fan for cooling the PV module, the opposite of active cooling [10]. In this regard, different passive cooling methods were applied to decrease temperature and enhance the PV module performance. Figure 3 shows the progress of PV cooling techniques in the recent decade. A passive cooling technique has been proposed, which consists of Phase Change Material (PCM), including different oils placed in a container designed as a zig-zag geometry to increase the heat transfer surface at the PV module's backside, as shown in Figure 4. Natural water circulating removes heat from the PCM container without any pump system. The technique used enhanced efficiency to 21.19%, 26.88% and 29.24% at solar radiation intensities of 410 W/m<sup>2</sup>, 530 W/m<sup>2</sup> and 690 W/m<sup>2</sup>, respectively. Mixed PCM with Boehmite nanopowder has better efficiency than the oils used [26]. Another proposed module consisted of cylindrical pin fins with a heat sink; pin fins were arranged uniformly to transmit heat from the PV module to air and enhance the heat exchange with the PV module. A moist wool wood pad was placed at the backside to ensure the touch with the backside surface of the heat sink, and water naturally dropped was used to provide a moist condition for the pad.

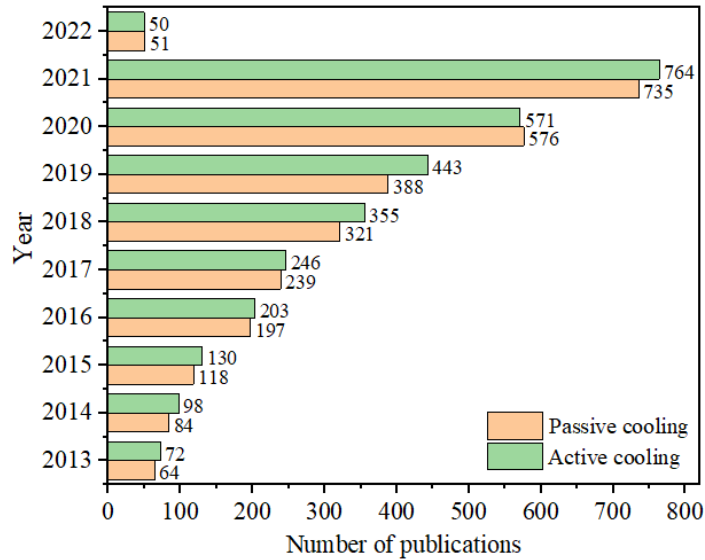


Figure 3. Statistics of publications used active and passive cooling of PV modules

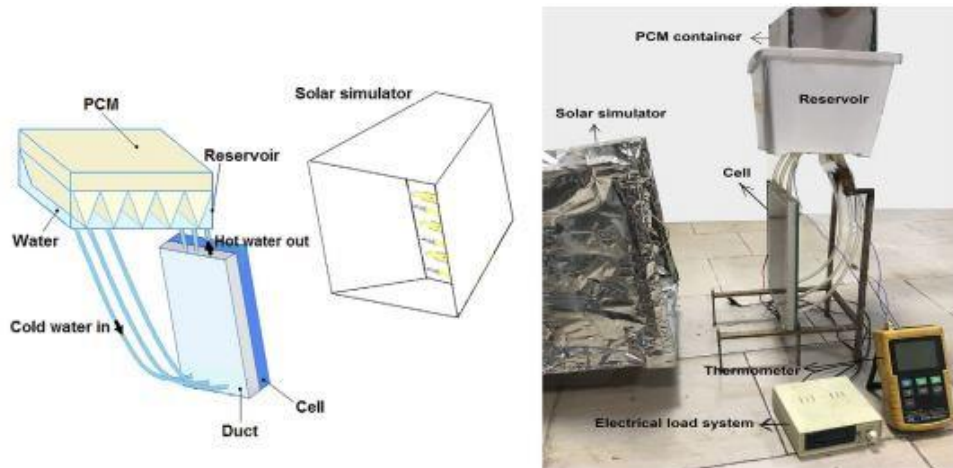


Figure 4. The cooling approach applied

The average temperature of the PV module decreased from 61 °C to 45 °C due to the prevailing moist condition at the backside of the PV module, then improving output power by 32.7% and PV efficiency by 31.7%. This cooling technique is characterized by easy maintenance and cost to reduce the PV module degradation [28]. Another method used thin rectangular fins placed longitudinally and integrated on the thin flat metallic sheet attached to the backside of the PV module. Fins helped release heat from the backside of the PV module to air effectively. Thus, increased the electrical and thermal efficiencies by 56.19% and 13.75%, respectively, using four fins under 700 W/m<sup>2</sup> of solar radiation [29]. The Evaporative cooling technique involves a synthetic clay layer covering a perforated copper sheet with a vaporizer and a measuring beaker filled with water used to spray the water on the clay attached at the backside of the PV module, as shown in Figure 5. The evaporating cooling allows to PV module to work at a suitable temperature due to evaporative cooling. The results indicate that this technique improved the performance of the PV module by increasing the voltage by 19.4% and electrical power to 19.1% [35].

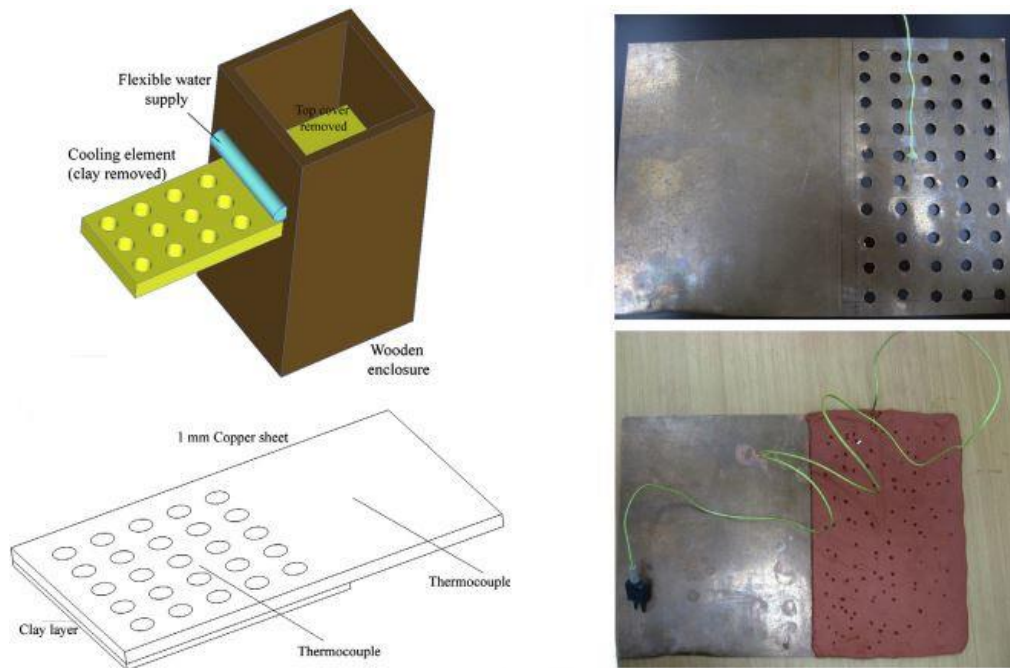


Figure 5. Evaporative cooling by synthetic clay layer covering a perforated copper sheet

Chandrasekar et al [36]. Propose fins in conjunction with cotton wicks attached at the backside of PV to control its temperature during operation. The cotton wick was provided with fluid from the bottom to the top of the PV module. The study shows that using fins integrated with cotton wicks increased the electrical yield of PV modules to 14% because of a 12% decrease in the PV module temperature. The use of clay was markedly effective, affordable and environment friendly. Another technique represents by the integration of the desiccants material on the backside of the PV module; at night, when the temperature decreases, desiccants work to adsorb water from the air when the relative humidity is high. During the day, when the temperature increases, water evaporates and takes excess heat from the PV module. The results referred to dropping the PV module's temperature lower than ambient air temperatures that may reduce to 30 °C with evaporative cooling. The yield of PV modules increases by over 10% in sunny conditions [37]. Another configuration representing a stainless-steel tube designed as a serpentine exchanger bonded on a stainless-steel sheet has been placed at the PV module's backside. A two-phase flow of CO<sub>2</sub> passes inside the exchanger by a heat pump system. Decreased solar absorber plate temperature led to an increase in the yield of electrical power of the PV module. The proposed design helped increase the electrical efficiency from 14.1% to 16% with 1.028 kW of thermal energy, and overall efficiency reached 72.3% [38]. A new trend to restore waste recycling materials in solar systems, aluminium beverage cans filled with paraffin wax have been used to improve the efficiency of PV modules and compare their performance with conventional PV modules simultaneously. Experimental results showed an increment in electrical efficiency from 10.69% to 12.60%, while output power efficiency was from 61.72% and 71.56%, respectively, for PV modules integrated with aluminium beverage cans filled with paraffin wax and conventional [39]. Another passive cooling approach consists of different numbers of aluminium and copper fins 5, 10, and 15 that are attached to the backside of the PV module; Figure 6 shows the fin configuration. Temperature distribution and wind speed vectors were simulating investigated. Passive cooling provided a potential cooling to

enhance the performance and decrease the temperature of the PV module. The number of copper fins increased to 15, with a drop in the PV module by 10.2 °C and electrical efficiency by 2.74% [40].

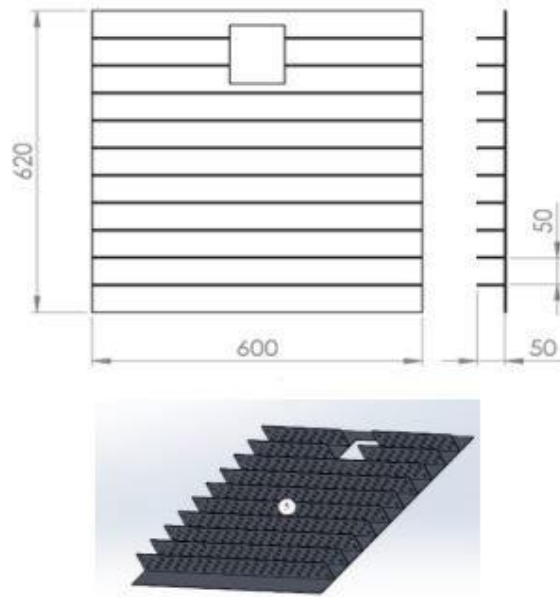


Figure 6. Fins configuration attached at the backside of the PV module

The passive cooling approaches applied in the studies above show interesting outcomes and achieve remarkable performance enhancement in the PVT system. However, some important research gaps are still not verified in this domain, such as adopting an evaporative cooling approach more efficient or hybrid passive cooling. Besides, few studies have investigated the thermodynamic performance of passive cooling, leaving an incomplete thermal view. In his PhD dissertation, two passive cooling approaches are applied, cotton wicks immersed in water and rectangular aluminium fins and cotton wicks combined by fins as a hybrid approach to study their effect on the PV module performance.

### 1.3.2 Active cooling system

#### 1.3.2.1 Cooling by conventional fluids

Several configurations and cooling fluids have been applied to improve the PV module performance under different conditions. Adopting forced cooling techniques such as circulating fluid into a heat exchanger consisting of tubes and absorb plate attached to the backside of the PV module [41]. The latter method is called a photovoltaic-thermal (PVT) system, which helps to reduce temperature, improve the electrical efficiency of the PV module, and then produce thermal and electrical energy simultaneously [42]. Circulation of air or fluids into pipes helps to absorb the excessive heat of the backside of the PV module through forced convection due to rising temperature, which improves the electrical efficiency of the PVT system [43]. The dynamic performance of a PVT system has been investigated with direct contact between a simple water box and a mono-crystal PV module. Water was adopted as a coolant to lower the PV module temperature, and it was observed an increment of the maximum thermal energy by

58% with a decrease in the PV module temperature due to heat loss. The electrical efficiency is dropped at noon due to rising solar radiation to the maximum value.

However, the cooling technique has increased the electrical efficiency from 15 to 21.5% compared to the conventional PV module [44]. Water circulation in a dual copper pipeline has been designed for a cooling PVT system tested under solar radiation from (600-1000)  $\text{W/m}^2$ , the mass flow rate from 2 to 5 L/min, and 26 °C inlet water temperature. The results indicated that the thermal efficiency was enhanced by 59.6% with the increased solar radiation and mass flow rate. Besides, the decreased PV cell temperature has improved the output power and the electrical efficiency by 11.71% compared with the reference module [45]. Another study adopted of water-to-air heat exchanger coupled with a PVT air collector; the heat exchanger consists of pipes with fins linked by the well that contains water at a constant temperature at 5 m depth and works as a geothermal energy source. Thus, the heat exchanger helps transfer energy from and to the water. The proposed system achieved the required heating and cooling and improved the PV module efficiency to 2 % in the winter and 5.1% in the summer. The saved electrical and thermal energies for cooling were 3.14 kWh/day and 24.79 kWh/day [46]. The spiral flow absorber consisting of rectangular hollow tubes made of stainless steel has been proposed as a heat exchanger. The tubes were connected by welding and attached to the backside of the PV module. The performances of PVT were tested under different solar radiation levels and mass flow rates. The results indicated that spiral flow absorbers provide superior performance at solar radiation of 800  $\text{W/m}^2$  and a mass flow rate of 0.041 kg/s. Electrical efficiency was 13.8%, with thermal efficiency reaching 54.6%, and the overall efficiency of PVT was 68.4% [47].

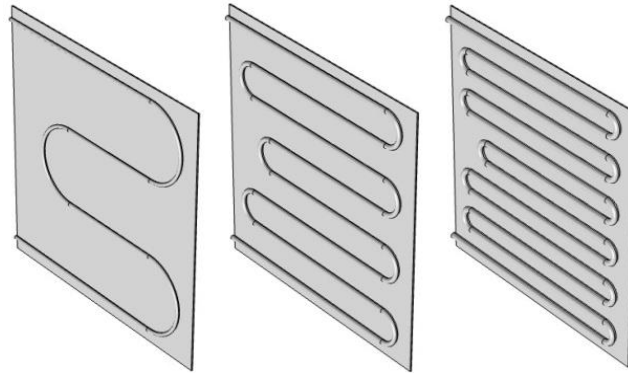


Figure 7. Different modes of tube design

An investigation used feed water of reverse osmosis for cooling the backside of a PV module, and its effect on the output power and efficiency of the PV module was studied. The output power generation and the electrical efficiency were improved by 14.1% and 19.8%, respectively, compared to a module without cooling [48]. A numerical study has investigated the impact of cooling system design on the electrical and thermal efficiency of the PVT system by using different tube diameters and lengths, as shown in Figure 7. The tube's diameters tested were 9.53, 12.70 and 15.88 mm under the flow rate range of 0.5 and 2.5 L/min. The results indicated that the highest electrical efficiency was 14.8% at a tube diameter of 9.53 mm, and a flow rate of 2.5 L/min, while the highest thermal efficiency was 79.1%, and overall efficiency was 92% at a used tube diameter of 15.88 mm and 1.5 L/min flow rate. Furthermore, using a 15.88 mm tube diameter and flow rate of 0.68 L/min leads to a lower temperature of the PV module and the increased outlet temperature of the PVT system [49]. Although using water or equivalent base fluids can enhance the performance of the PVT system, this enhancement is still meagre because

of the poor thermal conductivity of the conventional fluid (water). The thermophysical properties of the conventional fluid can be enhanced by adding nanoparticles to the fluid, which produces nanofluids with high thermal characteristics.

### 1.3.2.2 Cooling by nanofluids

In recent years, the use of nanofluids attracted attention because this fluid gives better heat transfer capacity due to its high thermal properties compared to conventional fluids [50]. The literature adopted various nanoparticles at specific volume concentrations, which achieved remarkable enhancement in the PVT system performance. For instance, an experimental study of the PVT system used a nanofluid consisting of carbon black nanoparticles mixed with water at different concentration ratios from 0-0.4 wt% to control rising PV cell temperature. The results indicated that a 0.21 wt% concentration ratio of nanoparticles in water lowered the surface temperature and increased the output power by 7% compared with pure water [51]. An investigation was conducted on the effect of used Ag/water nanofluid on the energy and exergy efficiencies of the PVT system under different flow regimes and nanoparticle concentrations. The results showed a significant enhancement of energy and exergy efficiencies of the PVT system, which was attributed to increased nanofluid concentration and flow rate close to turbulent flow. Thus, using 4 wt% nanofluids increased output power by 35% and 10%, and the exergy efficiency increased by 50% and 30% compared with water cooling and without cooling [52]. The performance of the unglazed PVT system was evaluated using water and CuO nanofluid circulated by the cooling system consisting of sheets and tubes placed at the backside of the PV module. The temperature of the PVT system dropped to 15 °C and 23.7 °C with the used water and nanofluid compared with the PV module without cooling, which reached 68.4 °C. The PV cell temperature reduction increases the average electrical efficiency to 35.67% with nanofluid and 12.98% with water, while without cooling is 12.32%. The overall efficiency of the PVT system with nanofluid was higher by 21% than the water-cooled due to the high heat absorption by CuO nanoparticles [53]. A new geometry of the PVT system has been studied with Al<sub>2</sub>O<sub>3</sub>/H<sub>2</sub>O nanofluid applied with a concentration of (0.05–0.5 wt.%) as a coolant working fluid to evaluate their effect on the performance of the PVT system. The cooling system attached at the backside of the PV module consists of the serpentine half-pipe; the PV cells are assembled on an aluminium plate of a 3 mm thickness, with removes the Tedlar to increase the heat transfer in the cooling section, as shown in Figure 8. The results show a remarkable increment of the PVT efficiency, especially at cooling by nanofluid with a concentration of 0.5 wt.% of nanoparticles into pure water. The thermal and electrical efficiency was enhanced by 126.71%, 7.38% compared with pure water, and the overall efficiency of the PVT system is 93.73%, which confirms the feasibility of nanofluids as a better coolant than water [25]. Experimental investigations were conducted on the performance of the PVT system using two types of nanofluids, Cu/water and TiO<sub>2</sub>/ water, at the variation of mass flow rate.

The experimental outcomes show enhancing of the PVT electrical efficiency to 5.98% at a 1% volume concentration of Cu/water nanofluid, and at a higher mass flow rate, the temperature of the PV module is reduced to 17.18 °C. Thereby enhancing the electric and thermal efficiency of the PVT system by 2.58% and 5.43%, respectively [54]. Energy and exergy evaluation of the PVT system was conducted using ZnO, TiO<sub>2</sub> and Al<sub>2</sub>O<sub>3</sub> nanoparticles dispersed in DI water as coolant fluids at a mass flow rate of 30 kg/h. Based on the data measured, the TiO<sub>2</sub> and ZnO nanofluids gave better energy and exergy efficiencies than Al<sub>2</sub>O<sub>3</sub> nanofluids. The overall exergy efficiencies of the PVT were enhanced by 15.45% ZnO/water, 15.93% TiO<sub>2</sub>/water, and 18.27% Al<sub>2</sub>O<sub>3</sub>/water compared with water cooling, which recorded 12.34%. Al<sub>2</sub>O<sub>3</sub>/water has a better

enhancement of entropy generation [33]. A numerical analysis of the PVT system using MgO/water nanofluid that circulated into copper tubes attached at the backside of the PV module, the volume concentration of nanoparticles was 0 and 1% in the base fluid and the volume flow rate from 0.5-4 L/min. The results indicated that it enhances the exergy output by lowering nanofluid flow rates while increasing the flow rate above 0.5 L/min causes reduces the efficiency.

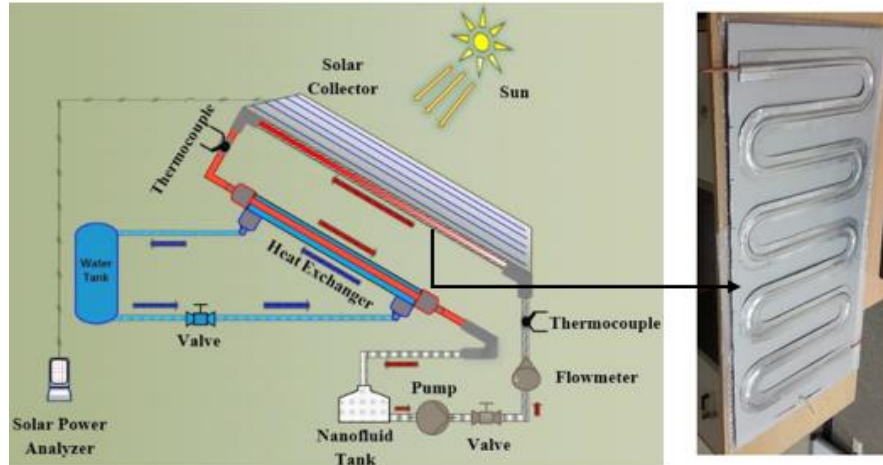


Figure 8. The schematic diagram of the experimental with serpentine half-pipe

The exergy efficiency increased by 0.45% by adding 1% volume concentration nanoparticles and 0.5 L/min volume flow rate [55]. A study has proposed using  $Al_2O_3$ /water and Cu/water nanofluids as a coolant and the effect of the diameter and number of pipes used on the performance of the PVT system. The results show that using Cu/water nanofluids gives better performance to the PVT system than using  $Al_2O_3$ /water nanofluids. The electrical and thermal efficiencies had improved by 4.98% and 5.23%, respectively, by Cu/water nanofluid. The performance of the PVT system was significantly enhanced by increasing the number of tubes with no substantial effect on the diameter of the pipes [56]. Multi-Wall Carbon Nanotubes (MWCNT)/water nanofluid has been used as a coolant to evaluate the PVT system performance at different volume concentrations (0-0.3%) and a constant mass flow rate of 1.2 L/min. Adding MWCNT nanoparticles to water enhanced the thermal properties, which are positively reflected by the electrical and thermal efficiency generated by the system. The temperature of the PV module was reduced by 12 °C at maximum incident radiation and achieved maximum overall efficiency of 83.26% [57]. Graphene nanofluid has been proposed as a coolant media to enhance the efficiency of a PVT system at different volume concentrations along with a surfactant (sodium deoxycholate). The results indicated a reduction in the PV module temperature by 20 °C with an increase in the volume concentration to 0.3 vol% at a mass flow rate of 0.085 kg/s. Then the energy efficiency of the PVT system and PV module was improved by 13% and 23%, respectively [58].

#### 1.4 Objectives of the dissertation

In the literature, it can observe all the methods and techniques used to improve the performance of the PVT systems somehow is similar, and it lacks a comprehensive analysis of quantitative and qualitative performance as a result of relying on quantitative analysis based on the first law of thermodynamics. In addition to qualitative analysis, it lacks comprehensive analysis, such as

exergy losses and entropy generation. Regarding the use of passive cooling in most of the techniques, we found that some technologies have achieved good results, but without mentioning their reliability in different operating conditions, economic feasibility, and scope of application. On the other hand, we found that active cooling techniques have occupied a wide range of applications due to their interesting outcomes and durability in simultaneously improving electrical and thermal performance. Nevertheless, limited improvements were made to improve its performance, such as the design of the heat exchanger attached to the back side of the solar panel, the type of coolant used, or the use of integrated cooling methods.

This PhD dissertation addresses the uncompleted gaps in the literature that contributes to improving the general performance of the PVT system by adopting reliable technologies that contribute to improving PVT system performance, such as:

- Comprehensive thermal analysis of the system included energy and exergy analysis, thermal parameters such as Reynolds number, Nusselt Number, fraction factor, pressure drop and heat transfer mechanism with identifying the cooling fluids (Chapter 2).
- Predictive study of the thermal and electrical behaviour of the PV module under different operating conditions and the factors affecting their output, which in turn determine the effective ways to improve performance (Chapter three).
- Investigation of the effect of thermal parameters of using nanofluids as a cooling fluid at various flow rates and temperatures by using the boiler system to ensure effective of nanofluids under different conditions (Chapter 4).
- Regarding passive cooling, in this PhD dissertation, cotton wicks immersed in water which arranged and stacked as one layer, then attached to the backside of the PV module as a first phase. The rectangular aluminium fins integrated with cotton wicks are used as a second phase to enhance evaporative cooling. These cooling techniques help increase the evaporating cooling that positively reflects on the PV module performance, and these techniques have been applied according to Iraq conditions (Chapter 5).
- Active cooling is a common cooling technique in most PVT system applications which adopt fluids as a cooling technique. Nowadays, nanofluid is one of the effective cooling fluids used in the PVT system; in this dissertation, new nanofluids have been used (mono and hybrid) nanofluids at different volume concentrations and according to Hungary and Iraq conditions (Chapter 6).
- Numerical investigation of the PVT system's energy and exergy and validation is an important issue that most consider demonstrating the reliability and feasibility of the system and the accuracy of the results by comparing them with the practical results. In this case, numerical simulation was conducted for the PVT system using nanofluid according to Iraq and Hungary conditions and then compared the numerical results by experimental results to determine the deviation of the simulation results (Chapter 7).
- Chapter 8 reviews the important new scientific of this dissertation.

## Chapter 2

### Methodology

#### 2.1 Thermal Analysis of heat transfer between the PVT system components

The efficiency of the PVT collector requires several factors that must be considered to achieve outstanding performance and stability of the PVT collector, such as solar radiation, ambient temperature, and wind speed. All the factors that have been mentioned affect the PVT collector performance. On the other hand, designed PVT collectors play an intrinsic role in their efficiency, such as absorber area, reduced heat loss, and collector tilt angle. The function of the heat exchanger, which represents the second part of the PVT collector fixed at the backside integrated with the PV, is to transform solar radiation by an absorber (copper plate) to thermal energy as a hot fluid and that depends on the input and output parameters that effect on the efficiency of the PVT collector. The input parameters include the form of design of the PVT collector (collector size, incidence angle, collector tilt angle, etc.), climatic conditions (ambient temperature, solar radiation, wind speed), and operation (nanofluid inlet temperature and the mass flow rate through the collector). While overall efficiency, nanofluid outlet temperature, power production, and quantity of useful heat gain are the output parameters. The mathematical model uses to describe the temperature that transfers across the different components of the PVT system. Therefore, it derived the heat balance transfer across different system components with arranged all the tubes in a parallel fashion, and the space between them is fixed. It is considering that both fluid flow rate and temperature are the same in all tubes. Assumptions that all the components' material properties are constant, the edge losses are neglected, calculation of all the heat transfer coefficients in real-time and the fluid flow rate in all tubes are the same. To mathematical modelling of the PVT collector, it writes the energy equation for all the different components of the system with the assumption that in one-dimensional energy balance analysis, the heat transfer is one-dimensional and steady.

In a steady state, the useful output energy of a collector of the area is the absorbed solar energy subtracted from the thermal loss. The absorbed solar radiation per unit area of the collector equals the variation amount between both the solar radiation and the optical losses. The concept of an overall loss coefficient is important for consideration in the calculation, where the absorbed energy (solar radiation) is distributed to thermal losses through the top and bottom and to useful energy gain; Figure 9 shows the heat transfer coefficient mechanism between the PVT system layers. The solar radiation incident on the PV cells with heating the PV cell. The absorber plate that attaches to the PV panel's backside will absorb the heat by conduction and transfer it to the pipes' region [59]. The temperature midway between the pipes will be higher than in the vicinity of the pipe. Because of the pipes' presence and weld metal, the temperature above the pipes will be nearly uniform. The heat energy is transferred to the fluid to heat the fluid, which causes a temperature gradient to exist in the flow direction. Thus, at any region of the PVT collector, the general temperature level is governed by the fluid's local temperature. Equation (1) represents the convection heat transfer coefficient between solar radiation and the glass cover of the PV collector.

$$h_{r,gl} = \sigma \varepsilon (T_s + T_{gl})(T_s^2 + T_{gl}^2)(T_{gl} - T_s) \quad (1)$$

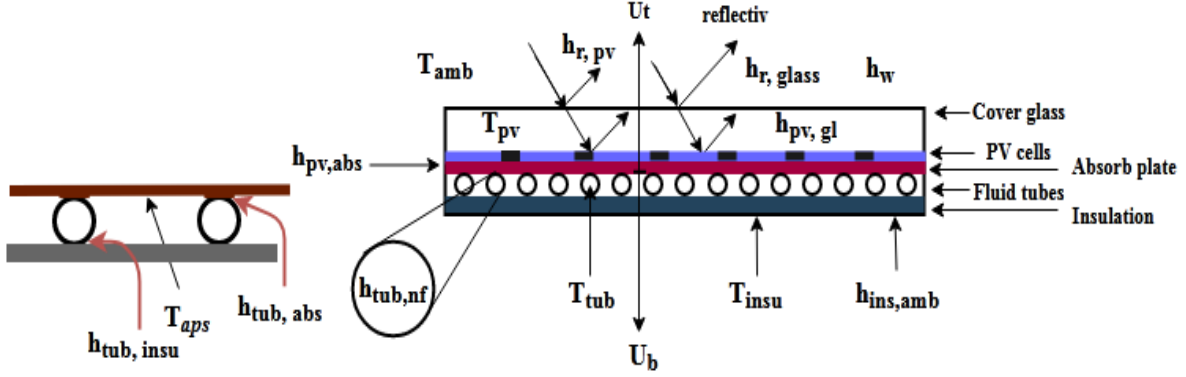


Figure 9. Heat transfer coefficient between PVT collector layers

The sky temperature  $T_s$ , is calculated by the equation below,  $T_{gl}$  is the glass cover temperature

$$T_s = 0.0522 * T_{amb}^{1.5} \quad (2)$$

The convection heat transfer coefficient between the glass cover and PV cells represents in Eq (3).

$$h_{gl,pv} = \frac{k}{L_{gl}} \cdot \left( 1 + 1.44 \left[ 1 - \frac{1708(\sin(1.8\beta))^{1.6}}{Ra \cos(\beta)} \right] \left[ 1 - \frac{1708}{Ra \cos(\beta)} \right] + \left[ \left( \frac{Ra \cos(\beta)}{5830} \right)^{\frac{1}{3}} - 1 \right] \right) \quad (3)$$

$$Ra = \frac{g(T_{pv}-T_{gl})L^3}{T_m \nu \alpha} \quad (4)$$

$$T_m = \frac{T_{pv}+T_{gl}}{2} \quad (5)$$

$T_{amb}$  is the ambient temperature,  $K$  is the thermal conductivity of the glass,  $L_{gl}$  is the distance between the PV cells and cover glass,  $\beta$  is the collector title angle and  $R_a$  is Rayleigh number which calculates from Eq (4). Thermal diffusivity ( $\alpha$ ), kinematic viscosity( $\nu$ ),  $g$  is the gravitational constant and  $T_{pv}$  The temperature of PV cells. The convection heat transfer coefficient between solar radiation PV cells is given in Eq (6).

$$h_{r,pv} = \frac{\sigma(T_{pv}^4 - T_{gl}^4)}{\frac{1}{\epsilon_{pv}} + \frac{1}{\epsilon_{gl}} - 1} \quad (6)$$

Where  $\sigma$  is the Stefan-Boltzman constant =  $5.67 \times 10^{-8}$  W/m<sup>2</sup> K,  $\epsilon_{pv}$ ,  $\epsilon_{gl}$  are the PV and glass emissivity. The collector overall loss coefficient  $U_L$  is the sum of the top, bottom, and edge loss coefficients; Figure 10 shows the thermal resistance to heat flow, and Table 1 shows the formulas used to calculate the thermal resistances.  $R_3 = \frac{k_{abs}}{L_{abs}}$

Table 1. Thermal resistance formulas

Formula	Thermal resistance
$R_1 = \frac{1}{h_w + h_{r,gl}}$	The thermal resistance between the surroundings and the glass cover
$R_2 = \frac{1}{h_{gl,pv} + h_{r,gl}}$	The thermal resistance between the glass cover and PV cells

$U_t = \frac{1}{R_1 + R_2}$	The total heat transfer coefficient top loss from the PVT system to the ambient
$R_3 = \frac{k_{abs}}{L_{abs}}$	The thermal resistance to heat flow through the absorbing plate
$R_4 = h_{tub, nf}$	The resistance of the convection heat transfer coefficient between the tube and nanofluid
$R_5 = \frac{k_{insu}}{L_{insu}}$	The resistance to heat flow through the insulation
$U_b = \frac{1}{R_3 + R_4 + R_5}$	The heat loss through the bottom of the PVT system
$U_L = U_t + U_b$	The overall loss coefficient

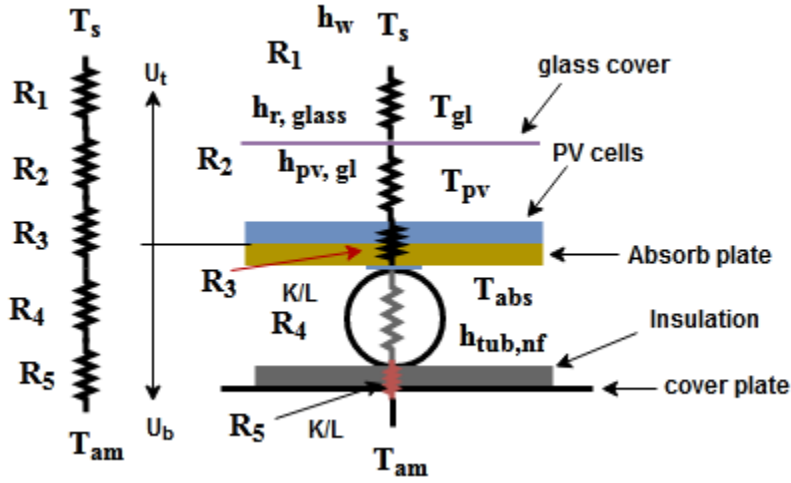


Figure 10. Thermal resistance between PVT collector layers

The heat loss from cover glass exposed to outside winds is important in calculating and by the used formula below [59] by Eq. (7)

$$q_{loss, top} = h_{gl, pv} + h_{r, pv} (T_{pv} - T_{gl}) \quad (7)$$

In a steady state, the useful output energy of the PVT collector is given by the equation below.

$$Q_u = A_c [S - U_L (T_{pv} - T_{amb})] \quad (8)$$

where  $S$  is solar radiation  $W/m^2$ , and  $A_c$  is collector area.

$$h_{wind} = 3u_a + 2.8 \quad (9)$$

where  $h_{wind}$  is the convection heat transfer coefficient between PV laminate and ambient air,  $u_a$  is the wind velocity [59]. The conduction heat transfer coefficient between the PV cells and the absorber plate  $h_{pv, abs}$  that can calculate using the following Eq (10)

$$h_{pv, abs} = \frac{k_{ad}}{\delta_{ad}} \quad (10)$$

where  $\delta_{ad}$  and  $k_{ad}$  are thickness and the thermal conductivity of the adhesive.

The conductive heat transfer coefficient between the absorber plate and the tube  $h_{abs,tub}$ ,  $h_{abs}$  that expressed by the equation below [60],

$$h_{abs, tub} = \frac{2k_{abs}}{(W-D_o)} \quad (11)$$

where  $k_{abs}$  is the thermal conductivity of the absorber copper plate = 398 W/m.k,  $W$  is the tube spacing = 5 cm,  $D_o$  is the outer diameter of the pipe = 0.095 cm. The convection heat transfer coefficient between the tube and nanofluid  $h_{tub,nf}$  that estimated by using the following correlation.

$$h_{tub, nf} = \frac{Nu_{nf}k_{nf}}{D_{ia}} \quad (12)$$

where  $Nu_{nf}$  is Nusselt number of nanofluid,  $K_{nf}$  is the thermal conductivity of the nanofluid,  $D_{ia}$  is the diameter of the tube. To calculate the conductive heat transfer coefficient between two layers neighbouring the tube and the insulation, it use the correlation [61].

$$h_{tub, insu} = \frac{1}{\frac{\delta_{tub}}{k_{tub}} + \frac{\delta_{insu}}{k_{insu}}} \quad (13)$$

where  $\delta_{tub}$  is the thickness of the tube,  $k_{tub}$  is the thermal conductivity of the tube.  $\delta_{ins}$  is the thickness of the insulation,  $k_{ins}$  is the thermal conductivity of the insulation. To calculate the conductive heat transfer coefficient between the insulation back cover, it uses the correlation [61].

$$h_{insu, bcov} = \frac{1}{\frac{\delta_{insu}}{k_{insu}} + \frac{\delta_{b,cov}}{k_{b,cov}}} \quad (14)$$

where  $\delta_{b,cov}$  is the thickness of the back cover,  $k_{cov}$  is the thermal conductivity of the back cover. The amount of heat transferred to the nanofluid can determine by the equation below.

$$q'_u = WF'[S - U_L(T_{nf} - T_a)] \quad (15)$$

where  $T_{nf}$ ,  $F'$  is the collector efficiency factor, and  $W$  is the distance between centre pipes, as shown in Figure 11.

$$F' = \frac{1/U_L}{W \left[ \frac{1}{U_L[D+(W-D)F]} + \frac{1}{C_b} + \frac{1}{\pi D_i h_{tub,nf}} \right]} \quad (16)$$

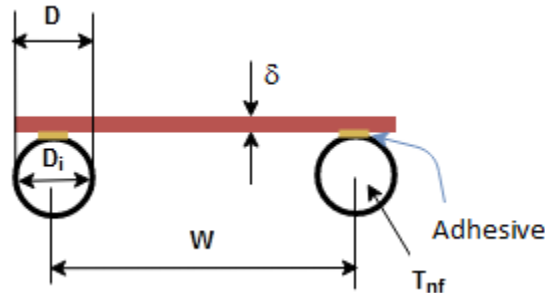


Figure 11. Contacting between absorbing plate and pipes

Adhesive  $k_b$ , the average adhesive thickness  $\gamma$ , and the adhesive width  $b$ ,  $D$  is the tube diameter and  $D_i$  is the inside diameter of the tube and  $h_{tube,nf}$  is the convection heat transfer coefficient between the tube and nanofluid.

$$C_b = \frac{k_b b}{\gamma} \quad (17)$$

The fin efficiency factor  $F$  [59].

$$F = \frac{\tanh [m(W-D)/2]}{m(W-D)/2} \quad (18)$$

$$m = \sqrt{\frac{U_L}{k\delta}} \quad (19)$$

## 2.2 Energy balance equations for the PVT system

The mathematical model of the hybrid PVT system involves two parts; the first part is related to calculating the overall efficiency of the PVT system (thermal and electrical efficiency of the PVT system). The second part is related to the properties of nanofluids and the governing equations for the thermo-physical properties of nanofluids. Evaluating the performance of the PV/T system is important to recognize the behaviour components of the system, considering the equations that are governed by the behaviour of the PV/T system. The PVT panel consists of five-part, as shown in Figure 12, cover glass, PV cells, absorb plate, copper pipes, insulation, and the outer cover. A mathematical equation governs each part. Different types of the working fluid are used with PVT systems considering thermo-physical proprieties that enhance the system's efficiency. Several assumptions are adapted to writing the heat balance mathematical equation of the PVT panel. We have adopted the heat balance mathematical equation similar to that used [62], as shown below. Solar radiation is the uniform distribution on the photovoltaic panel surface with constant thermal conductivity, particularly for solid materials.



Figure 12. Component of PVT collector

The temperature distribution is uniform for each solid material in the PVT system thermodynamic equilibrium with steady-state conditions and the computational domain element. The nanofluid inlet temperature differs from the outlet temperature as a linear variation, with negligible kinetic and gravitational energy balances.

$$\rho_g \delta_{gl} C_{p,gl} \frac{dT_{gl}}{dt} = \alpha_{gl} S + h_{r,gl} (T_{sky} - T_{gl}) + h_w (T_{amb} - T_{gl}) + h_{pv,gl} (T_{pv} - T_{gl}) \quad (20)$$

The left side of the equation represents the temporal energy changes in the glass covers. The first item on the right-hand side is the received irradiation by the glass cover; the second item is the irradiative heat transfer between the glass cover and the surroundings. The third item is the convective heat transfer between the glass cover and the outside environment, and the fourth item is the conductive heat transfer from the photovoltaic cells to the glass cover. The rate of absorbed solar radiation by photovoltaic minus the entire heat transfer from the photovoltaic to

absorb plate represents the PV module thermal balance [63]. Considering both convection and radiation heat exchange in the environment, as shown in Eq (22).

$$\rho_{pv}\delta_{pv}C_{p,pv}\frac{dT_{pv}}{dt} = \alpha_{pv}\tau_g S - E_{elec} + h_{pv,gl}(T_{gl} - T_{pv}) + h_{pv,abs}(T_{abs} - T_{pv}) \quad (21)$$

$$E = SP\eta_{el} \quad (22)$$

where  $S$  is the solar radiation,  $\alpha_{pv}$  is absorptivity of the PV cells and  $\rho_{pv}$  represent the density of the PV cells. while  $C_{p,pv}$  is the specific heat of the PV cells.  $E$ ,  $p$  and  $\eta_{el}$  are the electrical power, the packing factor, and the electrical efficiency.  $h_{pv,abs}$  is The conduction heat transfer coefficient between the PV laminate and the absorber plate and  $T_{abs}$  is absorber plate temperature. By the internal energy change of the plate, we can calculate the thermal balance of the absorber plate, where the heat transfer from the photovoltaic to the absorber plate minus the entire heat transfer from the plate absorber to the tube with considering the heat transfer from the absorber plate to the insulation [63].

$$\rho_{abs}\delta_{abs}C_{p,abs}\frac{dT_{abs}}{dt} = h_{pv,abs}A_{pv,abs}(T_{pv} - T_{abs}) - h_{abs,tub}A_{abs,tub}(T_{abs} - T_{tub}) - h_{abs,insu}A_{abs,insu}(T_{pv} - T_{insu}) \quad (23)$$

where  $T_{ins}$  is the insulation temperature,  $\rho_{abs}$  is the density of the absorber plate,  $\delta_{abs}$  is the thickness of the absorbing plate and  $C_{p,abs}$  is the specific heat of the absorber plate. The conductive heat transfer coefficients between the absorber and the insulation. The sum of the conduction heat transfer from the tube to the insulation and the convection heat transfer from the tube to the nanofluid minus heat transfer from the absorber plate to the tube represents the thermal balance of the tube [63], which is evaluated by the equation below.

$$\rho_{tub}\delta_{tub}C_{p,tub}\frac{dT_{tub}}{dt} = h_{abs,tub}A_{bt}(T_{abs} - T_{tub}) - A_{tub,f}h_{tub,nf}(T_{tub} - T_f) - A_{tub,insu}h_{tub,insu}(T_{tub} - T_{insu}) \quad (24)$$

where  $T_f$ ,  $\rho_{tub}$  are the circulating working fluid temperature, the density of the tube,  $\delta_{tub}$  tube thickness and  $C_{p,tub}$  is the specific heat of the tube. The energy balance equation of working fluid is evaluated by the equation below.

$$\dot{m}_{nf}C_{p,nf}\frac{dT_{nf}}{dt} = \dot{m}_{nf}C_{nf}(T_{out} - T_{in}) + A_{tub,nf}h_{tub,nf}(T_{tub} - T_{nf}) \quad (25)$$

where  $\dot{m}_{nf}$  is the fluid mass flow rate,  $T_{in}$  is the inlet temperatures and  $T_{out}$  is the outlet temperature of the fluid [64]. The energy balance for insulation is the sum of the conduction heat transfer from the tube to the insulation added to the heat transfer from the plate absorber to the insulation [63], which is evaluated by the equation below.

$$\rho_{insu}\delta_{insu}C_{p,insu}\frac{dT_i}{dt} = h_{abs,insu}A_{abs,insu}(T_{abs} - T_{insu}) + A_{tub,insu}h_{tub,insu}(T_{tub} - T_{insu}) + h_{insu,a}A_{insua}(T_{insu} - T_{amb}) \quad (26)$$

where  $\rho_{ins}$  is the density of the insulation material  $\delta_{insu}$  insulation thickness and  $C_{p,ins}$  is the specific heat of the insulation material.  $h_{ins,amb}$  represents the convective heat transfer coefficient between the insulation and the ambient air. The convection heat transfer coefficient between the outer aluminium cover plate of the collector and the ambient,  $h_{cov,amb}$  can calculate with the Mc-Adams equation below and depending on the wind velocity [65].

### 2.3 Energy and exergy assessment of PVT system

In this section, the energy and exergy analysis depend on the first and second laws of thermodynamics. The first law assesses the energy quantity, while the second law assesses the exergy quality of the system [51]. The PVT system produces electricity and thermal energy simultaneously; thereby, the energy analysis of the PVT system is divided into two parts: electrical and thermal performance. The electrical efficiency ( $\eta_{ele}$ ) is a measure of the electrical energy performance of the PVT system [66], which can be calculated from the equation below.

$$\eta_{ele} = \frac{P_{pv} \times FF}{S \times A} \quad (27)$$

$P_{pv}$  is the electrical power of the PV module, which is calculated by Eq (2),  $V_{pv}$  is the voltage,  $I_{pv}$  is the current, and (A) PVT module area. The fill factor (FF) represents the maximum power conversion efficiency of the PV module, which can be calculated from the equation below [36].

$$P_{pv} = V_{pv} \times I_{pv} \quad (28)$$

$$FF = \frac{V_{pv} \times I_{pv}}{V_{oc} \times I_{sc}} \quad (29)$$

The effect of using nanofluid as a cooling fluid on the electrical power of the PV module can be noticed by the percentage increment ( $P_{inc}$ ) of the electrical power [57]:

$$\%P_{inc} = \frac{P_{cooled} - P_{ref}}{P_{ref}} \times 100 \quad (30)$$

Thermocouples are placed on the PV module, PVT system surfaces and backsides for measuring the temperature; thus, Eq. (31) is used to measure the average temperature of the PV module and PVT system.

$$T_{avg} = \frac{T_{surface} + T_{back}}{2} \quad (31)$$

The thermal efficiency ( $\eta_{th}$ ) indicates the thermal performance of the PVT system. The thermal efficiency calculation of the PVT collector depends on the rate of thermal energy  $Q_u$  [67], which is calculated using the equation below.

$$Q_u = \dot{m} C_p \times (T_{out} - T_{in}) \quad (32)$$

$$\eta_{th} = \frac{Q_u}{S \times A} \quad (33)$$

where  $T_{out}$ ,  $T_{in}$  are the input and output fluids ( $^{\circ}\text{C}$ ),  $\dot{m}$  is the mass flow rate 1 L/min, and  $C_p$  is the specific heat of the fluid (kJ/kg. $^{\circ}\text{C}$ ). The overall efficiency of the PVT system is the collection of the electrical and thermal efficiencies, as presented in Eq. (34) [68]:

$$\eta_{ov} = \eta_{el} + \eta_{th} \quad (34)$$

In this dissertation, the nanofluids and DI water are circulated in the serpentine tubes placed at the backside of the PVT system. Thermophysical characteristics of the fluid affect the heat transfer properties and fluid flow velocity. Reynolds number is a parameter for predicting the fluid flow patterns, whether laminar or turbulent flow, which can be calculated from the equation below [69].

$$Re_{nf} = \frac{4\dot{m}}{\pi\mu_f D} \quad (35)$$

where  $D$  and  $\mu_f$  are the tube diameter and the viscosity of the fluid, respectively. Nusselt number represents the ratio of heat transfer by convection to the conductive heat transfer, which can be determined by Eq (36)[70,71].

$$Nu_f = \left( \frac{h D_h}{K_{nf}} \right) = \frac{\dot{m} C_p (T_{h,i} - T_{h,o})}{A (T - T_w)} \times \frac{D_h}{K_f} \quad (36)$$

where  $h$ ,  $D_h$ ,  $T$  and  $T_w$  are the heat transfer coefficient, the hydraulic diameter, the average inlet and outlet temperature and the average wall tube temperature, respectively. In addition, the friction factor is introduced as one of the causes of the pressure drop at the change of Reynold's number, which was calculated by Eq. (51) [72], while the pressure drop in the piping system is calculated by Eq. (52) [73].

$$f = [1.58 \ln Re - 3.82]^{-2} \quad (37)$$

$$\Delta P = \frac{f \rho_f L}{2D_{\text{tubes}}} \left( \frac{4 \dot{m}_{nf}}{n \rho_f \pi D^2} \right)^2 \quad (38)$$

Where  $n$  and  $L$  are the number of tubes and the riser length of tubes.

The second law of thermodynamics is used for exergy analysis to determine the realistic performance of the PVT systems and evaluate the quality of their electrical and thermal exergy. The change in temperature level destroys the exergy due to increasing the system's entropy compared to the surroundings [74].

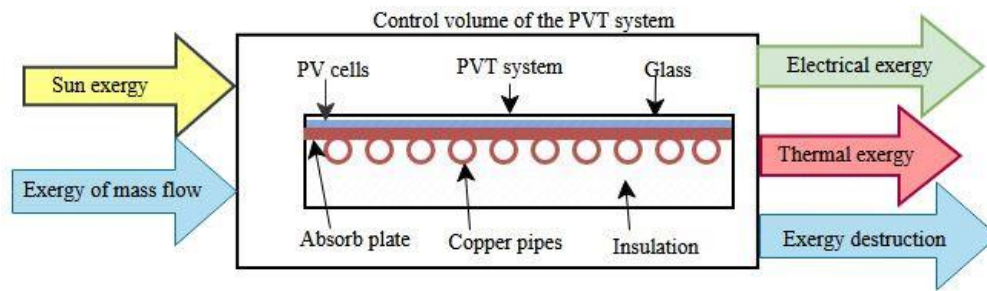


Figure 13. Schematic diagram of the Energy flow of a PVT system

Figure 13 shows the energy flow of the PVT system considering the PV module unit and the cooling system (absorbing plate and serpentine tube) as a united control volume assuming a steady state condition. The exergy balance equations for the PVT system are written as indicated in Eq. (53) [33]:

$$\sum \dot{E}x_{in} = \sum \dot{E}x_{out} + \sum \dot{E}x_{loss} \Rightarrow \dot{E}x_{solar} + \dot{E}x_{fluid, in} = \dot{E}x_{electrical} + \dot{E}x_{fluid, out} + \dot{E}x_{losses} \quad (39)$$

$\dot{E}x_{solar}$ , is the input exergy of the solar radiation to the PVT system, which can calculate by Eq. (40), [75].  $T_{amb}$  is ambient temperature and  $T_{sun}$  sun temperature which considered as (5800 K) [76].  $\dot{E}x_{electrical}$  is the electrical exergy equivalent to the electrical energy [75], which can be determined by Eq. (41).  $\dot{E}x_{fluid, in}$ , and  $\dot{E}x_{fluid, out}$  are the fluid exergy inlet and outlet,  $\dot{E}x_{loss}$  are the electrical exergy and exergy loss.

$$\dot{E}x_{solar} = S \left( 1 - \frac{T_{amb}}{T_{sun}} \right) \quad (40)$$

$$\dot{E}x_{ele} = V_{oc} \cdot I_{sc} \cdot FF \quad (41)$$

$\dot{E}x_{th}$  is thermal exergy, which is calculated by using Eq. (42),  $\dot{m}_f$  the mass flow rate and  $C_{p,f}$  is the specific heat of fluids.  $T_{out}$  and  $T_{in}$  are the inlet and outlet fluid temperatures. Then, the thermal and electrical exergy efficiencies are calculated from Eq. (43) and (44).

$$\dot{E}x_{th} = \dot{m}_f \cdot C_{p,f} \left[ (T_{out} - T_{in}) - T_{amb} \ln \left( \frac{T_{out}}{T_{in}} \right) \right] \quad (42)$$

$$\eta_{\dot{E}x_{th}} = \frac{\dot{m}_f \cdot C_{p,f} \left[ (T_{out} - T_{in}) - T_{amb} \ln \left( \frac{T_{out}}{T_{in}} \right) \right]}{S \left( 1 - \frac{T_{amb}}{T_{sun}} \right)} \times 100 \quad (43)$$

$$\eta_{\dot{E}x} = \frac{V_{oc} \cdot I_{sc} \cdot FF}{S \left( 1 - \frac{T_{amb}}{T_{sun}} \right)} \times 100 \quad (44)$$

The exergy efficiency of the PVT is the sum of thermal and electrical exergy efficiency. It can be calculated using Eq. (45) as follows:

$$\eta_{\dot{E}x} = \frac{\dot{E}x_{th} + \dot{E}x_{el}}{\dot{E}x_{solar}} \times 100 \quad (45)$$

The exergy loss (exergy destruction) is the other parameter which produces the frictional loss in the tubes and heat transfer losses [77], which can be calculated by Eq. (46) as follows:

$$\dot{E}x_{loss} = \dot{E}x_{in} - \dot{E}x_{ele} - \dot{E}x_{th} \quad (46)$$

The entropy generation is a thermodynamic parameter that determines the rate of entropy generation in the control volume PVT systems and could be calculated from the equation below.

$$\dot{S}_{gen} = \frac{\dot{E}x_{lost}}{T_{amb}} \quad (47)$$

## 2.4 Synthesized nanomaterials

### 2.4.1 Hybrid titanium oxide-iron oxide nanocomposite

TiO<sub>2</sub>-Fe<sub>2</sub>O<sub>3</sub> nanocomposite has been produced according to our previous work [78]. FeC<sub>13</sub>·6H<sub>2</sub>O precursor was dissolved in 100 mL of distilled water to create a homogenous solution. Then, 0.5 g of TiO<sub>2</sub> NWs that had already been produced were added to the solution. Drop by drop, NaOH solution was added while stirring, and when the solution had become base, it was poured into the autoclave and heated to 90 °C for 9 h. The product was dried, calcined at 500 °C for 2 h, and then rinsed with DI water to neutralize pH. The final composition of TiO<sub>2</sub>NWs- Fe<sub>2</sub>O<sub>3</sub> NPs is 50:50 wt%. To identify and describe the crystal structure of nanocomposite material, XRD was

performed. The diffraction peaks located at  $11.9^\circ$ ,  $24.2^\circ$ ,  $29.1^\circ$ ,  $43.1^\circ$  and  $60^\circ$  index to (200), (002), (310), (602) and (610) originating to  $K_2Ti_6O_{13}$  (PDF no. 40-0403). The other peaks at  $39.2^\circ$ ,  $48^\circ$ ,  $54.2^\circ$ ,  $56.5^\circ$  and  $68.8^\circ$ , corresponding to (220), (200), (105), (213) and (403), relate to the anatase phase of  $TiO_2$  (JCPDS 21-1272). The diffraction peaks located at  $27.4^\circ$ ,  $36.1^\circ$  and  $41.2^\circ$  index to (110), (101) and (111) refer to the rutile phase (JCPDS no-21-1276). The peaks relate to Hematite iron oxide ( $\alpha-Fe_2O_3$ ) (JCPDS 33-0664) located at  $62.4^\circ$ ,  $64^\circ$  and  $67.1^\circ$ , as shown in Figure 14 (a). These results are in good agreement with [79]. A scanning electron microscopy SEM technique is used for investigations of the surface morphology of hybrid nanocomposite, which is shown the superposition of  $TiO_2$  with  $Fe_2O_3$ , as shown in Figure 14 (b).

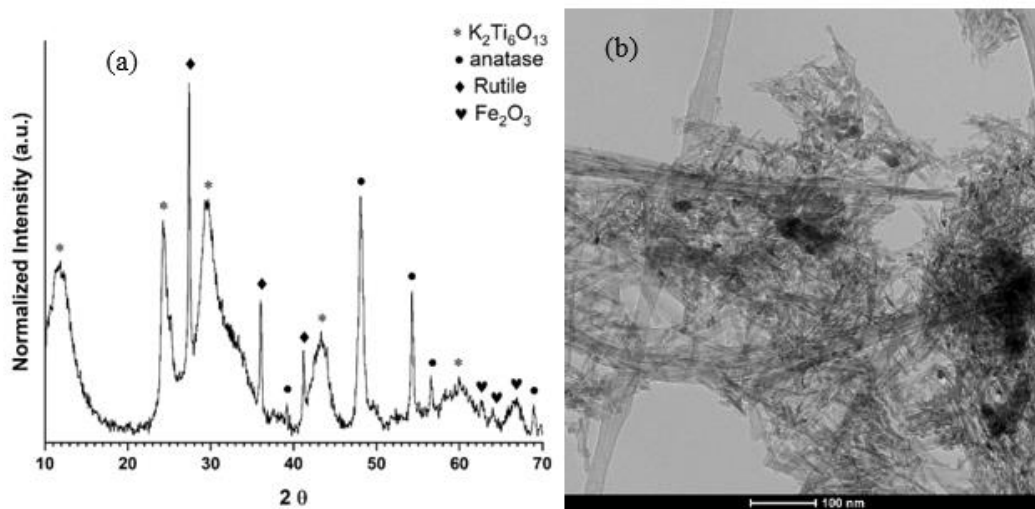


Figure 14. The XRD pattern of the synthesized  $TiO_2-Fe_2O_3$  (a) and (b) TEM image of  $TiO_2-Fe_2O_3$  nanocomposite

#### 2.4.2 Hybrid Titanium oxide-copper oxide nanocomposite

$TiO_2-CuO$  nanocomposite was prepared as the following procedure in [78], a calculated amount of  $(Cu(CH_3COO)_2 \cdot H_2O)$  was dissolved in 100 mL of ethanol and stirred vigorously for 30 min. After that, 0.5 g of  $TiO_2$  NW was added to the solution under vigorous stirring for 1 h. The solution was put in an autoclave and heated to  $150^\circ C$  in a static furnace for 12 h. The product was collected using vacuum filtration, washed, and then calcined at  $500^\circ C$  for 2 h. The final composition of  $TiO_2$  NWs-CuO NPs is 50:50 wt%. XRD has been performed to describe and identify the crystal structure of nanocomposite material. The diffraction peaks located at  $11.9^\circ$ ,  $24.2^\circ$ ,  $29.1^\circ$ ,  $43.1^\circ$  and  $60^\circ$  corresponding to (200), (002), (310), (602) and (610) refer to  $K_2Ti_6O_{13}$  (PDF no. 40-0403). The diffraction peaks located at  $25.2^\circ$ ,  $48^\circ$ ,  $54.2^\circ$  and  $56.6^\circ$  index to (101), (200), (105) and (213) originating to anatase phase (JCPDS 21-1272). The other peaks located at  $27.4^\circ$ ,  $36^\circ$  and  $41.2^\circ$  corresponding to (110), (101) and (111) relate to the rutile phase (JCPDS no-21-1276). Furthermore, the peaks at  $38^\circ$ ,  $62.7^\circ$ ,  $66.2^\circ$  and  $68.1^\circ$  corresponding to (111), (-113), (-311) and (220) refer to copper oxide (JCPDS card number 45-0937), as shown in Figure 15 (a). All these results agree with [78,79]. A scanning electron microscopy SEM technique is used for investigations of the surface morphology of hybrid nanocomposite, which is shown the superposition of  $TiO_2$  with  $CuO$ , as shown in Figure 15 (b).

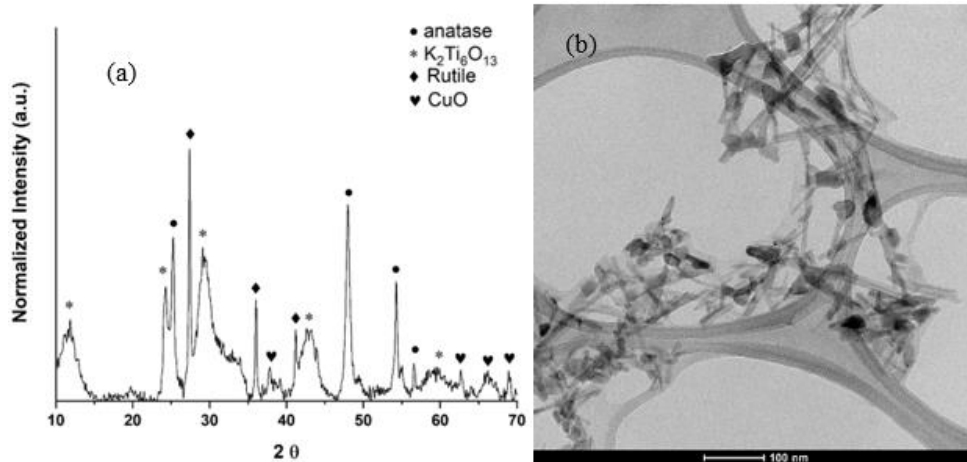


Figure 15. The XRD pattern of the synthesized  $TiO_2$ -CuO (a) and (b) TEM image of  $TiO_2$ -CuO nanocomposite

## 2.5 Preparation of nanofluids

Stability is an important advantage that nanofluids must have; achieving that is not easy. It undergoes several matters, such as nanoparticle types, purity, size, nanomaterials shapes and base fluid type. The purpose of preparing nanofluids is to improve the thermal properties of the fluids, particularly the thermal conductivity of fluids. Preparing stable nanofluid enhances heat transfer applications depending on the thermophysical characteristics of nanoparticles. The Two-type method is employed to prepare nanofluids, a one-step method consisting of either liquid chemical or physical vapour deposition method to prepare nanofluids. The two-step method is commonly used for dispersing nanomaterials into base liquids [80]. Dispersion of nanoparticles in the base fluid enhances the thermophysical properties of the new working fluid and then improves the heat transfer rate. The good dispersion of nanomaterials into the base fluid at low sedimentation and the high stability of nanofluids depends on the preparation method of nanofluids [81].

In this dissertation, various types of nanofluids have been prepared, such as  $WO_3$ /DI water,  $ZrO_2$ /DI water,  $TiO_2$ /DI water,  $Fe_2O_3$ /DI water, CuO/DI water nanofluids, and two types of hybrids nanofluids such as  $TiO_2$ -CuO/DI water,  $TiO_2$ - $Fe_2O_3$ /DI water. The two-type method is employed to prepare nanofluids at different volume concentrations dispersed in DI water were calculated from Eq. (10). The quantity of nanomaterials was scaled by an electronic scale (type: BOECO BAS of 0.0001g), then dispersed into DI water and mixed with a magnetic stirrer for a different period among 25-30 min depending on the type of nanomaterial employed. Ultrasonication probe (Bransonic type 220, Voltage: 240V, Vf: 48kHz) was used from 35-40min depending on the type of nanomaterial employed to avoid the agglomeration of nanoparticles in the nanofluid and to obtain a stable suspension for a long period, as shown in Figure 16. The time sediment and visualization methods were used to examine the nanofluid's stability for different periods from 3-5 h after sonication and from 2 to 4 days after sonication, as shown in Figure. 17 (a-j). The prepared nanofluid showed good stability. Thus, it was prepared in suitable quantities later and directly used in the experiment after the sonication.

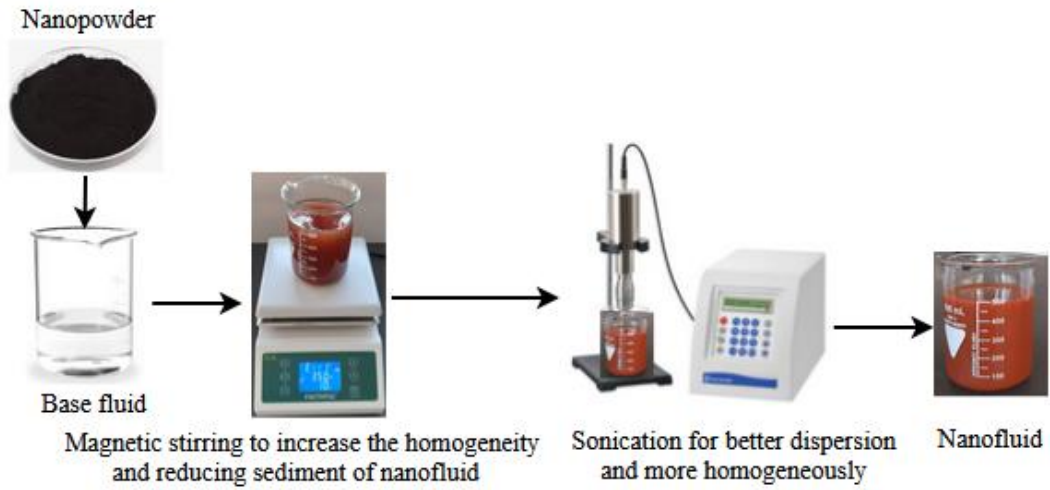
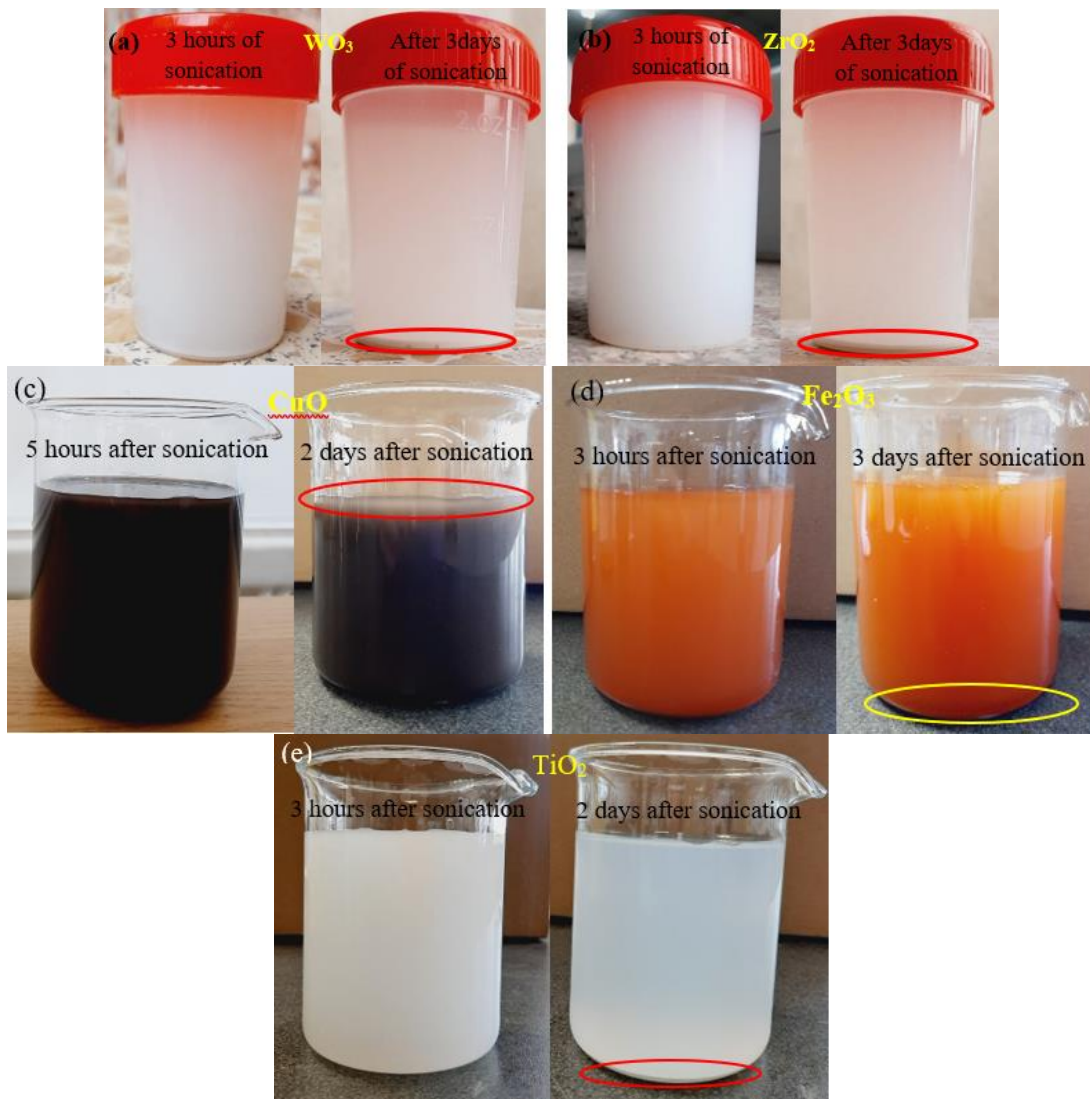


Figure 16. Preparation of nanofluid by using two steps method



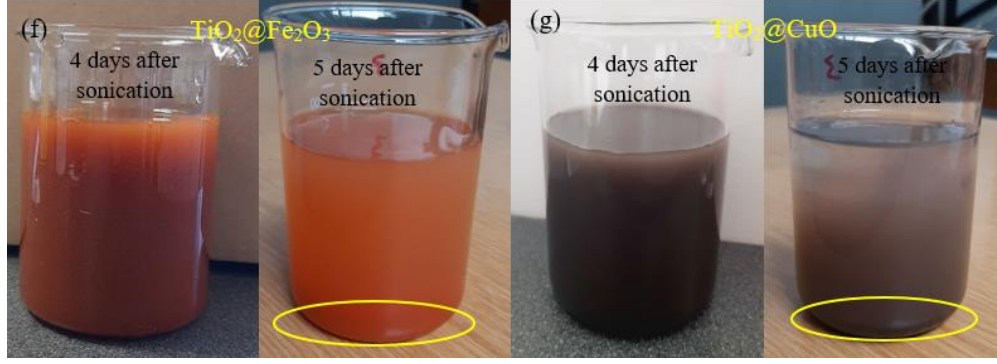


Figure 17. Stability of preparation of nanofluids (a)  $\text{WO}_3/\text{DI}$  water, (b)  $\text{ZrO}_2/\text{DI}$  water, (c)  $\text{CuO}/\text{DI}$  water, (d)  $\text{Fe}_2\text{O}_3/\text{DI}$  water, (e)  $\text{TiO}_2/\text{DI}$  water, (f)  $\text{TiO}_2\text{-Fe}_2\text{O}_3/\text{DI}$  water, (g)  $\text{TiO}_2\text{-CuO}/\text{DI}$  water

## 2.6 Thermophysical properties of nanofluids

### 2.6.1 Density and viscosity of nanofluid

Density is an essential property of the nanofluid that significantly affects the thermal system's sustainability and achieves a suitable extent of nanofluid stability [82]. Some parameters significantly affect the nanofluid's thermophysical, such as temperature, base fluid, volume fraction, the nanoparticles concentration, etc. The density of nanofluid is increased with increased volume concentration and reduced with rising temperature. Thus, an increase in density affects the pumping capacity by increasing power consumption, specifically in thermal applications [83]. On the other hand, increasing the density of nanofluids has a negative impact on the Reynolds number by boosting the friction factor [84]; increased temperatures lead to a low density of nanofluids [85]. The base fluid plays an essential role in nanofluids' density; a limited effect was found for nanoparticles' shape and size on nanofluid density [86]. Eq (48) is commonly used to determine nanofluids' density ( $\rho_{nf}$ ) which depends on the volume concentration ( $\phi$ ) of nanoparticles, the base fluid density ( $\rho_{bf}$ ), and the density of nanoparticles ( $\rho_{np}$ ).

$$\rho_{nf} = \phi \cdot \rho_{np} + (1 - \phi) \cdot \rho_{bf} \quad (48)$$

$$\phi = \left[ \frac{\frac{m_{np}}{\rho_{np}}}{\frac{m_{np}}{\rho_{np}} + \frac{m_{bf}}{\rho_{bf}}} \right] \times 100 \quad (49)$$

where,  $m_{np}$  the mass of the nanomaterials  $m_{bf}$  the mass of the base fluid.

Viscosity represents the essential factor that significantly affects the nanofluids' behaviour [87]. Increasing the nanoparticle concentration causes an increase in nanofluids viscosity, which leads to an increase in pumping power due to pressure drop [88]. The volume concentrations and temperature control the viscosity; the base fluid is the most important factor determining the nanofluid viscosity [89]. Thus, high thermal conductivity with low viscosity must be available by the ideal nanofluids. In contrast, nanofluid's viscosity is low with increasing temperature [90]. Increasing temperature contributes to increasing thermal conductivity, which leads to lower viscosity and reduces agglomeration of the nanoparticles [68]. Equation (50) is used to determine the nanofluid's viscosity, where  $\mu_{bf}$  is the viscosity of base fluid.

$$\mu_{nf} = \frac{\mu_{bf}}{(1-\phi)^{2.5}} \quad (50)$$

## 2.6.2 Thermal conductivity and specific heat of nanofluid

One of the most important nanofluid properties in the heat transfer field is thermal conductivity. Increasing the thermal conductivity of nanofluids is required to enhance the heat transfer of nanofluids. Conventional fluids are poor in heat transfer; the addition of solid nanomaterials materials into the base fluid enhances the high thermal conductivity of nanofluids [91]. On the other hand, increment temperature and concentration of nanoparticles in base fluid cause an increase in the thermal conductivity of nanofluid due to rising kinetic energy that strengthens the collision between particles [92]. Increased thermal conductivity is mainly associated with nanoparticles' type of material by their concentration and size. The shapes of nanoparticles have a role in increasing thermal conductivity [93]. It observes that nanoparticles' instability in base fluid causes agglomerates in the nanofluid, and it's one reason for decreasing thermal conductivity [94]. Equation (51) is used to determine the thermal conductivity of nanofluid, where  $k_{np}$ ,  $k_{bf}$ ,  $k_{nf}$  are thermal conductivity of nanomaterials, base fluid and nanofluid

$$\frac{k_{nf}}{k_{bf}} = \frac{k_{np} + 2k_{bf} + 2\phi(k_{np} - k_{bf})}{k_{np} + 2k_{bf} - \phi(k_{np} - k_{bf})} \quad (51)$$

The specific heat represents an important property of any thermal fluid; this property plays a vital role in providing the energy that transmits from one body to another [68]. In nanofluids, specific heat is different depending on the nanomaterials used, their concentration in the base fluid, and the type of base fluids [95]. Nanofluids' specific heat increases with increasing temperature while lowering at increased volume concentration [96]. Adding a small volume concentration of nanoparticles in the base fluids enhances the specific heat regardless of the particle shape or type [97]. The nanofluid's specific heat is determined using Eq. (52), where  $C_{p,nf}$ ,  $C_{p,bf}$ ,  $C_{p,np}$  are the specific heat of the nanofluid, base fluid and nanomaterials, respectively. Table 2 below shows the thermophysical properties of new hybrid nanocomposite used in this dissertation in all experiments.

$$C_{p,nf} = \frac{\phi \cdot (\rho_{np} \cdot C_{p,n}) + (1-\phi) \cdot (\rho_{bf} C_{p,bf})}{\rho_{nf}} \quad (52)$$

Table 2. Thermophysical properties of the hybrid nanocomposite

Properties	TiO <sub>2</sub> -Fe <sub>2</sub> O <sub>3</sub>	TiO <sub>2</sub> -CuO
Density (kg/m <sup>3</sup> )	3473	2791
Thermal conductivity (W/m·K)	75.32	79.9
Heat capacity (J/kg·K)	1334	1198

This chapter presented a deep analysis of the mechanism of heat transfer by conduction, convection and radiation between the components, considering the energy balance equations for each layer of the PVT system. The inputs and outputs parameters that affect the efficiency of the PV system has studied, and identified weak points that could improve by effectiveness methods by considering the experimental results. The maximum deviation has been noticed at 3.11% by applying the experimental results to the thermal analysis and energy balance equations. According to thermodynamics laws (first and second), energy and exergy analysis has been considered to demonstrate the quantity and quality of the energy produced, adding to identifying the value of exergy destruction. The chapter also presented a synthesis of new hybrid

nanocomposites used to prepare new hybrid nanofluids used as cooling fluids of the PVT system and their effect on improving the energy and exergy efficiency of the PVT system. Another mono nanomaterial has also been synthesized by different morphologies (in Appendix A) to use as cooling fluids to compare them with the hybrid nanofluid regarding their effect on the PVT system efficiency.

## Chapter 3

### Factors affecting the PV module performance

Investigation of the factors that affect the PV module performance is an important issue to avoid any problems facing its work. Climate conditions, such as solar radiation, temperature, wind speed, etc., are the main factors affecting the PV module's performance. Fluctuating incident solar radiation and increased temperature of the PV cells are common problems in most PV module applications. In this chapter, two case studies have been investigated:

The first case study is a numerical simulation by Ansys software to predict the thermal behaviour of the PV module at different operations conditions in hot and cold weather by adopting different values of solar radiation, temperatures, and wind speed. This case helps predict the PV cells' thermal behaviour at exposure to different solar radiation values and temperatures in different seasons. This case study help identify the problems faced by PV cells work and then determine the effective technique that improves PV performance.

The second case is an investigation of the electrical behaviour of the PV module depending on the mathematical equations governing PV module performance. The equations have been simulated using the MATLAB-Simulink program as a subsystem and then as one system that undergoes inputs that we can control. The simulation considers variable and constant values of solar radiation and temperature as input to observe output voltage and current and power of the PV module as outputs. This case contributes by giving a general vision of the factors which has the main effect on the PV module performance and helps select the appropriate methods to overcome.

#### 3.1 Simulation study of the photovoltaic module under different operation conditions

This case study studied the effects of temperature distribution on the PV module at various solar radiation values and temperatures under different operation conditions in January and July. A 3D module of the PV panel was simulated with ANSYS software, depending on the various values of temperatures and solar radiation values obtained using mathematic equations. The simulation depended on the layer's properties of the PV panel, solar radiation values, temperature, and convective heat transfer coefficient of the module to evaluate temperature distribution and identify the appropriate extent of operating conditions of the PV module.

##### 3.1.1 Operation conditions and governing equations

The PV module used type CL-SM50P Polycrystalline, consisting of glass covering, PV cells with two layers of Ethylene Vinyl Acetate (EVA), aluminium frame, and Tedlar (PVF) layer, as shown in Figure 18 below. Table 3 below shows the material properties of the PV components inserted in the ANSYS software engineering data. The PV panel datasheet has adopted a reference for comparing the simulation results and the PV panel values under stander test conditions STC (25 °C and 1000W/m<sup>2</sup>). According to the manufacturer datasheet, the PV module geometry is built by SolidWorks software with module dimensions. The materials are defined by the Ansys library data of all the PV panel layers. Then the PV module was imported to the Ansys software to analyse the PV module temperature distribution inserted in the software as variable values depending on the different values of beam solar radiation obtained using the mathematical equations below. Thus, according to STC, three solar radiation values have been used, two of them according to January and July with an estimation of clear-sky radiation and the third solar radiation value under STC.

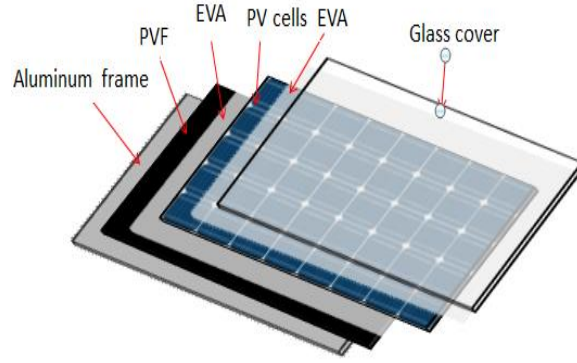


Figure 18. The layers of the PV module.

Table 3. The layer's properties of the PV panel [98]

Material (Layer)	$\rho$ (kg/m <sup>3</sup> )	$K$ (W/m.k)	$C_p$ (J/kg.k)
Glass	3000	1.8	500
EVA	960	0.35	2090
PV	2330	148	677
PVF	1200	0.2	1250
Aluminum Frame	2707	204	996

The heat flux changes with time, which causes a change in the temperature that influences the PV module performance. The temperature was fixed at 4 °C on January, 35 °C in July, and 25 °C in STC. The convective heat transfer coefficient is 14.8 W/m<sup>2</sup>. °C on the panel calculated by using equation (53) [99],  $V_m$  is the wind speed value that adopted 2.4 m/s according to Miskolc city [100]. The mesh element size of the PV module mesh was 0.002 m, and the number of meshes elements was 278964 with high smoothing; the time simulated was 43.1 min in all initial conditions.

$$h = 5.7 + 3.8V_m \quad (53)$$

The mathematical equations were used to predict and estimate direct radiations transmittance (beam radiation) for Miskolc city when a clear atmosphere on 7 January at solar time 11:30 AM and 13 July at solar time 12:30 PM. To achieve that, it needs to find some parameters that help achieve that such angular position of the sun (solar declination ( $\delta$ )) represents the angle between the line from the sun's centre to the earth's centre equator. The solar declination value is changeable because of the rotating of the earth around the sun and the tilt of the earth on its axis of rotation found by using Cooper's equation [99], where  $n$  is the day of the year of that selected ( $n = 7$  for January and  $n = 194$  for July).

$$\delta = 23.45 \sin \left( 360 \frac{284+n}{365} \right) \quad (54)$$

The zenith angle is the incidence beam solar radiation angle between the vertical and the line to the sun used with horizontal surfaces and determined by the following equation.

$$\cos \theta_z = \cos \phi \cos \delta \cos \omega + \sin \phi \sin \delta \quad (55)$$

Latitude between  $-90^\circ \leq \varphi \leq 90^\circ$  for Miskolc, Hungary, is  $48.1^\circ$ , which is an hour angle which is negative in the morning and afternoon positive. Solar time depends on the sun's angular motion in the sky, which may not synchronize with local time [59]. The extraterrestrial radiation incident is the quantity of solar energy received per unit of time at the mean distance between the sun to the earth. On the normal plane, it can calculate by Eq. (56) and is the solar constant.

$$G_o = G_{sc} \left( 1 + 0.033 \cos \frac{360n}{365} \right) \quad (56)$$

Calculating the daily and hourly solar radiation received on a horizontal surface is useful under standard conditions. To calculate the beam radiation transmitted from the sun without scattering by clear atmospheres, consider the zenith angle and altitude of the atmosphere for four climate types from equation (57) [101].

$$\tau_b = a_0 + a_1 \exp \left( \frac{-k}{\cos \theta_z} \right) \quad (57)$$

$$a_0^* = 0.4237 - 0.00821(6 - A)^2 \quad (58)$$

$$a_1^* = 0.5055 + 0.00595(6.5 - A)^2 \quad (59)$$

$$k^* = 0.2711 + 0.01858(2.5 - A)^2 \quad (60)$$

$a_0$ ,  $a_1$  are constant, and  $k$  represents the standard atmosphere at 23 Km visibility that can be found by using the equation (58), (59), (60), and  $A$  represents the altitude of the observer in kilometres. Hence, multiply the constant values by correction factors in Table 4,  $a_0^* \times r_o$ ,  $a_1 \times a_1^*$  and  $k \times r_k$  could calculate the beam radiation transmitted. Thus, it can determine the beam radiation for any zenith angle or altitude, even 2.5 km. The normal beam radiation in a clear sky which can be found by multiplying the value of the beam radiation transmitted during clear atmospheres  $\tau_b$  by the value of extraterrestrial radiation incident  $G_{on}$ . The value results multiply by the zenith angle to obtain solar radiation's value on the horizontal of the panel  $G_{cb}$  [102].

Table 4. Correction factors for climate types [99].

Climate Type	$r_o$	$r_1$	$r_k$
Tropical	0.95	0.85	1.02
Mid-latitude winter	1.03	1.01	1
Subarctic summer	0.99	0.99	1.01
Mid-latitude summer	0.97	0.99	1.02

### 3.1.2. Results and discussion

The PV panel has been simulated under different solar radiation values estimated by mathematical equations and various temperatures. For January, solar radiation values were  $176 \text{ W/m}^2$ , for July  $735 \text{ W/m}^2$  and under STC was  $1000 \text{ W/m}^2$ . January's temperature was  $4^\circ \text{C}$ , July's highest temperature was  $35^\circ \text{C}$ , and the PV panel temperature was under STC at  $25^\circ \text{C}$ . The results indicate that temperature distribution on the PV panels surface was high at the top of the PV panel while the aluminium frame's temperature was lower. The dark blue colour refers to the minimum temperature on the panel, the bright red colour refers to the maximum temperature on the panel, and other colours represent temperature variations. In January, when the temperature is low, the beam solar radiation is  $176 \text{ W/m}^2$ . The temperature distribution on the PV module is between a maximum of  $15.4^\circ \text{C}$  and a minimum of  $11.9^\circ \text{C}$ , as shown in Figure 19.

Thus, this solar radiation range influences PV panel performance represented by power output without leaving any damage or overheating because of the lower PV module temperature. At applied the July solar radiation  $735 \text{ W/m}^2$  when the temperature reaches  $35 \text{ }^\circ\text{C}$ , the simulation shows that the PV module is exposed to a maximum temperature of  $84.6 \text{ }^\circ\text{C}$ , while the minimum temperature was  $68.4 \text{ }^\circ\text{C}$ , as shown in Figure 20 below. Increasing the PV panel temperature by  $10 \text{ }^\circ\text{C}$  above the STC value causes a decrease in its efficiency. This extent of temperature causes other problems for the PV panel, such as overheating, which leads to the burning of some cells or reduced voltage, power, and the PV module output current; thus, the PV module becomes inoperative [103].

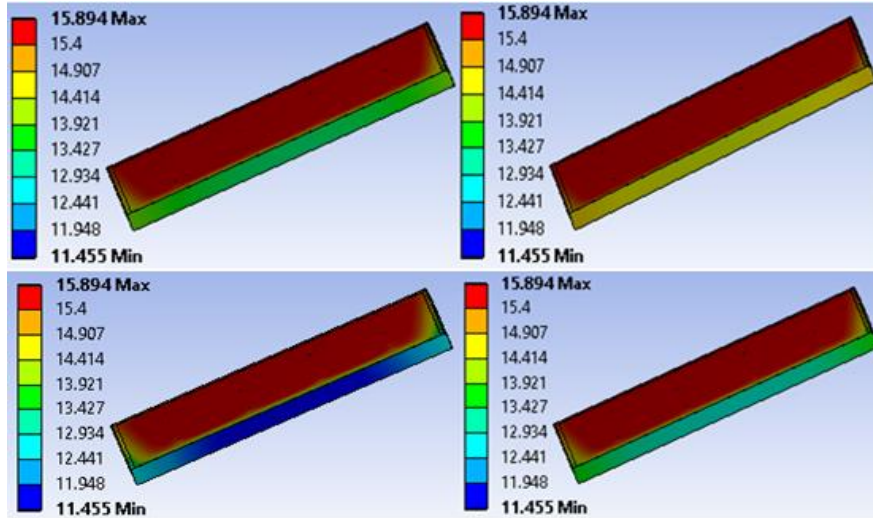


Figure 19. At solar radiation  $176 \text{ W/m}^2$  and temperature  $4 \text{ }^\circ\text{C}$

Under STC conditions of the PV module  $1000 \text{ W/m}^2$  and  $25 \text{ }^\circ\text{C}$ , the PV module temperature was observed until  $92.5 \text{ }^\circ\text{C}$ , while the lowest temperature was  $67.7 \text{ }^\circ\text{C}$ , as shown in Figure 21 below. Therefore, this temperature range is unsuitable for PV module operation due to the rising of the PV cell's temperature and causes the same problems of July values as overheating PV cells or reduced conversion efficiency and production of the PV module.

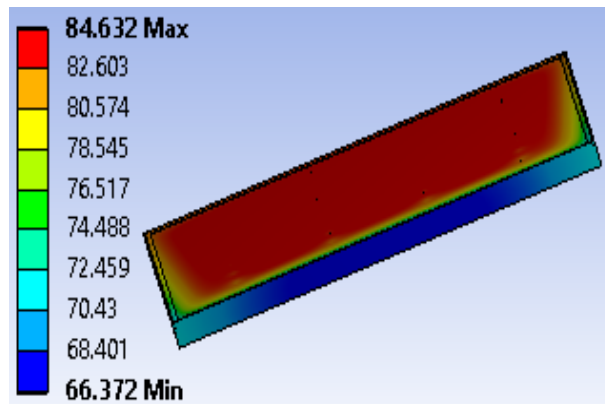


Figure 20. At solar radiation  $734 \text{ W/m}^2$  and temperature  $35 \text{ }^\circ\text{C}$

The temperature increase of the PV module is directly proportional to increasing solar radiation. Due to the PV layer's different properties, these layers' temperature is different, as shown in the Figures above; the PV module temperatures surface is different from the aluminium frame. The

maximum and average temperatures on the PV panel converged somewhat at increasing the solar radiation, as shown in Table 5, for July and STC values. Cooling the PV module to remove the excessive heat is important to continue its work under high temperatures, even with STC values.

Table 5. Temperatures on the PV panel at different solar radiation.

Solar radiation W/m <sup>2</sup>	Max temperature °C	Min temperature °C	Average temperature °C
176	15.8	11.4	15.2
735	84.6	66.3	82.1
1000	92.5	67.7	89.1

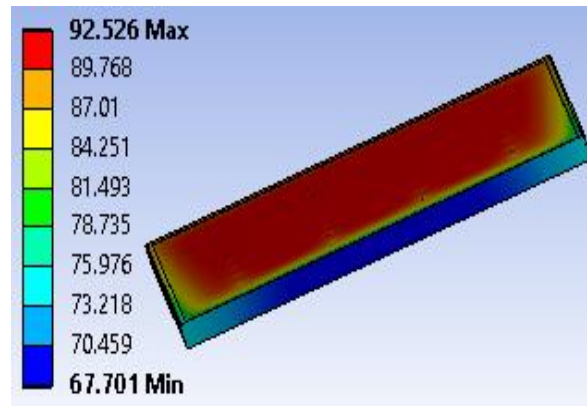


Figure 21. At solar radiation 1000 W/m<sup>2</sup> and temperature 25 °C

### 3.2. Test the mathematical of the photovoltaic module under different conditions by using MATLAB-Simulink

In this case study, we discuss temperature and solar radiation's effects on the voltage and current of the PV module. MATLAB-Simulink has been used to model the mathematical equations of the PV module to predict the behaviour of the output current and voltage of the PV module. Simulation depends on the constant temperature of the PV module with different solar radiation values and vice versa. Thus, the simulation results are compared with the PV module datasheet under standard test condition STC. The proposed module-derived is a single of the V-I characteristics that will extend for all the string/array of the PV cell depending on the five parameters module and based on the manufacturer datasheet.

#### 3.2.1. Mathematical modelling of PV module

A specified number of solar cells connected in series and parallel represent the unit build of the solar PV module. The study used MATLAB-Simulink to mathematical module equations of the PV module depending on the variable values of temperatures and solar radiation. The datasheet of the PV module is a reference for comparison with the simulation values with accurate parameters widely used for the analytical characterization of the PV module. The equivalent electric circuit of the PV module consists of a shunt resistor parallel  $R_{sh}$  with a higher value than a series resistor  $R_s$  with a single diode. Both the electrical characteristics of the PV module and climatic conditions determined the power output of the PV module. MATLAB-Simulink will module the mathematical equation as subsystems for each equation of the PV module, as shown in Figures (22 and 23), depending on the parameters of the equations. Thus, all the PV module

mathematical equations will simulate a PV module to study the PV module's behaviour of I-V and P-V, where Eq. (61) represents the I-V characteristic of the PV module.

$$I = I_{ph} - I_0 \left[ \exp\left(\frac{q \cdot (V + I \cdot R_s)}{nd \cdot N_{cs} \cdot B_c \cdot T_o}\right) - 1 \right] - I_{sh} \quad (61)$$

where  $I_{ph}$  is the PV current, which depends on the irradiation level,  $I_0$  is the saturation current obtained from equation (62).  $q$  represents the electron charge ( $1.60217646 \times 10^{-19}$  C),  $I$ ,  $V$ , representing both the output current and the PV module voltage.  $I_s$  is a series resistance (0.02  $\Omega$ ) of the equivalent electric circuit. While  $nd$  is (1.2) representing the diode's ideality factor (a number between 1 and 2 that typically increases as the current decreases),  $N_{sc}$  is the number of PV cells connected in parallel.  $B_c$  is Boltzmann's constant ( $1.3806503 \times 10^{-23}$  J/K). Thus, both  $T_o$  and  $I_{sh}$  represents an operating temperature of 24 K and the current resistor through the shunt.

$$I_{sh} = \frac{V + I \cdot R_s}{R_{sh}} \quad (62)$$

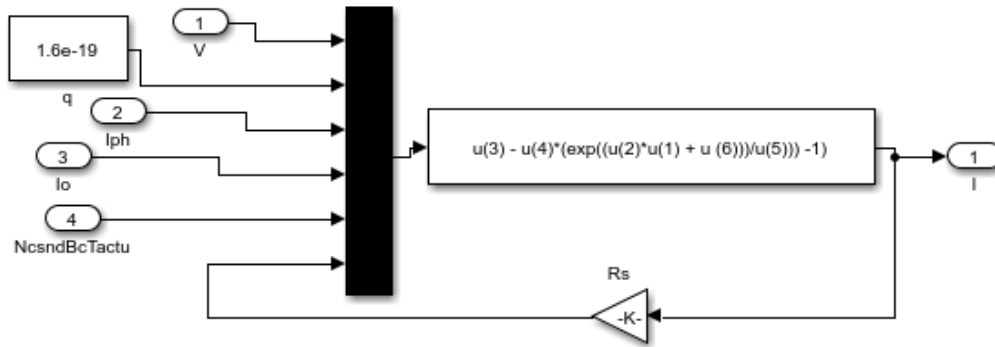


Figure 22. Modelling the output current of the PV module

Solar radiation and temperatures are the main parameters that define the value of the PV module current.  $R_{sh}$  is shunt resistance (485.5  $\Omega$ ).  $I_{ph}$  could determine by the equation below, and  $V$  represents the voltage across the diode.

$$I_{ph} = [I_{sc} + I_s(T_o - T_s)] \frac{S}{1000} \quad (63)$$

Where  $I_s$  represents the short-circuit current of the cell at STC,  $I_{sh}$  is the short circuit current (A).  $T_s$  represents a solar cell's absolute reference temperature at STC.  $S$  is solar irradiation. The difference between the cell saturation current  $I_0$  and cell temperature described in Eq. (64).

$$I_0 = I_{RS} \cdot \left(\frac{T_o}{T_N}\right)^3 \cdot \exp\left[\frac{qB_g}{nd \cdot B_g} \left(\frac{1}{T_N} - \frac{1}{T_o}\right)\right] \quad (64)$$

The reverse saturation current, as seen in Eq. (65), and  $B_g$  is the band-gap energy of the semiconductor with a value of (1.1 eV).  $T_N$  is the average temperature of 25  $^{\circ}\text{C}$ , and  $V_{oc}$  is open-circuit voltage (V).

$$I_{RS} = \frac{I_{sc}}{\exp\left(\frac{q \cdot V_{oc}}{nd \cdot B_c \cdot N_{cs} \cdot T_o}\right) - 1} \quad (65)$$

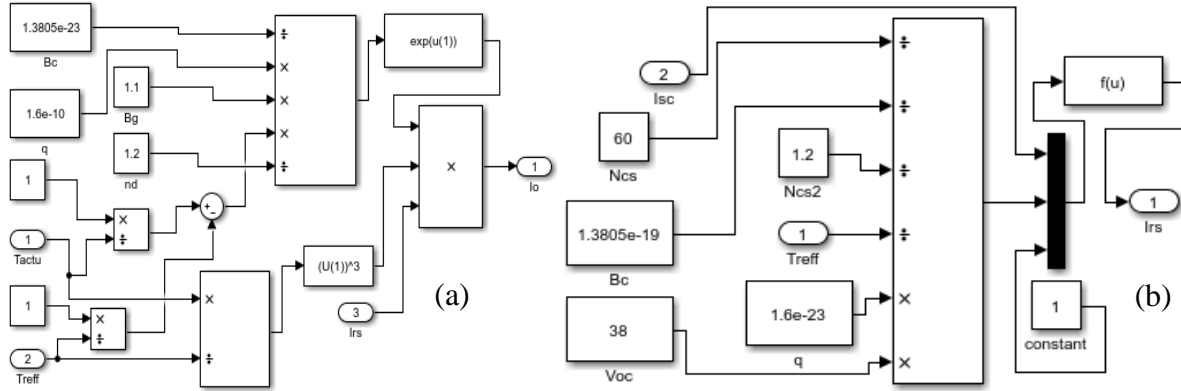


Figure 23. Modelling PV equations (a) Saturation current and (b) reverse saturation current

### 3.2.2 Simulation of the mathematic module

The simulation has conducted using MATLAB-Simulink for mathematic equations of the PV module with electrical characteristics that simulated as a subsystem, as shown in Figure 24, using variable and constant parameters. The MATLAB-Simulink illustrates the PV module building by investigating the  $V-I$  and  $P-V$  output characteristics. In general, the experiment has conducted under STC, as the first step after that used various values of solar irradiation and temperature.

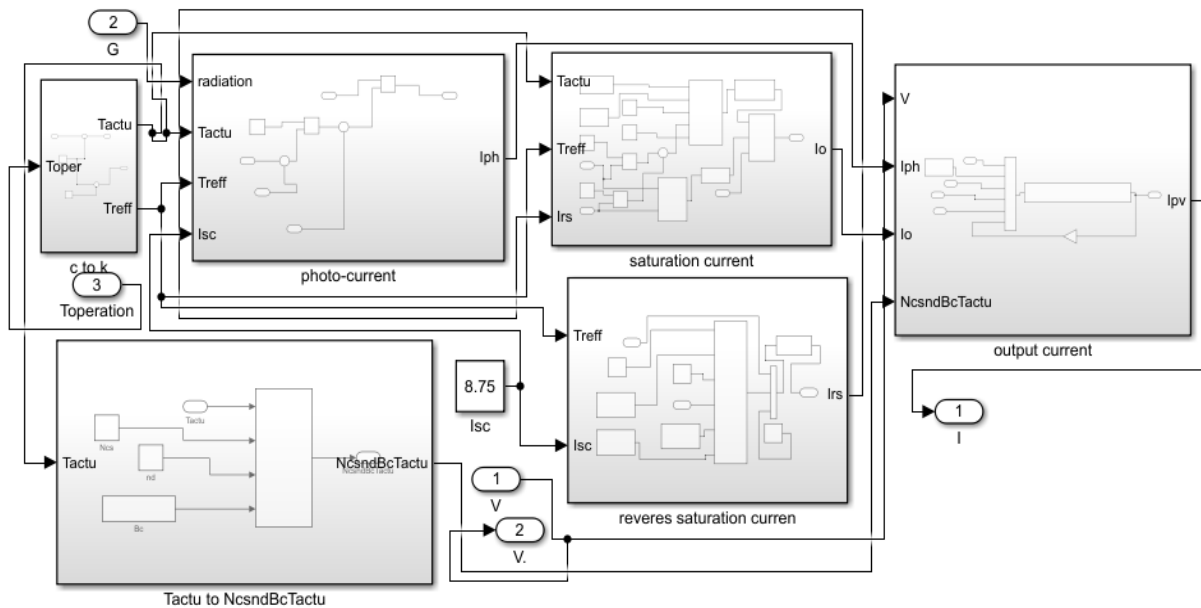


Figure 24. A subsystem of the PV module

Different values could change several times in the PV module as input variable parameters, as shown in Figure 25. Therefore, depending on the PV module equations, many subsystems have been created by using MATLAB-Simulink for each equation of the PV module (Saturation current, Reverses saturation current, Shunt current, Photo-current, and PV current) represented as a subsystem of the PV module. Thus, all the subsystems are simulated together after the PV module is linked.

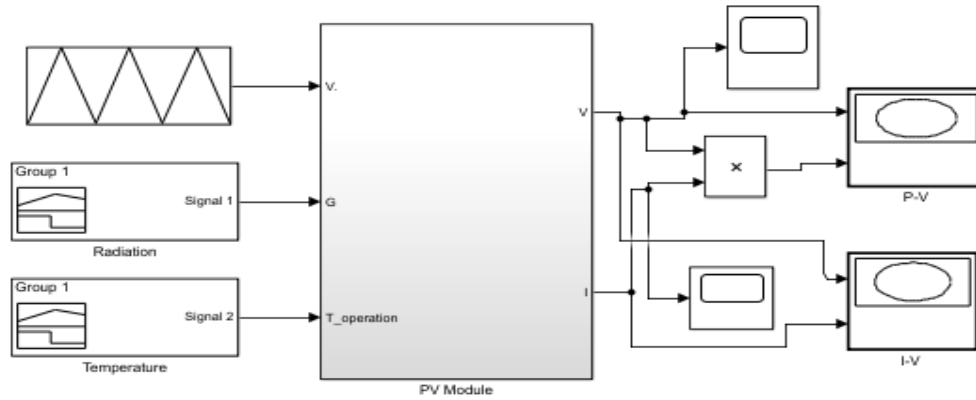


Figure 25. Simulink model of the PV module

### 3.3.3 Results and discussions

The results of simulations of the PV module depended on the variable values of solar radiation and temperatures in Miskolc climate conditions. The datasheet of the PV module under (STC) to recognize the behaviour of the PV module of the  $I$ - $V$  and  $P$ - $V$  values. The PV module current has been slightly affected by power output due to rising temperatures, even with the drop in solar radiation, as shown in Figure 26. This study considers two cases when solar irradiation values are constant with various temperatures and vice versa. The first case is when solar radiation values are lower than  $1000 \text{ W/m}^2$ , and the temperature is constant at  $25 \text{ }^\circ\text{C}$ .

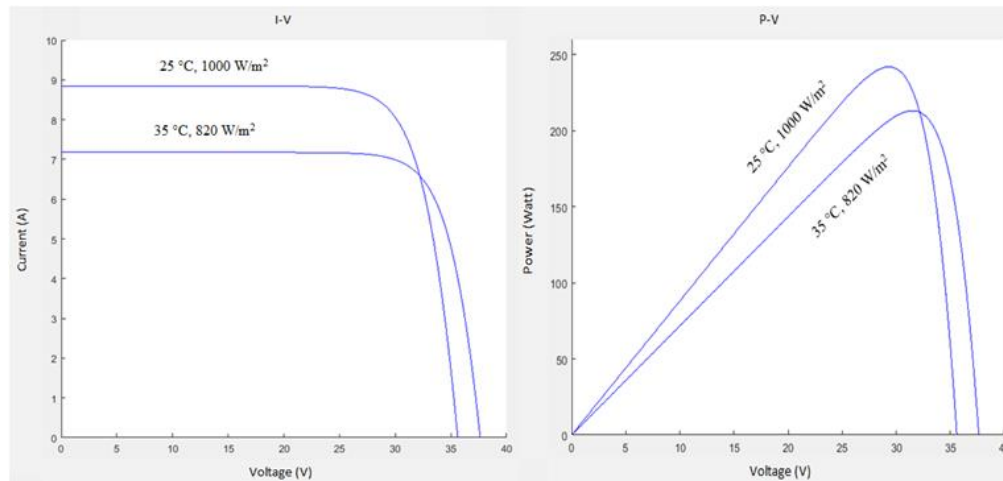


Figure 26. Characteristics of PV module under STC and  $35 \text{ }^\circ\text{C}$ ,  $820 \text{ W/m}^2$

The output current of the PV module dropped from  $8.75$  to  $\sim 7.2 \text{ A}$ , with little change with the PV module's output power of  $250 \text{ W}$  to  $\sim 220 \text{ W}$  compared with stander case STC at  $25 \text{ }^\circ\text{C}$ ,  $820 \text{ W/m}^2$ . Whereas notice the reduction in output current and power of the PV module from  $8.75 \text{ A}$  to  $\sim 4.8 \text{ A}$ , the output power value decreased from  $250 \text{ W}$  to  $\sim 140 \text{ W}$  when the temperature and solar radiation were  $25 \text{ }^\circ\text{C}$ ,  $535 \text{ W/m}^2$ . The continuous reduction in the solar irradiation value at  $25 \text{ }^\circ\text{C}$ ,  $185 \text{ W/m}^2$ , causes a significant drop in the output current of the PV panel from  $8.75 \text{ A}$  to  $\sim 1.7 \text{ A}$ . In contrast, the output voltage of the PV module dropped from  $250 \text{ W}$  to  $\sim 45 \text{ W}$  compared with the datasheet of the PV module under STC, as shown in Figure 27.

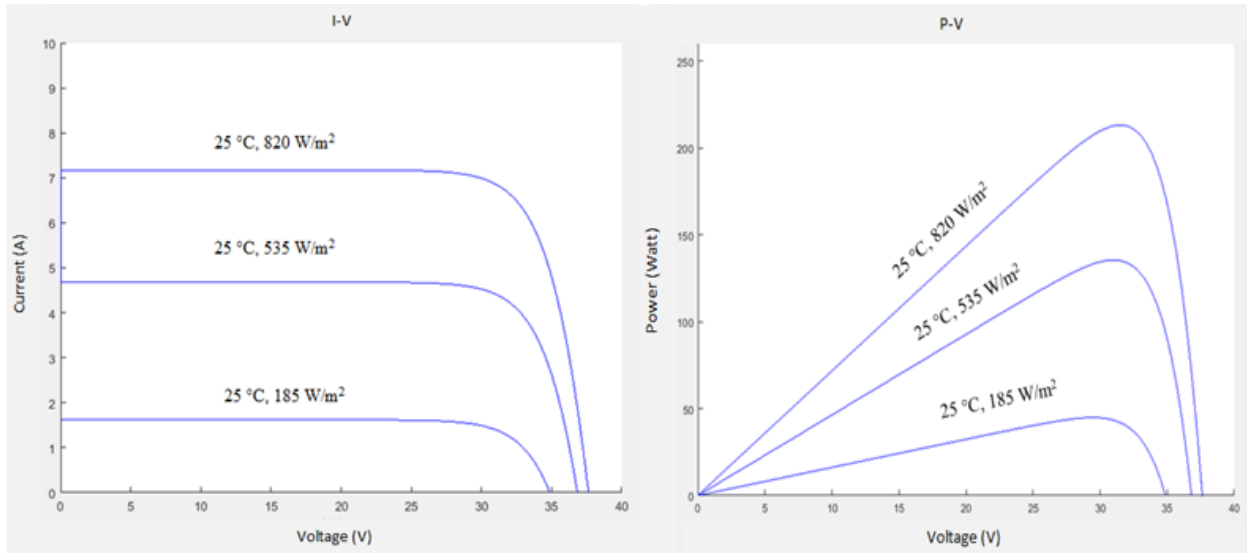


Figure 27. Characteristics of the PV module at 25 °C with various radiations

The second case is when the value of solar irradiation is constant at  $1000\text{W/m}^2$  with various temperature values at 35 °C, 24 °C, and 18 °C. The high temperatures cause to rise of PV cells, thus effected on the performance of the module. It's noticed at 35 °C,  $1000\text{W/m}^2$ , a slight drop by the PV module's output current (8.75 - 7.75) A, and the output power also decreased up to ~ 210 W compared with the datasheet of the PV module under STC. Increasing the output current and power of the PV module at 24 °C,  $1000\text{ W/m}^2$ , as shown in Figure 28.

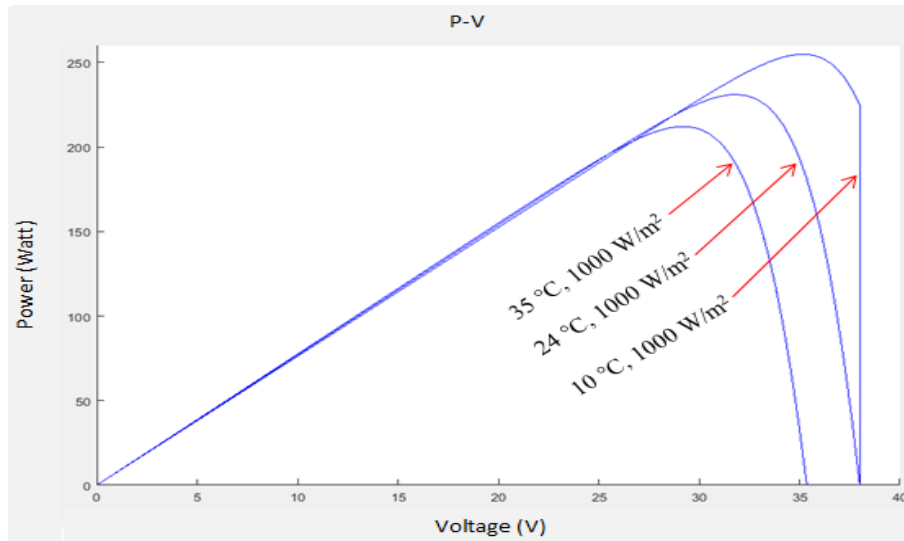


Figure 28. P-V characteristics PV module at various temperatures and constant radiation

Due to the closer temperature and radiation values of the stander datasheet of operation PV module parameters. The output current and power of the PV module continuously increase with a temperature reduction at 10 °C even with  $1000\text{W/m}^2$  of solar radiation, compared with the values when the temperature was high, as shown in Figure 28 above.

### 3.3 Conclusions

#### Contribution 1

- The first case study is characterized by using predicted equations that can be adopted to test the PV module's thermal behaviour under different conditions and give a general impression of temperature distribution on the PV module. Also, simulation was conducted according to the material properties of the PV module layers, such as thermal conductivity, densities, and specific heat for each layer, which give more precise heat transfer depending on the characteristics of each layer. The solar radiation values have been calculated depending on the mathematical equations for January and July of Miskolc city. It found that the thermal behaviour of the PV module is a variable with solar radiation change during the day, which was clear by temperature distribution on the PV module surface. The low the solar radiation value and temperature ( $176 \text{ W/m}^2$ ,  $4 \text{ }^\circ\text{C}$ ), the lower the intensity of solar radiation affects the PV module's short circuit current by the number of photons absorbed by the semiconductor material that PV cells are made from then, influenced by the PV module performance. The average temperature at the solar radiation mentioned above was  $15.2 \text{ }^\circ\text{C}$ . This temperature level is not causing damage to the PV module but reducing its electrical power and efficiency. Increasing solar radiation and temperature to ( $734 \text{ W/m}^2$ ,  $35 \text{ }^\circ\text{C}$ ) causes an increase in the PV module temperature that causes reduce in power output with damage to PV cells at continuously increased temperatures. An increase in the ambient temperature causes an increase of PV cells, which lead to a significant decrease in open-circuit voltage when the PV module temperature is above  $25 \text{ }^\circ\text{C}$  with a slight drop by short circuits current, then a reduction in power output. Rising temperature to  $82 \text{ }^\circ\text{C}$  causes degradation of the PV module performance and causes appearing of local hotspots when the temperature reaches the extreme range, which requires cooling of PV cells to remove the excessive heat and sustain its work. This case study help identify the problems faced by PV cells work and then determine the effective technique that improves PV performance.
- In the second case, we have modelled the PV module through equations that can control as one system undergoes controllable inputs and outputs that depend on the parameters we are setting. This investigation helps predict the PV module's electrical behaviour depending on input parameters and then identifies the appropriate parameters to achieve better electrical performance. The simulation considers variable and constant values of solar radiation and temperature as input to observe output voltage and current and power of the PV module as outputs. It found that reducing the solar radiation to less than STC, even with  $35 \text{ }^\circ\text{C}$ , reduces the PV module voltage and current to 21.52% and 13.63 %, respectively. Constant temperature with a gradual lowering of solar radiation is a significant effect by reducing the current and voltage of the PV module, which confirms the importance of the intensity of solar radiation on power produced. Constant solar radiation values and gradually lowering temperature has a slight effect on the current of the PV module and a higher effect by reducing the voltage compared with constant temperature and variable solar radiation. It was found that decreased temperature of the PV cells with constant solar radiation slightly affects the PV module performance. The second case has confirmed the effect of the intensity of solar radiation and temperature on the open-circuit voltage and short-circuit current that affects the PV module performance.

## Chapter 4

### Investigation of the effect of using nanofluids on the boiler system behaviour

In this chapter, thermal analytical calculations were conducted of the proposed nanofluids under laboratory conditions with validation of the results obtained. The current study contributes to increasing knowledge of the thermal behaviour of nanofluids proposed as a new cooling media and their influence on greater thermal system efficiency. Iron oxide ( $\text{Fe}_2\text{O}_3$ ) nanoparticles and tungsten trioxide ( $\text{WO}_3$ ) nanoflakes suspension at a specific volume concentration in DI water were proposed. Thus, investigate their effect on the heat transfer rate, Nusselt number and heat transfer coefficient, drop in the friction coefficient, friction factor and Reynolds number. MATLAB/Simulink has been used to validate the experimental and simulation to confirm the accuracy of the results and compare the results with other studies.

#### 4.1. Data reduction

The nanofluids of Iron oxide  $\text{Fe}_2\text{O}_3$  and Tungsten trioxide  $\text{WO}_3$  nanoparticles were prepared using two-step methods. More information about synthesizing the  $\text{Fe}_2\text{O}_3$  and  $\text{WO}_3$  nanoparticles is available in Appendix A. The volume concentration of  $\text{Fe}_2\text{O}_3$  was 0.015 vol%, and  $\text{WO}_3$  was 0.01 vol%, which calculate according to equation (49). The parameters of heat transfer rate, Reynolds number, Nusselt number, friction factor, and pressure drop were calculated from Eqs. (32, 35, 36, 37, and 38), as mentioned in subchapter 2.3, and the heat transfer coefficient was calculated by Eq. (66) [104] as follows:

$$h = \frac{m c_p \times (T_{out} - T_{in})}{A(T - T_w)} \quad (66)$$

Here,  $A$  is a pipe's peripheral area, which calculates in Eq (67), while  $T$  represents the average inlet and outlet temperature.

$$A = 2 \times (W + H)l \quad (67)$$

$W$ ,  $H$ , and  $l$  are the tube's width, height, and length.

#### 4.2 System description

The system consists of an electric water heater with 81 litres (Model: GCVS 804420 B11 TSR) and a heat exchanger with a surface area of  $0.21 \text{ m}^2$  inside the electric water heater. The heat exchanger of the electric heater is connected to a water tank (90 litres) which involves a second heat exchanger inside it with a 15 mm diameter connected with an electric water heater by an inlet pipe. The second tank contains a nanofluid with a pump and mass flow rate sensor (Model: YF-S201) connected to an inlet pipe, a nanofluid tank, and an electric water heater. Eight thermocouples (T-type of  $0.2 \text{ mm} \pm 1 \text{ }^\circ\text{C}$  accuracy and  $\pm 0.5 \text{ }^\circ\text{C}$  limits of error) were used to measure the temperature of each part of the system, as shown in Figure 29. Thermocouples were distributed of the inlet, outlet, water tank, nanofluid tank, electric heater wall, water inside of the electric heater, ambient temperature, and temperature between the water tank and nanofluid tank. The measured temperature is recorded by the National instrument model NI 9213 and read by IN Signal Express 2015 software. The National Instruments Compact DAQ (NIC) system contacts the thermocouples read and recorded by driver software installed by the laptop.

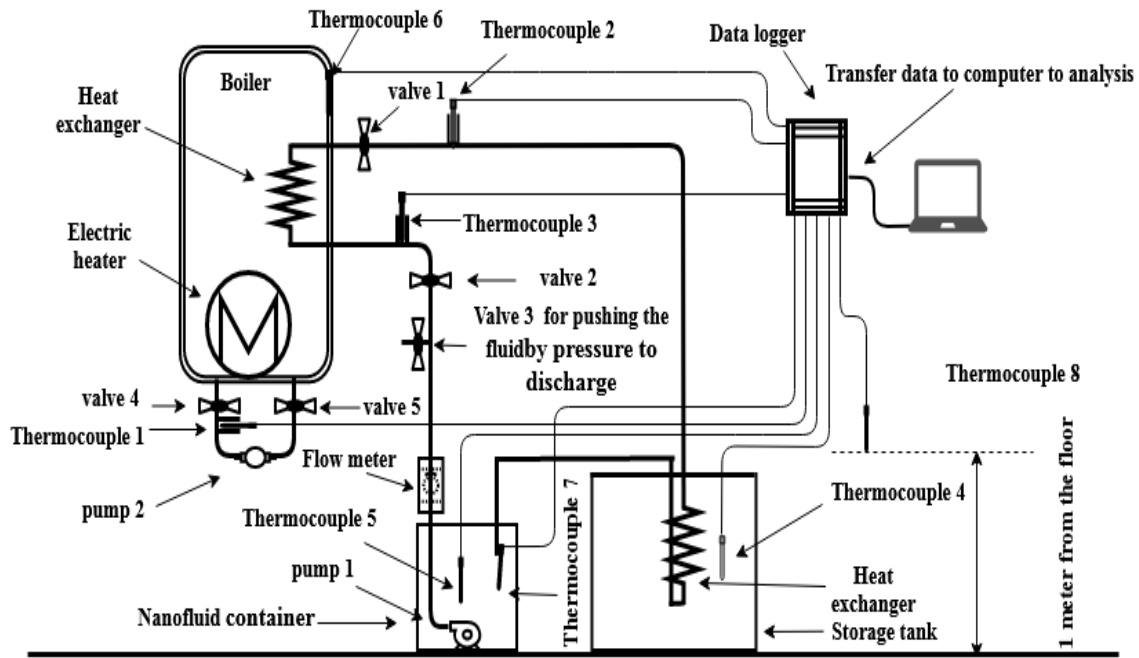


Figure 29. Schematic diagram of the boiler system

### 4.3 Validation of experimental

The system has been modelled with MATLAB/Simulink; this model represents a small water electric heater set to work between the temperature of 60-63 °C and a pressure of 0.6 MPa. Four ports were connected heat exchanger; the first port represents the (inlet cold fluid) connected by a reservoir involving cold water at a specific temperature with a pump and mass flow rate sensor, as shown in Figure 30. The second port is (the hot outlet fluid) connected by a temperature sensor to measure the temperature variation between the inlet and outlet.

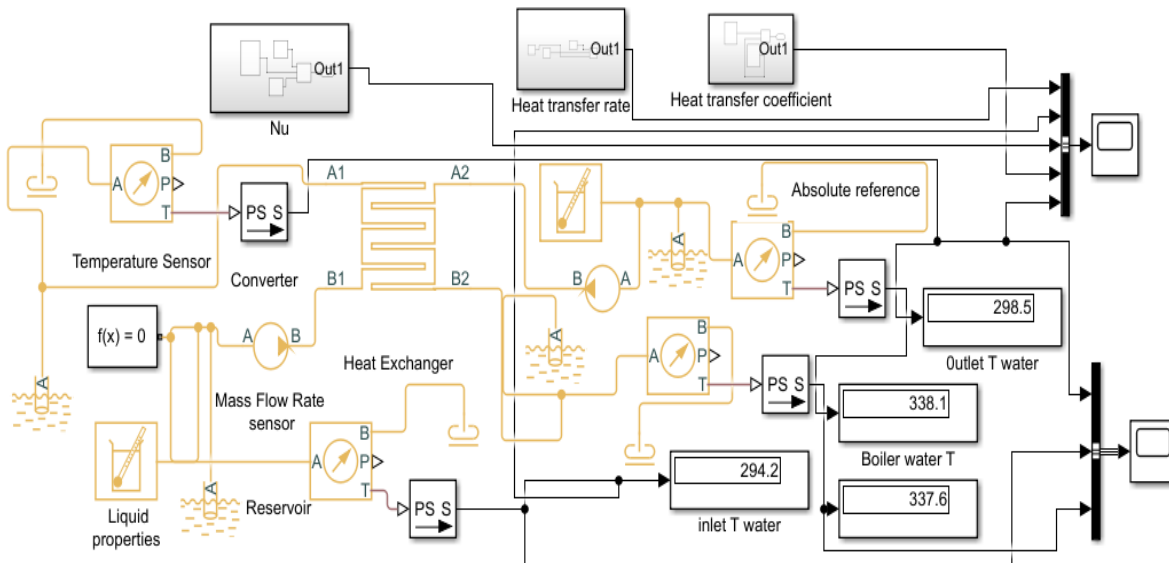


Figure 30. Simulink model of the heat exchanger

The other ports are connected to an electric water heater to circulate the hot water and make it homogeneous. The heat exchanger models the heating of fluids through conduction heat from hot water on the outer wall to water circulating inside heat exchanger pipes with a temperature less. The thermophysical properties of the liquid are defined and set on the thermal liquid tab. The simulation system undergoes governing equations into Simulink blocks that depend on variable parameters. The blocks of Simulink are built according to actual experiment results that were taken for a specific period to validate the effectiveness of the actual system.

#### 4.4 Results and discussion

##### 4.4.1. Effect of volume concentration on friction factor and Reynolds number

Adopted  $\text{Fe}_2\text{O}_3/\text{DI}$  water and  $\text{WO}_3/\text{DI}$  water as nanofluids, which achieved interesting changes in the heat transfer, thus affecting other parameters by improving the thermal characteristics. Heat transfer of the  $\text{Fe}_2\text{O}_3$  nanofluid used achieved better performance than  $\text{WO}_3$  nanofluids, reflecting enhanced working fluid characteristics due to increased thermal conductivity and decreased viscosity at the outlet. Figure 31 (a) shows the variation of inlet and outlet temperature of the DI water and nanofluids on the thermal performance of the working fluid. An increase in inlet hot fluids temperature causes decreased friction factor and a slight decrease in the viscosity of fluids. In contrast, the increase in Reynolds number leads to a decreased friction factor. The friction factor is affected by the volume concentration of nanoparticles; at 0.015 % and 0.01% nanoparticles volume concentration in the base fluid, the viscosity of nanofluids increases compared to DI water, and the friction factor increases. Figure 31 (b) shows the decreased friction factor with an increase of the average Reynolds number due to the volume concentration and viscosity of  $\text{Fe}_2\text{O}_3$  nanofluid being the highest compared with  $\text{WO}_3$  nanofluid and DI water.

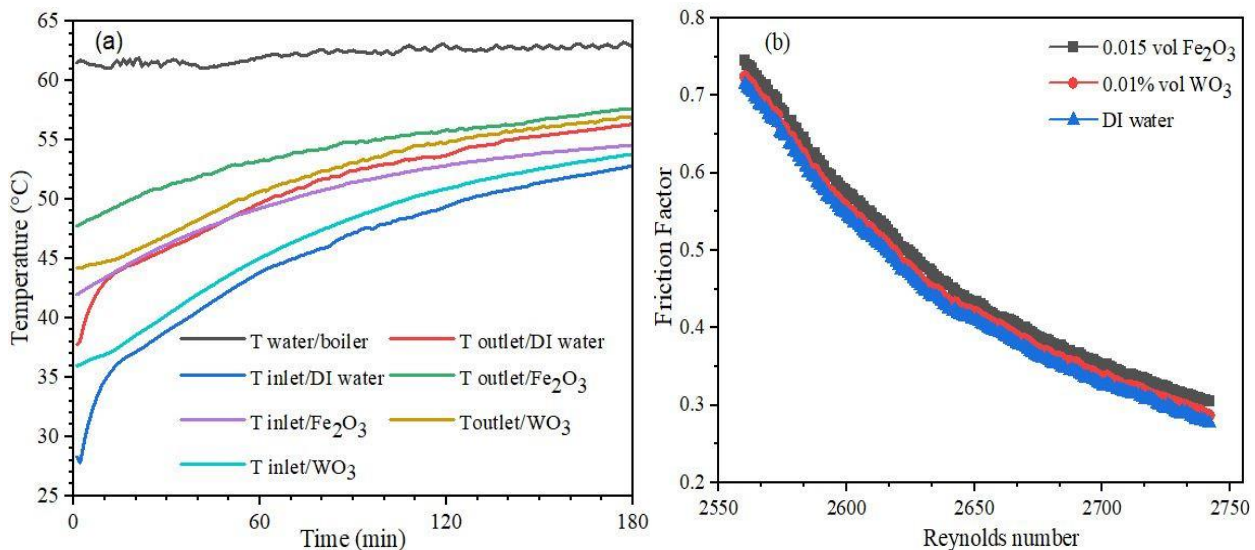


Figure 31. The temperature profile of working fluid (a) and (b) influence of Reynolds number on friction factor

Reynolds number is a measure of flow pattern, influenced by fluid inlet temperature and volume concentration of nanoparticles into the base fluid. Figure 32 shows the effect of mass flow rate on increasing Reynolds number at different volume concentrations of nanofluids. It can conclude that the increase in Reynolds number is related to the volume concentration of nanoparticles, flow rate, and inlet hot fluid temperature.  $\text{Fe}_2\text{O}_3$  nanofluid achieved increment by Reynolds

number of about 2.5% and 3.8% compared with  $\text{WO}_3$  nanofluid and DI water. Thus, increasing the Reynolds number and Nusselt number leads to an increased heat transfer rate to a more significant extent.

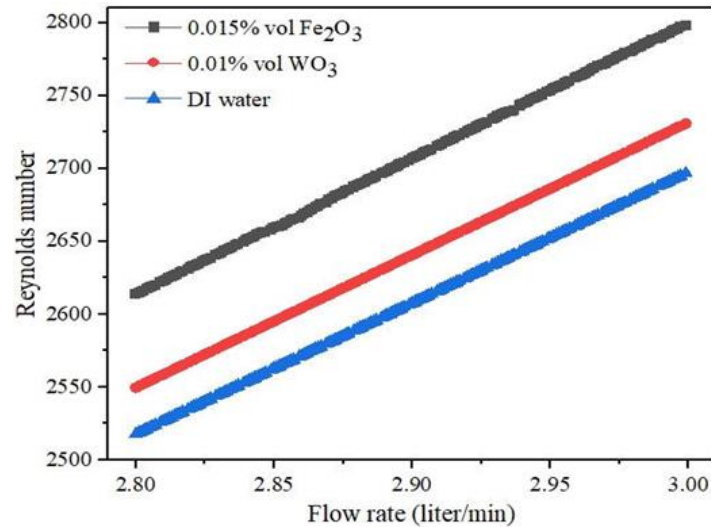


Figure 32. Effect of flow rate and volume concentration on Reynolds number

#### 4.4.2. Heat transfer coefficient and heat transfer rate

An increment in the thermal conductivity of the fluid has a positive effect on the convective heat transfer coefficient, thus enhancing the Nusselt number. Increasing the mass flow rate of the nanofluids achieved an increment in the heat transfer coefficient; thereby, the volume concentration of nanoparticles, inlet temperature, and flow rate contributed by an increment of the heat transfer coefficient of working fluid. Figure 33 shows the heat transfer coefficient enhancement with  $\text{Fe}_2\text{O}_3$  nanofluid at about 9.6%, which was higher than other studies [105] that used  $\text{Fe}_2\text{O}_3$  and  $\text{CuO}/\text{water}$  at 0.15 %, 0.4 %, 0.65 vol.%, and temperatures from 50 to 80 °C.

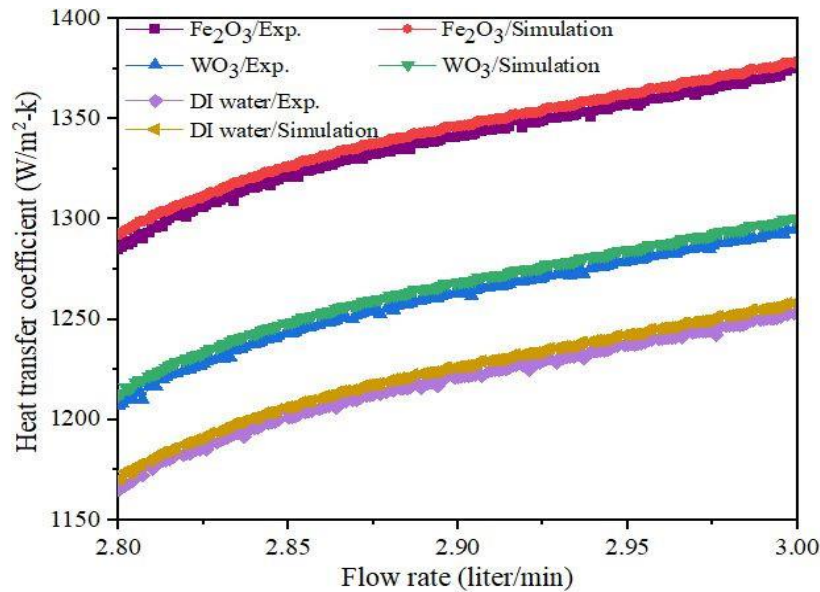


Figure 33. Influence of flow rate and inlet temperatures on heat transfer coefficient

Using  $\text{WO}_3$  nanofluid at 0.01 vol% achieved an increment of heat transfer coefficient higher than DI water and less than  $\text{Fe}_2\text{O}_3$  nanofluid by 6%. A slight variation was observed by the experimental and simulation results regarding the heat transfer coefficient of about 2% for the fluids used. Therefore, this experimental work adopting a low concentration of nanoparticles into base fluid achieved better heat transfer characteristics. Avoiding agglomeration and sedimentation of nanoparticles into pipes required a specific volume concentration for the nanoparticles that contribute to enhancing of thermal properties of nanofluid. Thus, increased volume concentration increases nanofluids' viscosity, causing more pump power consumption. Depending on the thermophysical properties of nanofluids and DI water to determine the heat transfer rate for both fluids, it considered the volume concentration of nanoparticles suspended by water and its effect on the thermal behaviour of the liquid. The experiment was conducted under a temperature range between 61-63 °C with a fluctuation flow rate between 2.8-3 L/min.  $\text{Fe}_2\text{O}_3$  nanofluid recorded increment by the heat transfer rate higher than  $\text{WO}_3$  nanofluids and DI water by about 4.1% and 5.8%, respectively, due to the high potential of their thermal properties that positively reflected on the heat transfer performance from the boiler to the storage tank. Figure 34 indicates the difference in heat transfer rate between used nanofluids and DI water; the increment of heat transfer rate was uniform under the operating temperature range and flow rate at three hours which confirms the stability of nanofluid used during the operation. Compared to another study by [106] that used silver nanoparticles mixed with water with 0.05 vol.% as a nanofluid, it achieved an increment of the heat transfer rate of about 4.4%. In the present study, 0.015 vol% of  $\text{Fe}_2\text{O}_3$  gives an increment of about 5.8% heat transfer rate, which indicates that  $\text{Fe}_2\text{O}_3$  nanofluid can be a cooling fluid more efficient than  $\text{WO}_3$  nanofluid that shows enhancement better than conventional cooling fluid. A slight variation in the heat transfer rate accidental during simulation compared with experimental results validate the measurement of experimental results, which is acceptable.

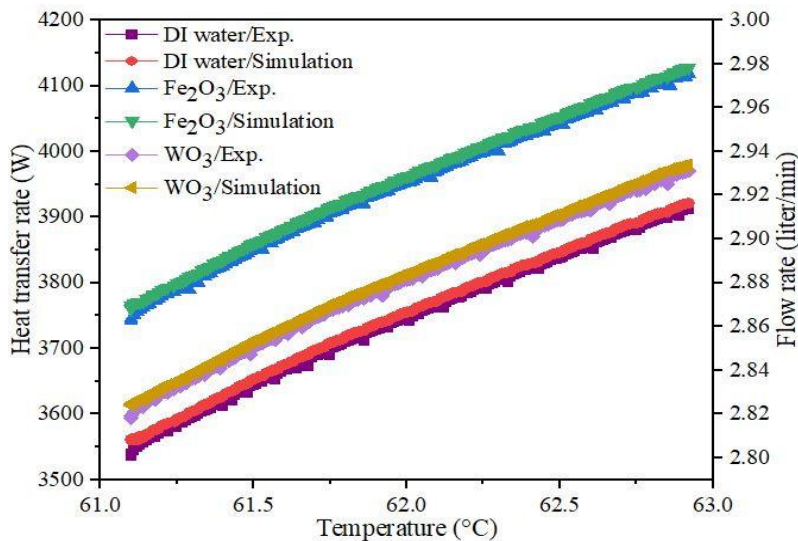


Figure 34. Heat transfer rate of working fluids at variation temperatures and flow rate

#### 4.4.3 Nusselt number (Nu)

Nusselt number is influenced by the volume concentration of nanoparticles and fluids temperature, as shown in Figure 35 (a). The Nusselt number significantly increases with an increase in the temperature of the working fluids; it can see the difference in the Nusselt number

used  $\text{Fe}_2\text{O}_3$  nanofluid compared to  $\text{WO}_3$  nanofluid and DI water. Using  $\text{Fe}_2\text{O}_3$  nanofluid led to an increment of Nusselt number about 6.2%, 8.5 % higher than  $\text{WO}_3$  nanofluids and DI water at a maximum temperature of 63 °C. It is evident in this study that three parameters have a significant effect on the Nusselt number such as thermal conductivity of the working fluid, Hydraulic diameter, and heat transfer coefficient of the working fluid. On the other side, the mass flow rate has a vital role in the Nusselt number; Figure 35 (b) show the increase in the Nusselt number with an increase in mass flow rate; the range of flow rate help suspend nanoparticles in the base fluid, thereby more stability of nanofluid. Compared with this study, an experiment conducted by [104] used aluminium nanoparticles mixed with water at 0.2 % and 0.3 vol % enhanced the Nusselt number by 3.37 % and 5.0877%. In present experiment used  $\text{Fe}_2\text{O}_3/\text{DI}$  water at 0.015 vol% enhancement of Nusselt number by 8.5%. A lower volume concentration of  $\text{Fe}_2\text{O}_3/\text{DI}$  water gave a high Nusselt number of Al/waters, and the variation of simulation and experimental results was convergent.

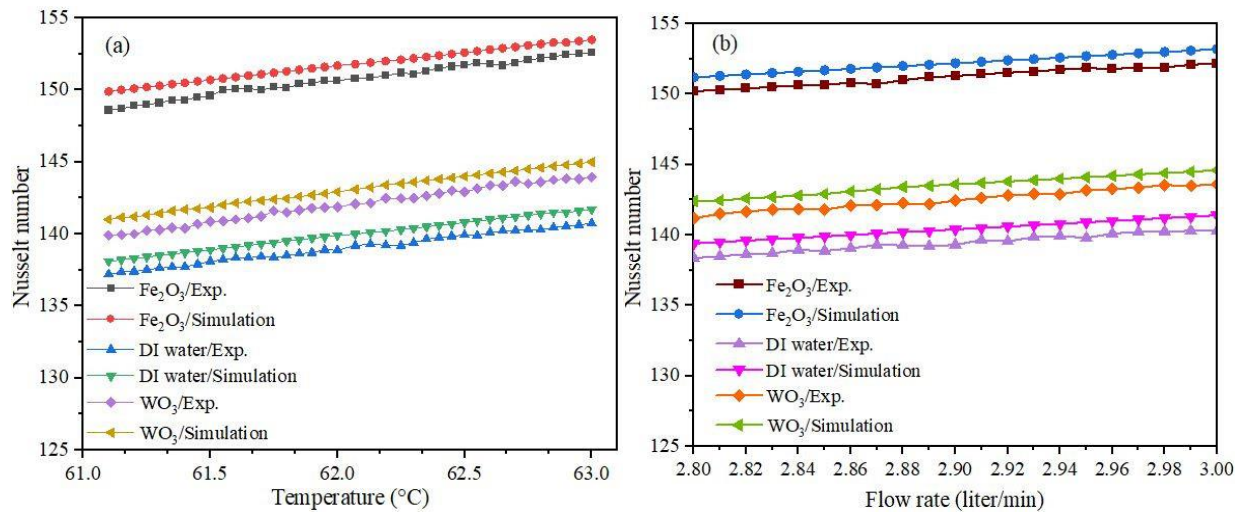


Figure 35. Influence Nusselt number by (a) inlet temperatures and (b) flow rate

#### 4.4.5 Conclusions

Heat transfer of the nanofluids used achieved better performance than DI water due to increased thermal conductivity. The volume concentration of nanoparticles, flow rate, and inlet hot fluid temperature influence an increase in Reynolds number. Increasing of volume concentration of nanoparticles cause an increased friction factor, while the increase of Reynolds number leads to a decrease in friction factor.  $\text{Fe}_2\text{O}_3$  nanofluid achieved increment by Reynolds number of about 2.5% and 3.8% compared with  $\text{WO}_3$  nanofluid and DI water. Furthermore, volume concentration, inlet temperature, and flow rate increase nanofluids' heat transfer coefficient by 9.6% and 6%, respectively, compared with DI water. Thereby, suspending 0.015 % vol of  $\text{Fe}_2\text{O}_3$  nanoparticles into DI water led to an increment of Nusselt number by 6.2%, 8.5% higher than  $\text{WO}_3$  nanofluids and DI water at a maximum temperature of 63 °C. Increasing the thermal conductivity and heat transfer coefficient of the  $\text{Fe}_2\text{O}_3$  nanofluid causes enhancement of the Nusselt number better than increases in heat transfer rate to a larger extent. A slight variation observed by the experimental and simulation results of about 2% confirms the accuracy of the results. Thus, lower volume concentrations of nanomaterials have been adopted in this study to avoid the agglomeration and sedimentation of nanoparticles into pipes. Thus, avoiding increasing the viscosity of nanofluids viscosity causing more power consumption of the pump.

## Chapter 5

### Effect of passive and active cooling on the efficiency of the PV and PVT system

This chapter consists of four experimental case studies which applied new cooling techniques under hot conditions; two of them will be discussed in this chapter, and two of them in Appendix B.

The first study investigates using evaporative cooling as a passive cooling technique to absorb the generated heat from the PV module and lower its temperature by using cotton wicks immersed in the water (CWIWs) attached to the backside PV module. The CWIWs help decrease air dry temperature and increase humidity, then produce cool air that helps cool PV modules.

The second study in (Appendix B) is investigating the effecting of cotton wicks integrated with rectangular aluminium fins (CWIRAFs). Integrated aluminium fins with cotton wicks immersed in water from the top to the bottom help to increase the heat transfer area and the effective evaporative cooling at the back surface of the PV module. This technique helps to reduce the temperature of the PV module in the surrounding air and then improves its performance. Under the same experimental condition, the passive cooling technique was compared with the active cooling of the PVT system, which used water as a cooling fluid. The cooling techniques' results are compared with other studies according to thermal behaviour, efficiency, and power yield to identify the appropriate cooling technique and calculate the payback period.

The third case is an investigation of using a new nanofluid zirconium oxide ( $ZrO_2$ ) as a coolant at different volume concentrations dispersed in DI water to reduce the temperature of the PV cells. The nanofluid is circulated in the tubes of the heat exchanger attached to the backside of the PV module to absorb excess heat and then enhance the performance of the PV module. Thus, energy and exergy efficiencies of the PVT system be analyzed from thermodynamic viewpoints to investigate the effect of the use of nanofluid on the PVT system entropy generation and exergy losses. Adding to the effect of dispersion of nanoparticles on heat transfer coefficient, Reynolds number, Nusselt number, friction factor and pressure drop.

The fourth case in (Appendix B) is a proposed heat exchanger consisting of fluid circulating in a serpentine tube and a thermal absorber plate attached at the backside of the PV module to reduce the PV cell's temperature and enhance their efficiency. This case experimentally investigates the effect of employing a new nanofluid tungsten trioxide ( $WO_3$ ) on a PVT system's energy and exergy efficiency at different volume concentrations 0.5 vol%, 0.75 vol%, and 1 vol%. Then, the effects of increased volume concentration of nanoparticles on the heat transfer coefficient, Nusselt number and Reynolds number, and pressure drop.

#### 5.1 Effect of evaporative cooling on PV module performance

The present work investigates using the evaporating cooling technique to absorb the heat generated at the backside of the PV by cotton wicks immersed in the water (CWIWs). The CWIWs help decrease air dry temperature and increase humidity, producing cool air and contributing to cool PV modules.

##### 5.1.1 Cooling technique and instruments used

Two polycrystalline 50 W PV modules were used with dimensions of 0.65 m × 0.55 m. The first PV modules were equipped with CWIWs, while the second was used as a reference without

cooling for comparison between them during operation. The height of PV modules from the ground and the tilt angle ( $29^\circ$ ) allow great air to flow on the backside of PV modules. The current technique contributes to generating the evaporating cooling by exposure of the wetted cotton wicks to the surrounding air, which decreases dry air temperature and increases humidity, producing evaporating cooling that can exploit it to absorb the rising heat from the backside of the PV module. The experiment used cotton wicks (CWs), commonly used for lanterns or locally available lamps. The CWs have a high absorbent ability, which helps in the transmission and distribution of water to all CWs arranged at the backside of the PV module and is characterized by a suitable heat transfer coefficient and lower thermal conductivity, as shown in Table 6. The appropriate cost and ease of use made its application feasible compared to other techniques. The internal structure of the cotton wicks consists of four small sub-cotton wicks collected and covered with a cotton cover. The CWs were arranged as serpentine forms and attached to the backside of the PV module. The arrangements of cotton wicks avoided any space between them and were fixed by thermal silicon, as shown in Figure 36. At the top edge of the PV module are eight ends of CWs immersed in the bottom of two plastic bottles full of water; this immersion method allows absorbing and transfer of the water from the top to the bottom of the PV module. The gravity-free flow of water helps transmit the water to the CWs without extra power. Thus, this method helps to distribute the water entirely from cotton wicks throughout the PV module. Thereby, the technique helps to create continuous cooling with less water consumption due to the effective absorption of cotton wicks.

Table 6. The properties of the cotton wicks

[107]	Cotton wick diameter	Cotton wick length	Thermal conductivity	Heat transfer coefficient
[108]	8 mm	50 m	0.048W/m·K	36 W/m °C

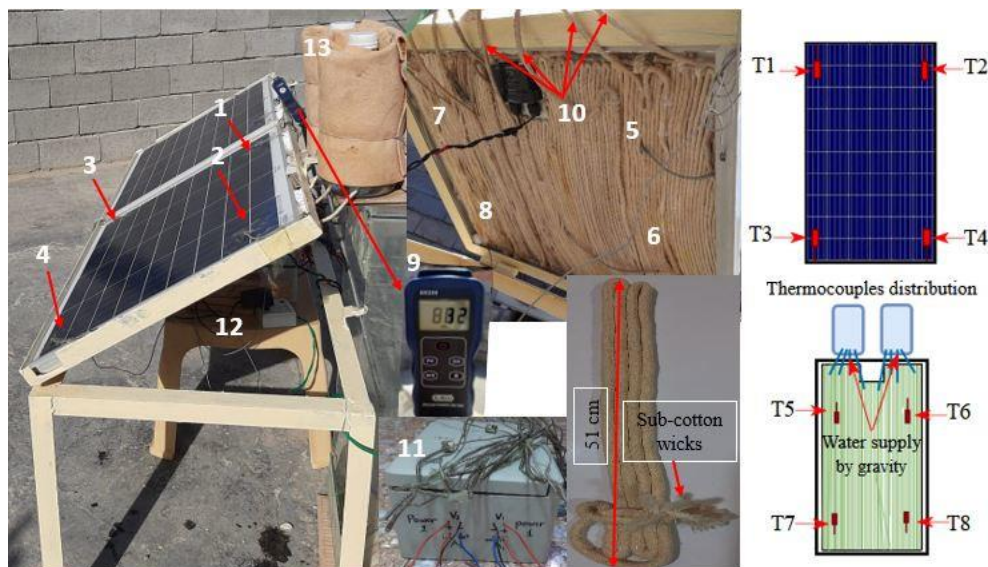


Figure 36. A sight of the experimental setup, (1-4) thermocouples distribution on the surface of the PV module, (5-8) on the backside, (9) solar power meter, (10) ends of CWs supplier for water, (11) data logger, (12) electric supply, (13), plastic bottles

Temperature and solar radiation are the operation parameters of the PV module work. In the present study, solar radiation was measured manually for 30 min using a solar power meter. The temperature was measured through thermocouples installed at different PV module surfaces and backsides. Temperature, voltage and current were measured using a data logger multi-channel Arduino, which was programmed to record the data. The data logger consisted of 17 thermocouples for measuring temperature, two sensors to measure the voltage and two current sensors. Table 7 shows the specifications of used devices used for the measure used in all experiments conducted in Iraq. The data logger recorded the measured data with 10 min time step throughout the experiment days and saved the data in portable storage memory of 8 GB. Two 18-V lamps completed the electrical circuit between the PV module voltage and current sensors.

Table 7. Specifications of the measurement devices and sensors.

Item	Model/Brand	Range	Accuracy
Thermocouples	K (2 m length)	-200 °C to 1350 °C	0.25 °C
Solar power meter	SM206	1-3999 W/m <sup>2</sup>	±0.1 W/m <sup>2</sup>
Current sensor	ACS712	up to 30 A	0.04 A
Voltage sensor	Module 25V	up to 25 V	0.02445 V
Flow rate sensor	YF-S201	1-30 L/min	-----
Electronic scale	BOECO BAS	3 Kg	0.0001g
Ultrasonication	Branson	240V, Vf: 48kHz	-----

### 5.1.2 Results and discussion

The experiments were conducted according in August 2021. August is characterized by a sunny month with high temperatures and low humidity on most days with moderate winds. There was no significant variation in the temperature recorded throughout the experiments, and the weather was sunny during the experiment days. The solar radiation values were obtained throughout the experiment days; Figure 37 shows the average solar radiation recorded at the beginning of the early morning; the solar radiation values increase until a higher value between 12:10 to 13 PM; after that, it decreases. Figure 37 also shows the average ambient temperature recorded during the experiment period, 43.8 °C, and according to (Iraqi Agricultural Meteorological Centre 2021), the average wind speed was between 2.84 - 6.64 m/s.

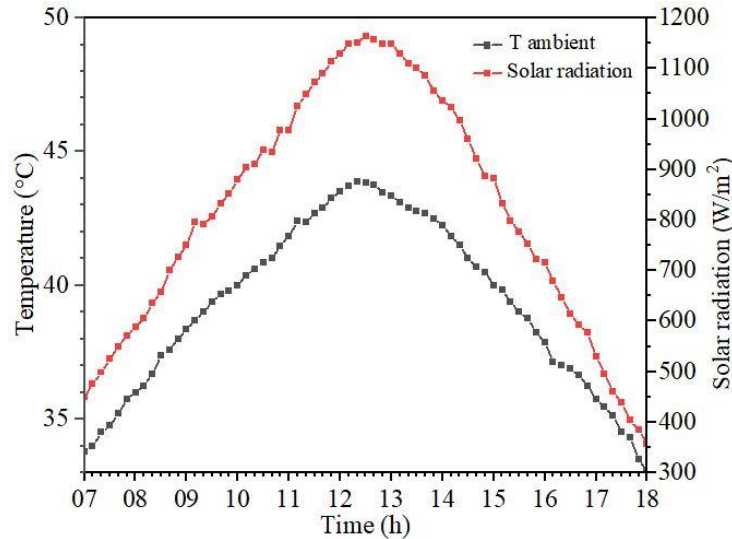


Figure 37. Average solar radiation and ambient temperature

### 5.1.2.1 Energy analysis of the PV modules with and without CWIWs

The PV modules were equipped with thermocouples to investigate the thermal behaviour of the PV modules is an important issue conducted by fixed four ( $T_1$ ,  $T_2$ ,  $T_3$ , and  $T_4$ ) thermocouples distributed in different places on the surface and other four ( $T_5$ ,  $T_6$ ,  $T_7$ , and  $T_8$ ) thermocouples on the backside of the PV modules. Depending on the average temperature recorded for each 10 min for the PV modules and throughout the experiment periods, it could notice that the variation in the temperature on the surface and backside of the PV module recorded by thermocouples was very slight, as shown in Figure 38 (a). Therefore, it adopted the average temperature for all experiment days and the average ambient temperature to evaluate the PV module's performance under similar operating conditions. The temperature of the PV module surface was higher than the backside due to being directly exposed to intense solar radiation. The increase obtained by the ambient temperature is related to the intensity of solar radiation. The PV module with CWIWs cooling showed thermal behaviour closer to the ambient temperature throughout the experiment due to evaporating cooling of CWs. The airflow on the wet surface of the cotton wicks has a major role in enhancing the evaporation process due to a convection mass transfer and decreasing the PV module temperature, which enhances the rate of evaporation cooling. The highest temperature recorded of the PV module with the CWIWs was 46.1 °C at 12:20 PM, while the ambient temperature was 43.8 °C.

In contrast, it increased the average PV module temperature without cooling to 56.4 °C simultaneously and during the experiment, as shown in Figure 38 (b). Rising the temperature at this level causes degradation of the PV cell's performance and drops the energy yield discussed in the next section. The wet CWIWs exposed to wind have provided adequate cooling that effectively reduces the PV module temperature to 10.3 °C, positively reflecting the PV module performance. The flowing of the air over the wetted surface of the cotton wicks causes water evaporates and cools the air that absorbs the heat from the PV module by forced convection and transfers it to air, which the productivity of the PV module enhances. The PV module without cooling causes an increase in the temperature, which influences the output voltage and current, thus causes to a dropped output power of the PV module. The maximum output voltage and

current obtained from the PV module without cooling were 8.9 V and 1.6 A, respectively, at 12:20 PM

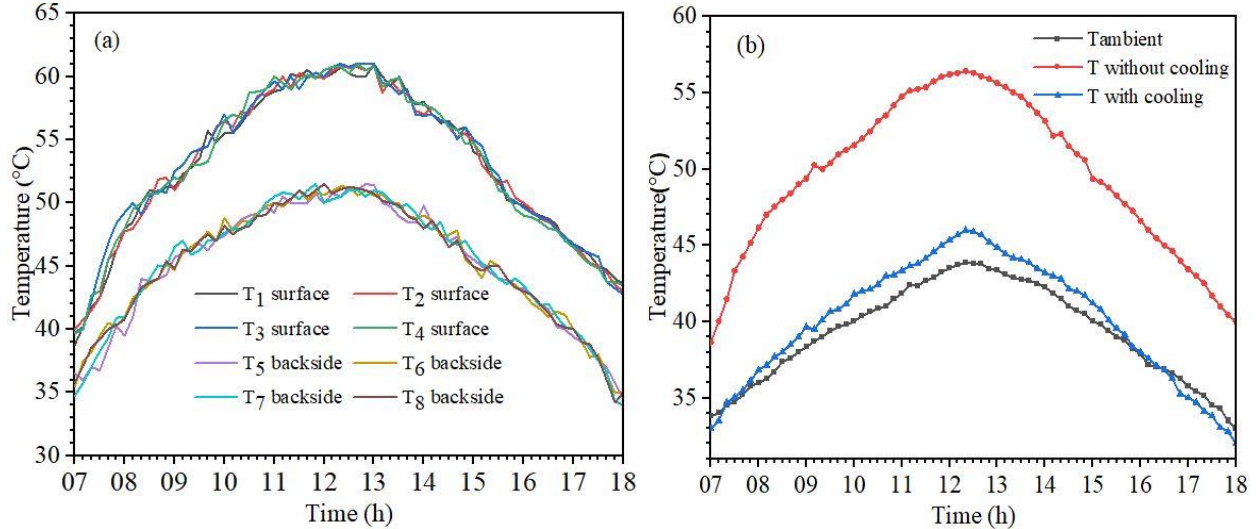


Figure 38. Temperature distribution on (a) PV module and (b) average temperature of the PV modules with and without CWIWs

Figure 39 (a) shows the maximum output power of the PV module without cooling was 14.2 W, which refers to the influence of an increase in the temperature on the PV module performance, and that was clear by dropping the efficiency to 3.4%, which confirmed the deterioration performance due to rising temperature. On another side, the effective absorption and transfer of the water from top to bottom of the PV module by natural flow helped achieve a good cooling rate throughout the experiment. Moreover, the tilt angle of the PV module helps run-off of wind in the backside of the PV modules; the airflow on the wet surface of the cotton wicks has a major role in enhancing the evaporation process due to a convection mass transfer and decreases the PV module temperature. Used CWIWs improved the output power of the PV module to 30.5 W due to an increase in the output voltage values and current to 16.3 V 1.872 A, respectively.

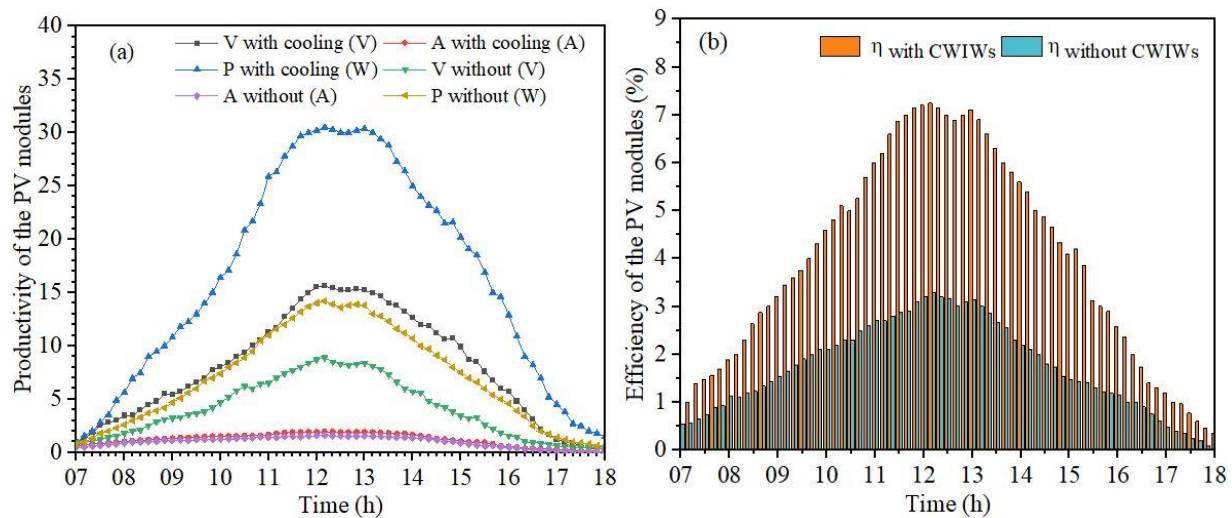


Figure 39. The variation value of (a) productivity of PV modules and (b) Efficiencies  $\eta$  of the PV modules with and without CWIWs

Because the cotton bristles immersed in water and exposed to the wind have provided, continuous cooling improved, the power yield with an increment of about 16.3 W compared without cooling. Figure 39 (b) shows the variation of the PV module's efficiency of both cooling and without cooling, maximum efficiency of the PV module with CWIWs being 7.25%. The decrease in the PV module temperature and improved performance is attributed to cotton wicks immersed in water from the top to the bottom. The cotton wick immerses helped the distribution of water entirely on the backside of the PV module, which gave continuous cooling throughout the experiment. The mechanism of evaporative cooling used has enhanced the performance of the PV module better than in other studies conducted by [36,109 and 110] used different evaporation cooling techniques, which makes it more reliable for application. Table 8 shows the PV module performance compared with previous studies that used similar cooling methods to improve the PV module performance.

Table 8. The PV module performance compared with previous studies

Ref.	Passive cooling techniques	$\eta_{electric}$ increment	Power increment (W)	Temperature reduction ( $^{\circ}$ C)
Current study	Cooling by CWWs/ PV 50W	7.25	16.3	10.3
[110]	Inclined duct with water flows on a piece of cloth/PV 130W	6.7	5	10
[111]	Evaporative cooling by a wool/ PV 80 W	0.6	9.7	12
[40]	Aluminium fins / PV 50 W	2.3	20	5.5
[112]	Cotton wick structures/ PV 25W	1.4	12.2	5.9

### 5.1.2.2 Exergy and entropy generation

Exergy analysis is important for estimating the real performance of the PV module. The maximum average PV module temperature without cooling was recorded at 56  $^{\circ}$ C at 12: 20 PM. The evaporating cooling helped absorb the generated thermal exergy and dissipate it into the surrounding air, reducing the PV module temperature. As mentioned in Eq (55), the output electrical power of the PV module is equal to the exergy electrical. Figure 40 (a) shows the relation of the electrical exergy with temperature; it can observe the increment gradual of the electrical exergy and exergy efficiency with increased temperature until 56  $^{\circ}$ C. Maximum electrical exergy and exergy efficiency was 29.8 W, 7.2%; it was a slight variation from electrical energy and efficiency, as shown in Table 9, which confirms the effect of evaporative cooling on the performance of the PV module. Using CWIWs with a PV module reduces the exergy losses due to absorbing the heat generated by PV cells by the CWIWs and dissipating it to the surroundings. Based on the second law of thermodynamics, lowering the exergy losses affect the entropy generation in the PV module because of the irreversibilities. Figure 40 (b) shows the average entropy generation; using CWIWs leads to a decrease in entropy generation due to reducing the exergy losses exergy by about 14% lower than the PV module without cooling. The lower average entropy generation of the PV module with CWIWs compared to that of the PV module without cooling. Maximum entropy generation with CWIWs 8.45 W/ $^{\circ}$ C and without cooling was 9.66 W/C at 12:20 PM; after that, it dropped with a lowering of the temperature. Comparing performance with and without passive cooling, the PV module that used CWIWs was distinguished with high performance during the experiment by achieving higher power yield and efficiency than the PV module without cooling. Water absorbed by cotton wicks

with rising temperature led to created evaporation cooling helps absorb heat from the backside of the PV module. Figure 41 shows the comparison of the PV module performance using CWIWs and without; the PV module temperatures used CWIWs have a noticeable effect that contributed by decreasing about 22 % of the PV temperature compared with the PV module without cooling. Reduction of the temperature effectively contributes to enhanced productivity of the PV module by incrementing the power yield of the PV module to 16.3 W. Due to the increase in output voltage and current of the PV module, the efficiency enhanced to 7.25% compared to cooling, which recorded 3.4% with 14.2 W output power. According to evaporating cooling, the generated heat at the backside of the PV module is absorbed and dissipated into the surrounding air.

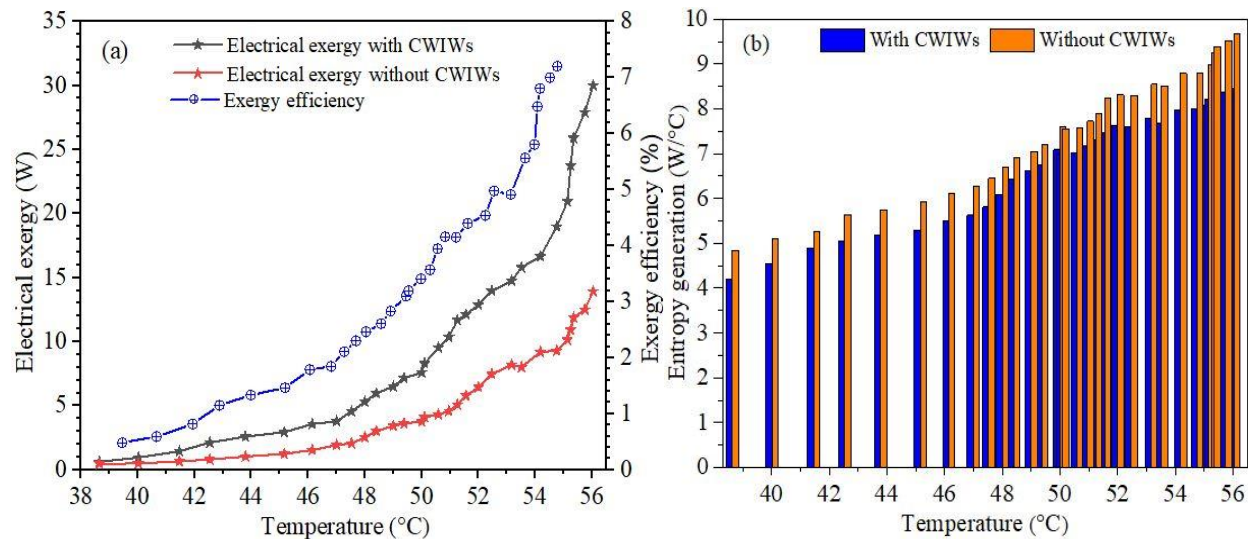


Figure 40. The effect of temperature on (a) electric exergy and exergy efficiency and (b) Entropy generation with and without CWIWs

Table 9. The variation of energy and exergy analysis

Performance of PV module	PV with CWWs
Electrical energy (power output)	30.5 W
Efficiency	7.25 %
electrical exergy	29.8 W
Exergy efficiency	7.2 %

The electrical energy (output power) under evaporating cooling was the same as the electrical exergy at high temperatures. Enhancing the PV module performance is attributed to using CWIWs to provide the appropriate cooling, decrease the temperature, and increase the electrical exergy and exergy efficiency. It was observed a significant deterioration in the PV module performance without cooling, thus causes negatively influence the power yield and efficiency in areas with hot climate conditions.

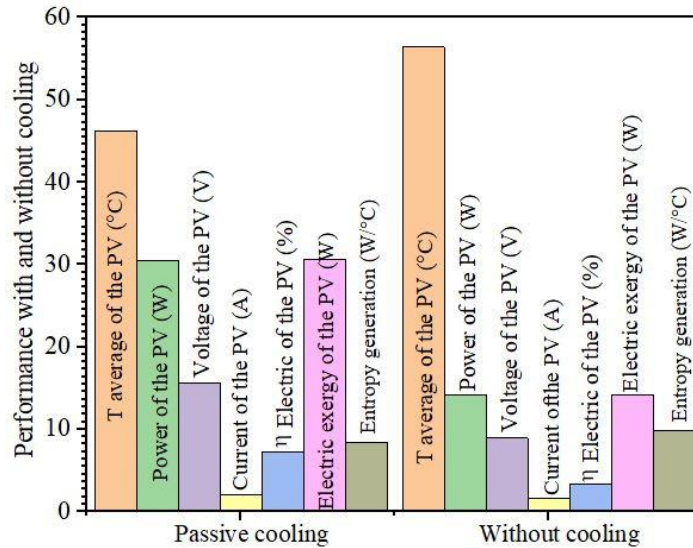


Figure 41. Comparison of PV module's performance

## 5.2 Effect of Zirconium Oxide (ZrO<sub>2</sub>) nanofluid on the behaviour of PVT System

Experimental investigation of using new zirconium oxide (ZrO<sub>2</sub>) nanofluid and serpentine tubes soldered on absorb plate and placed at the backside of the PV modules. Circulating ZrO<sub>2</sub> nanofluid in serpentine tubes helps absorb high heat and enhance the performance of the PV module. Thus, the effect of different volume concentrations (0.015 vol%, 0.025 vol%, 0.0275 vol%) in DI water on energy and exergy efficiencies of the PVT system be analyzed from thermodynamic viewpoints. Then, the effect of dispersion of different volume concentrations of nanoparticles on heat transfer coefficient, Reynolds number, Nusselt number, fraction factor and pressure drop at flow rate 1 L/min.

### 5.2.1 Experimental setup and work procedure

The experiments were conducted on a typical sunny day from 7:00 am to 5:00 pm, with no significant variation in temperature and solar radiation during the experiment period. Three PV modules of 50 W type polycrystalline were used in this experiment. The first PV module was a reference without cooling, the second PVT module used water as a cooling medium, and a nanofluid cooled the third PVT module. The PVT modules consist of an absorber copper plate integrated at the backside of the PV module with copper pipes arranged in serpentine and fixed on the absorber plate. A thermal wool insulation layer has been placed on the copper pipes and then covered by an aluminium plate. Two copper coils were immersed in a water tank of 35 litres; the first one was connected between the copper coil and the outlet of the nanofluid to reduce the nanofluid temperature. The second was connected between the outlet water and copper coil, then inlet water as a close loop. Thermocouples are placed on the surface and backside of the modules to measure their thermal behaviour of them. A thermocouple was fixed at each inlet and outlet of the PVT modules to measure the variation in fluid temperature. The modules are fixed at a tilt angle of 29° towards the southern. Four thermocouples are distributed on each surface of the PVT modules, and three are on the backside. Thermocouples were placed in the inlet and outlet of the first and second PVT module to measure the temperature of the cooling medium during the experiment period. Figure 42 above shows the experimental setup of the PVT modules.

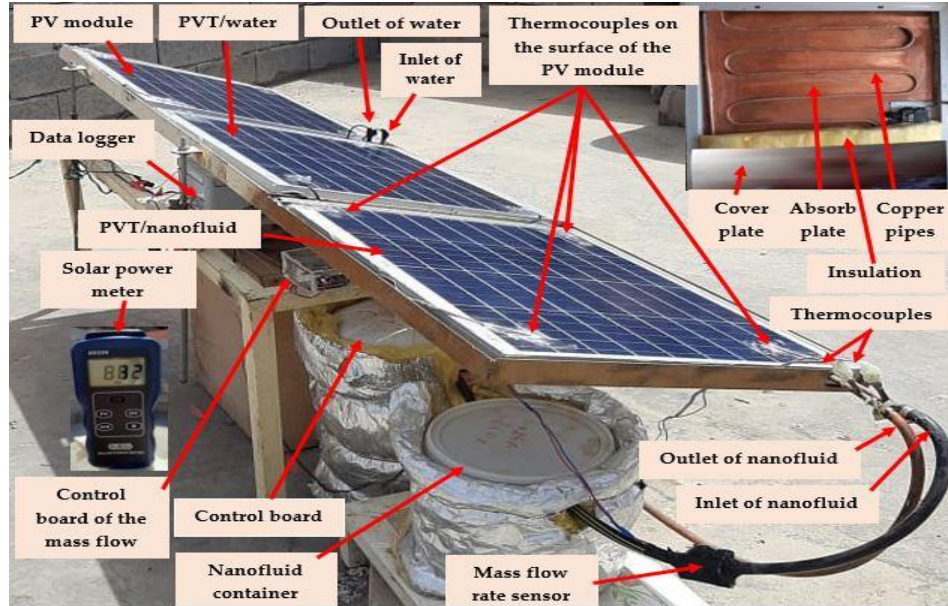


Figure 42. A view of the experimental setup

## 5.2.2 Results and discussion

### 5.2.2.1 Energy analysis results

Figure 43 (a) shows the average ambient temperature and solar radiation values recorded. The maximum ambient temperature was  $42.7\text{ }^{\circ}\text{C}$ , while solar radiation was  $1004\text{ W/m}^2$ , specifically at 12:20 pm. According to the Iraqi agricultural meteorological centre, the average wind speed was  $2.75\text{-}2.37\text{ m/s}$  [113] during the experiment days.

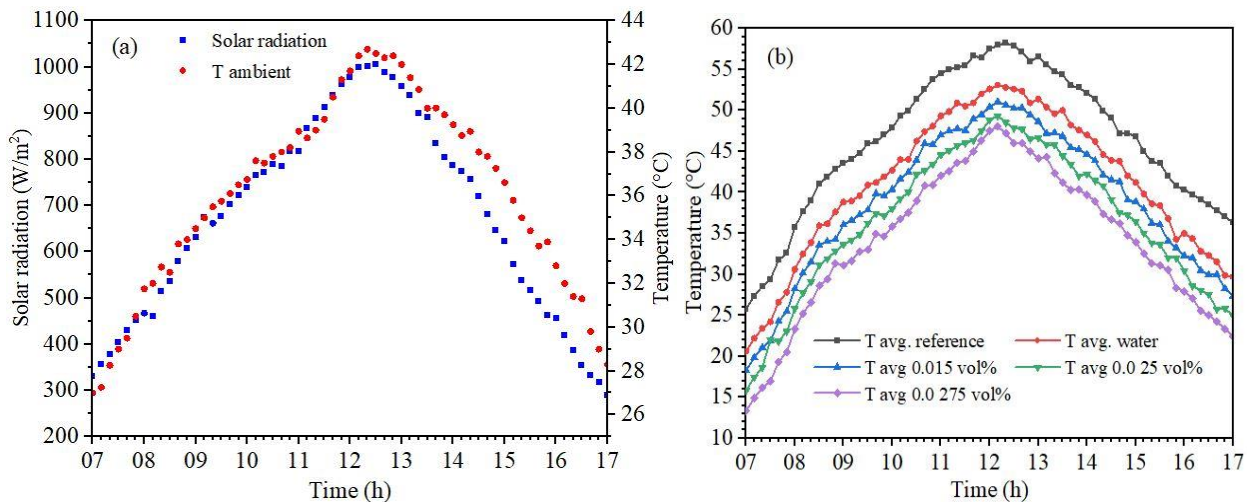


Figure 43. Average ambient temperature and solar radiation and (b) The temperature of the PVT system cooling by  $\text{ZrO}_2$  nanofluid

The thermocouples distributed on the surface and backside for measuring the PV module's temperature show a very slight variation of the measured temperature. It has adopted the average temperature of the temperatures measured for both sides to assess the thermal behaviour of the PVT system considering the ambient temperature. Figure 43 (b) shows the variation of the

average temperature of the PVT system at different volume concentrations of ZrO<sub>2</sub> fluids, compared with water as coolant and the reference PV module. The average temperature of the reference PV module was recorded at 58.2 °C; circulated DI water in the serpentine pipes attached to the backside of the PV module helped absorb the heat and reduced the PV module temperature by 9.7%. Circulate ZrO<sub>2</sub> nanofluids achieved a remarkable reduction in the PVT system temperature. The gradual increase in the volume concentration of the ZrO<sub>2</sub> nanofluid is accompanied by a noticeable decrease in temperature. At volume concentrations, 0.015 vol%, 0.025 vol%, and 0.0275 vol%, the PVT system temperatures have been reduced to 14%, 18.1% and 21.2%, respectively. Thereby, improving the thermal conductivity of fluids leads to increased heat absorption at the backside of the PV module; using ZrO<sub>2</sub> nanofluid has achieved higher heat absorbed from the PV module than water.

Figure 44 (a) confirms the necessity of having a cooling system to enhance the performance of the PV module. It can be observed that the electrical power output of the reference PV module is at a minimum level compared to others that have been coolant. Reduced PV module temperatures effectively contribute to enhancing their performance due to cooling. The increased volume concentration of ZrO<sub>2</sub> nanofluid with a constant mass flow rate of 1 L/min gradually increased the electrical power output. The maximum electrical power of the reference PV module was recorded at 18 W. Using nanofluids at different concentrations of 0.015 vol%, 0.025 vol%, 0.0275 vol% incremented the electrical power output by 11.4 W, 14.7 W and 15.72 W, respectively, compared to DI water that recorded 8.5 W. Figure 44 (b) shows the effect of volume concentrations of ZrO<sub>2</sub> nanofluids and water on the enhancing of electrical power, replacing nanofluid with water resulted in a noticeable enhancing due to their thermal properties. The electrical power increment by 15.72 W at 0.0275 vol% compared with DI water. The electrical power output enhancement is positively reflected in the electrical efficiency of the PVT system. Figure 44 (c) indicates the growth in the electrical efficiency with increasing volume concentrations of the ZrO<sub>2</sub> nanofluids. At 0.0275 vol%, the electrical efficiency of the PVT system was enhanced by around 54 % compared to DI water. Thermal efficiency is an important parameter to evaluate the thermal performance of a PVT system which is affected by the temperature, design of the cooling system applied and type of cooling fluid. Figure 44 (c) show the values of thermal efficiency at different volume concentration; during the experiment's days, the thermal efficiency starts with a low value and then increase to reach a maximum value at noon and then drop until the end of the experiment. Increasing the volume concentration of ZrO<sub>2</sub> nanoparticles in base fluid enhanced the heat removal capacity because of the increased thermal conductivity and convection heat transfer coefficient of the ZrO<sub>2</sub> nanofluid. Thereby the overall efficiency of the PVT system has been boosted by 8.9%, 18.8 % and 24.4%, respectively, compared with DI water cooling at 0.0275 vol%. The effect of increasing the volume concentration of ZrO<sub>2</sub> nanoparticles in base fluid and Nusselt number as a function of Reynolds number has been investigated. Figure 45 (a) shows an increase in the Nusselt number, with Reynold's number increasing due to a gradual increase in the volume concentration of ZrO<sub>2</sub> nanoparticles. Dispersion of ZrO<sub>2</sub> nanoparticles in the base fluid has enhanced the Nusselt number at a maximum value of about 51.7% at 0.0275 vol% compared to the DI water and then enhancement of the thermal properties of the cooling fluid. The increment of Reynolds number leads to an increased heat transfer coefficient of the nanofluid due to enhancing the thermal conductivity of the nanofluid. Figure 45 (b) shows the heat transfer coefficient values with Reynold's number at different volume concentrations.

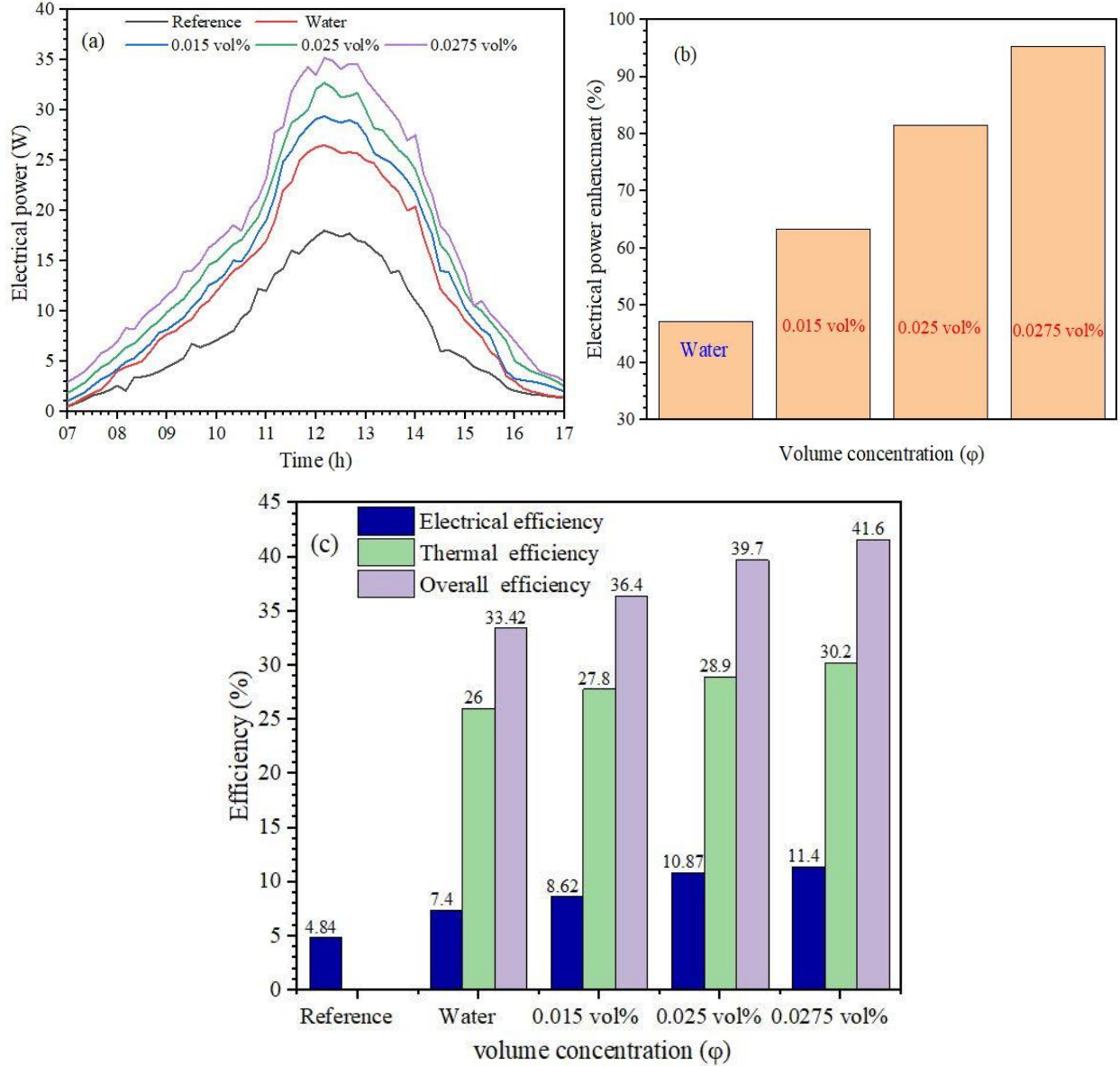


Figure 44. The performance of the PVT system Electrical power (a), (b) electrical power-enhancing and (c) overall efficiency as a function of volume concentration

Compared with DI water, the maximum enhanced heat transfer coefficient is 13% at 1 vol %; thus,  $ZrO_2$  nanofluids can increase the heat transfer coefficient, which positively reflects a lower PV temperature than DI water. Increasing the volume concentration enhances the thermal conductivity of nanofluid and increases the density, which affects the pressure drop. Figure 46 (a) shows the effect of increased Reynolds number and volume concentrations in the pressure drop; it can notice increased the pressure drop by using  $ZrO_2$  nanofluid to 31.5% compared with DI water which was less due to the low flow resistance of DI water.

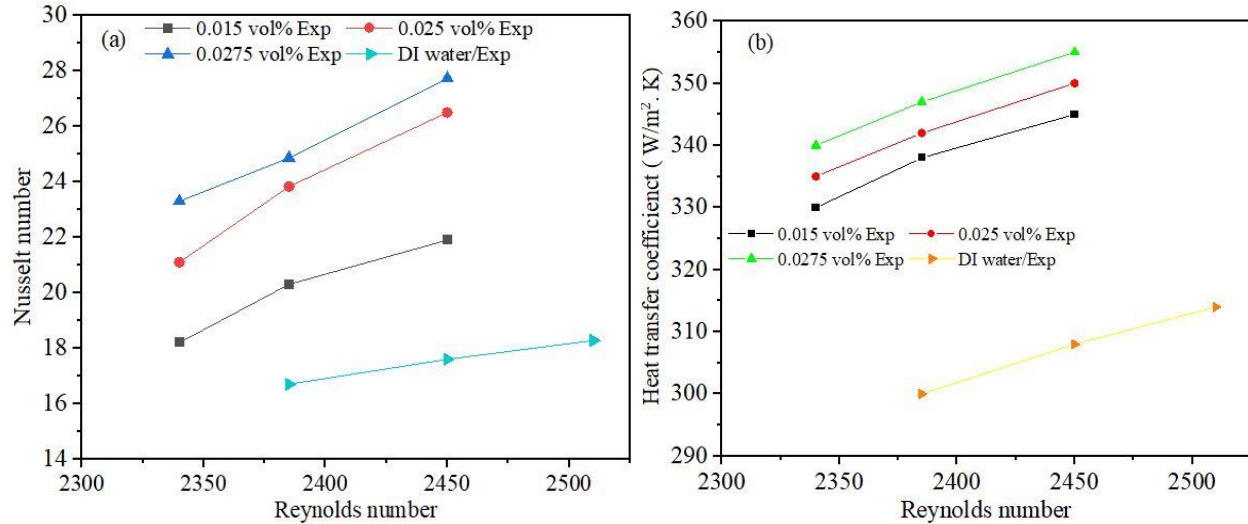


Figure 45. Effect of Reynolds number and volume concentration on (a) Nusselt number and (b) heat transfer coefficient

Figure 46 (b) shows the effect of increased volume concentration and Reynolds number on the decrease of friction factor. Compared with DI water, the friction factor of ZrO<sub>2</sub> nanofluid was high, which returned to the increased viscosity of nanofluids. At a high Reynolds number with 0.1% volume concentration, the friction factor was 0.37 higher than DI water, which recorded 0.29 due to lower density.

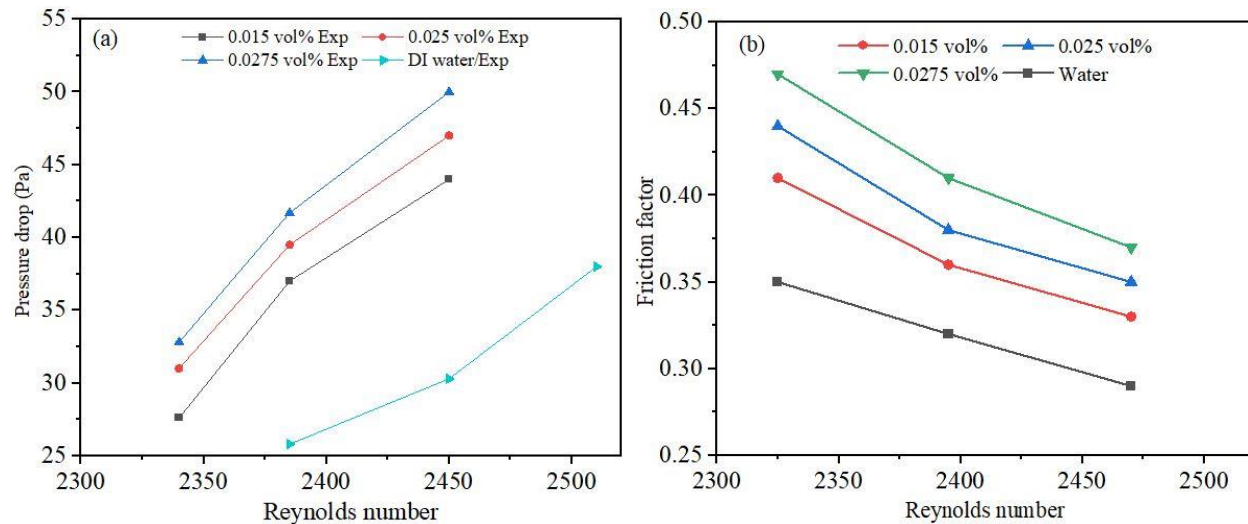


Figure 46. Effect of Reynolds number and volume concentration on (a) friction factor and (b) pressure drop

### 5.2.2.2 Exergy analysis results

Depending on the second law of thermodynamics, this subsection evaluates the effect of using ZrO<sub>2</sub> nanofluid and water on the thermal exergy and electrical exergy efficiency, entropy generation and exergy losses of the PVT system. Based on Eq. (40), the inlet exergy that comes from solar irradiation has been calculated for the maximum, average and minimum solar exergies

during experiments days to be  $997 \text{ W/m}^2$ ,  $668.33 \text{ W/m}^2$  and  $328.58 \text{ W/m}^2$ , respectively. Figure 47 (a) shows the value of the thermal exergy that was significantly lower than the electrical exergy due to the closer of the fluid outlet temperature of the PVT system to the ambient temperatures. The output thermal exergy is influenced by the specific heat of the working fluid and mass flow rate. Due to the high thermal properties of the nanofluid, it was noticed that the thermal exergy is enhanced more with the  $\text{ZrO}_2$  nanofluid than with water.

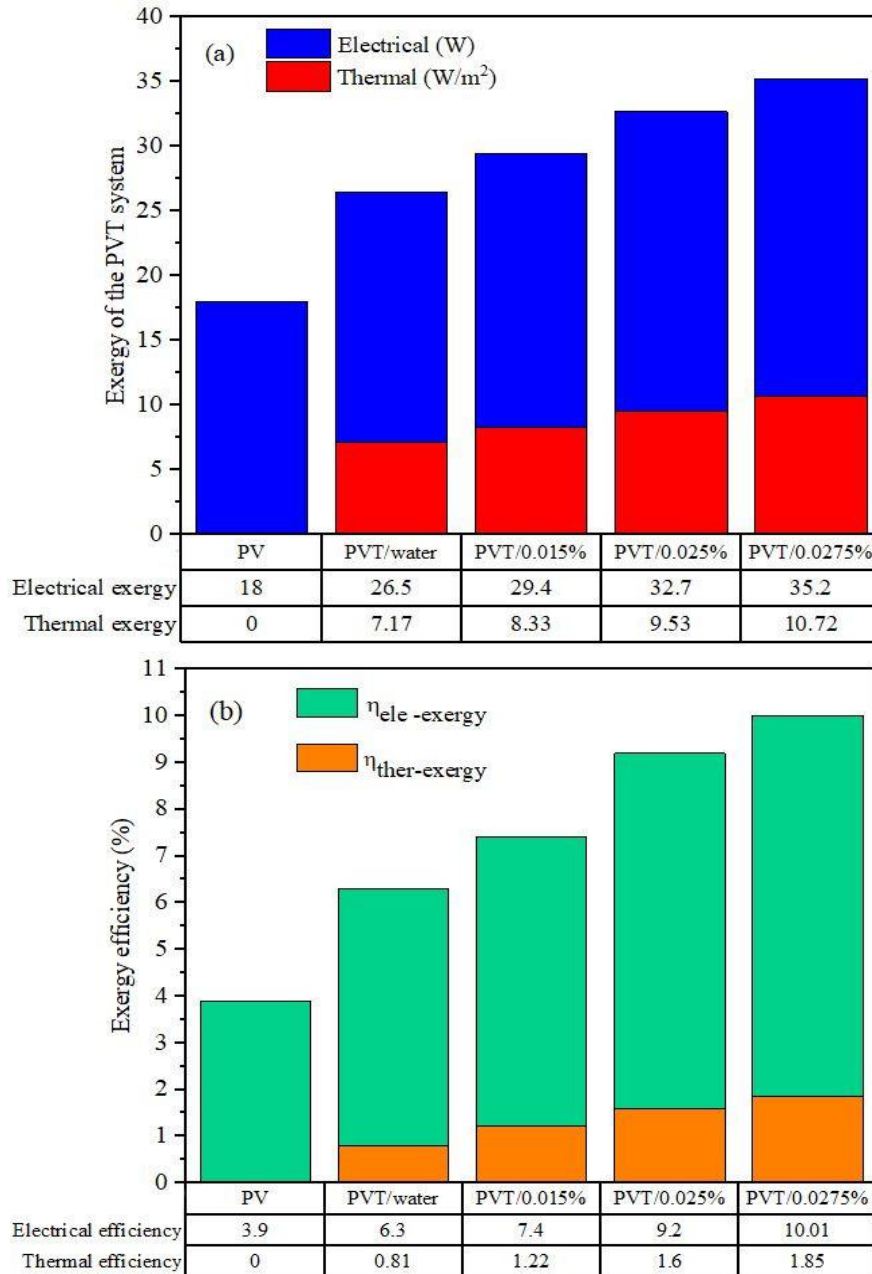


Figure 47. Exergy of the PVT system (a) electrical and thermal exergy (b) electrical and thermal efficiency

To evaluate the quality of the thermal and electrical efficiencies, Figure 47 (b) shows the effects of  $\text{ZrO}_2$  nanofluid on the PVT system's thermal and electrical exergy efficiencies. The low

thermal exergy value significantly affects the thermal exergy efficiency; however, a relative increment of the thermal exergy was noticed by increases in the volume concentrations of  $ZrO_2$  nanofluid compared with DI water. The overall exergy efficiency is impacted by the thermal exergy efficiency, the electrical exergy efficiency, the exergy of solar radiation and ambient temperature. Thereby, the exergy efficiency effectively contributes to the increment of the overall exergy efficiency of the PVT system, the maximum overall exergy efficiency obtained at 0.0275 vol% is 11.86%, while cooling by DI water was 7.11%, which confirms the feasibility of  $ZrO_2$  nanofluid as a working fluid. Using nanofluids as a coolant for the PVT system instead of conventional fluids help enhances the performance of the PVT system due to its high thermal conductivity that increases the convective heat transfer. Evaluation of each thermodynamic system's exergy loss and entropy generation is important for specifying the system losses and irreversibilities. In this case, the exergy loss of the PVT system was calculated using Eq. (40) with  $ZrO_2$  nanofluid and DI water. Figure 48 (a) shows the high exergy losses of the PVT system and PV module without cooling due to a drop in the overall exergy efficiency of the systems lower than the input exergy, specifically thermal exergy efficiency and increased temperature of the PV module surface.

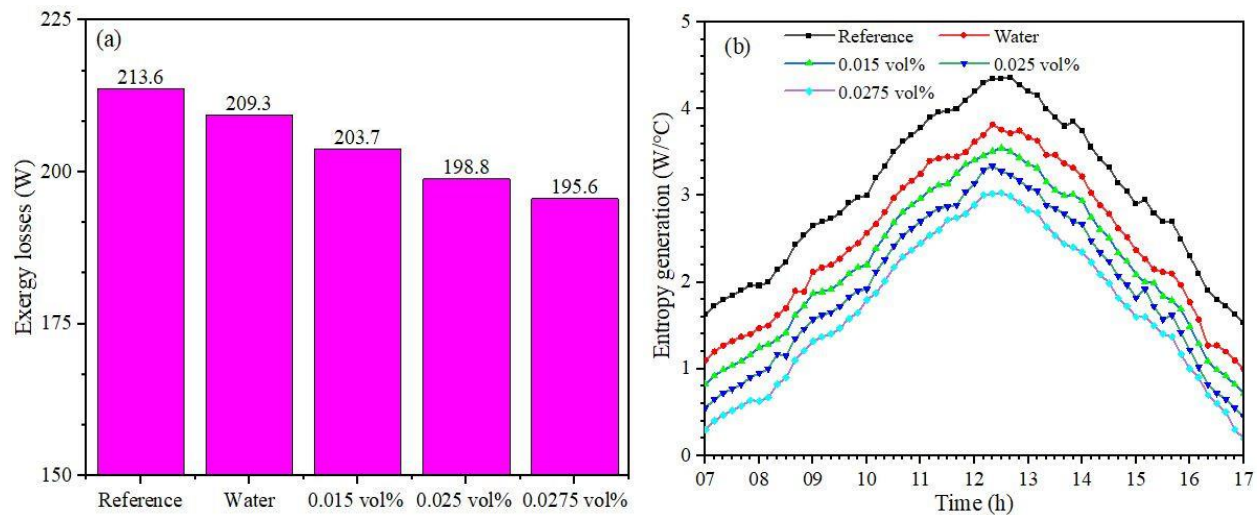


Figure 48. Exergy evaluation of the PVT system (a) exergy losses (b) entropy generation

### 5.2.3 New contributions results

#### Contribution 2

The passive cooling applied in the first case showed sustained performance of the PV modules in hot conditions. The energy yield, efficiency and exergy analyses were investigated based on the results of the experiment as follows:

- The CWIWs technique has good potential cooling to control the heat of the PV module, lower cost, and has an easy configuration with less water consumption.
- The CWIWs attached to the backside of the PV module are effective passive cooling techniques that contributed to reducing the PV module temperature by 22% compared with the PV module without cooling. The moist condition resulting from the cotton bristles immersed in water and exposed to the wind has provided appropriate cooling that enhances efficiency to 7.25 % and the power yield increment of about 16.3 W.

- Using CWIW's decreases the entropy generation of the PV module by 14.32% due to reducing the losses exergy by 14% of the PV module compared to the PV module without cooling. The electrical energy (output power) was the same as the electrical exergy, and the exergy efficiency of the PV module with evaporating cooling was higher than the PV module without cooling.
- The passive cooling applied enhanced the performance of the PV module higher than in another similar study, making it more reliable for application.
- Significant power yield deterioration and the PV modules' efficiency were observed due to the PV cell's temperature increase to 56.4 °C.

### **Contribution 3**

The second case investigated the effects of cooling PV modules using ZrO<sub>2</sub>/water nanofluids and water on their thermal behaviour, energy, and exergy. Different volume concentrations of ZrO<sub>2</sub> nanoparticles have been applied in water to investigate their effect on heat transfer coefficient, Nusselt number fraction factor and pressure drop compared with water as a coolant. Based on the results, the conclusions are summarized as follows:

- Improving the thermal conductivity of ZrO<sub>2</sub> nanofluid leads to increasing the heat absorption at the backside of the PV module, then reduces the PV module temperature to 21.2% compared to water. Reduced the PV module temperature effectively increased the electrical power to 33.72 W.
- The electrical and thermal efficiency was enhanced by using nanofluids, which positively reflected the overall efficiency of the PVT system increased to 60% compared with water at 0.0275 vol%. Increased nanoparticle concentration increased the thermal conductivity of nanofluids, and then more heat was absorbed from the PV module.
- Increasing the volume concentration of ZrO<sub>2</sub> nanoparticles in base fluid and Reynolds number has enhanced the heat transfer coefficient and Nusselt number due to the increase in the thermal conductivity of the nanofluid. On another side, the density and viscosity have increased, which causes reduced friction factors and increased pressure loss.
- Exergy analysis indicates lower thermal exergy of the PVT system than electrical exergy, which is attributable to the closing of the fluid outlet temperature of the PVT system to the ambient temperatures. Despite that, a remarkable relative increment of the thermal exergy has been found with increases in the volume concentrations of ZrO<sub>2</sub> nanofluid compared with water.
- The overall exergy efficiency is affected by the thermal and the electrical exergy efficiencies, which incremented with using nanofluid by 11.86 at 0.0275 vol% compared with water due to the high thermal conductivity enhancing of the convective heat transfer.
- Exergy losses and energy generation has reduced by 7 % and 26% at 0.0275 vol% compared to water because of their effects on convective heat transfer. The PV module, without cooling, is exposed to significant degradation in its performance.

## Chapter 6

### Effect of active cooling by nanofluids on the PVT system efficiency

This chapter consists of five experimental case studies, which applied mono nanofluids and a new hybrid nanofluid as cooling fluids, in addition to DI water as a reference cooling fluid used with a PVT system:

The first case study investigates the effects of CuO nanoparticles at different volume concentrations that dispersion in DI water on the PVT system performance. The results obtained are compared with previous studies to show the effectiveness of the nanofluid prepared and the cooling method on the PVT energies produced.

The second case study investigates the effect of TiO<sub>2</sub> nanowire, which has been synthesized and prepared with specific mixing ratios to cool the PV cells and enhance their efficiency by reducing their temperature. Then exploit the heat extracted from the backside of the PV module to maximize the thermal energy depending on the improved thermal properties of TiO<sub>2</sub> nanofluid.

The third case study investigates the effect of Fe<sub>2</sub>O<sub>3</sub> nanorod dispersion in DI water on the PVT system's electrical power generation and efficiency. Then determining the enhanced percentage of the electrical power and efficiencies of the PVT system at different volume concentrations.

The fourth and fifth cases investigate the effects of a new hybrid nanocomposite such as TiO<sub>2</sub>-Fe<sub>2</sub>O<sub>3</sub> and TiO<sub>2</sub>-CuO at different volume concentrations that dispersion in DI water on the energy and exergy of the PVT system. These cases are characterized by the comprehensive study of the PVT system according to the laws of thermodynamics (first and second laws) to demonstrate the quantity and quality of the energies produced by the PVT system. Then compared, the result obtained by previous studies by considering parameters such as system size, nanofluid type, volume concentrations, and operating conditions to show the effectiveness of the new hybrid nanofluid as a cooling fluid in the PVT system.

#### 6.1 Instruments used in experiments

Experiments were conducted in Miskolc city, Hungary, on typical sunny days from 8:30 am to 3:00 pm. Two polycrystalline PV modules of 50 W were used. The first PV module was referenced without cooling, and the second PV module was cooled with DI water as conventional fluid and then cooled with mono and hybrid nanofluids. The PVT modules consist of a copper absorber plate integrated with serpentine copper tubes soldering together and attached at the backside of the PV module by thermal grease HP, which has high thermal conductivity. High-performance insulation type SLENTEX was placed on the copper pipes, and an aluminium plate covered the PV module. The PV modules have fixed with a tilt angle of 14.8° towards the southern. Four thermocouples (T type) were placed on each surface, the backside of the PV modules, the PVT system, the inlet, the outlet of the PVT system, the inside nanofluid tank, and the water tank. The outlet of the PVT system is connected to a copper coil placed inside the water tank, and the outlet of the coil is linked to the nanofluid tank. Figure 49 shows the experimental setup of the reference PV module and PVT system. Data logger type National instrument model NI cDAQ-9178 consists of 24 channels for measuring temperatures, voltage, current of PV modules, solar radiation, and flow rate. The data logger connected with IN SignalExpress 2015 software for recording and reading the data every 10 minutes; Table 10 shows the measurement devices and sensors' specifications used in the current study.

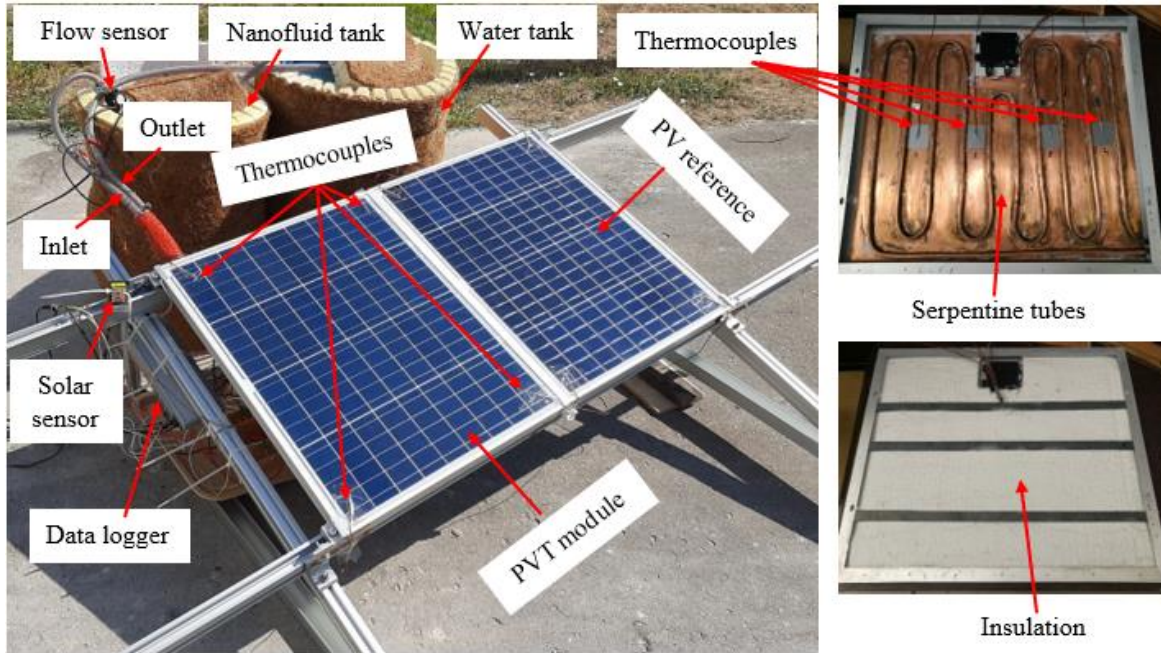


Figure 49. A sight of the experimental setup

Table 10. Specifications of the measurement devices and sensors

Item	Model/Brand	Range	Accuracy
Thermocouples	T-type 0.2 mm	-250°C to 400°C	± 0.5 °C
Solar sensor	SS11.303	1-3999 W/m <sup>2</sup>	± 0.1 W/m <sup>2</sup>
Flow rate sensor	YF-S201	1-30 L/min	±10%
Electronic scale	BOECO BAS	3 kg	0.0001 g
Current sensor	ACS712	up to 30 A	0.04 A
Voltage sensor	Module 25V	up to 25 V	0.02445 V
Pump	AD20P-1230C	240 L/H	-----
Ultrasonication	Bransonic	240V, Vf: 48 kHz	-----

## 6.2 Effect of DI water on the PVT system efficiency

To the investigation effect of cooling the PV module on their performance, this case employed DI water as a cooling fluid of the PVT system and compared their performance with the reference PV module. Figure 50 (a) shows the variation of solar radiation and ambient temperature; the maximum solar radiation was 940.17 W/m<sup>2</sup> and the ambient temperature was 37.6 °C. Rising PV cell temperature represents a critical problem facing the conversion efficiency of PV cells, which causes degradation in their performance. Under standard test conditions (25 °C and 1000 W/m<sup>2</sup>), the PV module gives maximum efficiency; in reality, that is difficult to achieve due to the weather fluctuation during the day. The direct incident solar

radiation on the PV module raised the temperature of the PV cells to a high level, significantly decreasing their efficiency. Figure 50 (b) shows the reference PV module temperature, which rises to 55.6 °C at 12:20 pm; this temperature range cause lowers the PV module efficiency

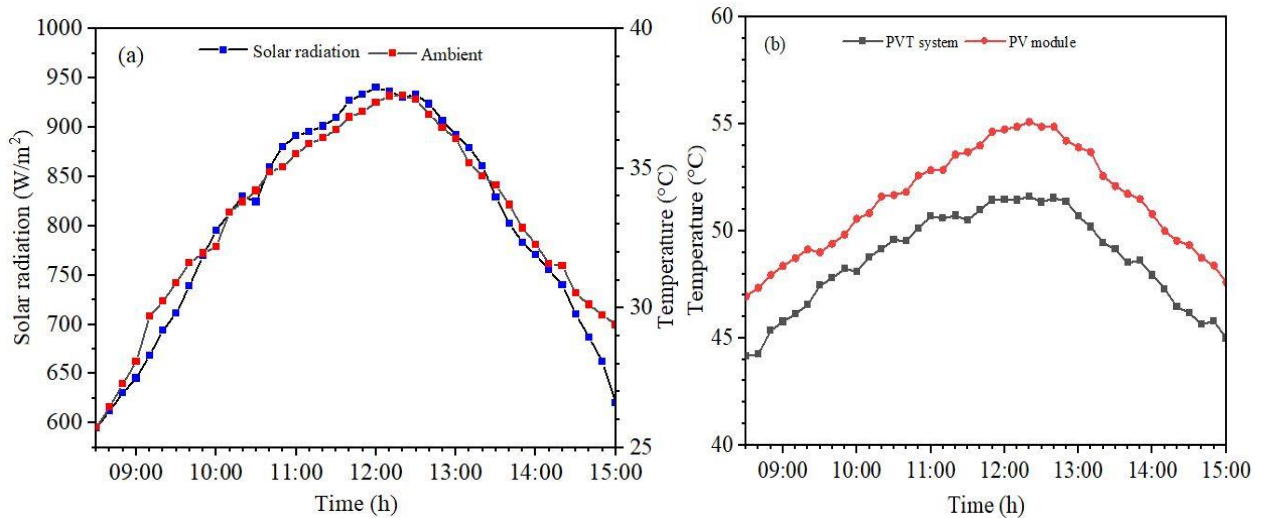


Figure 50. The various values of (a) solar radiation and ambient temperature and (b) temperature of the PV module

In contrast, the circulated DI water was into serpentine tubes that were soldered on absorb plate attached at the back side of the PV module to reduce the PV cell's temperature to 51.6 °C. Due to the removal of the heat from the backside of the PV module and the effect of the increase of heat convection between tubes and DI water into tubes, which helped to reduce the PV cell's temperature by 6.74% compared to the reference PV module.

Reduced the PV cell's temperature positively affects the electrical power of the PV module performance, which confirms the necessity of cooling the PV module at rising temperatures. Figure 51 (a) shows the lowering of the electrical power of the reference PV module, which recorded 19.32 W. It is observed that the electrical efficiency of the PVT system was higher than the reference PV module due to cooling by DI water which helps to reduce the PV temperature and boosts the electrical power yield of the PVT system. Thus, cooling the PVT system with DI water at a constant mass flow rate of 1.4 L/min reduced PV module temperatures and contributed to enhancing the electrical power of the PVT to 22.19 W. Circulation of DI water in serpentine tubes helped to remove the heat of the PV cells and to maximize the thermal efficiency of the PVT system which recorded maximum value at noon is 30.25%. Figure 51(b) shows the maximum electrical efficiency of the PVT system recorded at 12:30 pm is 6.32 %, while the reference PV module recorded 5.11%, which reflects the capacity of the DI water as a cooling fluid. The electrical and thermal efficiency significantly contribute to the increased overall efficiency of the PVT system to 36.57%.

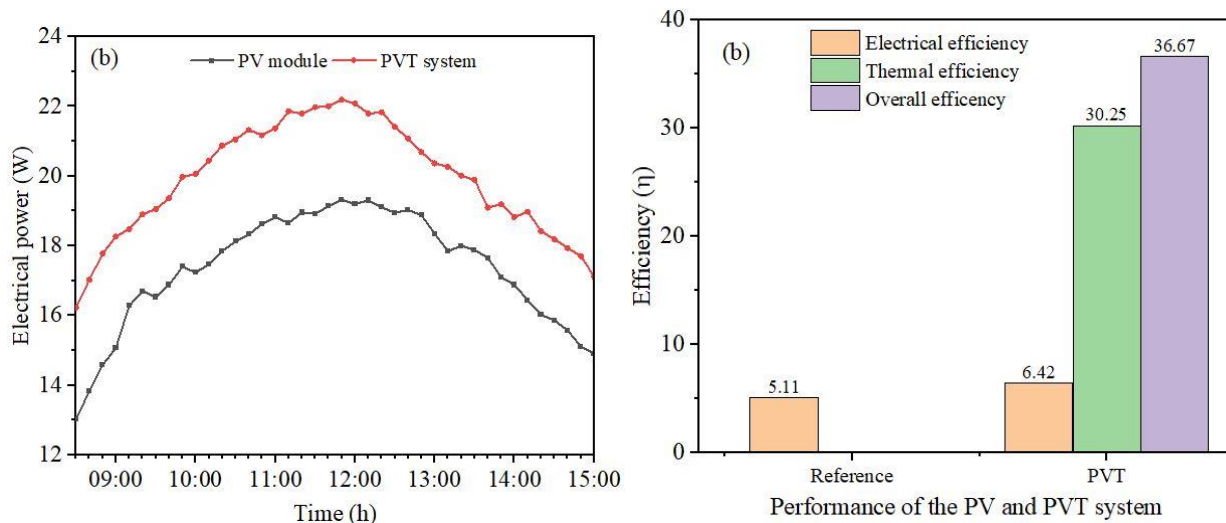


Figure 51. Performance of the PV, PVT system (a) electrical power, and (b) efficiency

### 6.3 Effect of CuO nanofluid on the PVT system efficiency

According to the climatic conditions of Miskolc city, the weather was sunny, and no significant variation was recorded regarding the solar radiation and the ambient temperature measured during the experiment period. The hourly variations of solar radiation and ambient temperature were recorded from 8:30 am. to 3 pm. Figure 52 (a) shows the maximum solar radiation values, which recorded  $941.48 \text{ W/m}^2$ , and the ambient temperature was  $35.75 \text{ }^\circ\text{C}$ , specifically at 12:30 pm. It can observe that the ambient temperature is directly proportional to solar radiation, which both reduced with sunset. The thermocouples placed on the surface and backside of the PV module show the variation of the measured temperature compared with the PVT system. Because of the direct exposure to intensive solar radiation and increased temperature, the reference PV module recorded a higher temperature, reached to  $52.86 \text{ }^\circ\text{C}$ . The thermal properties of the CuO nanoparticle suspended in the base fluid have improved the convective heat transfer of the nanofluid. Thereby, using CuO nanofluid helps to reduce the temperature of the PVT system differently depending on the CuO volume concentration in the base fluid. Figure 52 (b) shows the average temperature of the PV module and PVT system at 0.2 vol% and 0.3 vol% nanofluids, which reduced to  $45.6 \text{ }^\circ\text{C}$  and  $42.82 \text{ }^\circ\text{C}$ , respectively. The high thermal properties of nanofluid circulated in the serpentine tubes placed on the PVT system's backside helped reduce the temperature by 16 % and 23.44% compared to the reference PV module. The electrical power of the PV module and PVT system is calculated by the voltage of the PV module, which is affected by the PV cell's temperature, and its current, which is affected by the intensity of solar radiation. Figure 53 (a) illustrates the electrical power generated by PV, PVT system with CuO nanofluid and without cooling throughout the testing. The maximum PV module voltage recorded at 12:20 PM was 20.78 W, at 0.2 vol% of CuO in the base fluids helped to increment the PVT system power to 32.76 W. In contrast, at 0.3 vol%, the electrical power increment to 35.47 W. Improved electrical power due to the high thermal conductivity of the CuO nanoparticles suspension into DI water increased the heat transfer rate of the backside of the PVT system and achieved effective cooling. Thereby suspensions of CuO nanoparticles into DI water have proven their ability to withdraw the heat of the backside of the PV module and improve the electrical power by 70.6%, 57.65% compared to the reference PV module.

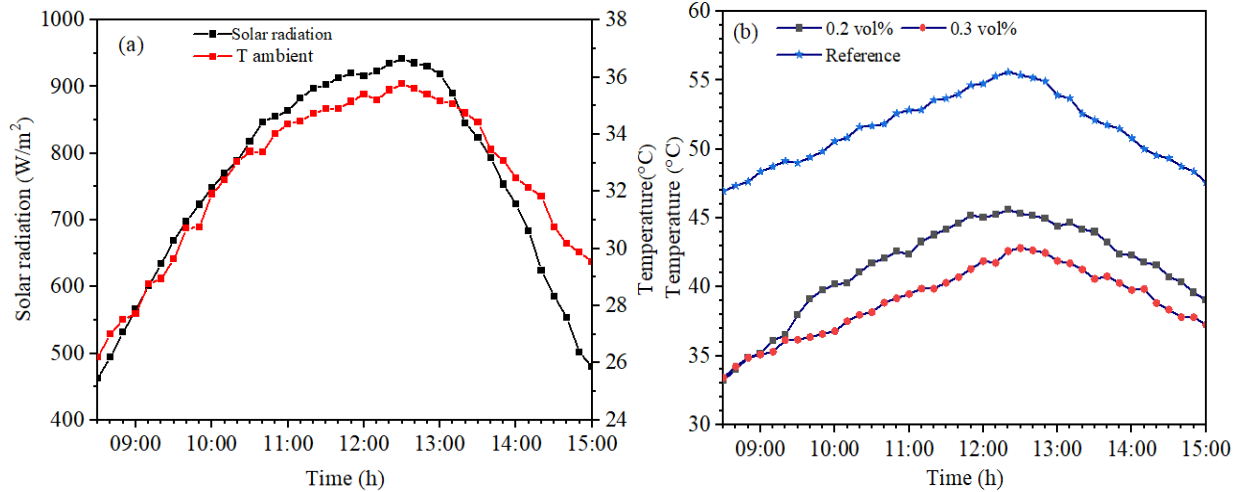


Figure 52. The average values of (a) ambient temperature and solar radiation, and (b) PV, PVT system temperature

Figure 53 (b) shows the efficiency of the PV module and PVT system, the intensity of solar radiances and rising temperature caused degradation of the electrical efficiency of the reference PV module, which was recorded by about 5.42%. Using CuO nanofluid improved the electrical power positively reflected in the electrical efficiency of the PVT system, which increments to 9.2%, 10.3% at 0.2 vol% and 0.3 vol, respectively. The heat of the backside of the PV module is dropped due to the circulated CuO nanofluid, which enhances the thermal energy of the PVT system and then improves the thermal efficiency of the PVT system. Figure 53 (b) shows the impact of CuO nanofluid on the thermal efficiency at different volume concentrations of CuO nanoparticles in the base fluids. The difference in temperature of the inlet and outlet of the nanofluid and the higher thermal properties of the nanofluid improve the thermal efficiency. Improving the thermal and electrical efficiencies led to increasing the PVT system's overall efficiency exponentially with an increasing volume concentration of CuO nanoparticles. Table 11 compares current results with previous studies results in the literature that used CuO nanofluid for cooling PVT systems. According to some factors such as the size of the PV module, the design of the heat exchanger applied, the flow rate used, and measurement conditions, the current results may not be the best among the results of other studies, but it was not the least.

Table 11. Performance of the PVT system compared with previous studies

Ref.	PV module power	Volume concentration (vol%)	Temperature reduction (°C)	Power increased (W)	Electrical efficiency (%)	Thermal efficiency (%)
Current study	50 W	0.2	7.2	11.9	9.2	36.7
		0.3	10.06	14.6	10.3	38.9
[114]	250 W	0.2	12	9.5	11.2	43
[31]	100 W	0.05	15	11.2	12.9	71.7
[115]	50 W	0.1	6	3.6	9.5	-

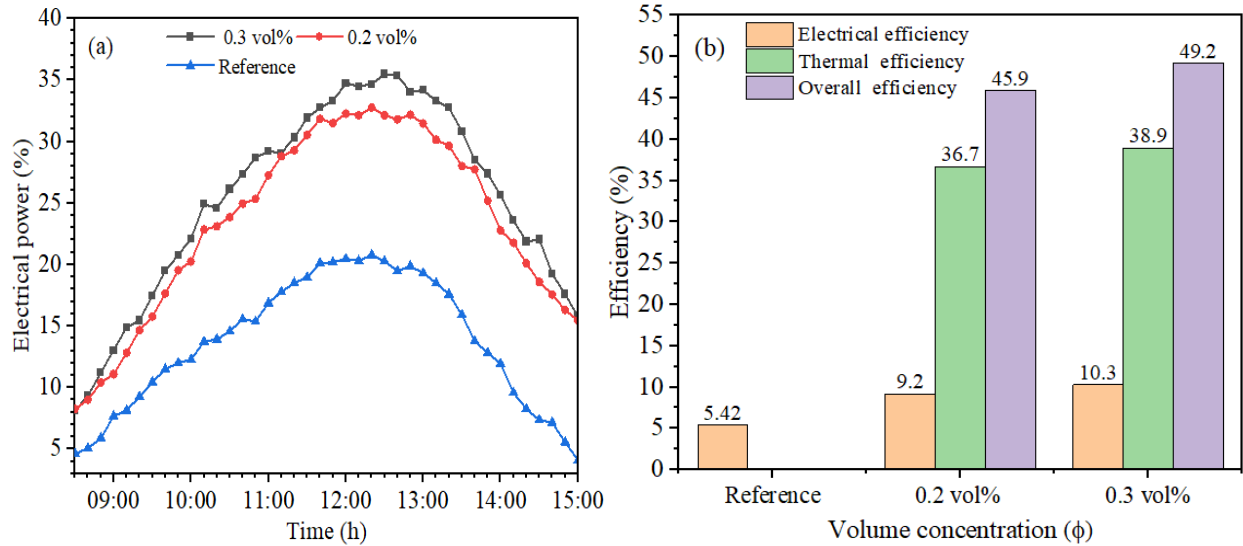


Figure 53. The performance of the PVT system (a) electrical power and (b) effect volume concentration on the efficiency

#### 6.4 Effect of TiO<sub>2</sub> nanofluid on the PVT system efficiency

In this case, TiO<sub>2</sub> nanofluids are used to cool PV modules and PVT systems under different solar radiation and ambient temperature values. Figure 54 (a) presents the solar radiation values during the experiment period, which gradually increases with operation hours until 12:20 PM, which recorded the maximum solar radiation is 918.9 W/m<sup>2</sup>, then lower with sunset. Rising the ambient temperature is associated with increased solar radiation intensity, in which the average ambient temperatures are variable along the experiment period. At the beginning of the experiment, the ambient temperature increased gradually, and the maximum ambient temperature was 34.16 °C at 12:20 PM. After that, it decreased to 30.83 °C when the experiment was over. The temperature of the PV module and the PVT system were measured by thermocouples placed on the surface and backside. The temperature measured at four points on the surface of the PV module and the back side also gives significant convergence between them, which is logical to depend on the average temperature. The temperature for the PV module and PVT system gradually increased during the day because of the increasing solar radiation and ambient temperature. The maximum temperature of the reference PV was recorded at 52.58 °C at 12:20 PM; this temperature range negatively influences the PV module performance. On the other side, using TiO<sub>2</sub> nanowires at different volume concentrations, 0.2 vol% and 0.3 vol% in the base fluid helps to reduce the PVT system temperature to 47.31 °C and 46.11 °C compared with the reference PV module, as shown in Figure 54 (b). The improved thermal properties of the TiO<sub>2</sub> nanowires suspended in the base fluid that circulated in the serpentine tubes help to remove the heat of the backside of the PVT system. Thus, reduced the PVT system temperature by about 5.27 °C at 0.2 vol%, while increasing the volume concentration to 0.3 vol% decreased the PVT system temperature by about 6.47 °C. The temperature increase of the PV modules during operation affects their performance due to reduced electrical power generation. Figure 55 (a) shows the PV module's electrical power drop compared with the PVT system cooled with TiO<sub>2</sub> nanofluid. Because of the rising PV module temperature, the maximum electrical power of the reference PV module was 21.15 W.

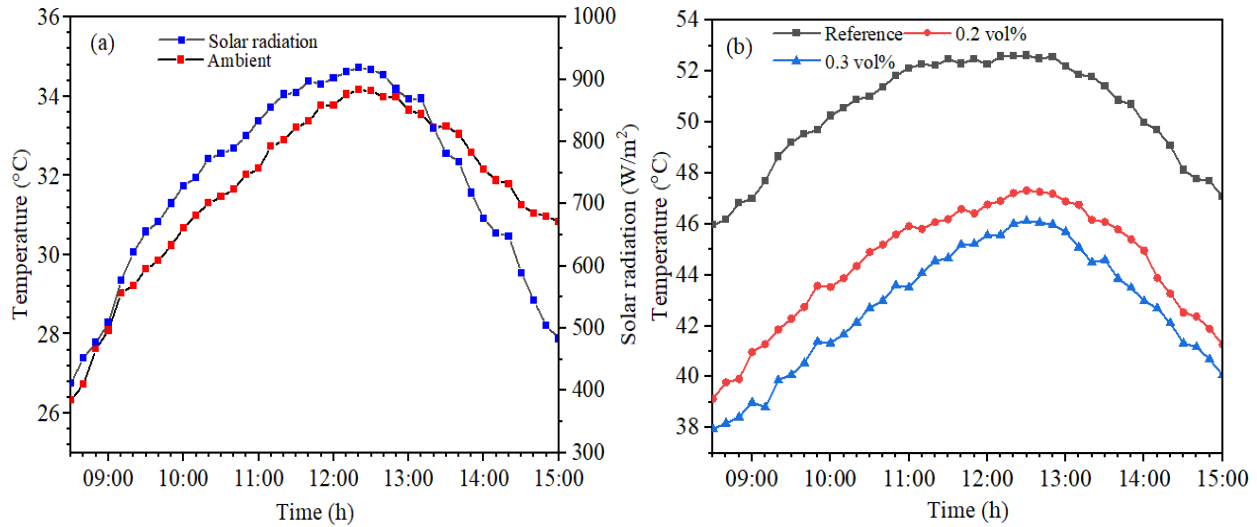


Figure 54. The variation values of (a) solar radiation and ambient temperature, and (b) temperature of the PV, PVT system

Employing TiO<sub>2</sub> nanofluid contributed to the increment of the electrical power of the PVT system to 30.31 W at 0.2 vol% and 31.66 at 0.3 vol% due to improving thermal properties of the TiO<sub>2</sub> nanofluid. TiO<sub>2</sub> nanofluid reduced PVT system temperatures and effectively improved the electrical power by 45.45% and 49.7 %, compared with the reference PV module, at increased volume concentration of 0.2 vol% and 0.3 vol% nanowires in the base fluid. Therefore, the excessive heat removed by the circulation of TiO<sub>2</sub> nanofluid into serpentine tubes maximizes the PVT system's thermal efficiency. Figure 55 (b) shows an increase in the suspension of TiO<sub>2</sub> nanowires in base fluid at 0.2 vol% and 0.3 vol%, incrementing thermal efficiency to 32.7% and 34.63%; thus, the overall efficiency increased to 40.32% and 43%. The PVT system exhibits a better performance with TiO<sub>2</sub> nanofluid as a cooling fluid by comparing reference PV modules, using TiO<sub>2</sub> nanowires at different volume concentrations, improving the PV module's thermal and electrical efficiency compared with DI water.

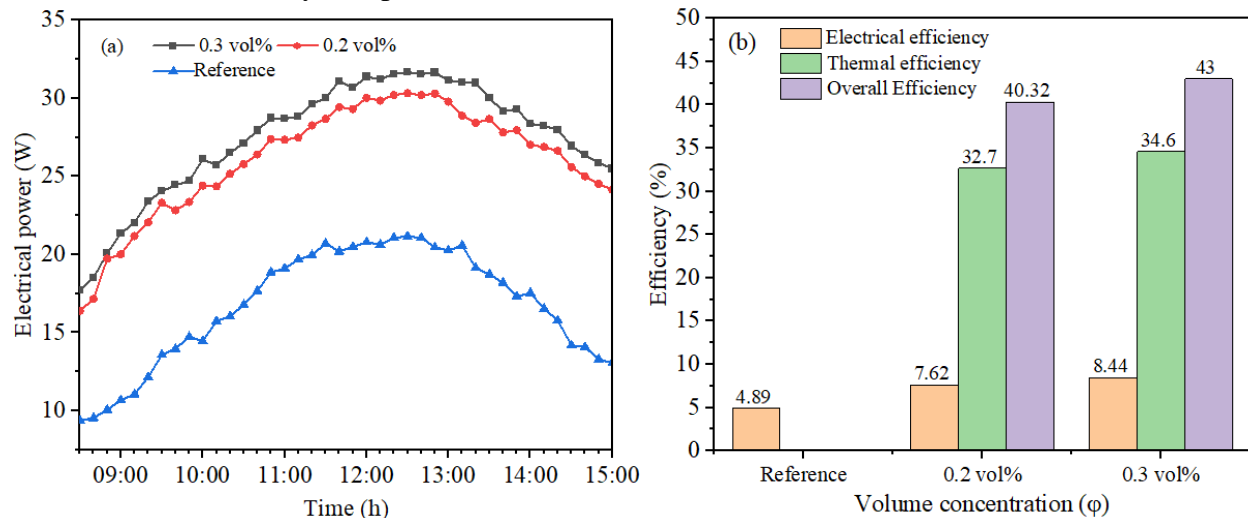


Figure 55. Performance of PVT system (a) electrical power, and (b) the overall efficiency

## 6.5 Effect of Fe<sub>2</sub>O<sub>3</sub> nanofluid on the PVT system efficiency

A gradually increased solar radiation intensity was recorded from the first morning hours and continued to reach its maximum value of 925 W/m<sup>2</sup> at 12:30 PM. By the increase of solar radiation intensity, an increase in the ambient temperature was recorded at 12:40; the maximum ambient temperature was 32.97 °C. Figure 56 (a) shows the variation value of the solar radiation and ambient temperature during the experiment. Four thermocouples were placed at different points on both sides of the PV module and PVT system to measure the temperature during the experiment. In this case, iron oxide Fe<sub>2</sub>O<sub>3</sub> nanofluid was used for cooling the PVT system, and two volume concentrations of Fe<sub>2</sub>O<sub>3</sub> nanorod (0.2 vol% and 0.3 vol%) were suspended in the base fluid. The nanofluid is circulated inside serpentine tubes at 1.4 L/min to increase the heat removal of the PVT system backside. The performance of the reference PV module is degraded due to increased temperature; at noon, the maximum temperature of the reference PV module was 50.9 °C, as shown in Figure 56 (b).

In contrast, using Fe<sub>2</sub>O<sub>3</sub> achieved a remarkable decrease in the PVT system temperature. Suspended 0.2 vol% of Fe<sub>2</sub>O<sub>3</sub> in base fluid improved the convection heat transfer, which helped to reduce the PVT system temperature to 42.6 °C. Increased the volume concentration to 0.3 vol% decreases the temperature to 39.26 °C; this confirms the ability to use Fe<sub>2</sub>O<sub>3</sub> nanofluid for cooling and improve the PVT performance compared with water cooling. Thus, reducing the PVT system temperature by 19.45% and 29.64% led to improved PVT system performance. Figure 57 (a) demonstrates that using Fe<sub>2</sub>O<sub>3</sub> nanofluid improves the electrical power due to lowered PVT system temperature compared to the reference PV module. The reduced temperature is attributed to the enhancement of the Fe<sub>2</sub>O<sub>3</sub> nanofluid thermal conductivity, then enhanced convective heat transfer between the Fe<sub>2</sub>O<sub>3</sub> nanofluid circulated in tubes and the backside of the PVT system. It observed an increment of the electrical power of the PVT system with an increase in the Fe<sub>2</sub>O<sub>3</sub> nanorod in the base fluid; at 0.2 vol and 0.3 vol%, the electrical power increased to 36.7 W and 37.76 W, respectively. The electrical power of the reference PV module was recorded at about 21.37 W. Thereby, using Fe<sub>2</sub>O<sub>3</sub> nanofluid has improved the electrical power to 71.73% and 76.68 % compared with the reference PV module.

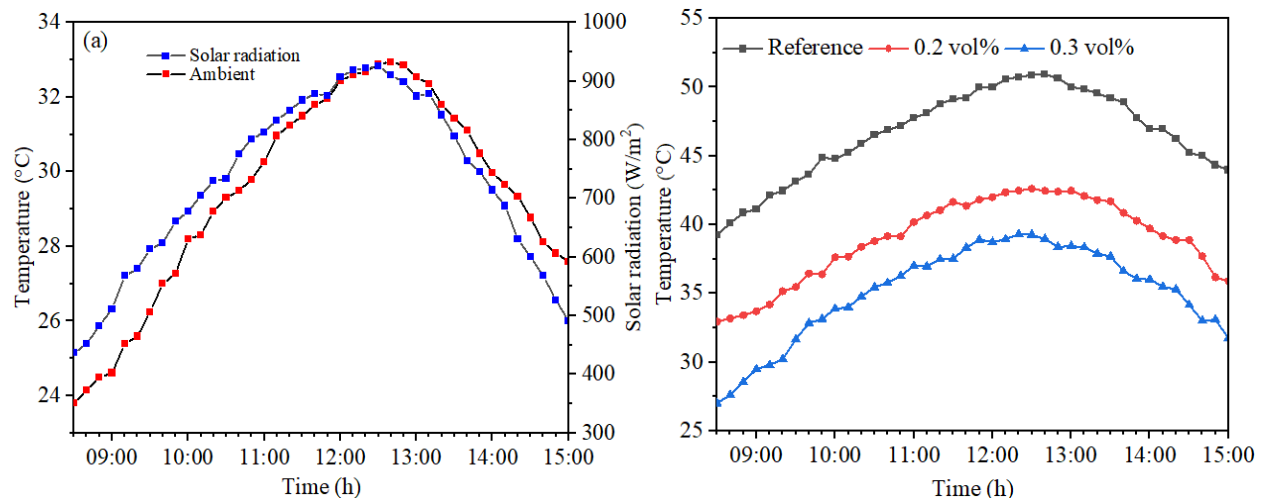


Figure 56. The variation value of (a) Solar radiation and ambient temperature, and (b) temperature of the PV, PVT system

Thus, improved output electrical power of the PVT system has positively reflected the electrical efficiency. Figure 57 (b) shows the maximum electrical efficiency of the reference PV module, which was 5.75 %, which confirms the effect of the rising temperature on the PV module efficiency. The maximum electrical efficiency of the PVT system using  $\text{Fe}_2\text{O}_3$  nanofluid was 11.3% and 12.1 at 0.2vol% and 0.3 vol%, respectively. Improved the heat transfer convection between the backside of the PV module and the circulating nanofluid in the heat exchanger attached at the back side of the PVT system contributed to removing the heat of the PVT system. Thus, a gradual increase in the thermal efficiency with increased volume concentrations of the  $\text{Fe}_2\text{O}_3$  nanorod in the base fluid. The maximum thermal efficiency recorded at 0.2 vol% was 40.8%, while at 0.3 vol%, the thermal efficiency increments to 43.3%. The overall efficiency of the PVT system is the summation of thermal and electrical efficiencies; with increasing the volume concentrations in the base fluid, the overall efficiency increments to 52.1% and 55.4%.

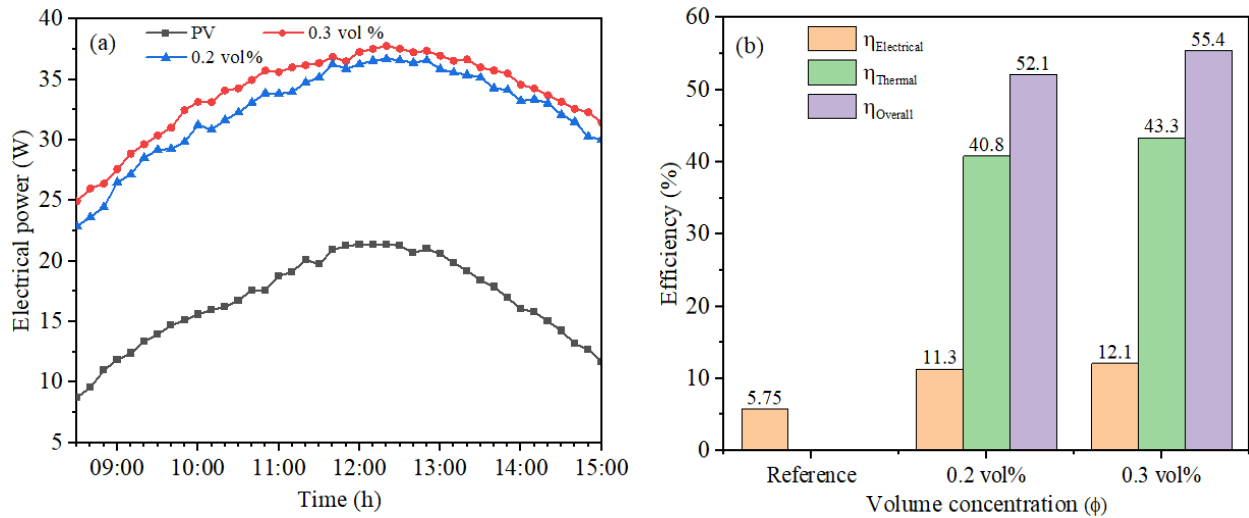


Figure 57. Performance of PVT system (a) electrical power, and (b) the overall efficiency

## 6.6 Effect of hybrid $\text{TiO}_2\text{-Fe}_2\text{O}_3$ nanofluid on the PVT system efficiency

### 6.6.1 Energy analysis results

A hybrid  $\text{TiO}_2\text{-Fe}_2\text{O}_3$  nanofluid and DI water have been employed as a cooling fluid to improve the PVT system performance and compare their performance with the reference PV module. The performance PVT system is influenced by the rise in temperature and the incident solar radiation during the day. Figure 58 (a) shows the average solar radiation values and ambient temperature recorded during the experiment days. The maximum solar radiation recorded was  $899.23 \text{ W/m}^2$  at 12:30 pm. The ambient temperature is about  $32.76 \text{ }^\circ\text{C}$ . Thus, increased solar radiation coincides with rising ambient temperature, which affects the PV cells by reducing their conversion efficiency. Figure 58 (b) shows the temperature of the PV module and PVT system from the experiment's beginning until the period's end. The maximum temperature of the reference PV module was recorded at  $49.85 \text{ }^\circ\text{C}$  at noon when the ambient temperature of  $32.76 \text{ }^\circ\text{C}$  increased the PV cell's temperature and caused decreased electrical efficiency. Circulation of DI water in the PVT system reduces the temperature of the PV cells to  $45 \text{ }^\circ\text{C}$  due to removing the heat from the backside of the PV module. Using hybrid nanofluid as a cooling fluid reduced the temperature of the PV cells, and loading of  $\text{CuO}$  NPs over the  $\text{TiO}_2$  NWs has increased the surface area of the nanocomposite suspended in the base fluid and improved the thermal

characteristics, which led to an increase in convective heat transfer and a decrease in the PV module temperature. The circulation of hybrid  $\text{TiO}_2\text{-Fe}_2\text{O}_3$  nanofluid at volume concentrations 0.2 vol% and 0.3 % inside the serpentine tubes helps to increase the heat transfer convection and extract excessive heat of the PV module, then reduced the temperature to  $37.46^\circ\text{C}$  and  $36.37^\circ\text{C}$ . Compared to the reference PV module, cooling by DI water decreased the PV module temperature by 10.7%, cooling by hybrid nanofluid at 0.2 vol%, 0.3 vol% reduced the PV module temperature by 33% and 37%, which confirms the ability of hybrid  $\text{TiO}_2\text{-Fe}_2\text{O}_3$  nanofluids as a cooling fluid.

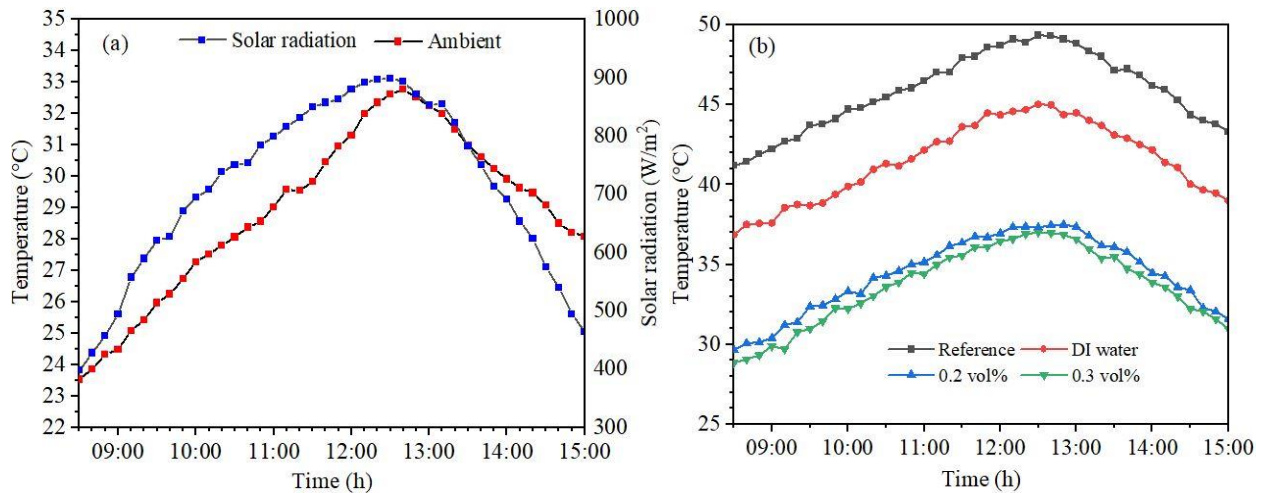


Figure 58. The variation values of (a) solar radiation and ambient temperature, (b) temperature of PV and PVT system

The electrical power of the reference PV module was low because of the rising temperature, which affected the PV cell conversion efficiency. Maximum electrical power was recorded at 23.14 W; reduced PV cells temperature helped to increment the electrical power. Figure 59 (a) shows the effect of DI water, hybrid nanofluid on the electrical power of the PV and PVT system, using DI water as a cooling fluid increment of electrical power of the PVT system to 27.22 W. Increased  $\text{TiO}_2\text{-Fe}_2\text{O}_3$  nanomaterials suspension in the base fluid enhanced the thermal properties of the working fluids, which positively reflected of the electrical power produced of the PVT system. Using nanofluids at different volume concentrations of 0.2 vol% and 0.3 vol% at constant mass flow rate incremented the electrical power output of the PVT system by 38.95 W and 39.71W, respectively. Compared with the electrical power of the reference PV module, using DI water and hybrid nanofluid at 0.2% and 0.3% enhanced the electrical power by 17.63%, 68.32% and 71.6%, respectively. The hybrid nanofluid, characterized by higher thermal properties than DI water, increased the volume concentration of hybrid nanocomposite in the base fluid, increasing the heat transfer coefficient of the nanofluid thus, more heat removed from the PV cells and maximizing the thermal energy of the PVT system. The increment of electrical power has increased the PVT system's electrical efficiency compared with the reference PV module. Figure 59 (b) shows the electrical efficiency of the reference PV module and PVT system cooling by DI water and hybrid nanofluid. At maximum solar radiation and ambient temperature, the electrical efficiency of the reference PV module was 5.7%. Enhanced electrical power of the PVT system directly affects the electrical efficiency of the PVT system due to cooling. The maximum electrical efficiency of the PVT system was 7.1%, 12.44% 12.62% at cooling by DI water and hybrid nanofluid at 0.2 vol% and 0.3 vol%.

On the other hand, increased volume concentrations of hybrid nanocomposite in the base fluid by increment the thermal efficiency of the PVT system compared with DI water. Circulation of hybrid nanofluid into tubes helps to increase the heat removal by convection and increment thermal efficiency to 45.4% and 48.2% at 0.2 vol% and 0.3 vol% respectively, while used DI water has incremented the thermal efficiency to 32.6%. The overall efficiency is the sum of thermal and electrical efficiencies; maximum overall efficiency has been recorded using a hybrid nanofluid at 57.84% and 59.82% compared with DI water, which was 39.7%. This is attributed to the high thermal properties of the hybrid  $\text{TiO}_2\text{-Fe}_2\text{O}_3$  nanofluid. The results obtained are compared with previous studies to show the ability of  $\text{TiO}_2\text{-Fe}_2\text{O}_3$  nanofluids as a cooling fluid to improve the PVT system performance, as shown in Table 12. Considering some factors, such as the size of the PVT system, the nanofluids used and volume concentrations of nanocomposite in the base fluid, measurement conditions, and their effect on temperature drop, the thermal and electrical energy efficiencies of the PVT system. The present results may not be better than the results in the literature studies, but its highlight of a new type of nanofluid that can use as a cooling fluid helps to improve the energy and exergy of the PVT system. The employed volume concentrations of the hybrid  $\text{TiO}_2\text{-Fe}_2\text{O}_3$  nanocomposite enhanced PVT performance compared with DI water and achieved better performance than other studies that used different nanofluids, which confirmed the effectiveness of the applied nanofluid. Dispersion of  $\text{TiO}_2\text{-Fe}_2\text{O}_3$  nanocomposite in the host fluid causes an improvement in their thermal properties because the nanomaterials have higher thermal properties than conventional fluids. This study investigated the influence of adding  $\text{TiO}_2\text{-Fe}_2\text{O}_3$  nanocomposite at different volume concentrations in DI water on Reynolds number, heat transfer coefficient, Nusselt number, pressure drop and friction factor. Depending on the maximum, average and minimum, it has calculated heat transfer coefficient, Nusselt number, pressure drop, and fraction factor from Eq. (15-17).

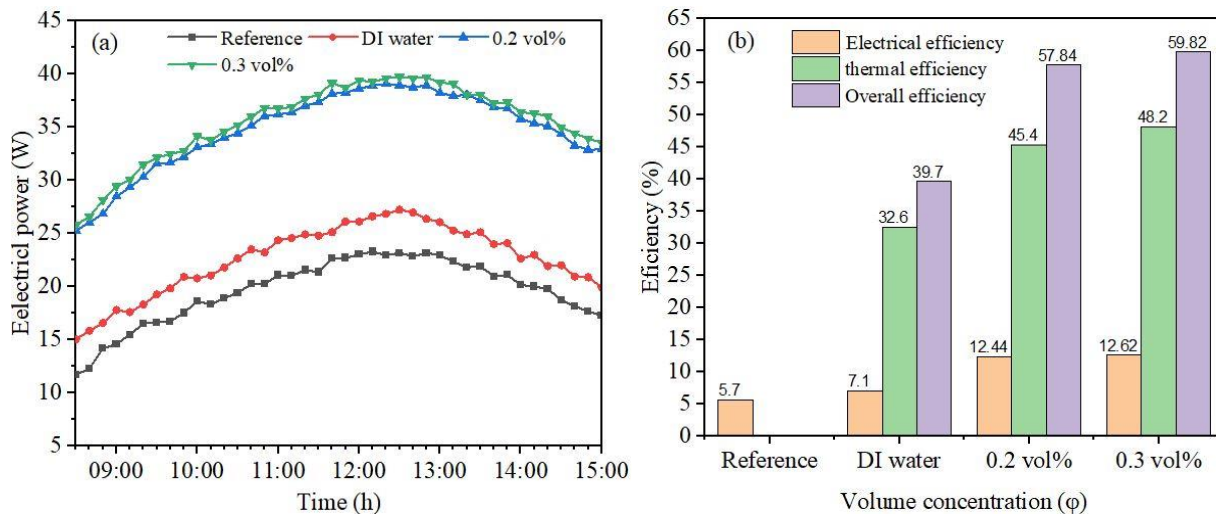


Figure 59. Performance of the PV and PVT system (a) electrical power, (b) overall efficiency

Figure 60 (a) shows the effect of increased volume concentration of the  $\text{TiO}_2\text{-Fe}_2\text{O}_3$  nanocomposite on the Nusselt number as a function of Reynold's number; it was gradually increased by Nusselt number with increased Reynold's number. Suspension of  $\text{TiO}_2\text{-Fe}_2\text{O}_3$  nanocomposite by 0.2 vol% and 0.3 vol% in the base fluid enhanced the Nusselt number by 25 % at 0.3 %vol compared to the DI water. An increase in Nusselt numbers of the  $\text{TiO}_2\text{-Fe}_2\text{O}_3$  nanofluid has positively increased the heat transfer coefficient.

Table 12. Compare the energy result obtained by other previous studies

Ref.	PV module peak power	Type of nanofluid	Volume concentration %	Temperature drop %	Electrical efficiency %	Thermal efficiency %
Current study	50 Watts	TiO <sub>2</sub> -Fe <sub>2</sub> O <sub>3</sub>	0.2	12.04	12.44	45.4
		TiO <sub>2</sub> -Fe <sub>2</sub> O <sub>3</sub>	0.3	12.45	12.62	48.2
[116]	35 Watts	Al <sub>2</sub> O <sub>3</sub> /SiO <sub>2</sub>	0.5	19.2	1.99	9.09
[117]	250 Watts	Al <sub>2</sub> O <sub>3</sub> /ZnO-Fe <sub>3</sub> O <sub>4</sub>	1	5.14	13.43	54.11
[118]	250 Watts	Al <sub>2</sub> O <sub>3</sub> /ZnO	1.7	21	13.8	55.9
[119]	150 Watts	CNT/Al <sub>2</sub> O <sub>3</sub>	2	15	17.2	27.23

The increase in the Reynolds number has enhanced the heat transfer coefficient of the nanofluid. Figure 60 (b) shows the increase of the heat transfer coefficient with Reynold's number increased at different volume concentrations, which is attributed to the high thermal conductivity of the hybrid nanofluid. Adding 0.2 vol% and 0.3 vol% in DI water enhanced the heat transfer coefficient of hybrid nanofluid by 28.95% and 43.33%, which contributes to lower PV temperature more than DI water. Despite increasing the heat transfer coefficient due to increasing thermal conductivity, the density of the hybrid nanofluid is increased because of the volume concentration, which influences the pressure drop.

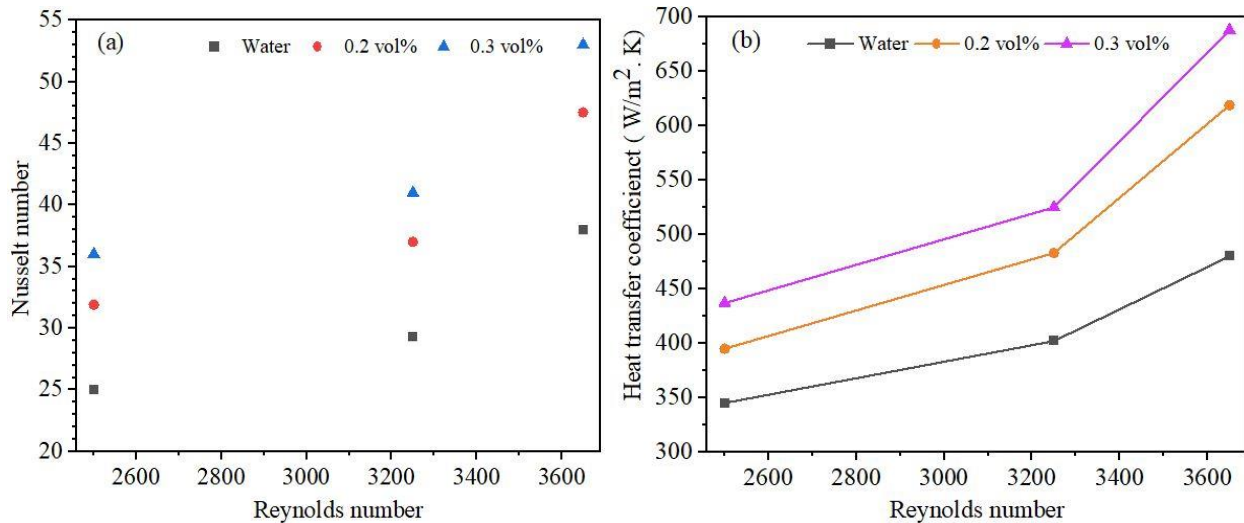


Figure 60. The effect volume concentration of TiO<sub>2</sub>-Fe<sub>2</sub>O<sub>3</sub> on (a) Nusselt number and (b) heat transfer coefficient

Thus, the nanofluid's increased density and viscosity increased the pressure drop using a hybrid nanofluid compared to DI water, as shown in Figure 61 (a). The nanocomposite dispersed in DI water worked to the resistance of the flow and increased the pressure drop, increasing the volume concentration of nanocomposite pressure drop by 23.61% and 36.12% as a function of increased Reynolds number. Figure 61 (b) shows the decreased friction factor of the TiO<sub>2</sub>-Fe<sub>2</sub>O<sub>3</sub> nanofluid with increased Reynolds number and volume concentration of nanocomposite in DI water. The friction factor of the DI water was lowest than hybrid nanofluids because of the increase in the

viscosity of the hybrid nanofluids. The friction factor dropped by 5.26% and 10.52% at increased Reynolds number and volume concentration by 0.2 vol%, 9% and 0.3 vol %, respectively.

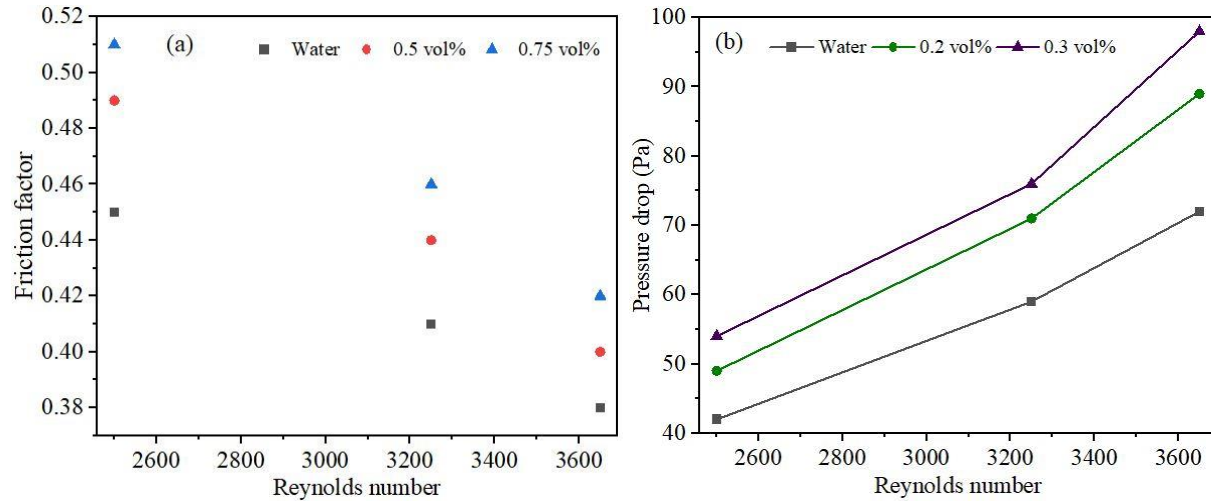


Figure 61. The effect volume concentration of TiO<sub>2</sub>-Fe<sub>2</sub>O<sub>3</sub> on (a) fraction factor and (b) pressure drop

### 6.6.2 Exergy analysis results

The thermal exergy of the system is proportional to the specific heat of the cooling fluid, the flow rate, and the exit temperature of the cooling fluid. Figure 61 (a) shows the thermal exergy of using TiO<sub>2</sub>-Fe<sub>2</sub>O<sub>3</sub> nanofluid compared with DI water, where increasing the TiO<sub>2</sub>-Fe<sub>2</sub>O<sub>3</sub> nanocomposite in base fluid increments the thermal exergy of the system. This is attributed to enhanced cooling fluid thermal conductivity reflected on enhanced convective heat transfer between circulating cooling fluid and tubes placed on the absorbing plate. It can notice that the value of the thermal exergy system is lowest than the electrical exergy because of its higher quality compared to the thermal energy [66]. Maximum thermal and electrical exergies were recorded at the solar noon, and this is returning to the rising of the solar irradiation. Thus, enhancing thermal properties such as specific heat and increasing the flow rate of the cooling fluid may achieve comparable with electrical exergy. According to Eq. (43), the thermal exergy efficiency of the system is influenced by the outlet fluid temperature. Increases in the volume concentrations of nanocomposite in the DI water and the mass flow rate caused an increment of the thermal exergy. Figure 61 (b) shows that the relative increase of the nanocomposite in DI water led to a gradual increment of the thermal exergy efficiency to 2.43%, 2.28%, at 0.2 vol% and 0.3 vol%, respectively, compared with DI water which recorded 1.48%. Thereby, it can be observed that the thermal exergy efficiency was much lower than the electrical exergy efficiency. This is attributed to the outlet temperature of the fluids being closer to the ambient temperature, which agrees with [120]; the low quality of the thermal exergy is one of the reasons that causes reduced thermal exergy efficiency.

The electrical exergy efficiency is relatively enhanced with increased volume concentrations; maximum electrical exergy recorded was 12.4 %, 11.52% at 0.3 vol% and 0.2 vol%, respectively, while cooling with DI water recorded at about 6.8%, as shown in Figure 61 (b). Thus, using TiO<sub>2</sub>-Fe<sub>2</sub>O<sub>3</sub> nanofluid increment the electrical exergy efficiency of the PVT system by 82.3%, 69.4% with increased the TiO<sub>2</sub>-Fe<sub>2</sub>O<sub>3</sub> nanocomposite in DI water by 0.3% and 0.2% compared with DI water. An increment in the electrical energy efficiency significantly increased

the overall exergy of the PVT system than thermal exergy efficiency. It can be observed that increasing the volume concentration of  $\text{TiO}_2\text{-Fe}_2\text{O}_3$  nanocomposite in base fluid increased the overall exergy to 14.83% and 13.8% at 0.3% and 0.3%, respectively, while used DI water achieved 8.28%. Compared with previous studies that used different PVT system sizes, volume concentrations, and types of nanomaterials, Table 13 shows the effect of hybrid  $\text{TiO}_2\text{-Fe}_2\text{O}_3$  nanofluid on the thermal and electrical efficiencies of the PVT system. The exergy analysis results show the effect of hybrid  $\text{TiO}_2\text{-Fe}_2\text{O}_3$  nanofluid on the thermal and electrical exergy efficiencies, which achieved quite results. However, the limited suspension of  $\text{TiO}_2\text{-Fe}_2\text{O}_3$  nanocomposite in the base fluid gives high exergy efficiency compared with some studies.

Table 13. The exergy performance compared with previous studies

Ref.	PV module peak power	Type of nanofluid	Volume concentration %	Thermal exergy %	Electrical exergy %
Current study [121]	50 W	$\text{TiO}_2\text{-Fe}_2\text{O}_3$	0.2	2.28	11.52
			0.3	2.43	12.4
			0.5	0.76	7.87
[33]	50 W	$\text{WO}_3$	0.75	0.91	8.81
			1	1.2	9.3
			0.2	1.01	10.87
[33]	40 W	$\text{Al}_2\text{O}_3$	0.2	1.18	10.99
		$\text{ZnO}$	0.2	0.91	11.02
		$\text{TiO}_2$	0.2	0.25	15.25
[51]	60 W	Carbon black	0.1	0.52	15.98
			0.2	0.34	15.55
			0.3	0.19	14.45
[122]	40 W	$\text{ZnO}$	0.2	0.89	11.48
		PCM	-	1.6	12.01

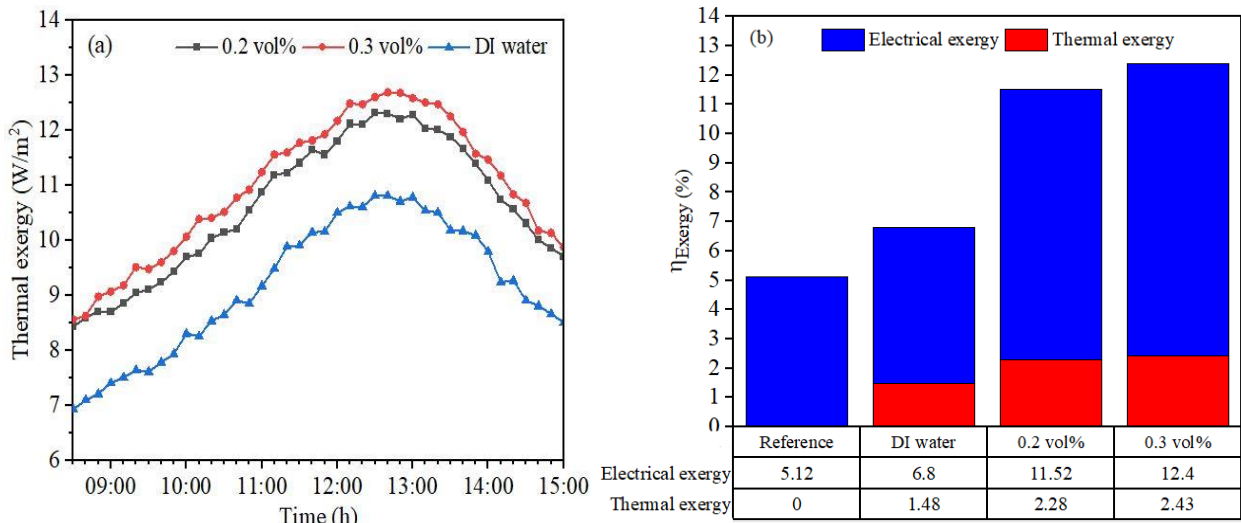


Figure 61. Exergy performance of the PV and PVT system (a) thermal exergy, (b) overall exergies

Assessment of energy losses and entropy generation in thermodynamic systems is important to determine the system losses and irreversibilities. The PVT system's exergy loss and entropy generation are calculated using Eq. (46) using DI water and hybrid nanofluid at different volume concentrations. Raising the PV module temperature means increased exergy losses; employing hybrid nanofluid help in reducing the exergy losses due to enhanced thermal properties. Using a hybrid  $\text{TiO}_2\text{-Fe}_2\text{O}_3$  nanofluid reduced the exergy losses in the PVT system by converting the heat generated by the PV cells to useful thermal energy due to the circulating of the hybrid nanofluid in tubes. Figure 62 shows the relatively reduced exergy losses of the PVT system compared with the reference PV module using DI water and hybrid nanofluid at 0.2 vol%, 0.3 vol% the exergy losses reduced to 13.57%, 42.33% and 47.3%, respectively.

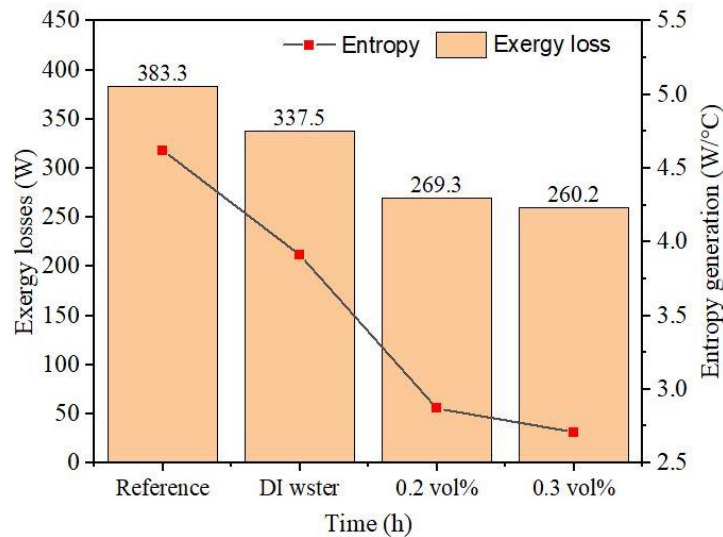


Figure 62. Exergy losses and entropy generation

On the other side, the reference PV module has the highest entropy generation due to rising temperature because of the increase in the heat transfer between the PVT system and the environment. Increasing volume concentrations enhances electrical exergy efficiency due to the reduced temperature of PV cells and then reduces entropy generation. Figure 84 shows the influence of DI water and hybrid nanofluid by reducing the entropy generation by 18.15%, 60.9% and 70.47%, respectively, compared with the reference PV module. Thereby, both the exergy losses and entropy generation of the PVT system have lowered at cooling the hybrid nanofluid was higher than cooling by DI water; this is important to reducing the work lost in the PVT system.

### 6.6.3 Economic analysis of the PVT system

The economic analysis of the proposed cooling approach is important to show the payback period [20], the feasibility of a hybrid PVT system for the long term and compare it with conventional PV modules. Considering the daily maintenance, which may be non-existent on some days of the month, operation cost, including pump and flow sensor electrical consumption and others. Synthesizing nanomaterials in the laboratory and preparing the nanofluid helped significantly reduce the cost of nanofluid compared to purchasing from companies, as well as the purity and morphology of nanomaterials that can be improved. The nanofluid cost was calculated each day after dividing the total price by days in the year. The configuration of the PVT system includes an absorbing part, copper tubes, an aluminium cover, insulation, a pump, a flow sensor,

plastic tanks, etc. The net profit is calculated from Eq. (68) [123] depending on the cost of each element mentioned in Table 14. Compared with conventional PV modules, the hybrid PVT system used hybrid nanofluid achieved less payback period of 630 days than conventional PV modules with a payback period of about 727 days with more than 3 months difference. This difference is logically acceptable and confirms the effectiveness of using nanofluids in improving the PVT system efficiency and its economic feasibility.

$$\text{Net profit} = \text{Energy produces cost (electric and thermal energy)} - \text{Nanofluid cost} - \text{Operation cost} - \text{Maintenance cost} \quad (68)$$

Table 14. Economic analysis of PV module and PVT system cooled by hybrid nanofluid

Element cost	PVT system costs \$	Conventional PV costs \$
Configuration	179.86 \$	39.76 \$
Maintenance	0.007 \$/ day	0.00397 \$/day
Nanofluid supply	0.06 \$/day	-
Operation cost	0.00363 \$/ day	-
Energy productivity	0.356 \$/day	0.0587 \$/day
Net profit	0.285	0.0547
Payback period	630 days	727 days

## 6.7 Effect of hybrid TiO<sub>2</sub>-CuO nanofluid on the PVT system efficiency

### 6.7.1 Energy analysis results

In this case, using a hybrid TiO<sub>2</sub>-CuO nanofluid as a cooling fluid improves the efficiency of the reference PV module by decreasing its temperature. During the experiment, the sky was clear, and no significant variation in solar radiation or temperature was recorded. The reference PV module and PVT system were oriented to face south with installed at a 14.8° tilt angle. Figure 63 (a) shows the average ambient temperature and solar radiation; at the beginning, the temperature and solar radiation values were low, then increased at noon to reach maximum values and dropped with sunset. The maximum ambient temperature and solar radiation recorded between 12:20 PM to 1:50 PM were 32.6 °C and 903.5 W/m<sup>2</sup>. Increased intensity of incident solar radiation on the PV module causes the PV module temperature to rise because of increased solar radiation absorbed by the PV cell temperature. The electrical efficiency of the PV module and PVT system is directly influenced by incident solar radiation and ambient temperature. The mechanism of conduction heat transfer from the backside of the PV modules to the absorbing plate, then to serpentine tubes and by heat convection to hybrid nanofluids that pass inside tubes has reduced the temperature rise in the PV module. Figure 63 (b) shows the peak temperature of the reference PV module was 51.63 °C; with cooling by DI water, the average temperature decreased to 48.85 °C, at 0.2 vol% and 0.3 vol% of hybrid nanomaterials in the base fluid, the average temperature dropped to 37.9 °C and 37.1 °C, respectively. The loaded of CuO NPs over the TiO<sub>2</sub> NWs increased their surface area and improved the thermal characteristics of the hybrid nanofluid, which led to an increase in convective heat transfer and a decrease in the PV module temperature. The flowing hybrid nanofluid at different volume concentrations inside the serpentine tubes attached beneath the PV module helps to extract the excessive heat and reduced of PV module temperature by 36.1%, 39%, compared to the reference PV module. Cooling by water achieved a slight decrease in temperature by 5.6% compared to the reference PV module, confirming the efficient hybrid nanofluids proposed as cooling fluids. The proposed cooling approach of the PVT system contributed to decreased PV cell temperature and improved their

performance. Removing excessive heat from the backside of the PVT system using DI water and hybrid nanofluids helps to increment electrical power compared to the reference PV module. Figure 64 (a) show the maximum electrical power generated by the reference PV module, PVT system at cooling by water and hybrid nanofluid at different volume concentration.

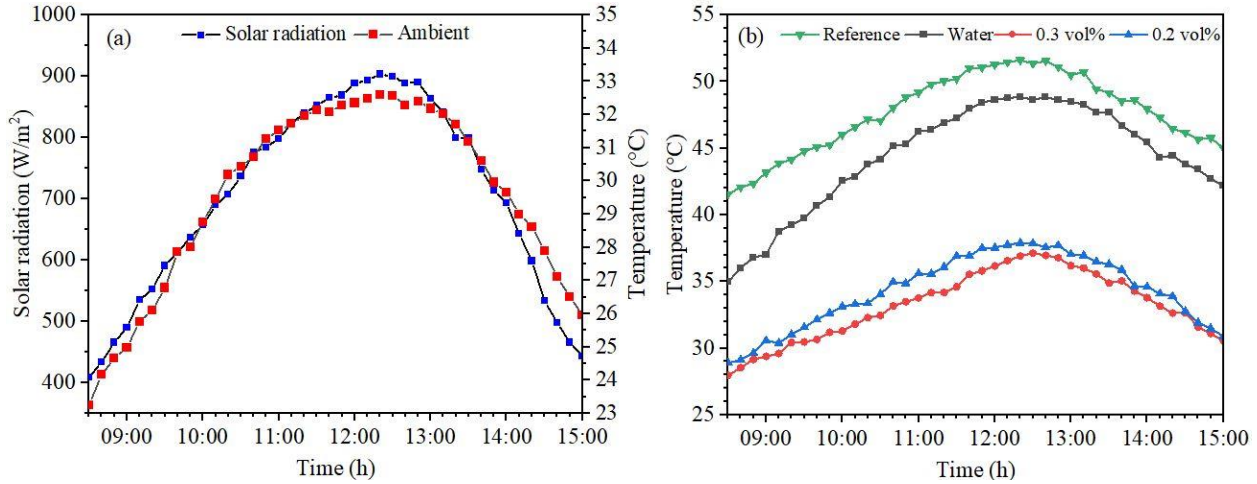


Figure 63. Variations values of (a) solar radiation and ambient temperature, (b) temperature of the PV and PVT system

The reference PV module has recorded lower electrical power, about 21.9 W, which confirms the degradation of the PV cell's work due to increased temperature. Circulation water inside serpentine tubes with absorb plate helps slightly increment the electrical power to 24.2 W. Using hybrid nanofluids at 0.2 vol % and 0.3 vol %, the electrical power of the PVT system increments to 38.1 W and 38.88 W, respectively. The loaded of CuO NPs on TiO<sub>2</sub> NWs at equal ratios and dispersion in DI water helped improve the hybrid nanofluid's thermal properties by increasing the hybrid nanofluid's thermal conductivity and heat capacity. Improving the nanofluid's thermal conductivity increased the PV module's absorbing heat and then reduced its temperature. The electrical power produced was enhanced by 73.9 5% and 77.5% with the used hybrid nanofluid at 0.2 vol% and 0.3 vol%, while the used DI water improved by 10.4% compared to the reference PV module. The effectiveness of hybrid nanofluid caused a decrease in the PV cell's temperature and an increment in electrical power generation of the PVT system hence positively reflecting of electrical efficiency of the PVT system. Figure 64 (b) it can observed the electrical efficiency of the reference PV module was 5.8 % due to a drop in the electrical power; with DI water cooling, the electrical efficiency of the PVT system is an increment to 6.4%. The improvement of electrical power of the PVT system with the used hybrid nanofluid led to an increment in the PVT electrical efficiency to 12.28%, 12.4%, at 0.2 vol% and 0.3 vol%, respectively, that attributed to reducing PV module temperature. The higher heat transfer capacity of using hybrid nanofluids caused decreasing the PV module operation temperature, thus incrementing the thermal efficiency of the PVT system. Figure 46 (b) shows the variation of thermal efficiency increase in the volume concentration of nanocomposite in DI water; the increase in volume concentration achieved a relative increase in thermal efficiency due to the increased thermal conductivity of nanofluids. Compared with DI water, using a hybrid nanofluid led to an increment in thermal efficiency to 44.2% and 45.8% with increased volume concentration by 0.2 vol% and 0.3 vol%. Thus, incrementing the overall efficiency of the PV

module to 54.1%, 58.8%, compared with cooling by DI water. Compared with previous studies in the literature, Table 15 compares the current study with previous studies that used mono nanofluids such as CuO, TiO<sub>2</sub> and hybrid nanofluids for cooling PVT systems. It can remark that the hybrid TiO<sub>2</sub>-CuO fluid achieved good performance by temperature drops and increment in the electrical and thermal efficiency attributed to the improving thermal characteristics of hybrid nanofluids. According to some factors such as the size of the PV module, the design of the heat exchanger applied, the flow rate used, and measurement conditions, the current results may not be the best among the results of other studies, but it was not the least.

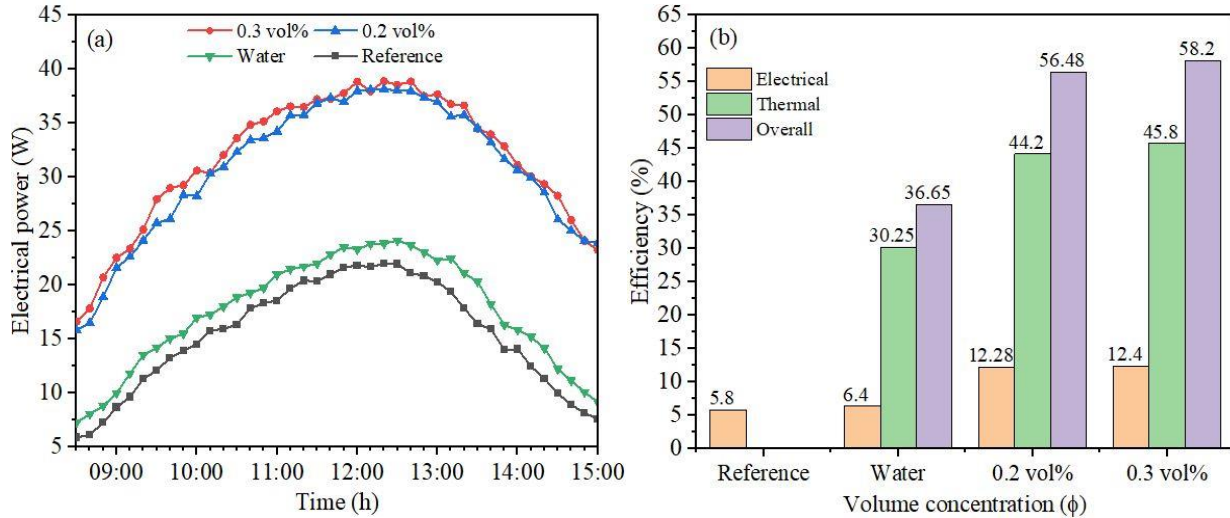


Figure 64. Performance of the PV and PVT system (a) electrical power, (b) overall efficiencies

Table 15. The energy analysis of the PVT system compared with previous studies

Ref.	PV module peak power	Type of nanofluid	Temperature drop %	Electrical efficiency %	Thermal efficiency %
Current study	50 Watts	TiO <sub>2</sub> -CuO/0.2 vol%	13.7	12.28	44.2
		TiO <sub>2</sub> -CuO/ 0.3vol%	14.5	12.4	45.8
[114]	250 W	CuO	12	11.2	43
[31]	100 W	CuO	15	12.9	71.1
[124]	80 W	TiO <sub>2</sub>	12.3	7.32	41
[125]	50 W	TiO <sub>2</sub>	9.6	18.8	45
[119]	150 Watts	CNT/Al <sub>2</sub> O <sub>3</sub>	15	17.2	27.23
[116]	35 Watts	Al <sub>2</sub> O <sub>3</sub> /SiO <sub>2</sub>	19.2	1.99	9.09
[118]	250 Watts	Al <sub>2</sub> O <sub>3</sub> /ZnO	21	13.8	55.9
[117]	250 Watts	Al <sub>2</sub> O <sub>3</sub> /ZnO-Fe <sub>3</sub> O <sub>4</sub>	5.14	13.43	54.11

### 6.7.2 Exergy analysis results

Exergy analysis is important for appearing the actual work and determining the losses of the PVT system. Similar to the energy analysis of the PVT system, the exergy analysis shows the effect of an increase in the solar radiance and the ambient temperature on the exergy performance of the PVT system. Based on Eq. (40), the solar exergy calculated for the maximum, average, and minimum values during experiments days were 897 W/m<sup>2</sup>, 654.33W/m<sup>2</sup>

and  $320.58 \text{ W/m}^2$ , respectively. According to Eq. (41), the electrical exergy was equal to the electrical power produced by the PVT system. The electrical exergy produced was higher than the thermal exergy, in contrast to thermal energy in energy analysis, which is attributed to the outlet fluid's temperature convergence with an ambient temperature. Based on Eq. (42), it can observe the thermal exergy depends on the difference between the  $T_{f \text{ out}}, T_{f \text{ in}}$  fluid temperature, ambient temperature, the logarithm of  $\left(\frac{T_{f \text{ out}}}{T_{f \text{ in}}}\right)$ , and the specific heat of fluids applied. The convergence of  $T_{f \text{ out}}$  to ambient temperature leads to dropping thermal exergy, then influencing thermal exergy efficiency. Nevertheless, using nanofluid achieved a remarkable improvement of thermal exergy to  $11.86 \text{ W/m}^2$  %,  $12.18 \text{ W/m}^2$ , at 0.2 vol% and 0.3 vol%, while cooling by DI water was  $8.8 \text{ W/m}^2$ , as shown in Figure 65. Circulating the hybrid nanofluid into the serpentine tubes helps to remove excess heat from the backside of the PV module and reduces their temperature, which improves the electrical exergy. Figure 66 (a) shows the effect of DI water and hybrid nanofluid at 0.2 vol% and 0.3 vol% by increasing electrical exergy efficiency to 5.4 %, 11.33 %, and 12.18%, respectively. The thermal exergy drop influences the thermal exergy efficiency because of the low quality of the thermal exergy. The overall exergy efficiency of the PVT system is the sum of the thermal and electrical exergy efficiencies. Enhancing hybrid nanofluid's thermal properties increments the PVT system's overall exergy efficiency to 13.44 % and 14.97 % at different volume concentrations. In contrast, overall exergy efficiency with cooling by DI water does not exceed 6.28 %. An increase in the volume concentration of hybrid nanomaterials in the base fluid remarkably influences the increment of the overall exergy efficiency. It is important to evaluate exergy loss and entropy generation for specifying the PVT system losses and irreversibilities. The exergy loss increases with the rising temperature of the PV module surface.

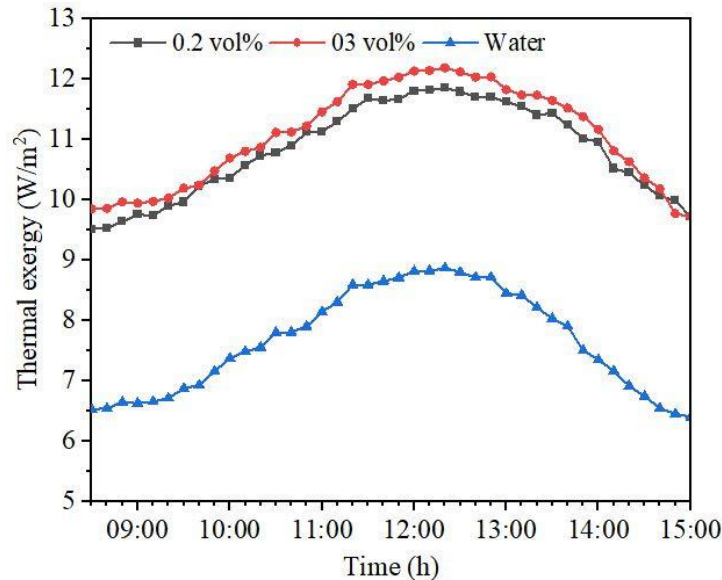


Figure 65. Thermal exergy of the PVT system

Enhancing the thermal characteristics of hybrid nanofluids helped to reduce the exergy losses; Figure 66 (b) shows a reduction of exergy losses by 38.4%, 44.3% at 0.2 vol% and 0.3 vol%. In contrast, using DI water has reduced entropy generation by about 4.5% compared to the reference PV module. Rising the temperature of the PV module causes increased entropy generation due to increased heat transfer between the PVT system and the environment.

Minimizing the entropy generation is necessary to reduce the work lost in the system. Figure 66 (b) shows the effect of hybrid nanofluid by lowering the entropy generation; compared with the reference PV module, hybrid nanofluid reduced the entropy generation by 62.2 % and 69.6%, while DI water by 8.46 %, which confirms the effectiveness of hybrid nanofluid used. Moreover, using hybrid nanofluids effectively reduces exergy loss because of their efficient effects on heat transfer.

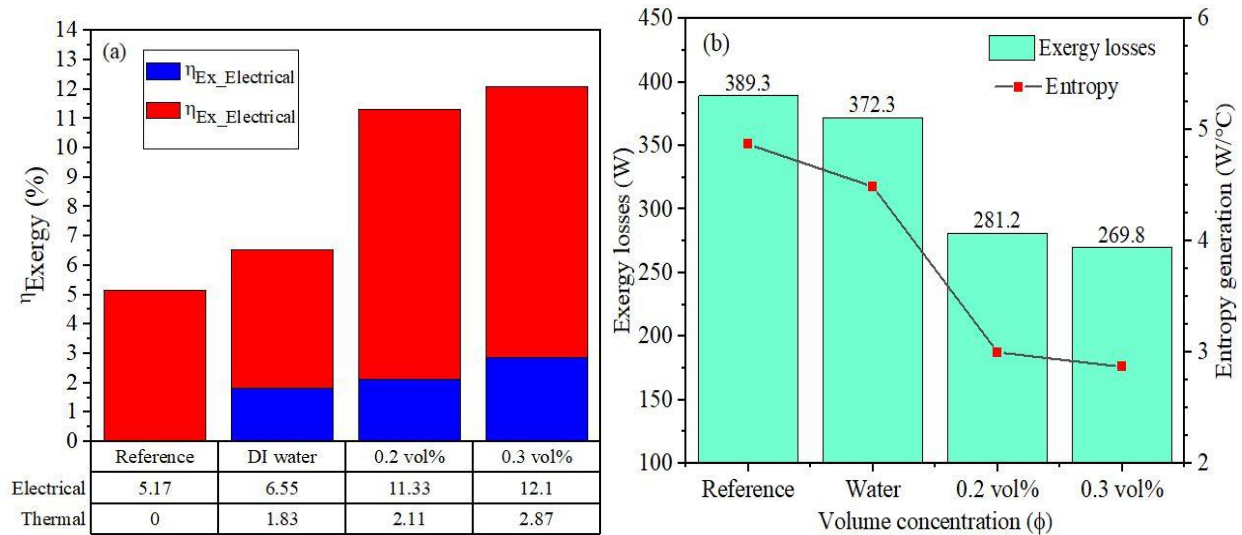


Figure 66. Exergy performance of the PV and PVT system (a) exergy efficiencies, (b) exergy losses and entropy generation

## 6.8 New contributions results

### Contribution 4

Dispersion of CuO nanofluid at different volume concentrations for cooling the PVT system gives good results, which improves the PVT system performance. Copper oxide nanoparticles are characterized by higher thermal conductivity, which is positively reflected by a reduced PVT system temperature of 23.44%. Reduced PVT system temperature helped increment the electrical power from 20.78 W to 35.47 W at 0.3 vol%, thus enhancing the electrical efficiency from 5.43% to 10.3%, which confirms the effectiveness of the nanofluid used. The CuO nanofluid thermal properties helped to improve the heat transfer coefficient, which led to more absorption of excess heat from the backside of the PVT system, then increased the thermal efficiency to 38.9%.

Most studies use TiO<sub>2</sub> nanoparticles to prepare nanofluids as a cooling fluid for different PVT system configurations; in the current case, TiO<sub>2</sub> nanowires have been adopted, which are characterized by having a surface area to help increase heat absorption. Compared with the reference PV module, using TiO<sub>2</sub> nanofluid decreased the PVT system temperature to 14% at 0.3 vol% and increased the electrical power to 49.7%. Reduced temperature and increment of electrical power improve the electrical PVT system efficiency by 27.5%, while increased thermal conductivity of nanofluid increases heat absorbing from PV cells and then increases thermal efficiency to 34.6%.

Suspension of 0.3 vol% of Fe<sub>2</sub>O<sub>3</sub> nanoparticles in DI water improved the convection heat transfer, which helped to reduce the PVT system temperature by 29.64%. Compared with DI

water, the electrical power increased from 21.37 W to 37.76 W, that is, by 76.68%, enhanced the electrical power positive reflected to increase the electrical efficiency to 12.1% at increased the volume concentration to 0.3 vol%. Thermophysical properties of Fe<sub>2</sub>O<sub>3</sub> nanoparticles significantly help to improve the heat transfer convection between the backside of the PV module and the heat exchanger, then increase heat removal from the PV cells, thus increasing the thermal efficiency to 43.3%.

Table 16 shows the effect of different cooling fluids on the PVT system, which contributes to reducing the PV cell temperature and increasing the efficiency of the PVT system higher than DI water. At 0.3 vol%, the Fe<sub>2</sub>O<sub>3</sub> nanofluids achieved better performance by reducing the temperature, incrementing electrical power, and increasing electrical and thermal efficiency more than other nanofluids. This is attributed to the high thermal conductivity of Fe<sub>2</sub>O<sub>3</sub> nanofluids compared to CuO and TiO<sub>2</sub> nanofluids, which help increase the heat transfer convection between nanofluids and tubes, which is reflected by reducing the PVT system temperature. CuO nanofluid achieved higher performance than TiO<sub>2</sub> nanofluid because of their high thermal properties, which positively reflected the PVT system performance.

Table 16. Effect of different nanofluids on the PVT system performance

Cooling applied	$PV_{ref}$	Cooling by DI water	$PV_{ref}$	Cooling by CuO nanofluid	$PV_{ref}$	Cooling by TiO <sub>2</sub> nanofluid	$PV_{ref}$	Cooling by Fe <sub>2</sub> O <sub>3</sub> nanofluid
$T_{PV}$ °C	55.6	-	52.86	-	52.57	-	50.9	-
$T_{PVT}$ °C	-	55.6	-	42.82	-	46.11	-	39.26
$P_{PV}$ W	19.3	-	20.78	-	21.15	-	21.37	-
$P_{PVT}$ W	-	22.19	-	35.47	-	31.66	-	37.76
$\eta_{ele-PV}$ %	5.11	-	5.42	-	4.89	-	5.75	-
$\eta_{ele-PVT}$ %	-	6.32	-	10.3	-	8.44	-	12.1
$\eta_{ther-PVT}$ %	-	30.25	-	49.2	-	43	-	55.4

### Contribution 5

The hybrid TiO<sub>2</sub>-Fe<sub>2</sub>O<sub>3</sub> nanofluid consisting of 50% nanowires and 50% nanoparticles has created a new hybrid nanofluid having new thermophysical properties that help improve the hybrid nanofluid performance used with PVT system more than mono nanofluid. Loading TiO<sub>2</sub> NWs over Fe<sub>2</sub>O<sub>3</sub> NPs has increased the surface area of the nanocomposite, which positively reflected heat absorbing then enhanced the PVT system performance as follows:

- Compared to the reference PV module, circulation of DI water decreased the PV module temperature by 9.67%, using hybrid nanofluid at 0.2 vol%, 0.3 vol% reduced the PV module temperature by 25% and 33.63%. Due to decreased PV cell temperature, the PVT system's electrical power has increased by 17.63%, 68.32% and 71.6% at DI water and hybrid nanofluids, respectively.
- Increment in the electrical power has enhanced the electrical efficiency of the PVT systems to 7.1%, 12.44%, and 12.62% at cooling by DI water and hybrid nanofluid at different volume concentrations compared with the reference PV module. Increasing the volume concentrations by 0.2 vol% and 0.3 vol% in the base fluid has increased the nanofluid heat

transfer coefficient and heat removal from the PV cells, then enhanced the thermal efficiency of the PVT system by 39.26% and 47.85% compared to used DI water.

- Compared with DI water, using a hybrid nanofluid enhanced the Nusselt number by 25 % at 0.3 %vol. An increase in Nusselt numbers has positively increased the heat transfer coefficient by 43.33% at 0.3 vol%, which helped lower PV temperature and increased thermal efficiency. Increased volume concentration causes increased nanofluid density and effect by the pressure drop of about 36.12%; increased Reynolds number and volume concentrations lead to dropping the friction factor to 10.52%.
- The thermal exergy is affected by the specific heat of the cooling fluid, flow rate and temperature. An increase in the TiO<sub>2</sub>-Fe<sub>2</sub>O<sub>3</sub> nanocomposite in base fluid increments the thermal exergy by 17.29% and 13.87% compared to DI water. The relative increase of the volume concentrations increments the thermal exergy efficiency to 2.43%, 2.28% compared with DI water, which was lower than electrical exergy efficiency due to the low quality of the thermal exergy.
- Increment of electrical exergy has a positive reflection to enhance the electrical exergy efficiency of the PVT system by 69.4% and 82.3% compared to cooling by DI water, which significantly increments the overall exergy of the PVT system by 79.1% and 66.67%, even with a relative increment in thermal exergy efficiency. The exergy losses increase with the rising PV module temperature. Compared to cooling by DI water, employing hybrid nanofluid help in reducing the exergy losses by 13.57% and 42.33%. Thereby reducing entropy generation by 60.9% and 70.47%, which contributes to reducing the work lost in the PVT system.
- Compared with previous studies, which adopted different sizes of the PVT system, the nanofluids and volume concentrations of the nanocomposite. The employed hybrid TiO<sub>2</sub>-Fe<sub>2</sub>O<sub>3</sub> nanofluid enhanced the energy and exergy of the PVT system better than previous studies, confirming the effectiveness of the hybrid nanofluid employed.
- The economic analysis of cooling by hybrid nanofluid achieved a satisfying payback period for the PVT system, which produces electrical and thermal energy compared to the reference PV module with a difference of more than 3 months.

## **Contribution 6**

Energy and exergy of the PVT system have been conducted to evaluate the quantity and quality of the PVT system's productivity. The following points summarized the new findings of using hybrid TiO<sub>2</sub>-CuO nanofluid as follows:

- The effectiveness of the hybrid nanofluid at different volume concentrations helps to extract the excessive heat and reduces PV module temperature by 36.1% and 39%, while DI water by 5.6 % compared with the reference PV module. The electrical power improved of the PVT system by 73.95% and 77.5% at increased volume concentrations due to improving the hybrid nanofluid's thermal properties, while using DI water improved it by 10.4%. Thus, the electrical efficiency of the PVT system increased by 12.28% and 12.4%.
- The high thermal characteristics of hybrid nanofluids increment heat transfer convection and then improve the thermal efficiency of the PVT system to 56.48% and 58.2%, then increment the overall efficiency of the PV module, reaching 36.25% and 56.48%.

- Convergence of the outlet fluids temperature with ambient temperature causes decreased thermal exergy and thus reduced thermal exergy efficiency. Cooling by hybrid nanofluid has improved the electrical exergy efficiency by 11.33 % and 12.18%, while a slight improvement was recorded using DI water. The overall exergy efficiency has increased to 13.44 %, 14.97 % and 6.28 % at different nanocomposite volume concentrations and DI water.
- The exergy losses were reduced by 32.3% and 37.9% due to enhancing the thermal characteristics of hybrid nanofluids, while used DI water was reduced by 4.5% compared to the reference module. The effective cooling by hybrid nanofluid causes reduced entropy generation by 62.2 % and 69.6%, compared with DI water.

Improving the performance of nanofluids positively reflected in their performance the TiO<sub>2</sub> nanofluid was less effective than CuO and Fe<sub>2</sub>O<sub>3</sub> nanofluids. Thus, loading Fe<sub>2</sub>O<sub>3</sub> nanorods over TiO<sub>2</sub> nanowires and loading CuO nanoparticles over TiO<sub>2</sub> nanowires produced new hybrid nanocomposites with high thermal properties than mono nanomaterials. Dispersion of the hybrid nanocomposites in DI water achieved high performance than the mono nanofluids; Table 17 shows the improvement of the PVT system at 0.3 vol% of TiO<sub>2</sub>-Fe<sub>2</sub>O<sub>3</sub> and TiO<sub>2</sub>-CuO nanofluids compared with mono nanofluid used, as mentioned in Table 15. Using TiO<sub>2</sub>-Fe<sub>2</sub>O<sub>3</sub> nanofluid achieved higher performance than TiO<sub>2</sub>-CuO due to the high specific heat and low density of Fe<sub>2</sub>O<sub>3</sub> nanorods that help to enhance the thermal properties of the TiO<sub>2</sub> nanowire, and the results in Table 17 confirm the effectiveness of hybrid nanofluid as a cooling fluid.

Table 17. Effect of hybrid nanofluid on the PVT system performance

Cooling applied	$PV_{ref}$	Cooling by TiO <sub>2</sub> -Fe <sub>2</sub> O <sub>3</sub> nanofluid	$PV_{ref}$	Cooling by TiO <sub>2</sub> -CuO nanofluid
$T_{PV}$ °C	49.85	-	51.63	-
$T_{PVT}$ °C	-	36.37	-	37.1
$P_{PV}$ W	23.14	-	21.9	-
$P_{PVT}$ W	-	39.71	-	38.88
$\eta_{ele-PV}$ %	5.7	-	5.8	-
$\eta_{ele-PVT}$ %	-	12.62	-	12.4
$\eta_{ther-PVT}$ %	-	59.82	-	58.2

Another two contributions can be found in (Appendix B)

## Chapter 7

### Numerical simulation of the PVT system by using different nanofluids

In this chapter, a numerical simulation has been conducted of the effects of  $ZrO_2$ /water nanofluid and  $TiO_2-Fe_2O_3$  hybrid nanofluid as cooling fluids on the temperature, energy efficiency, exergy efficiency, heat transfer coefficient, Nusselt number, Reynold number, and pressure drops in system PVT system. The methodology of this chapter involved a numerical simulation via ANSYS Fluent 19.2 software by (computational fluid dynamics (CFD)) of a 3D model. The proposed model involved a PV module, an absorber plate and serpentine tubes attached at the backside of the PV module. The numerical results are validated by comparing the experimental results obtained. The numerical simulation results of the PVT system cooled by  $ZrO_2$ /water nanofluid have been compared with experimental results conducted according to the Iraq condition, while the  $TiO_2-Fe_2O_3$  hybrid nanofluid according to experimental results conducted in Hungary condition.

#### 7.1 The model geometry and assumptions

The proposed model consists of a glass cover, photovoltaic cells, absorb plate, and tubes directly in contact with the absorbing plate. Figure 67 shows the geometry of the PVT system used for the current simulation. The geometry model is created by SolidWorks with all dimensions and then imported to ANSYS 19.2; Table 18 presents the properties of the geometry model proposed. The effect of the cover glass and the PV module are indirectly used through the boundary conditions; the solar radiation value received by the copper absorber plate depends on the transmissivity of the cover glass section beside and the absorptivity of the PV module, which is interpreted as constant heat flux and that agrees with [126]. The conduction heat transfer among absorber plates and tubes and the convection heat transfer of the fluid circulation inside the tube are important mechanisms in this chapter employed by CFD in the numerical domain proposed. The assumptions below have been applied to the numerical simulation model:

- The fluid is steady-state, uniform and incompressible.
- Part of the absorbed solar radiation by PV cells converts to electrical, whereas the rest part cause is rising in PV cell temperature.
- In reality, the nanoparticles and base fluid are two-phase; in calculations, both are in thermal equilibrium and single phase; this assumption is repeatedly in literature [127-129].
- Due to the lowering of temperature in the PVT system, the radiation heat loss is neglected.
- The contact area between the surface tubes and the bottom surface of the absorber plate is adiabatic.
- The thermal grease thickness between the PV module and the copper absorber plate is ignored.
- Assumed a perfect contact between the PV module and absorber plate. Thus, the temperature is the same in these layers, which agrees with [130,129].

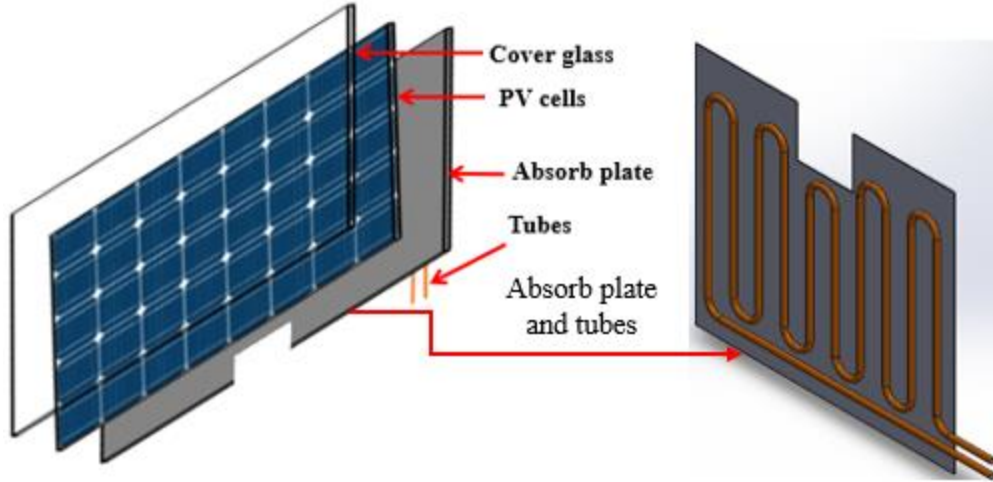


Figure 67. Sketch of the initial model and its components

Table 18. The model component's characteristics

Glass	Emissivity 0.88
PV module	Number of riser cells: 60 Area: 0.355 m <sup>2</sup> Absorptance: 0.9 Emissivity: 0.88 $\eta_r = 15\%$ $\beta_r = 0.0045 \text{ } ^\circ\text{C}^{-1}$
Absorb plate	Area: 0.2928 m <sup>2</sup> Thickness: 0.002 m Material: Copper $C_p = 381 \text{ J/kg K}$ , $k = 387.6 \text{ W/m K}$ , $\rho = 8978 \text{ kg/m}^3$
Tubes	Length of tubes: 5 m The thickness of the tube: 0.001 m Outer diameter: 0.01 m Material: Copper

## 7.2 Boundary conditions and numerical procedure

In this numerical study, the computational fluid dynamic (CFD) approach was used to investigate the performance of the PVT system cooled by nanofluids. According to the assumption above, the fluid flow inside the tubes is steady and incompressible, and the PVT system is considered the control volume; the governing equations adopted in the simulation are energy, continuity, and momentum [86]. These equations are represented the boundary conditions for the current cases in a simple form.

$$\text{Energy equation} \quad \nabla \cdot (\rho_{nf} U_{nf} C_{p_{nf}} T) = \nabla \cdot (k_{nf} \nabla T) \quad (69)$$

$$\text{Continuity equation} \quad \nabla(\rho_{nf} U_{nf}) = 0 \quad (70)$$

$$\text{Momentum equation} \quad \nabla \cdot (\rho_{nf} U_{nf} U_{nf}) = -\nabla P + \nabla \tau + \rho_{nf} g \quad (71)$$

The equations are solved using the finite volume method through the ANSYS Fluent 19.2 software. According to the boundary condition, the heat flux value has been set and specified the fluid velocity at the inlet and temperature of the inlet fluid, then the specification method of the turbulent intensity from Eq (72) and the hydraulic diameter. At the tube outlet, the outflow is adapted as a fully developed fluid flow. For the flow regime, the k-epsilon model has been used through the calculations with activation of the enhanced wall treatment for both pressure gradient effects and thermal effects. The properties of the PVT system component and thermophysical properties of the nanofluids have been inserted from a fluent database. The boundary conditions of the external tube surface and the backside of the absorbing plate are an adiabatic wall, and the heat flux is zero. The heat generation rate on the top surface of the PVT system (geometry model) as a wall is equal to the value of absorbed solar irradiation, with the assumption that this wall transfers heat to the surrounding in a convection and radiation mechanism. The three-dimensional meshing generation is important to the conducted computational domain of the proposed CFD simulation model.

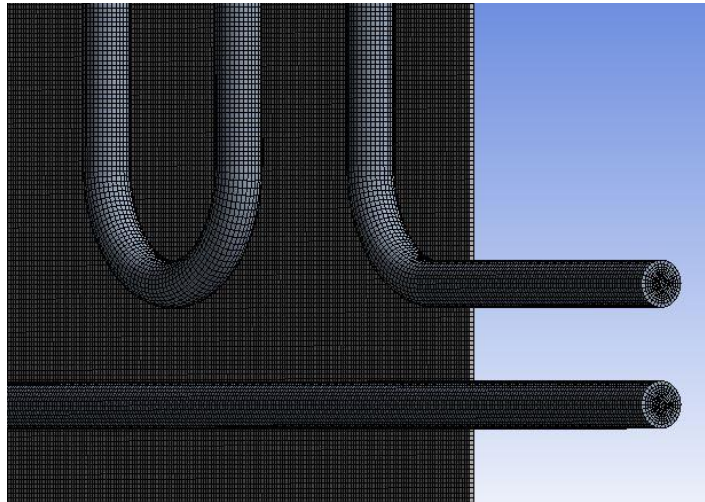


Figure 68. The meshing of the model proposed

The absorber plate and tubes were meshed with a mesh element size of 0.1mm, as shown in Figure 68 above, and the number of meshes elements was 779755 with high smoothing. Using the expression of the Re, Nu, and heat transfer coefficient, we calculated theirs for minimum, average and maximum values to compare with experimental results. The gravitational acceleration is an important parameter that works as a function of the system setup tilt angle and affects buoyancy force convection terms. This feature has been activated in the simulation and is defined in Eq (75-77) [86]. For turbulent flow in tubes and a smooth surface and fully turbulent conditions, the Dittus-Boelter equation used Eq (73).

$$I = 0.16 Re^{\frac{1}{8}} \quad (72)$$

$$Nu = 0.023 Re^{\frac{4}{5}} Pr^n \quad (73)$$

$$\text{Pr} = \frac{c_p \mu}{k} \quad (74)$$

$$g_x = -g \sin \theta \quad (75)$$

$$g_y = 0 \quad (76)$$

$$g_z = +g \cos \theta \quad (77)$$

### 7.3 Results and discussions

To validate the results of the simulation model, it has been compared with experimental studies that adopt ZrO<sub>2</sub>/DI water, CuO/DI water, TiO<sub>2</sub>/DI water, Fe<sub>2</sub>O<sub>3</sub>/DI water, and TiO<sub>2</sub>-Fe<sub>2</sub>O<sub>3</sub>/DI water and TiO<sub>2</sub>-CuO/DI water nanofluid. In this chapter, the simulation results are validated with results obtained according to Iraq and Hungary conditions by using ZrO<sub>2</sub>/DI water nanofluid and Fe<sub>2</sub>O<sub>3</sub>/DI water nanofluid.

#### 7.3.1 Temperature distribution on the proposed model

Figure 69 (a) shows the temperature distribution on the absorber plate directly in contact with tubes at used TiO<sub>2</sub>-Fe<sub>2</sub>O<sub>3</sub> nanofluid; a similar trend was observed with cooling by ZrO<sub>2</sub> nanofluid. It can be observed the gradual temperature distribution increased at the end of the outlet fluid due to heat accumulated during nanofluid flow inside the serpentine tubes. The temperature distribution on the absorber plate was conducted at the tilt angle of 26 when 0.2vol% nanofluid enters the inlet tube at 0.323 m/s, 295 K, and solar radiation of 900 W/m<sup>2</sup>. Thus, the cooling fluid's effect on the temperature distribution of the absorbing plate is positively reflected by decreased PV cells temperature. Figure 69 (b) shows the thermal behaviour of the cooling fluid inside the tubes that enters the inlet tube at low temperatures. Then it increases gradually due to heat transfer conduction from absorbing plate to tubes and by heat transfer convection to circulated fluid.

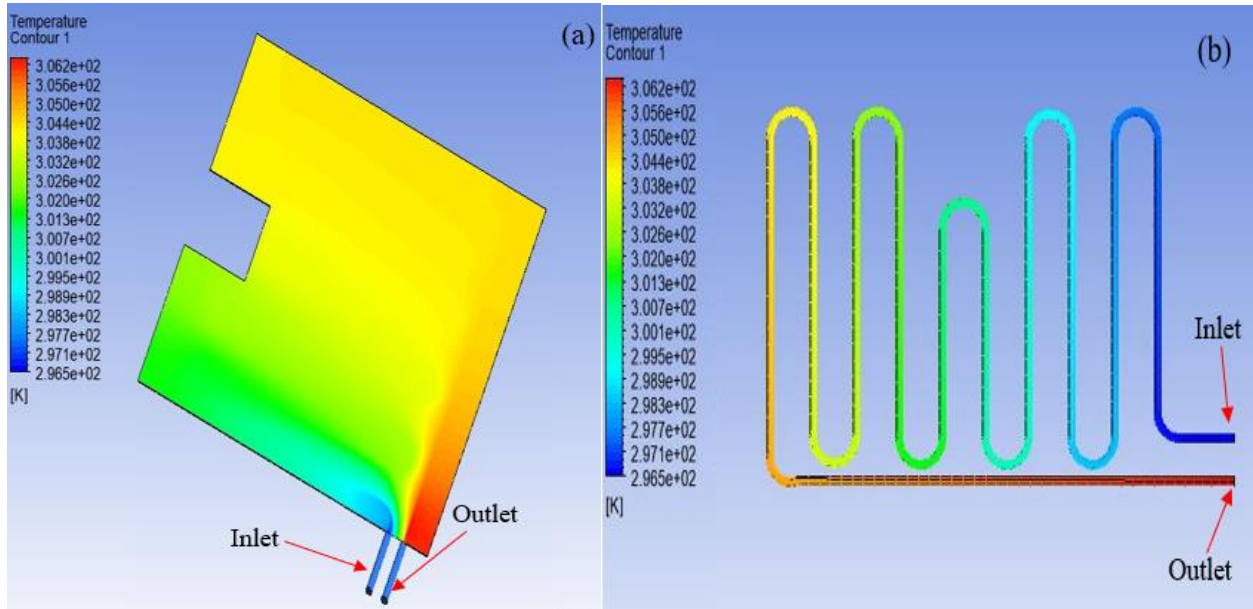


Figure 69. Temperature distribution contour (a) absorb plate and (b) serpentine tube

Thereby by entering the cooling fluid inside the tubes, the temperature of the PV cells at the entrance area is reduced due to decreased absorb plate temperature. The cooling fluid temperature is gradually raised by circulating the coolant fluid through the tubes, which gain heat from the PV cells by the absorbing plate. Figure 70 shows a simplification of one tube contacted with absorb plate taken from the tubes connected to the entire absorbed plate, which can show the gradual temperature of a nanofluid along the tube tested under the same condition. Temperature contour shows the temperature path increased from the tube wall to fluid, which was high at the contact area of the tube and absorbed plate because there was no cooling effect at this area.

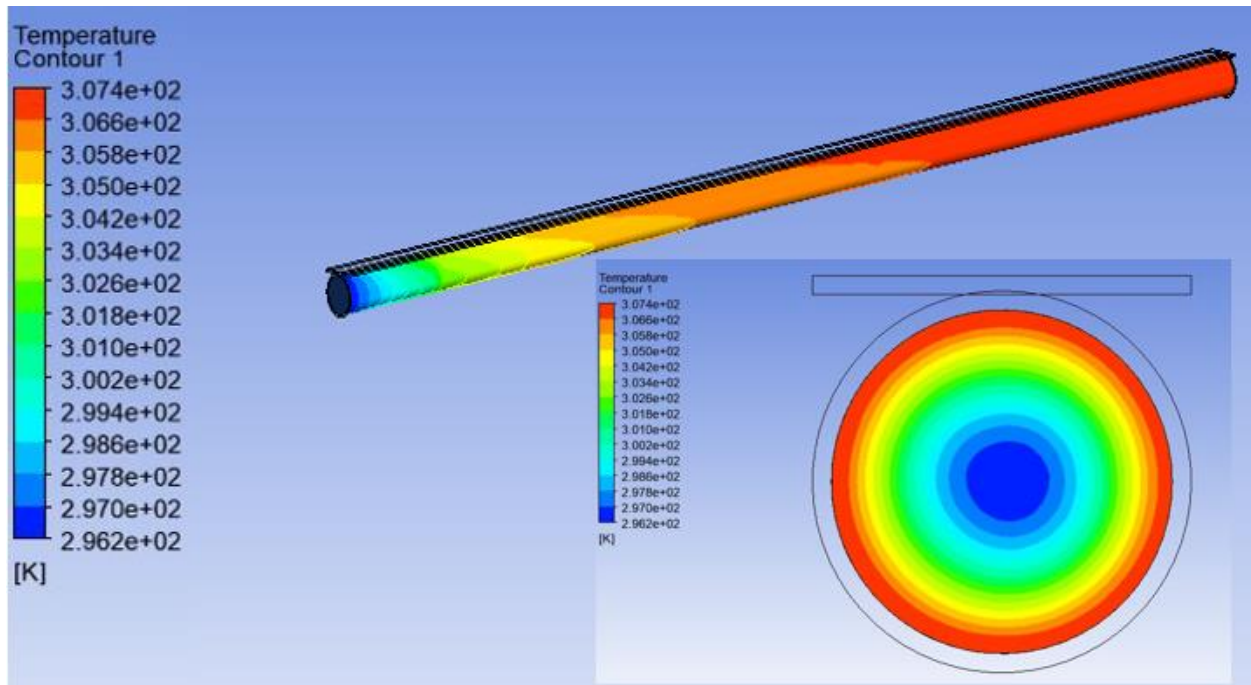


Figure 70. Gradual heat transfer

### 7.3.2 Energy evaluation of the PVT model

Figure 94 (a and b) shows the effect of the increase in the volume concentration of nanomaterials on the PVT temperature. The gradual volume concentration increases in base fluid enhanced the thermal conductivity of nanofluid and then increased the heat absorbed by the backside of the PV module. Using  $ZrO_2$ /DI water nanofluid for cooling the PV module help decrease its temperature. Figure 71 (a and b) show the simulation results of maximum, average and minimum PVT system temperature, recorded at 0.015 vol%, 0.025 vol%, and 0.0275% were 51.93 °C, 50.32 °C and 48.8 °C, respectively. A gradual decrease in the temperature to the increased thermal conductivity of nanofluid can be observed due to an increase in the volume concentration of nanoparticles in base fluid compared with the PVT system cooled by DI water. Validation of the numerical simulation results with experimental results regarding the PVT system temperature was performed in May according to Iraq conditions. It can see the deviation

of the simulation results of maximum, average, and minimum were 1.7%, 2.3% and 2.7%; this percentage is reasonable. In contrast, using a hybrid  $\text{TiO}_2\text{-Fe}_2\text{O}_3$  nanofluid achieved a remarkable decrease in the PVT system temperature due to enhanced thermal properties. Suspension 0.2 vol% and 0.3 vol% of hybrid nanocomposite in base fluid helped decrease the PVT system temperature compared with cooling by DI water. Thus, cooling by hybrid nanofluid achieved a maximum reduction of the PVT system at 38.7 °C, 38 °C at 0.2 vol% and 0.3 vol% compared to cooling by DI water. By validation with experimental results obtained according to Hungary conditions in August, the maximum, average, and maximum deviation between the simulation and experimental results regarding TPV system temperature was 2.86%, 2.73 and, respectively.

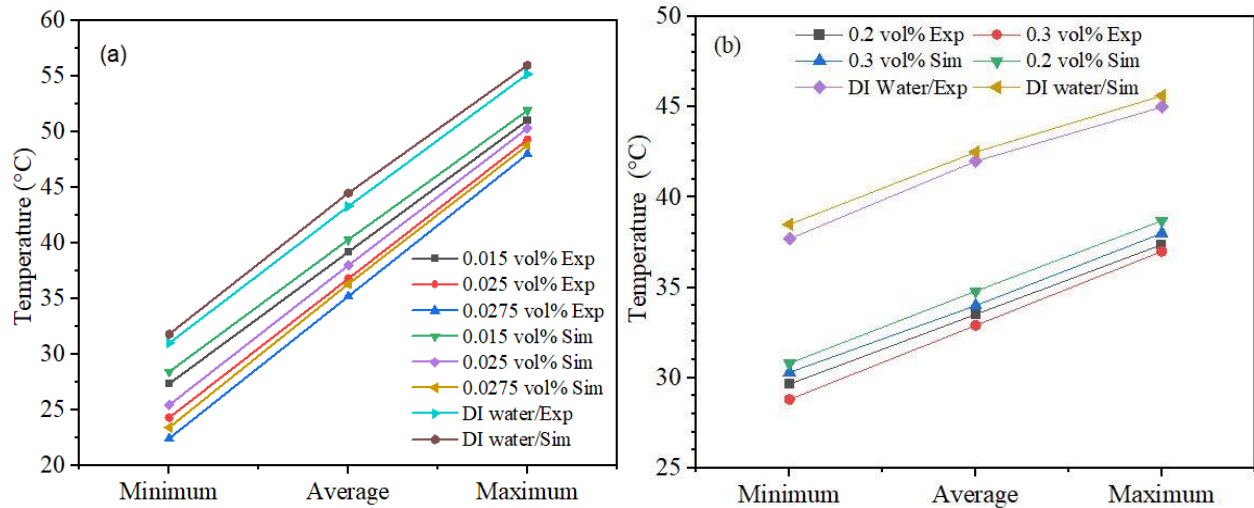


Figure 72. The numerical and experimental results of the effect of nanofluid on the PVT system temperature (a)  $\text{ZrO}_2$  nanofluid and (b)  $\text{TiO}_2\text{-Fe}_2\text{O}_3$  nanofluid

The energy efficiency of the PVT system is an important parameter to demonstrate the quantitative performance of the PVT system, which consists of electrical and thermal efficiencies. Circulating the fluids at the backside of the PV module reduces the PV cell's temperature and enhances the PV cells' conversion efficiency. The cooling of the PVT system  $\text{ZrO}_2$  nanofluid contributed by reducing the temperature and positively reflected by increased electrical efficiency. Figure 73 (a) shows the increase in the electrical efficiency of the PVT system cooled by  $\text{ZrO}_2$  nanofluid at different volume concentrations compared to cooling by DI water. Enhancing the thermal conductivity of the nanofluid helps increase the excess absorbing heat at the backside of the PV module, then gradually increments the electrical efficiency. Compared with DI water, the  $\text{ZrO}_2$  nanofluid improved electrical efficiency by 11.4 % at 0.0275 vol%. Dispersion of  $\text{ZrO}_2$  nanoparticles in the base fluid has enhanced thermal conductivity and then increased the absorption of excess heat, which causes an increase in the thermal efficiency of the PVT system. Thermal efficiency depends on mass flow rate, the specific heat of fluid used, and the temperature variation between inlet and outlet fluid. The maximum thermal efficiency achieved by cooling with  $\text{ZrO}_2$  nanofluid was 30.79% at 0.0275 vol% compared to DI water, with achieved 26.8 %. Compared with experimental results, the deviation of simulation results is about 2.7% of the electrical efficiency and 2.83%.

On the other hand, using the new hybrid nanofluid at different volume concentrations has noticeably improved electrical and thermal efficiencies. The new synthesis of  $\text{TiO}_2\text{-Fe}_2\text{O}_3$  nanocomposite dispersed into DI water significantly helped to decrease the PV cell's temperature more than mono nanofluid, then improved the electrical efficiency to 12.93% at 0.3 vol% compared to DI water which achieved 7.31 %. The high thermophysical properties of the hybrid nanofluid caused more heat absorption at the backside of the PV module, which reflected to increase in the thermal efficiency to 49.5% at 0.3 vol%. The simulation result of electrical and thermal efficiencies is validated with experimental results as shown in Figure 73 (b); the deviation of electrical efficiency was 3.61% 2.98% of  $\text{ZrO}_2$  and hybrid nanofluid, while thermal efficiency was 2.95 %, 3.1% which confirms the reasonable result of the module proposed.

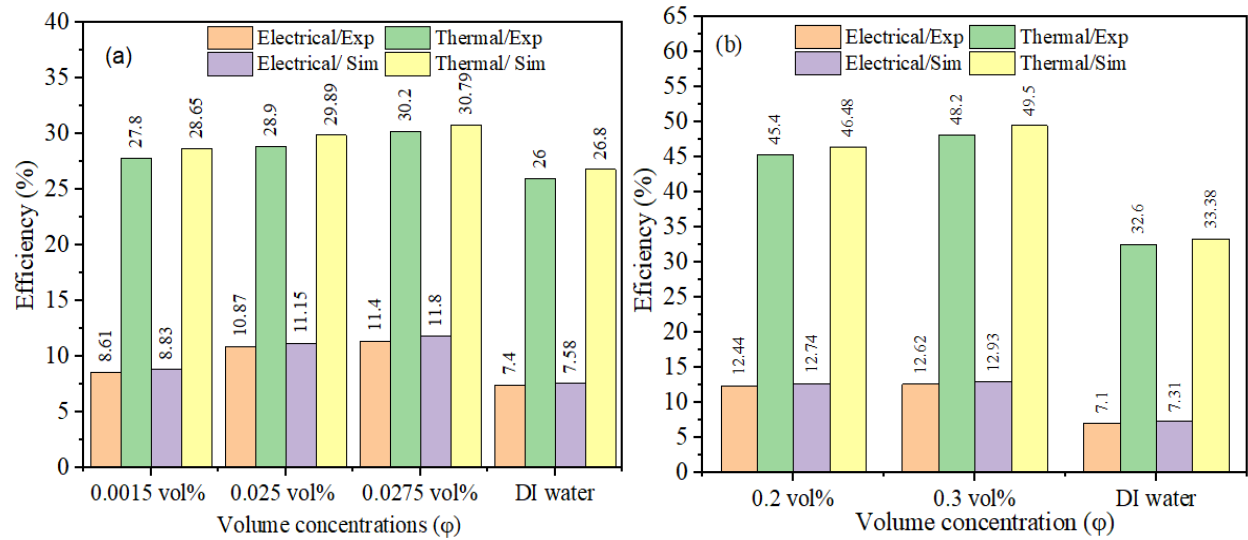


Figure 73. The electrical and thermal efficiencies of the PVT system cooled by (a)  $\text{ZrO}_2$  nanofluid and (b) hybrid  $\text{TiO}_2\text{-Fe}_2\text{O}_3$  nanofluid

Dispersion of nanomaterials in the base fluid improves their thermal properties because the nanomaterials have higher thermal properties than fluids. This chapter investigated the influence of adding  $\text{ZrO}_2$  nanoparticles and  $\text{TiO}_2\text{-Fe}_2\text{O}_3$  nanocomposite at different volume concentrations in DI water on Reynolds number, heat transfer coefficient, Nusselt number, and pressure drop. Depending on the maximum, average and minimum, it has calculated heat transfer coefficient, Nusselt number, and pressure drop from Eq. (15-17). Figure 74 (a and b) shows the effect of increased volume concentration of the  $\text{ZrO}_2$  and  $\text{TiO}_2\text{-Fe}_2\text{O}_3$  nanocomposite on the Nusselt number as a function of Reynold's number. There was a gradually increased in Nusselt number with increased Reynold's number with increased nanomaterials in the base fluid. Suspension of  $\text{ZrO}_2$  nanoparticles at 0.015 vol%, 0.025 vol% and 0.0275 vol% enhanced the Nusselt number by 12.6%, 17.3% and 19.6% compared to DI water. In contrast, the suspension of  $\text{TiO}_2\text{-Fe}_2\text{O}_3$  nanocomposite by 0.2 vol% and 0.3 vol% in the base fluid enhanced the Nusselt number by 25 % at 39.47% compared to the DI water. Increasing Nusselt numbers has a positive effect by increasing the heat transfer coefficient; thus, increasing the Reynolds number enhances the hybrid nanofluid's heat transfer coefficient. The maximum deviation between simulation and experimental results regarding using  $\text{ZrO}_2$  nanofluid was 2.46% and with  $\text{TiO}_2\text{-Fe}_2\text{O}_3$  was 2.3%.

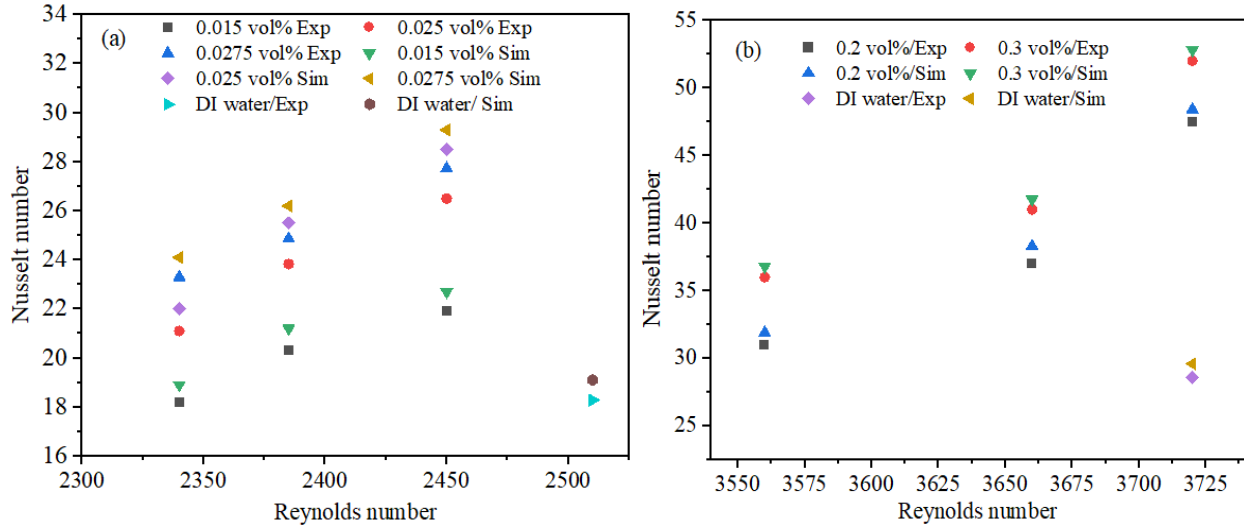


Figure 74. Effect of Reynolds number and volume concentration on Nusselt number at used (A) ZrO<sub>2</sub> nanofluid and (b) TiO<sub>2</sub>-Fe<sub>2</sub>O<sub>3</sub> nanofluid

Figure 75 (a) shows the increment of the heat transfer coefficient with Reynold's number increased at different volume concentrations due to the high thermal conductivity of the thermophysical properties of nanofluid. The gradual increase of ZrO<sub>2</sub> volume concentrations in host fluid enhanced the heat transfer coefficient by 9.1%, 10.75%, and 12.34 % compared with DI water. On the other side, Figure 75 (b) shows that adding 0.2 vol% and 0.3 vol% of TiO<sub>2</sub>-Fe<sub>2</sub>O<sub>3</sub> nanocomposite in DI water enhanced the heat transfer coefficient of hybrid nanofluid by 28.95% and 43.33%, which contributes to lower PV temperature more than DI water. Despite increasing the heat transfer coefficient due to increasing thermal conductivity, the density of the hybrid nanofluid is increased because of the volume concentration, which influences the pressure drop. Thereby, the deviation between experimental and simulation results is recorded at 2.65% at the used ZrO<sub>2</sub> nanofluid and with the used TiO<sub>2</sub>-Fe<sub>2</sub>O<sub>3</sub> nanocomposite is 2.96%. Despite the remarkable enhanced in thermal conductivity of nanofluid and the enhancement of the Nusselt number and heat transfer coefficient with the increase in volumetric concentration, there was a percentage increase in the nanofluid density, which effect on the pressure drop. Figure 76 (a) shows the pressure drop values when increased Reynolds number due to the increase in the nanofluid density at adding ZrO<sub>2</sub> nanoparticles at different volume concentrations in the DI water. Thus, the nanofluid's increased density and viscosity increased the pressure drop using ZrO<sub>2</sub> nanofluid to 18.7% at 0.0275 vol% compared to DI water. Figure 76 (b) shows the effect of the TiO<sub>2</sub>-Fe<sub>2</sub>O<sub>3</sub> nanocomposite dispersed in DI water, which worked to the flow's resistance and increased the pressure drop. Increasing the volume concentration of nanocomposite in the base fluid increased the pressure drop by 22.97% and 35.12% compared with DI water. Thereby the deviation of pressure drop in the simulation result was higher than the experimental result by 3.1% for the ZrO<sub>2</sub> nanofluid and 2.6% for the TiO<sub>2</sub>-Fe<sub>2</sub>O<sub>3</sub> hybrid nanofluid.

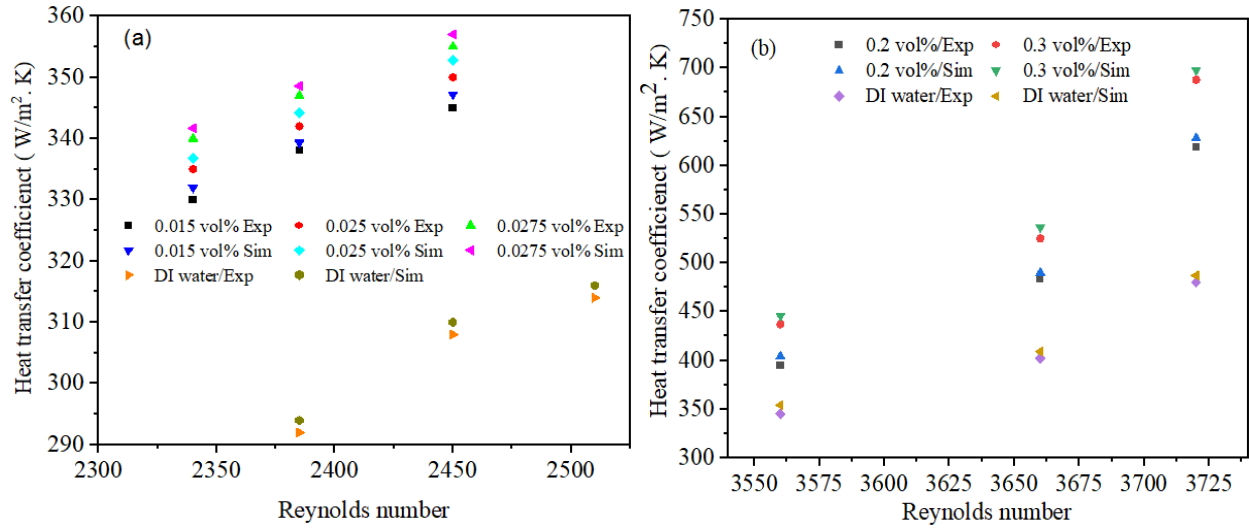


Figure 75. Effect of Reynolds number and volume concentration on heat transfer coefficient at used (A) ZrO<sub>2</sub> nanofluid and (b) TiO<sub>2</sub>-Fe<sub>2</sub>O<sub>3</sub> nanofluid

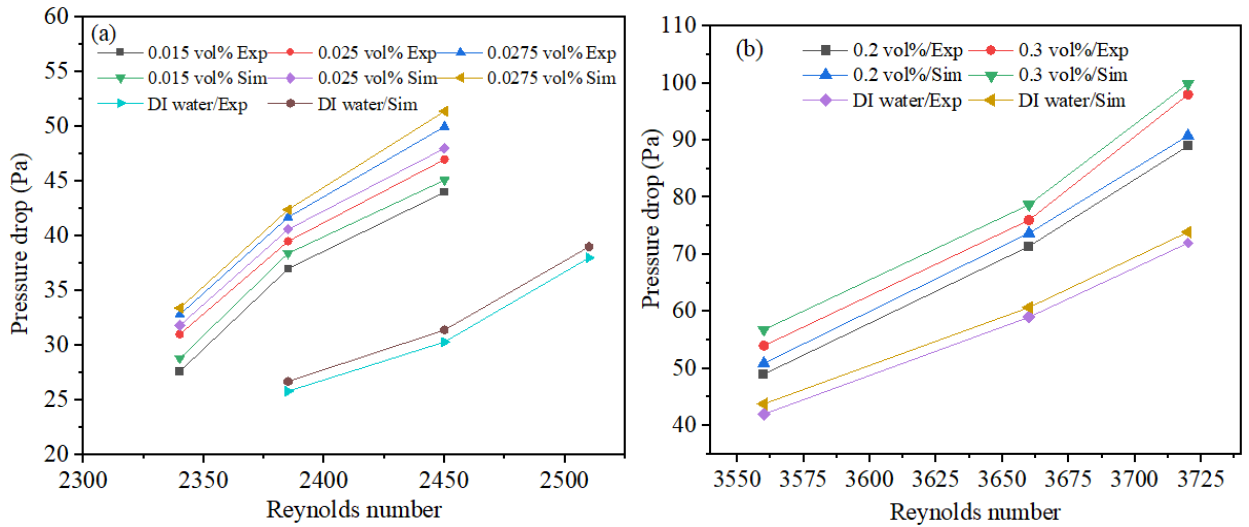


Figure 76. Effect of Reynolds number and volume concentration on pressure drop using (a) ZrO<sub>2</sub> nanofluid and (b) TiO<sub>2</sub>-Fe<sub>2</sub>O<sub>3</sub> nanofluid

### 7.3.3 Exergy evaluation of the PVT model

The outlet fluid temperature, the volume concentrations of nanomaterials in the DI water and the mass flow rate influence the thermal exergy efficiency of the system. Figure 77 (a and b) shows that the relative increase of the ZrO<sub>2</sub> nanoparticles and TiO<sub>2</sub>-Fe<sub>2</sub>O<sub>3</sub> nanocomposite in DI water led to a gradual increment of the thermal exergy efficiency higher than used DI water. Thereby, it can be observed that the thermal exergy efficiency was much lower than the electrical exergy efficiency. This is attributed to the outlet temperature of the fluids being closer to the ambient temperature, which agrees with [86]; the low quality of the thermal exergy is one of the reasons that causes reduced thermal exergy efficiency. The electrical exergy efficiency has relatively enhanced with increased volume concentrations and due to the enhanced heat transfer coefficient

of the nanofluid. Figure 99 (a) shows the gradual increment of the electrical exergy with increased volume concentrations, where the maximum electrical exergy recorded at used  $ZrO_2$  nanofluid to 10.324% at 0.0274 vol% compared to DI water. Figure 77 (b) demonstrates the ability of the  $TiO_2-Fe_2O_3$  nanofluid to enhance the electrical exergy of the PVT system, adding 0.2 vol% and 0.3 vol of nanocomposite in base fluid increased the electrical exergy to 11.8% and 12.62%, respectively, compared by cooling with DI water.

Nevertheless, using  $TiO_2-Fe_2O_3$  nanofluid increments the electrical exergy efficiency of the PVT system by 82.3%, 69.4% with increased the  $TiO_2-Fe_2O_3$  nanocomposite in DI water by 0.3% and 0.2% compared with DI water. Increment in the electrical energy efficiency significantly increased the overall exergy of the PVT system than thermal exergy efficiency; Figure 77 (b) shows the exergy efficiency of the PVT system cooled with DI water and hybrid  $TiO_2-Fe_2O_3$ . This is attributed to enhanced cooling fluid thermal conductivity reflected on enhanced convective heat transfer between circulating cooling fluid and tubes placed on the absorbing plate. The variation between simulation results, electrical and thermal exergy efficiencies of using  $ZrO_2$  nanofluid and experimental results were 2.61% and 3.12% respectively. While using, hybrid nanofluid has recorded 2.87% thermal exergy efficiency and 3.3% electrical exergy efficiency.

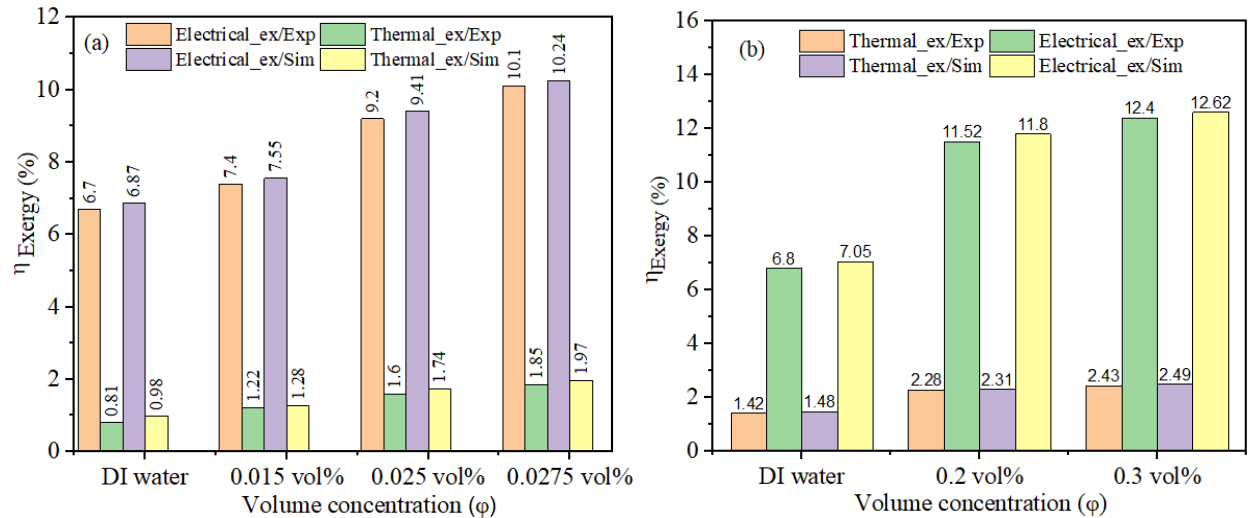


Figure 77. The exergy efficiency of the PVT system cooled by (a)  $ZrO_2$  nanofluid, (b)  $TiO_2-Fe_2O_3$  nanofluid

## 7.4 New contributions results

### Contribution 7

This chapter presents a numerical simulation study to investigate the effect of  $TiO_2-Fe_2O_3$  nanofluid and  $ZrO_2$  nanofluid at different volume concentrations on the energy, exergy, heat transfer coefficient, Nusselt number, and pressure drop of the PVT system. The important results of the simulation study are summarized as points below:

- Dispersion of nanomaterials in base fluid improves the thermophysical properties of cooling fluid higher than ID water, then accelerates heat exchange between circulated nanofluids in tubes and absorbs plate, which positively reflects on decreasing the PV cells temperature. The PVT system temperature decreased by 14.75% at cooling with  $ZrO_2$  nanofluid at 0.0275

vol% and by 20.7% by cooling with hybrid nanofluid at 0.3 vol%. Improving the thermal properties of nanofluid help increase heat absorption and reduces the PV cell's temperature, which affects by increased energy and exergy efficiency.

- Reduction of the PV cell's temperature increased their electrical and thermal efficiency, attributed to the improvement of the heat transfer coefficient between the absorbing plate, which has a low temperature, and the backside of the PV module, which has a high temperature. The heat exchange helped decrease the temperature and increased the electrical efficiency to 55.6% and 76.8% using  $ZrO_2$  and  $TiO_2-Fe_2O_3$  nanofluid. The heat absorption by absorb plate has maximized the thermal efficiency of the PVT system by 15% of  $ZrO_2$  nanofluid and 28.29% of  $TiO_2-Fe_2O_3$  hybrid compared to DI water.
- Because the solid material has higher thermal properties than fluids, the dispersion of nanomaterials in DI water improves the thermal properties of the nanofluid. The thermal parameters have improved with an increased volume concentration of nanofluid; increasing of Nusselt number led to an increase of heat transfer coefficient by 12.34 % at used  $ZrO_2$  nanofluid and 43.33% with hybrid nanofluid. An increase in volumetric concentration affects the pressure drop due to an increase in the nanofluid density, then increased the pressure drop by 18.7% using  $ZrO_2$  nanofluid, while using  $TiO_2-Fe_2O_3$  nanofluid increased the pressure drop to 35.12%.
- The exergy efficiency of the PVT system improved with the dispersion of nanomaterial in the DI water, which caused of increase in the exergy efficiency of the PVT system due to improving heat exchange between the heating body of the PV module backside and absorber plate, which has low temperature. Thus, improving the thermal conductivity of nanofluid helped to increase the electrical exergy by 10.324% with  $ZrO_2$  nanofluid, while using hybrid nanofluid enhanced electrical exergy to 12.62%. The low quality of the thermal exergy due to the closer of the outlet temperature to the ambient temperature, which affected the thermal energy of the PVT system.
- For validating the simulation result work, a comparison study has been implemented between the simulation results and the experimental results, as shown in Table 19 below, and it was observed reasonable conformity between the numerical results and the experimental results.

Table 19. The variation between simulation and experiments results

Nanofluid	Temperature	Electrical efficiency	Thermal efficiency	Heat Transfer coefficient	Nusselt number	Pressure drops	Electrical exergy efficiency	Thermal exergy efficiency
$ZrO_2$	2.86%	3.61%	2.95	2.46	2.56	3.1	2.61	2.87
$TiO_2-Fe_2O_3$	2.73%	2.98%	3.1	2.3	2.96	2.6	3.12	3.3

## Chapter 8

### Contributions to the scientific knowledge

This dissertation presents new scientific results that contribute to increasing the knowledge of readers and researchers about new methods that help increase the efficiency of solar energy systems (PV module and PVT system). The cooling approaches are discussed in an experimental and numerically scientific detailed manner to show the capabilities and modernity of the cooling approaches used to improve the energy and exergy of the PVT system. Thus, demonstrating the quantity and quality of the PVT system produced using different cooling approaches and operation conditions. The points below summarize the new scientific results, and full contributions are found at the end of chapters 3, 5, 6,7, and Appendix B.

#### 8.1 Prediction of PV module thermal and electrical behaviour under different conditions

Predicting any system behaviour is important to know the effect of changeable parameters on its performance. The PV module work mainly depends on the incident solar radiation, ambient temperature, and other parameters such as wind speed, manufacturing, etc. It's necessary to study the thermal behaviour of PV modules under different conditions to know their influence on the electrical behaviour and then specify the weak points that affect their performance. According to the properties of each layer which consists of the PV module, and the climatic conditions such as solar radiation, temperatures, and wind speed, the PV module was simulated by ANSYS software. The simulation study adopted various solar radiation values obtained by predictive mathematical equations for different seasons and at various temperatures to predict the thermal behaviour of the PV module. I found that the electrical power and efficiency of the PV module dropped with a low solar radiation value of  $176 \text{ W/m}^2$  and temperature between a maximum of  $15.4 \text{ }^\circ\text{C}$  and a minimum of  $11.9 \text{ }^\circ\text{C}$ ; this range did not cause damage to the PV cells but lowering the performance. Increasing solar radiation to  $735 \text{ W/m}^2$  with an ambient temperature of  $35 \text{ }^\circ\text{C}$  causes an increase in the PV module temperature, affecting the open circuit voltage and output power. Thus, this range of solar radiation and ambient temperature caused to increase in the PV module temperature to  $84.6 \text{ }^\circ\text{C}$ , which may lead to damage to PV cells.

On the other side, the electrical behaviour of the PV module has been investigated by MATLAB-Simulink by modelling the governing equations, which predict the  $P$ - $V$  and  $V$ - $I$  of the PV cell depending on the various values of solar radiation and temperature. The simulation mainly depends on the PV module datasheet under STC as a reference point for comparison with other changeable parameters. The model can predict electrical behaviour at different values of solar radiation and ambient temperature, which help to identify the appropriate range of PV module work under different conditions. I found that, at a constant temperature of  $25 \text{ }^\circ\text{C}$  and variable solar radiation from  $820$ ,  $535$ , and  $185 \text{ W/m}^2$ , the current of the PV module has reduced to  $21.5\%$ ,  $82.3\%$ , and  $414.7\%$ , respectively. In contrast, the voltage was reduced to  $13.6\%$ ,  $0.78.57\%$  and  $455.5\%$ , respectively, compared with the STC condition.

Furthermore, at constant solar radiation  $1000 \text{ W/m}^2$ , various temperature values at  $35 \text{ }^\circ\text{C}$ ,  $24 \text{ }^\circ\text{C}$ , and  $18 \text{ }^\circ\text{C}$ , the current of the PV cells is slightly decreased at  $35 \text{ }^\circ\text{C}$  by  $12\%$  and voltage by  $19\%$  compared with STC. The decreased temperature has enhanced the current and voltage of the PV module; the better condition was at  $1000 \text{ W/m}^2$  and  $24 \text{ }^\circ\text{C}$ , which was closer to STC conditions. Both simulation cases help us know the thermal and electrical behaviour of the PV module, thus specifying the best methods to improve their performance under different conditions.

## 8.2 Effect of passive cooling approaches applied

Cooling approach by cotton wicks immersed in water (CWIWs). The passive cooling approach represented by cotton wicks immersed in water generated continuous evaporative cooling, which decreased the PV module temperature by 22.34% and made it near ambient temperature. The generation of evaporative cooling helped increment the output power and efficiency by 114.8% and 113.2%, respectively, which were higher than the previous studies that used similar approaches. The reason returned to the type of cotton wicks used and the setting of the PV module. The internal structure consists of four small sub-cotton wicks collected together and covered with a cotton cover that helps absorbent, then transmission and distribution of water to all CWs arranged at the backside of the PV module adequately. The tilt angle and the height of the PV module from the ground allow great air to circulate on the backside of PV modules. Thus, the flowing of the air over the wetted surface of the cotton wicks causes water evaporates and cools the air that absorbs the heat from the PV module by forced convection and transfers it to air, which the productivity of the PV module enhances. In addition, water supplied to cotton wicks by gravity helped to sustain wetted cotton wicks throughout the experiment and avoid using external power. The quality of the PV module production has improved by incrementing the electrical exergy and exergy efficiency by 29.8% and 7.2 %, respectively. The exergy losses have dropped to 14%, while entropy generation has by 14.32% due to temperature reduction due to the effective cooling approach of CWIWs.

Cooling by cotton wicks integrated with rectangular aluminium fins (CWIRAFs). This case study compares passive (CWIRAF) cooling and active cooling (circulated water) and their effect on the PV module's performance. The passive cooling approach has been developed by integrating the cotton wicks with rectangular aluminium fins to increase evaporative cooling. Integrating wetted cotton wicks with aluminium fins that made direct contact with the backside of the PV module helped increase the heat transfer dissipation and reduced the PV module temperature higher than the first approach (without aluminium fins). The higher thermal conductivity of the cooled aluminium fins helps to enhance the heat exchanger at the backside of the PV module. Then it increases the conversion efficiency of the PV cells due to a temperature drop of 46.34%. Thereby, integrated cotton wicks by aluminium fins as on cooling approach achieved effective evaporative cooling applicable in hot conditions. The CWIRAFs cooling approach shows improved behaviour, which significantly enhanced the output power and efficiency of the PV module by 199.82% and 175.6% compared with the reference PV module. The CWs are characterized as an easy configuration that does not require maintenance, is locally available, cost-effective and does not react with the back layer of the PV module after immersing in water.

Nevertheless, some cons of utilizing cotton wicks, such as the water consumption in hot weather; thus, this approach may not be feasible for large-scale installations. Randomly increasing the quantity of CWs on the backside of the PV module affects its adhesion due to increased water absorption and becomes heavier. Incorrect arrangement of CWs leaves voids that lead to the uneven distribution of water in all the CWs and rising temperature in some places, which affect the PV module performance. In contrast, the active cooling approach performed less than passive cooling under similar conditions. This is attributed to indirect cooling, heat transfer across different PVT system layers, the thermal resistance of the layers, and the low thermal conductivity of the fluid circulated in tubes. However, The PVT collector enhances power yield and electrical efficiency by 131.2% and 153.2% compared with the reference module due to

removing excess heat from the backside by circulation water, then improving the thermal and overall efficiency of the PVT collector.

### **8.3 Effect of active cooling approaches applied**

Active cooling approaches are represented by different circulated types of mono and new hybrid nanofluids in copper tubes arranged in serpentine form by decreasing the distance between tubes to increase the heat exchanger area. The tubes have soldered on thin copper absorb plates to reduce thermal resistance and are attached to the PV module as a hybrid PVT system. The tubes and absorb plate work on absorbing the excess heat from the PV cells by conduction and convection heat transfer between the PVT system layers. The PVT system design has been enhanced by using thermal grease between the absorbing plate and the backside of the PV module, and new insulation (SLENTEX) having low thermal conductivity help to maximize thermal energy. According to hot climate conditions, new mono nanofluids not used by other researchers or studies, such as ( $ZrO_2$  and  $WO_3$ ) have been used as a cooling fluid to reduce the PV cells' high temperature and increase the PVT system energy and exergy. Using  $ZrO_2$  nanofluid helps decrease the PV cell temperature by 21.2%, and increasing the volume concentrations of the nanomaterials in the host fluid cause to enhance the heat transfer coefficient and Nusselt number by 13% and 51.7%. Thus, increased heat exchange between the absorbing plate (less hot) and the backside of the PV module (The hottest) helps increase the electrical power and efficiency to 87.3% and 54%, respectively. On the other hand, increased the exergy efficiency by 11.86% due to lowering the temperature, and the exergy losses and entropy generation were improved by 7% and 26%, respectively. Using  $WO_3$  nanofluid helped to reduce the temperature of the PV cells by 21%, which was reflected in enhanced electrical power and electrical efficiency by 62%, and 52% due to improved heat transfer coefficient to 5.3% with increased volume concentration to 1%. Increased volume concentration and Reynolds number caused an improved Nusselt number by 51.2% and increased the pressure drop by 49.2% compared to DI water. The exergy efficiency increased with the temperature low, effectively reducing the exergy loss and entropy generation by 15.32% and 53.5% because of their heat transfer enhancement and reduced fluid friction in PVT systems. Using both  $ZrO_2$  and  $WO_3$  nanofluids, the thermal exergy was lower than the electrical exergy because of the convergence of the fluid outlet temperature to the ambient temperature.

Therefore, both nanofluids achieved enhanced PVT system performance due to reduced PV cells temperature and increased electrical power. A slightly better variation has been observed of the PVT system performance at used  $ZrO_2$  nanofluid higher than  $WO_3$  nanofluid, and this is because the thermal conductivity of  $ZrO_2$  nanoparticles, which reflected heat transfer convection between absorb plate and circulated nanofluid. Thus, using  $ZrO_2$  nanofluids has effectively enhanced the exergy efficiency and reduced the exergy loss due to enhancing the heat transfer coefficient. Enhancing the heat transfer and reducing fluid friction led to a drop in the PVT system's entropy generation compared to the reference PV module. Cooling by different improving types of mono nanofluids represented by dispersion of the CuO NPs in DI water has improved the performance of the PVT system due to the decreased temperature of the PV cells by 23.44%, and this is attributed to the effectiveness of CuO NPs synthesized, which have high purity, and high thermal properties contribute to enhance the heat transfer convection between tubes and CuO nanofluid. Thus, increased the electrical power and efficiency of the PVT system by 70.7% and 90%, which was higher than the previous studies that used conventional approaches cooling by CuO

nanofluid. This returns to the effective PVT system design and effectiveness of CuO NPs synthesized.

Dispersion TiO<sub>2</sub> NEWs in DI water achieved higher performance of the PVT system than ZrO<sub>2</sub> and WO<sub>3</sub> nanofluid due to their low thermophysical properties compared with TiO<sub>2</sub> nanofluid. On another side, using TiO<sub>2</sub> nanofluid achieved lower performance of the PVT system compared with CuO nanofluid, despite the low density and increased specific heat of the TiO<sub>2</sub> NWs, but the thermal conductivity of CuO NPs has a major role by enhancing the heat transfer of nanofluid, which reflected of performance of the PVT system. Nevertheless, cooling with TiO<sub>2</sub> nanofluid reduced the PV cell reaches by 14%, reflecting an increment of power produced by 49.69%, then improved the electrical efficiency to 72.6% compared with DI water. Dispersion Fe<sub>2</sub>O<sub>3</sub> NPs in DI water achieved the highest performance of the PVT system than all the mono nanofluids used because of their high thermal properties. The gradually increased in the Fe<sub>2</sub>O<sub>3</sub> NPs in the base fluid caused an increase in heat transfer convection between the Fe<sub>2</sub>O<sub>3</sub> nanofluid and tubes, which caused a lower temperature of the absorbing plate due to direct contact between tubes and the absorbing plate by 29.64%. Thus, heat transfers from the hot body (backside of the PV module) to a relatively cold body (absorb plate). This heat transfer mechanism decreases the PV cell's temperature and then improves the electrical power and efficiency of the PVT system by 76.7% and 110.43%, respectively, compared with DI water. Thereby, using Fe<sub>2</sub>O<sub>3</sub> nanofluid achieved higher temperature reduction of the PVT system than CuO and TiO<sub>2</sub> nanofluids by 26.45% and 111.7%, respectively. In contrast, electrical power and electrical efficiency of the PVT system cooled with Fe<sub>2</sub>O<sub>3</sub> nanofluid were higher than cooling by CuO and TiO<sub>2</sub> nanofluids by 8.48%, 54.35%, 22.7% and 52.1%, respectively, which confirm the effectiveness of Fe<sub>2</sub>O<sub>3</sub> nanofluid as a cooling fluid.

The new hybrid nanocomposite synthesized has a positive effect on the nanofluid preparation by improving its thermal properties. Loading TiO<sub>2</sub> NWs over Fe<sub>2</sub>O<sub>3</sub> NPs, and TiO<sub>2</sub> NWs over CuO NPs led to the increased surface area of the hybrid nanocomposite, increased thermal conductivity and specific heat. Improving the nanocomposite's thermophysical properties significantly affects the heat transfer coefficient, Heat transfer rate, Nusselt number, and Reynolds Number of the hybrid nanofluids, which affects PVT system performance. I have found that dispersion of TiO<sub>2</sub>-Fe<sub>2</sub>O<sub>3</sub> hybrid nanocomposite in DI water increased the heat transfer coefficient by 25% of nanofluid, which was reflected by enhancing the heat transfer convection between hot tubes and nanofluid. This caused a lowering of the absorb plate temperature that dropped the temperature of the PV cells by 37.06% due to heat exchange. Reducing the PV cell's temperature has enhanced the electrical power output by 71% and the overall efficiency of the PVT system by 50.68% compared to DI water. Compared with DI water, it found that using TiO<sub>2</sub>-Fe<sub>2</sub>O<sub>3</sub> reduced the exergy loss and entropy generation by 47.3% and 70.47% due to temperature reduction, which led to increments in the exergy efficiency of the PVT system by 79.1%. It was observed that a slight increment in the thermal exergy efficiency was due to the closer of the outlet fluid temperature to the ambient temperature. Also found increased the pressure drop value by 36.12% with increased volume concentration in DI water, which caused an increase in the density and viscosity, then increased flow resistance of nanoparticles compared with cooling by DI water. On the other hand, dispersion of TiO<sub>2</sub>-CuO nanocomposite in DI water achieved cooling not less effective than TiO<sub>2</sub>-Fe<sub>2</sub>O<sub>3</sub> nanofluid. I found that using TiO<sub>2</sub>-CuO nanofluid helps improve the energy and exergy efficiency of the PVT system. Loading of TiO<sub>2</sub> NWs over the CuO NPs achieved higher thermal conductivity and less density than TiO<sub>2</sub>-Fe<sub>2</sub>O<sub>3</sub> nanocomposite, which decreased the PV cell's temperature by 39.16 %,

which was higher than the other nanofluids used. Then enhanced the energy and exergy efficiencies by 113.8% and 78.6%, with fewer exergy losses than  $\text{TiO}_2\text{-Fe}_2\text{O}_3$  by 44.3%. Lowering the PV cell's temperature reduced the entropy generation by 69.6% more than DI water. It was observed that lower thermal exergy efficiency, which also attributed to the low quality of the thermal exergy. Compared with mono nanofluids, I found that the hybrid nanofluid has a higher ability as a cooling fluid than mono nanofluids because of their new thermophysical properties and the new morphology of the nanocomposite shape. Preparation of the volume concentrations selected in DI water helped enhance the performance of nanofluid. Thus avoid the agglomerate of nanomaterial in DI water and decrease the pumping power consumption. It was found that the PVT system's performance is convergent at both hybrid nanofluids with slight variation in temperature drop and electrical power at using  $\text{TiO}_2\text{-CuO}$  nanofluid, which is slightly higher than used  $\text{TiO}_2\text{-Fe}_2\text{O}_3$  nanofluid. This is attributed to the slight increase in thermal conductivity of the  $\text{TiO}_2\text{-CuO}$  nanofluid than  $\text{TiO}_2\text{-Fe}_2\text{O}_3$  nanofluid.

#### **8.4 Numerical simulation effect nanofluids on the PVT system performance**

In this chapter, a numerical simulation of the effects of  $\text{ZrO}_2$ /water nanofluid and  $\text{TiO}_2\text{-Fe}_2\text{O}_3$  hybrid nanofluid as cooling fluids on the temperature, energy efficiency, exergy efficiency, heat transfer coefficient, Nusselt number, Reynold number, and pressure drops in system PVT system. The numerical simulation has been conducted for a proposed model consisting of PVT components by ANSYS Fluent 19.2; the numerical simulation results have been validated with the experimental results. Dispersion of nanomaterials in base fluid improves the thermal properties of the nanofluid due to the high thermal conductivity of solid materials, which leads to improved thermal parameters of nanofluids with increased volume concentrations. By increasing the volume concentration, the Nusselt number increased and improved of heat transfer coefficient by 12.34 % and 43.33% at used  $\text{ZrO}_2$  and hybrid nanofluid. It was observed increased the pressure dropped by 18.7% and 35.12% at using  $\text{ZrO}_2$  and hybrid nanofluid because the increased volume concentration caused to increase in the nanofluid density. The simulation results show that the adopted  $\text{ZrO}_2$  nanofluid helped decrease the PV cell's temperature to 14.75%, while a hybrid  $\text{TiO}_2\text{-Fe}_2\text{O}_3$  nanofluid reduced the temperature by 20.7%. Because of the high thermophysical properties of hybrid nanofluids, which accelerate heat exchange between circulated nanofluids in tubes and absorbing plates, thus cause decreasing the PV cell's temperature.

The maximum deviation regarding decreased PV cell temperature between simulation results and experimental results was 2.79%. Improving the heat transfer coefficient has positively affected the heat exchange between the hot backside of the PV module and the absorbing plate, which have a lower temperature, which causes reduced temperature and improved the electrical efficiency by 55.6% and 76.8% using  $\text{ZrO}_2$  and hybrid nanofluid. While absorbing the excess heat from by absorb plate has maximized the thermal efficiency by 15% and 28.29% at used  $\text{ZrO}_2$  nanofluid and  $\text{TiO}_2\text{-Fe}_2\text{O}_3$  nanofluid. The deviation was 3.93% and 3.025% between the simulation and experimental results for the electrical and thermal efficiencies. Improved heat exchange area due to enhancing the thermal conductivity of nanofluid led to increasing the electrical exergy by 10.324% at using  $\text{ZrO}_2$  nanofluid; this percentage is an increment to 12.625 with using hybrid nanofluid. Thermal exergy efficiency was lower than electrical exergy efficiency, which was proven in experimental results due to the low quality of the thermal exergy. The maximum deviation of the thermal and electrical exergy efficiencies was 3.285% and 2.86% between the simulation and experimental results.

## **Bibliography**

### **Papers published in international journals**

- [J1] Alktranee, M. & Péter, B. Energy and exergy analysis for photovoltaic modules cooled by evaporative cooling techniques. *Energy Reports* 9, 122–132 (2023).
- [J2] Alktranee, M. et al. Energy and Exergy Assessment of Photovoltaic-Thermal System Using Tungsten Trioxide Nanofluid: An Experimental Study. *Int. J. Thermofluids* 100228 (2022).
- [J3] Alktranee, M. et al. Effect of Zirconium Oxide Nanofluid on the Behaviour of Photovoltaic-Thermal System: An Experimental Study. *Energy Reports* 9, 122–132 (2023).
- [J4] Alktranee, M. & Bencs, P. Experimental comparative study using different cooling techniques with photovoltaic modules. *Journal of Thermal Analysis and Calorimetry*. 2023.
- [J5] Alktranee, M. & Bencs, P. Effect of Evaporative Cooling on Photovoltaic Module Performance. *Process Integr. Optim. Sustain.* 1–10 (2022)
- [J6] Alktranee, M. & Bencs, P. Applications of nanotechnology with hybrid photovoltaic/thermal systems: A review. *J. Appl. Eng. Sci.* 19, 292–306 (2021).
- [J7] Alktranee, M. & Bencs, P. Test the mathematical of the photovoltaic model under different conditions by using Matlab–Simulink. *J. Mech. Eng. Res. Dev.* 43, 514–521 (2020).
- [J8] Bencs, P. & Alktranee, M. The potential of vehicle cooling systems. *Journal of physics: Conference series* vol. 1935 12012 (IOP Publishing, 2021).

### **Papers published in Hungarian journals**

- [J1] Alktranee, M. & Bencs, P. Simulation study of the photovoltaic panel under different operation conditions. *ACTA IMEKO* 10, 62–66 (2021).
- [J2] Alktranee, M. & Bencs, P. Overview of the hybrid solar system. *Analecta Tech. Szeged.* 14, 100–108 (2020).
- [J3] Bencs, P., Al-Ktranee, M. & Mészáros, K. M. Effects of solar panels on electrical networks. *Analecta Tech. Szeged.* 14, 50–60 (2020).
- [J4] Péter, B., Dávid, F. & Alktranee, M. Áramlás-és Hőtechnikai fejlesztések az EFOP-361 projekt keretében. *Multidiszcip. Tudományok* 11, 107–115 (2021).

### **Conferences participation**

- [C1] Spring wind conference, Hungary, 28 May 2021.
- [C2] International conference on vehicle and automotive engineering (VAE 2022) 8-9 September 2022, Miskolc, Hungary.
- [C3] 17th Miklós Iványi International PhD and DLA Symposium 25-26 Oct, Pécs, Hungary 2021
- [C4] 5th Agria Conference on Innovative Vehicle Technologies and Automation Solutions InnoVeTAS 2021 Digitization is the new normal, Hungary, 13th May 2021.
- [C5] International Conference on Vehicle and Automotive Engineering (VAE2022) 8-9 September 2022, Miskolc, Hungary

### **Papers not related to the dissertation**

- [O1] Alktranea, M. H. R., Al-Yasiric, Q. & Kabele, A. E. Improving the productivity of single-slope solar still using Fresnel lenses under Iraq climatic conditions. *Desalin Water Treat* 205, 22–30 (2020).
- [O2] Alktranee, M. H. R., Al-Yasiri, Q. & Sahib, M. M. Power output enhancement of grid-connected PV system using dual-axis tracking. *Renew. Energy Environ. Sustain.* 5, 8 (2020).

## References

- [1] P. A. Østergaard, N. Duic, Y. Noorollahi, H. Mikulcic, and S. Kalogirou, “Sustainable development using renewable energy technology,” *Renewable Energy*, vol. 146. Elsevier, pp. 2430–2437, 2020.
- [2] P. J. T. Straatman and W. G. Van Sark, “A new hybrid ocean thermal energy conversion–Offshore solar pond (OTEC–OSP) design: A cost optimization approach,” *Sol. Energy*, vol. 82, no. 6, pp. 520–527, 2008.
- [3] M. Ball, M. Wietschel, and O. Rentz, “Integration of a hydrogen economy into the German energy system: an optimising modelling approach,” *Int. J. Hydrogen Energy*, vol. 32, no. 10–11, pp. 1355–1368, 2007.
- [4] P. Yilmaz, M. H. Hocaoglu, and A. E. S. Konukman, “A pre-feasibility case study on integrated resource planning including renewables,” *Energy Policy*, vol. 36, no. 3, pp. 1223–1232, 2008.
- [5] D. Das, P. Kalita, and O. Roy, “Flat plate hybrid photovoltaic-thermal (PV/T) system: A review on design and development,” *Renew. Sustain. Energy Rev.*, vol. 84, pp. 111–130, 2018.
- [6] D. H. W. Li, L. Yang, and J. C. Lam, “Zero energy buildings and sustainable development implications—A review,” *Energy*, vol. 54, pp. 1–10, 2013.
- [7] A. Hepbasli, “A key review on exergetic analysis and assessment of renewable energy resources for a sustainable future,” *Renew. Sustain. energy Rev.*, vol. 12, no. 3, pp. 593–661, 2008.
- [8] M. Alktrane and P. Bencs, “Overview of the hybrid solar system,” *Analecta Tech. Szeged.*, vol. 14, no. 1, pp. 100–108, 2020, doi: 10.14232/analecta.2020.1.100-108.
- [9] A. Dawar, A. Wakif, T. Thumma, and N. A. Shah, “Towards a new MHD non-homogeneous convective nanofluid flow model for simulating a rotating inclined thin layer of sodium alginate-based Iron oxide exposed to incident solar energy,” *Int. Commun. Heat Mass Transf.*, vol. 130, p. 105800, 2022.
- [10] N. Kannan and D. Vakeesan, “Solar energy for future world review,” *Renew. Sustain. Energy Rev.*, vol. 62, pp. 1092–1105, 2016.
- [11] V. Tomar, B. Norton, and G. N. Tiwari, “A novel approach towards investigating the performance of different PVT configurations integrated on test cells: An experimental study,” *Renew. Energy*, vol. 137, pp. 93–108, 2019.
- [12] Y. Wang, M. L. Kamari, S. Haghghat, and P. T. T. Ngo, “Electrical and thermal analyses of solar PV module by considering realistic working conditions,” *J. Therm. Anal. Calorim.*, vol. 144, no. 5, pp. 1925–1934, 2021.
- [13] A. F. Abed, D. M. Hachim, and S. E. Najim, “A Novel Hybrid PV/T System for Sustainable Production of Distillate Water from the Cooling of the PV Module,” in *IOP Conference Series: Materials Science and Engineering*, 2021, vol. 1094, no. 1, p. 12049.
- [14] Z. Fu, X. Liang, Y. Li, L. Li, and Q. Zhu, “Performance improvement of a PVT system using a multilayer structural heat exchanger with PCMs,” *Renew. Energy*, vol. 169, pp. 308–317, 2021.
- [15] J. Siecker, K. Kusakana, and et B. P. Numbi, “A review of solar photovoltaic systems cooling technologies,” *Renew. Sustain. Energy Rev.*, vol. 79, pp. 192–203, 2017.
- [16] S. Odeh and M. Behnia, “Improving photovoltaic module efficiency using water cooling,” *Heat Transf. Eng.*, vol. 30, no. 6, pp. 499–505, 2009.

- [17] M. Aghaei *et al.*, “Review of degradation and failure phenomena in photovoltaic modules,” *Renew. Sustain. Energy Rev.*, vol. 159, p. 112160, 2022.
- [18] I. W. G. on the E. of C. R. to Humans, “Solar and ultraviolet radiation,” *Radiation*, 2012.
- [19] L. J. Piotrowski, M. G. Simões, and F. A. Farret, “Feasibility of water-cooled photovoltaic panels under the efficiency and durability aspects,” *Sol. Energy*, vol. 207, pp. 103–109, 2020.
- [20] D. C. Jordan, S. R. Kurtz, K. VanSant, and J. Newmiller, “Compendium of photovoltaic degradation rates,” *Prog. Photovoltaics Res. Appl.*, vol. 24, no. 7, pp. 978–989, 2016.
- [21] M. Suthar, G. K. Singh, and R. P. Saini, “Performance evaluation of sun tracking photovoltaic systems: a case study,” 2013.
- [22] W. Luo *et al.*, “Potential-induced degradation in photovoltaic modules: a critical review,” *Energy Environ. Sci.*, vol. 10, no. 1, pp. 43–68, 2017.
- [23] B. V Chikate, Y. Sadawarte, and B. Sewagram, “The factors affecting the performance of solar cell,” *Int. J. Comput. Appl.*, vol. 1, no. 1, pp. 975–8887, 2015.
- [24] K. Sudhakar, N. Jain, and S. Bagga, “Effect of color filter on the performance of solar photovoltaic module,” in *2013 International Conference on Power, Energy and Control (ICPEC)*, 2013, pp. 35–38.
- [25] P. Dwivedi, K. Sudhakar, A. Soni, E. Monomin, and I. Kirpichnikova, “Advanced cooling techniques of P.V. modules: A state of art,” *Case Stud. Therm. Eng.*, vol. 21, no. June, p. 100674, 2020, doi: 10.1016/j.csite.2020.100674.
- [26] N. Abdollahi and M. Rahimi, “Potential of water natural circulation coupled with nano-enhanced PCM for PV module cooling,” *Renew. Energy*, vol. 147, pp. 302–309, 2020.
- [27] Y. Xu, Y. Xuan, and L. Yang, “Full-spectrum photon management of solar cell structures for photovoltaic–thermoelectric hybrid systems,” *Energy Convers. Manag.*, vol. 103, pp. 533–541, 2015.
- [28] I. A. Hasan and D. A. Attar, “Effect of evaporative cooling combined with heat sink on PV module performance,” *J. Univ. Babylon Eng. Sci.*, vol. 27, no. 2, pp. 252–264, 2019.
- [29] M. Chandrasekar, S. Rajkumar, and D. Valavan, “A review on the thermal regulation techniques for non integrated flat PV modules mounted on building top,” *Energy Build.*, vol. 86, pp. 692–697, 2015.
- [30] A. S. Abdelrazik, F. A. Al-Sulaiman, R. Saidur, and R. Ben-Mansour, “A review on recent development for the design and packaging of hybrid photovoltaic/thermal (PV/T) solar systems,” *Renew. Sustain. Energy Rev.*, vol. 95, pp. 110–129, 2018.
- [31] G. S. Menon, S. Murali, J. Elias, D. S. Aniesrani Delfiya, P. V. Alfiya, and M. P. Samuel, “Experimental investigations on unglazed photovoltaic-thermal (PVT) system using water and nanofluid cooling medium,” *Renew. Energy*, vol. 188, pp. 986–996, 2022, doi: 10.1016/j.renene.2022.02.080.
- [32] H. Fayaz, R. Nasrin, N. A. Rahim, and M. Hasanuzzaman, “Energy and exergy analysis of the PVT system: Effect of nanofluid flow rate,” *Sol. Energy*, vol. 169, pp. 217–230, 2018.
- [33] M. Sardarabadi, M. Hosseinzadeh, A. Kazemian, and M. Passandideh-Fard, “Experimental investigation of the effects of using metal-oxides/water nanofluids on a photovoltaic thermal system (PVT) from energy and exergy viewpoints,” *Energy*, vol. 138, pp. 682–695, 2017, doi: 10.1016/j.energy.2017.07.046.
- [34] M. I. Hussain, J.-H. Kim, and J.-T. Kim, “Nanofluid-powered dual-fluid photovoltaic/thermal (pv/t) system: Comparative numerical study,” *Energies*, vol. 12, no. 5, p. 775, 2019.

- [35] A. H. Alami, “Effects of evaporative cooling on efficiency of photovoltaic modules,” *Energy Convers. Manag.*, vol. 77, pp. 668–679, 2014.
- [36] M. Chandrasekar and T. Senthilkumar, “Passive thermal regulation of flat PV modules by coupling the mechanisms of evaporative and fin cooling,” *Heat Mass Transf. und Stoffuebertragung*, vol. 52, no. 7, pp. 1381–1391, 2016, doi: 10.1007/s00231-015-1661-9.
- [37] L. J. Simpson, J. Woods, N. Valderrama, A. Hill, N. Vincent, and T. Silverman, “Passive Cooling of Photovoltaics with Desiccants,” in *2017 IEEE 44th Photovoltaic Specialist Conference (PVSC)*, 2017, pp. 1893–1897.
- [38] P.-L. Paradis, D. R. Rouse, L. Lamarche, and H. Nesreddine, “A hybrid PV/T solar evaporator using CO<sub>2</sub>: Numerical heat transfer model and simulation results,” *Sol. Energy*, vol. 170, pp. 1118–1129, 2018.
- [39] A. D. Tuncer, A. Khanlari, İ. Aytaç, E. Çiftçi, A. Sözen, and H. İ. Variyenli, “Passive thermal management of photovoltaic panel by using phase change material-filled aluminium cans: an experimental study,” *Heat Transf. Res.*, vol. 53, no. 5, 2022.
- [40] Z. Arifin, S. Suyitno, D. D. D. P. Tjahjana, W. E. Juwana, M. R. A. Putra, and A. R. Prabowo, “The effect of heat sink properties on solar cell cooling systems,” *Appl. Sci.*, vol. 10, no. 21, p. 7919, 2020.
- [41] T. Nabil and T. M. Mansour, “Augmenting the performance of photovoltaic panel by decreasing its temperature using various cooling techniques,” *Results Eng.*, p. 100564, 2022.
- [42] A. Parthiban, K. S. Reddy, B. Pesala, and T. K. Mallick, “Effects of operational and environmental parameters on the performance of a solar photovoltaic-thermal collector,” *Energy Convers. Manag.*, vol. 205, p. 112428, 2020.
- [43] Z. Wang, J. Wei, G. Zhang, H. Xie, and M. Khalid, “Design and performance study on a large-scale hybrid CPV/T system based on the unsteady-state thermal model,” *Sol. Energy*, vol. 177, pp. 427–439, 2019.
- [44] A. Rahaei, R. Rafee, and M. R. Zargarabadi, “A photovoltaic thermal system with a complete contact between water and PV modules suitable for district heating and electric power generation,” *Sustain. Energy Technol. Assessments*, vol. 47, p. 101325, 2021.
- [45] S. Misha, A. L. Abdullah, N. Tamaldin, M. A. M. Rosli, and F. A. Sachit, “Simulation CFD and experimental investigation of PVT water system under natural Malaysian weather conditions,” *Energy Reports*, vol. 6, pp. 28–44, 2020.
- [46] P. Chidambaram, R. Govindan, and K. C. Venkatraman, “Study of Thermal Comfort Properties of Cotton / Regenerated Bamboo Knitted Fabrics,” vol. 4, no. 2, pp. 60–66, 2012, doi: 10.5829/idosi.ajbas.2012.4.2.1032.
- [47] A. Fudholi, K. Sopian, M. H. Yazdi, M. H. Ruslan, A. Ibrahim, and H. A. Kazem, “Performance analysis of photovoltaic thermal (PVT) water collectors,” *Energy Convers. Manag.*, vol. 78, pp. 641–651, 2014.
- [48] S. M. Shalaby, M. K. Elfakharany, B. M. Moharram, and H. F. Abosheiasha, “Experimental study on the performance of PV with water cooling,” *Energy Reports*, vol. 8, pp. 957–961, 2022.
- [49] S. Aghakhani, M. Afrand, A. Karimipour, R. Kalbasi, and M. M. Razzaghi, “Numerical study of the cooling effect of a PVT on its thermal and electrical efficiency using a Cu tube of different diameters and lengths,” *Sustain. Energy Technol. Assessments*, vol. 52, p. 102044, 2022.
- [50] T. Le Ba *et al.*, “Experimental Study of Halloysite Nanofluids in Pool Boiling Heat

- Transfer,” *Molecules*, vol. 27, no. 3, p. 729, 2022, doi: 10.3390/molecules27030729.
- [51] M. Firoozzadeh, A. H. Shiravi, M. Lotfi, S. Aidarova, and A. Sharipova, “Optimum concentration of carbon black aqueous nanofluid as coolant of photovoltaic modules: A case study,” *Energy*, vol. 225, 2021, doi: 10.1016/j.energy.2021.120219.
- [52] S. Aberoumand, S. Ghamari, and B. Shabani, “Energy and exergy analysis of a photovoltaic thermal (PV/T) system using nanofluids: An experimental study,” *Sol. Energy*, vol. 165, no. January, pp. 167–177, 2018, doi: 10.1016/j.solener.2018.03.028.
- [53] G. S. Menon, S. Murali, J. Elias, D. S. A. Delfiya, P. V Alfiya, and M. P. Samuel, “Experimental investigations on unglazed photovoltaic-thermal (PVT) system using water and nanofluid cooling medium,” *Renew. Energy*, vol. 188, pp. 986–996, 2022.
- [54] S. Diwania, R. Kumar, S. K. Singh, G. S. Dua, and P. Khetrapal, “Performance assessment of a serpentine tube PVT system using Cu and TiO<sub>2</sub> nanofluids: an experimental study,” *J. Brazilian Soc. Mech. Sci. Eng.*, vol. 44, no. 2, pp. 1–18, 2022, doi: 10.1007/s40430-022-03366-5.
- [55] M.-W. Tian *et al.*, “Energy, exergy and economics study of a solar/thermal panel cooled by nanofluid,” *Case Stud. Therm. Eng.*, vol. 28, p. 101481, 2021.
- [56] S. Diwania, A. S. Siddiqui, S. Agrawal, and R. Kumar, “Modeling and assessment of the thermo-electrical performance of a photovoltaic-thermal (PVT) system using different nanofluids,” *J. Brazilian Soc. Mech. Sci. Eng.*, vol. 43, no. 4, pp. 1–18, 2021, doi: 10.1007/s40430-021-02909-6.
- [57] S. R. Abdallah, H. Saidani-Scott, and O. E. Abdellatif, “Performance analysis for hybrid PV/T system using low concentration MWCNT (water-based) nanofluid,” *Sol. Energy*, vol. 181, pp. 108–115, 2019.
- [58] T. Venkatesh, S. Manikandan, C. Selvam, and S. Harish, “Performance enhancement of hybrid solar PV/T system with graphene based nanofluids,” *Int. Commun. Heat Mass Transf.*, vol. 130, p. 105794, 2022, doi: 10.1016/j.icheatmasstransfer.2021.105794.
- [59] J. A. Duffie and W. A. Beckman, *Solar engineering of thermal processes*. John Wiley & Sons, 2013.
- [60] T. T. Chow, “Performance analysis of photovoltaic-thermal collector by explicit dynamic model,” *Sol. Energy*, vol. 75, no. 2, pp. 143–152, 2003.
- [61] O. Rejeb, H. Dhaou, and A. Jemni, “A numerical investigation of a photovoltaic thermal (PV/T) collector,” *Renew. Energy*, vol. 77, pp. 43–50, 2015.
- [62] O. Rejeb, M. Sardarabadi, C. Ménézo, M. Passandideh-Fard, M. H. Dhaou, and A. Jemni, “Numerical and model validation of uncovered nanofluid sheet and tube type photovoltaic thermal solar system,” *Energy Convers. Manag.*, vol. 110, pp. 367–377, 2016.
- [63] M. Sardarabadi and M. Passandideh-Fard, “Experimental and numerical study of metal-oxides/water nanofluids as coolant in photovoltaic thermal systems (PVT),” *Sol. Energy Mater. Sol. Cells*, vol. 157, pp. 533–542, 2016.
- [64] M. I. Hussain and J.-T. Kim, “Performance optimization of unglazed nanofluid photovoltaic/thermal system: Energy and exergy analyses,” *Int. J. Photoenergy*, vol. 2018, 2018.
- [65] D. L. Evans, “Simplified method for predicting photovoltaic array output,” *Sol. energy*, vol. 27, no. 6, pp. 555–560, 1981.
- [66] M. Hosseinzadeh, M. Sardarabadi, and M. Passandideh-Fard, “Energy and exergy analysis of nanofluid based photovoltaic thermal system integrated with phase change material,” *Energy*, vol. 147, pp. 636–647, Mar. 2018, doi: 10.1016/j.energy.2018.01.073.

- [67] F. Abbas *et al.*, “Towards convective heat transfer optimization in aluminum tube automotive radiators: Potential assessment of novel Fe<sub>2</sub>O<sub>3</sub>-TiO<sub>2</sub>/water hybrid nanofluid,” *J. Taiwan Inst. Chem. Eng.*, vol. 124, pp. 424–436, 2021.
- [68] M. Alktrane and P. Bencs, “Applications of nanotechnology with hybrid photovoltaic/thermal systems: A review,” *J. Appl. Eng. Sci.*, vol. 19, no. 2, pp. 292–306, 2021, doi: 10.5937/jaes0-28760.
- [69] P. Naphon, “Heat transfer characteristics and pressure drop in channel with V corrugated upper and lower plates,” *Energy Convers. Manag.*, vol. 48, no. 5, pp. 1516–1524, 2007.
- [70] A. H. A. Al-Waeli, M. T. Chaichan, H. A. Kazem, K. Sopian, and J. Safaei, “Numerical study on the effect of operating nanofluids of photovoltaic thermal system (PV/T) on the convective heat transfer,” *Case Stud. Therm. Eng.*, vol. 12, pp. 405–413, 2018.
- [71] S. Devireddy, C. S. R. Mekala, and V. R. Veeredhi, “Improving the cooling performance of automobile radiator with ethylene glycol water based TiO<sub>2</sub> nanofluids,” *Int. Commun. heat mass Transf.*, vol. 78, pp. 121–126, 2016.
- [72] A. M. Hussein, R. A. Bakar, K. Kadirgama, and K. V Sharma, “Experimental measurement of nanofluids thermal properties,” *Int. J. Automot. Mech. Eng.*, vol. 7, p. 850, 2013.
- [73] Z. Qiu, X. Zhao, P. Li, X. Zhang, S. Ali, and J. Tan, “Theoretical investigation of the energy performance of a novel MPCM (Microencapsulated Phase Change Material) slurry based PV/T module,” *Energy*, vol. 87, pp. 686–698, 2015.
- [74] Y. Demirel, “Thermodynamic analysis,” *Arab. J. Sci. Eng.*, vol. 38, no. 2, pp. 221–249, 2013.
- [75] T. T. Chow, G. Pei, K. F. Fong, Z. Lin, A. L. S. Chan, and J. Ji, “Energy and exergy analysis of photovoltaic–thermal collector with and without glass cover,” *Appl. Energy*, vol. 86, no. 3, pp. 310–316, 2009.
- [76] A. Fudholi *et al.*, “Energy and exergy analyses of photovoltaic thermal collector with V-groove,” *Sol. Energy*, vol. 159, pp. 742–750, 2018.
- [77] A. Farzanehnia and M. Sardarabadi, “Exergy in photovoltaic/thermal nanofluid-based collector systems,” in *Exergy and Its Application-Toward Green Energy Production and Sustainable Environment*, IntechOpen, 2019.
- [78] M. A. Shehab *et al.*, “Preparation and Photocatalytic Performance of TiO<sub>2</sub> Nanowire-Based Self-Supported Hybrid Membranes,” *Molecules*, vol. 27, no. 9, p. 2951, 2022.
- [79] M. Sołtys-Mróz, K. Syrek, J. Pierzchała, E. Wiercigroch, K. Malek, and G. D. Sulka, “Band gap engineering of nanotubular Fe<sub>2</sub>O<sub>3</sub>-TiO<sub>2</sub> photoanodes by wet impregnation,” *Appl. Surf. Sci.*, vol. 517, p. 146195, 2020.
- [80] Y. Li, S. Tung, E. Schneider, and S. Xi, “A review on development of nanofluid preparation and characterization,” *Powder Technol.*, vol. 196, no. 2, pp. 89–101, 2009.
- [81] M. Awais, A. A. Bhuiyan, S. Salehin, M. M. Ehsan, B. Khan, and M. H. Rahman, “Synthesis, heat transport mechanisms and thermophysical properties of nanofluids: A critical overview,” *Int. J. Thermofluids*, vol. 10, p. 100086, 2021.
- [82] M. Milanese, G. Colangelo, A. Cretì, M. Lomascolo, F. Iacobazzi, and A. De Risi, “Optical absorption measurements of oxide nanoparticles for application as nanofluid in direct absorption solar power systems–Part II: ZnO, CeO<sub>2</sub>, Fe<sub>2</sub>O<sub>3</sub> nanoparticles behavior,” *Sol. Energy Mater. Sol. Cells*, vol. 147, pp. 321–326, 2016.
- [83] N. Gupta, S. M. Gupta, and S. K. Sharma, “Synthesis, characterization and dispersion stability of water-based Cu–CNT hybrid nanofluid without surfactant,” *Microfluid.*

- Nanofluidics*, vol. 25, no. 2, pp. 1–14, 2021.
- [84] N. S. Binti Rukman, A. Fudholi, N. F. Mohd Razali, M. Hafidz Ruslan, and K. Sopian, “Investigation of TiO<sub>2</sub> and MWCNT Nanofluids-based Photovoltaic-Thermal (PV/T) System,” *IOP Conf. Ser. Earth Environ. Sci.*, vol. 268, no. 1, 2019, doi: 10.1088/1755-1315/268/1/012076.
- [85] A. H. A. Al-Waeli, M. T. Chaichan, H. A. Kazem, and K. Sopian, “Evaluation and analysis of nanofluid and surfactant impact on photovoltaic-thermal systems,” *Case Stud. Therm. Eng.*, vol. 13, p. 100392, 2019.
- [86] Y. Khanjari, F. Pourfayaz, and A. B. Kasaeian, “Numerical investigation on using of nanofluid in a water-cooled photovoltaic thermal system,” *Energy Convers. Manag.*, vol. 122, pp. 263–278, 2016.
- [87] S. M. S. Murshed, K. C. Leong, and C. Yang, “Thermophysical and electrokinetic properties of nanofluids—a critical review,” *Appl. Therm. Eng.*, vol. 28, no. 17–18, pp. 2109–2125, 2008.
- [88] D. A. Vincely and E. Natarajan, “Experimental investigation of the solar FPC performance using graphene oxide nanofluid under forced circulation,” *Energy Convers. Manag.*, vol. 117, pp. 1–11, 2016.
- [89] Z. Said, M. H. Sajid, M. A. Alim, R. Saidur, and N. A. Rahim, “Experimental investigation of the thermophysical properties of AL<sub>2</sub>O<sub>3</sub>-nanofluid and its effect on a flat plate solar collector,” *Int. Commun. heat mass Transf.*, vol. 48, pp. 99–107, 2013.
- [90] A. N. Al-Shamani, K. Sopian, S. Mat, H. A. Hasan, A. M. Abed, and M. H. Ruslan, “Experimental studies of rectangular tube absorber photovoltaic thermal collector with various types of nanofluids under the tropical climate conditions,” *Energy Convers. Manag.*, vol. 124, pp. 528–542, 2016.
- [91] M. J. Muhammad, I. A. Muhammad, N. A. C. Sidik, M. N. A. W. M. Yazid, R. Mamat, and G. Najafi, “Retracted: the use of nanofluids for enhancing the thermal performance of stationary solar collectors: a review.” Elsevier, 2016.
- [92] M. R. Safaei, A. Hajizadeh, M. Afrand, C. Qi, H. Yarmand, and N. W. B. M. Zulkifli, “Evaluating the effect of temperature and concentration on the thermal conductivity of ZnO-TiO<sub>2</sub>/EG hybrid nanofluid using artificial neural network and curve fitting on experimental data,” *Phys. A Stat. Mech. its Appl.*, vol. 519, pp. 209–216, 2019.
- [93] T.-K. Hong, H.-S. Yang, and C. J. Choi, “Study of the enhanced thermal conductivity of Fe nanofluids,” *J. Appl. Phys.*, vol. 97, no. 6, p. 64311, 2005.
- [94] R. Mehmood, S. Nadeem, and N. Sher Akbar, “Non-aligned ethylene-glycol 30% based stagnation point fluid over a stretching surface with hematite nano particles,” *J. Appl. Fluid Mech.*, vol. 9, no. 3, pp. 1359–1366, 2016.
- [95] S. K. Verma and A. K. Tiwari, “Progress of nanofluid application in solar collectors: a review,” *Energy Convers. Manag.*, vol. 100, pp. 324–346, 2015.
- [96] R. S. Vajjha and D. K. Das, “Measurements of specific heat and density of Al<sub>2</sub>O<sub>3</sub> nanofluid,” in *AIP Conference Proceedings*, 2008, vol. 1063, no. 1, pp. 361–370.
- [97] O. Arthur and M. A. Karim, “An investigation into the thermophysical and rheological properties of nanofluids for solar thermal applications,” *Renew. Sustain. Energy Rev.*, vol. 55, pp. 739–755, 2016.
- [98] S. Armstrong and W. G. Hurley, “A thermal model for photovoltaic panels under varying atmospheric conditions,” *Appl. Therm. Eng.*, vol. 30, no. 11–12, pp. 1488–1495, 2010.
- [99] P. I. Cooper, “The absorption of radiation in solar stills,” *Sol. energy*, vol. 12, no. 3, pp.

- 333–346, 1969.
- [100] “Weather and climate, Miskolc, Hungary,” 2021.
- [101] J. A. D. Deceased and W. A. Beckman, *Solar engineering of thermal processes*, vol. 3, no. 3. 1982. doi: 10.1016/0142-694x(82)90016-3.
- [102] H. C. Hottel, “A simple model for estimating the transmittance of direct solar radiation through clear atmospheres,” *Sol. energy*, vol. 18, no. 2, pp. 129–134, 1976.
- [103] I. Bodnár, P. Iski, D. Koós, and Á. Skribanek, “Examination of electricity production loss of a solar panel in case of different types and concentration of dust,” in *Advances and Trends in Engineering Sciences and Technologies III*, CRC Press, 2019, pp. 313–318.
- [104] F. Abbas *et al.*, “Towards convective heat transfer optimization in aluminum tube automotive radiators: Potential assessment of novel Fe<sub>2</sub>O<sub>3</sub>-TiO<sub>2</sub>/water hybrid nanofluid,” *J. Taiwan Inst. Chem. Eng.*, vol. 124, pp. 424–436, 2021, doi: 10.1016/j.jtice.2021.02.002.
- [105] S. M. Peyghambarzadeh, S. H. Hashemabadi, M. Naraki, and Y. Vermahmoudi, “Experimental study of overall heat transfer coefficient in the application of dilute nanofluids in the car radiator,” *Appl. Therm. Eng.*, vol. 52, no. 1, pp. 8–16, 2013.
- [106] E. M. C. Contreras, G. A. Oliveira, and E. P. Bandarra Filho, “Experimental analysis of the thermohydraulic performance of graphene and silver nanofluids in automotive cooling systems,” *Int. J. Heat Mass Transf.*, vol. 132, pp. 375–387, 2019.
- [107] R. S. Hansen, C. S. Narayanan, and K. K. Murugavel, “Performance analysis on inclined solar still with different new wick materials and wire mesh,” *Desalination*, vol. 358, pp. 1–8, 2015.
- [108] P. Chidambaram, R. Govindan, and K. C. Venkatraman, “Study of thermal comfort properties of cotton/regenerated bamboo knitted fabrics,” *African J. Basic Appl. Sci.*, vol. 4, no. 2, pp. 60–66, 2012.
- [109] K. S. Hanumanth Ramji, J. Vinoth Kumar, and A. Amar Karthik, “Experimental Investigation of Automobile radiator using Tungsten trioxide Nano-fluid,” *IOP Conf. Ser. Mater. Sci. Eng.*, vol. 995, no. 1, 2020, doi: 10.1088/1757-899X/995/1/012017.
- [110] Z. A. Haidar, J. Orfi, and Z. Kaneesamkandi, “Photovoltaic panels temperature regulation using evaporative cooling principle: Detailed theoretical and real operating conditions experimental approaches,” *Energies*, vol. 14, no. 1, p. 145, 2020.
- [111] A. Pandey, S. Chakrabarti, and P. Daghe, “A systematic approach for a better thermal management of photovoltaic systems-a review,” *J. Comput. Appl. Res. Mech. Eng.*, vol. 10, no. 1, pp. 1–24, 2020, doi: 10.22061/JCARME.2019.5814.1734.
- [112] M. Chandrasekar and T. Senthilkumar, “Experimental demonstration of enhanced solar energy utilization in flat PV (photovoltaic) modules cooled by heat spreaders in conjunction with cotton wick structures,” *Energy*, vol. 90, pp. 1401–1410, 2015, doi: 10.1016/j.energy.2015.06.074.
- [113]: : “Agrometeorological Network::” <http://www.agromet.gov.iq/stations.php?id=6> (accessed Jun. 24, 2022).
- [114] P. Jidhesh, T. V Arjunan, and N. Gunasekar, “Thermal modeling and experimental validation of semitransparent photovoltaic-thermal hybrid collector using CuO nanofluid,” *J. Clean. Prod.*, vol. 316, p. 128360, 2021.
- [115] M. Chandrasekar, S. Suresh, T. Senthilkumar, and M. Ganesh Karthikeyan, “Passive cooling of standalone flat PV module with cotton wick structures,” *Energy Convers. Manag.*, vol. 71, pp. 43–50, 2013, doi: 10.1016/j.enconman.2013.03.012.
- [116] N. Hooshmandzade, A. Motevali, S. R. M. Seyedi, and P. Biparva, “Influence of single

- and hybrid water-based nanofluids on performance of microgrid photovoltaic/thermal system,” *Appl. Energy*, vol. 304, p. 117769, 2021.
- [117] H. Adun *et al.*, “Synthesis and application of ternary nanofluid for photovoltaic-thermal system: Comparative analysis of energy and exergy performance with single and hybrid nanofluids,” *Energies*, vol. 14, no. 15, p. 4434, 2021.
- [118] I. Wole-Osho, H. Adun, M. Adedeji, E. C. Okonkwo, D. Kavaz, and M. Dagbasi, “Effect of hybrid nanofluids mixture ratio on the performance of a photovoltaic thermal collector,” *Int. J. Energy Res.*, vol. 44, no. 11, pp. 9064–9081, 2020.
- [119] R. Sathyamurthy, A. E. Kabeel, A. Chamkha, A. Karthick, A. Muthu Manokar, and M. G. Sumithra, “Experimental investigation on cooling the photovoltaic panel using hybrid nanofluids,” *Appl. Nanosci.*, vol. 11, no. 2, pp. 363–374, 2021.
- [120] M. Sardarabadi, M. Passandideh-Fard, and S. Z. Heris, “Experimental investigation of the effects of silica/water nanofluid on PV/T (photovoltaic thermal units),” *Energy*, vol. 66, pp. 264–272, 2014.
- [121] M. Alktranee, M. A. Shehab, Z. Németh, P. Bencs, K. Hernadi, and T. Koós, “Energy and Exergy Assessment of Photovoltaic-Thermal System Using Tungsten Trioxide Nanofluid: An Experimental Study,” *Int. J. Thermofluids*, p. 100228, 2022.
- [122] M. Hosseinzadeh, M. Sardarabadi, and M. Passandideh-Fard, “Energy and exergy analysis of nanofluid based photovoltaic thermal system integrated with phase change material,” *Energy*, vol. 147, pp. 636–647, 2018.
- [123] P. Pounraj *et al.*, “Experimental investigation on Peltier based hybrid PV/T active solar still for enhancing the overall performance,” *Energy Convers. Manag.*, vol. 168, pp. 371–381, 2018.
- [124] N. S. B. Rukman, A. Fudholi, N. F. M. Razali, M. H. Ruslan, and K. Sopian, “Energy and exergy analyses of photovoltaic-thermal (PV/T) system with TiO<sub>2</sub>/water nanofluid flow,” in *IOP Conference Series: Earth and Environmental Science*, 2019, vol. 268, no. 1, p. 12075.
- [125] T. K. Murtadha, A. A. dil Hussein, A. A. H. Alalwany, S. S. Alrwashdeh, and M. Ala’a, “Improving the cooling performance of photovoltaic panels by using two passes circulation of titanium dioxide nanofluid,” *Case Stud. Therm. Eng.*, vol. 36, p. 102191, 2022.
- [126] C. D. Corbin and Z. J. Zhai, “Experimental and numerical investigation on thermal and electrical performance of a building integrated photovoltaic–thermal collector system,” *Energy Build.*, vol. 42, no. 1, pp. 76–82, 2010.
- [127] A. H. Mahmoudi, M. Shahi, A. M. Shahedin, and N. Hemati, “Numerical modeling of natural convection in an open cavity with two vertical thin heat sources subjected to a nanofluid,” *Int. Commun. Heat Mass Transf.*, vol. 38, no. 1, pp. 110–118, 2011.
- [128] K. C. Lin and A. Violi, “Natural convection heat transfer of nanofluids in a vertical cavity: Effects of non-uniform particle diameter and temperature on thermal conductivity,” *Int. J. Heat Fluid Flow*, vol. 31, no. 2, pp. 236–245, 2010.
- [129] H. Demir, A. S. Dalkilic, N. A. Kürekci, W. Duangthongsuk, and S. Wongwises, “Numerical investigation on the single phase forced convection heat transfer characteristics of TiO<sub>2</sub> nanofluids in a double-tube counter flow heat exchanger,” *Int. Commun. Heat Mass Transf.*, vol. 38, no. 2, pp. 218–228, 2011.
- [130] E. Ekramian, S. G. Etemad, and M. Haghshenasfard, “Numerical analysis of heat transfer performance of flat plate solar collectors,” *J. Fluid Flow, Heat Mass Transf.*, vol. 1, pp.

- 38–42, 2014.
- [131] Y. Wang and J. Zhang, “Ultrafine TiO<sub>2</sub> (B) nanowires for ultrahigh-rate lithium-ion batteries,” *Ionics (Kiel)*, vol. 26, no. 3, pp. 1159–1164, 2020.
- [132] A. Mulik, P. Hegade, S. Mulik, and M. Deshmukh, “CuO nanoparticles and nanobelts catalyzed potent synthesis of benzopyran derivatives,” *Res. Chem. Intermed.*, vol. 45, no. 11, pp. 5641–5647, 2019.
- [133] C. Han, J. Han, Q. Li, and J. Xie, “Wet chemical controllable synthesis of hematite ellipsoids with structurally enhanced visible light property,” *Sci. World J.*, vol. 2013, 2013.
- [134] S. O. Giwa, M. Sharifpur, and J. P. Meyer, “Experimental study of the thermo-convection performance of hybrid nanofluids of Al<sub>2</sub>O<sub>3</sub>-MWCNT/water in a differentially heated square cavity,” *Int. J. Heat Mass Transf.*, vol. 148, p. 119072, 2020, doi: 10.1016/j.ijheatmasstransfer.2019.119072.
- [135] B. yuan Han *et al.*, “WO<sub>3</sub> thermodynamic properties at 80–1256 K revisited,” *J. Therm. Anal. Calorim.*, vol. 142, no. 4, pp. 1533–1543, 2020, doi: 10.1007/s10973-020-09345-z.
- [136] E. B. Ögüt, “Natural convection of water-based nanofluids in an inclined enclosure with a heat source,” *Int. J. Therm. Sci.*, vol. 48, no. 11, pp. 2063–2073, 2009.
- [137] A. H. A. Al-Waeli, M. T. Chaichan, H. A. Kazem, and K. Sopian, “Comparative study to use nano-(Al<sub>2</sub>O<sub>3</sub>, CuO, and SiC) with water to enhance photovoltaic thermal PV/T collectors,” *Energy Convers. Manag.*, vol. 148, pp. 963–973, 2017.
- [138] M. Faizal, R. Saidur, S. Mekhilef, and M. A. Alim, “Energy, economic and environmental analysis of metal oxides nanofluid for flat-plate solar collector,” *Energy Convers. Manag.*, vol. 76, pp. 162–168, 2013.
- [139] A. B. Colak, “Experimental study for thermal conductivity of water-based zirconium oxide nanofluid: developing optimal artificial neural network and proposing new correlation,” *Int. J. Energy Res.*, vol. 45, no. 2, pp. 2912–2930, 2021.
- [140] J. Kim, S. Bae, Y. Yu, and Y. Nam, “Experimental and numerical study on the cooling performance of fins and metal mesh attached on a photovoltaic module,” *Energies*, vol. 13, no. 1, p. 85, 2019.
- [141] M. Firoozzadeh, A. H. Shiravi, and S. S. Chandel, “An experimental analysis of enhancing the efficiency of photovoltaic modules using straight and zigzag fins,” *J. Therm. Anal. Calorim.*, 2022, doi: 10.1007/s10973-021-11178-3.

## Appendix A

### Synthesized mono nanomaterials

The nanomaterials are the main part of nanofluids; all the nanomaterials used to prepare nanofluids have been synthesized in the faculty of materials and chemical engineering at the University of Miskolc, except  $ZrO_2$  nanoparticles, which were purchased. The thermophysical properties of all mono nanomaterials are shown in Table A1, and it has depended on the previous studies. Table A1 shows the thermophysical properties of the new hybrid  $TiO_2-Fe_2O_3$  and  $TiO_2-CuO$  nanocomposites measured thermal properties at the University of Miskolc.

Table A1. Thermophysical properties of mono nanomaterials

Properties	DI Water [134]	$Fe_2O_3$ [67]	$WO_3$ [109,135]	$TiO_2$ [67,136]	$CuO$ [137,138]	$ZrO_2$ [139]
Density ( $kg/m^3$ )	997	5240	7160	3900	6310	5890
Thermal conductivity ( $W/m \cdot K$ )	0.613	20	1.63	8.9	32.9	2.7
Heat capacity ( $J/kg \cdot K$ )	4179	650	335	686	551	0.455

#### A.1 Tungsten trioxide ( $WO_3$ NPs)

Hydrothermal treatment is used to fabricate  $WO_3$  nanoparticles, which involves dissolving 5 g of sodium tungstate dihydrate ( $Na_2WO_4 \cdot 2H_2O$ ) into 200 mL of DI water under continuous stirring (500 rpm) for 2 hours. Then Hydrochloric acid (HCl) was dropwise by 3 M into the solution even tungsten acid was precipitated thoroughly, thus putting the solution into a Teflon-lined autoclave with a capacity of 500 ml, then sealed and maintained the autoclave at 150 °C for 12 hours. Left the autoclave to cool to room temperature naturally after the reaction was completed; after that, washed with DI water several times by centrifuge to reach pH 7. Moreover, the solution is dried in an oven at 100 °C for 1 hour and calcination under 500 °C for 2 hours. Figure A1 shows the steps of nanoparticle  $WO_3$  synthesis.

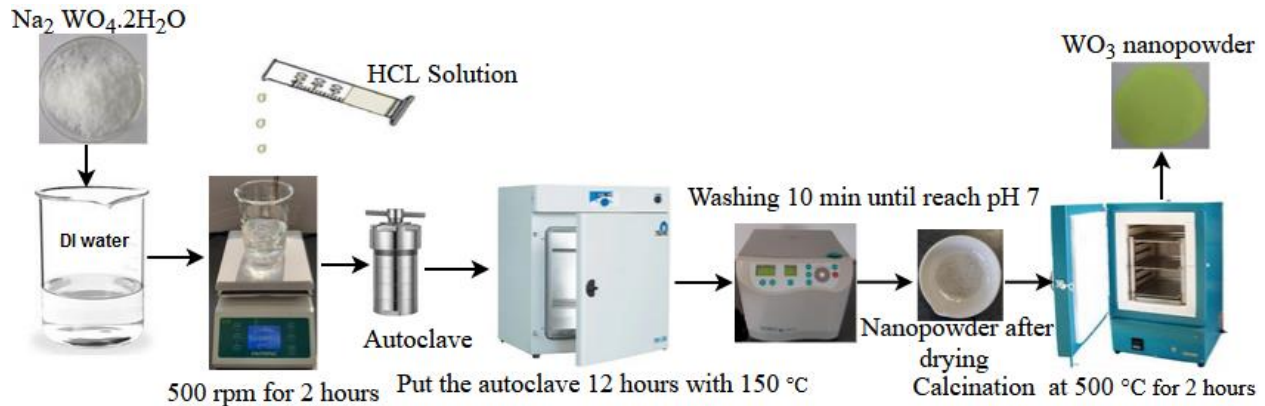


Figure A1. Schematic of the synthesis process of  $WO_3$  nanopowder by hydrothermal method

The crystal structure of the prepared samples was determined using X-ray powder diffraction (XRD) (Bruker D8 Advance diffractometer) at ( $CuK \alpha = 0.15418 \text{ nm}$ ) (40 kV and 40 mA) in parallel beam geometry (Göbel mirror) with a position-sensitive detector (Vantec1, 1° opening). On top-loaded specimens in zero-background  $WO_3$  sample containers, measurements were made

in the 2-100° (2 Theta) range using a 0.007° (2 Theta)/14-sec goniometer speed. Based on the qualitative phase analysis of WO<sub>3</sub> synthesized by the hydrothermal method, the sample consists of a hexagonal lattice WO<sub>3</sub> phase found in more significant amounts, and there are few monoclinic lattice WO<sub>3</sub>. Based on the Rietveld refinement, the sample is 100% crystalline with green colour with no amorphous phase found; Figure A2 (a) shows the XRD pattern of WO<sub>3</sub> nanopowder. Figure A2 (b) shows the shape and distribution of the WO<sub>3</sub> nanopowder sample synthesized by the scanning electron microscope (SEM). The morphology of WO<sub>3</sub> appeared as nanoflakes formed in irregular shapes.

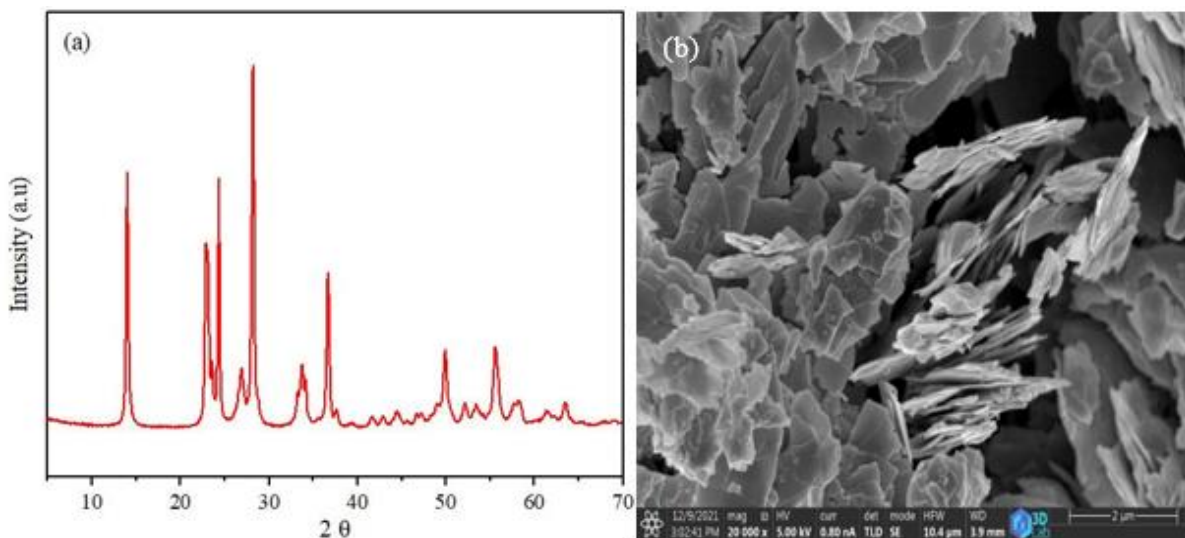


Figure A2. The XRD pattern of the synthesized WO<sub>3</sub> (a) and (b) SEM image of WO<sub>3</sub> nanoflakes

## A.2 Titanium oxide nanowires (TiO<sub>2</sub> NWs)

TiO<sub>2</sub> NWs produced using a hydrothermal method as published in our earlier work, the homogenous suspension was formed using 3 g of TiO<sub>2</sub> nanoparticles dissolved in 100 mL KOH aqueous solution (10 M) and kept stirred for 30 min, then transferred to a Teflon<sup>®</sup>-lined autoclave at 160 °C for 24 h. The product was collected using vacuum filtration and washed several times with 0.1 M HCl and DI water until the pH value became 7. After drying the products overnight in a furnace, the white TiO<sub>2</sub> NWs powder was obtained and calcined at 400 °C for 1 h. XRD has been performed to identify and describe the crystal structure of TiO<sub>2</sub> NWs, as shown in Figure A3 (a). The diffraction peaks are located at 33.8°, 39.2°, 48°, 54.2°, 56.5°, 66.4° and 68.8°, corresponding to (211), (220), (200), (105), (213), (004) and (403) refer to anatase phase (JCPDS 21-1272). The other peaks located at 27.4°, 36.1° and 41.2° index to (110), (101) and (111) relate to the rutile phase (JCPDS no-21-1276). Furthermore, the diffraction peaks located at 11.4°, 24.1°, 29.2°, 42.9° and 59.8° corresponding to (200), (002), (310), (602) and (610) refer to K<sub>2</sub>Ti<sub>6</sub>O<sub>13</sub> (PDF no. 40-0403). All these results agreed with [78] [131]. A scanning electron microscopy SEM technique is used for investigations of the surface morphology of TiO<sub>2</sub>, which is shown as nanowires, as shown in Figure A3 (b).

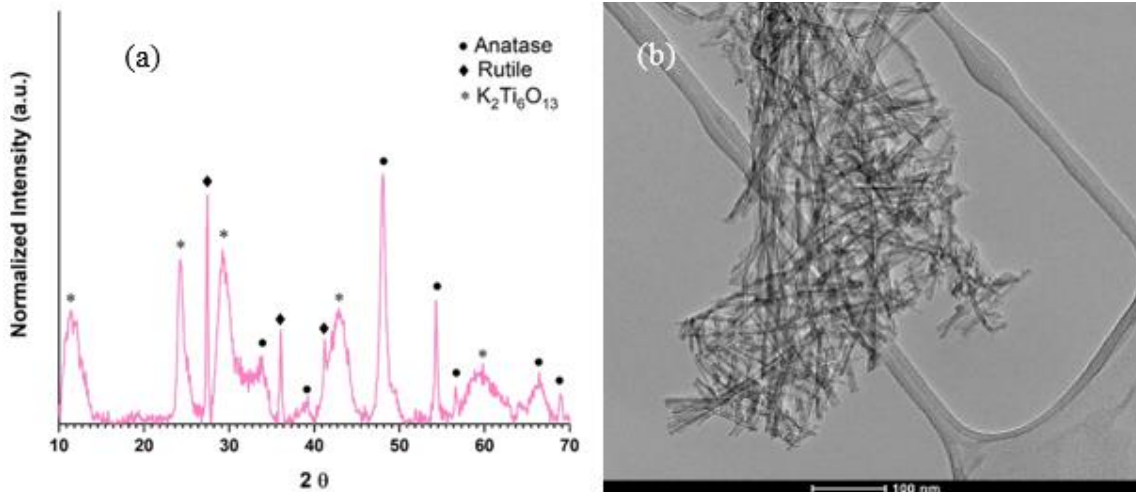


Figure A3. The XRD pattern of the synthesized TiO<sub>2</sub> (a) and (b) TEM image of TiO<sub>2</sub> nanowires

### A.3 Copper oxide nanoparticles (CuO NPs)

In order to produce the copper oxide, a calculated amount of  $(\text{Cu}(\text{CH}_3\text{COO})_2 \cdot \text{H}_2\text{O})$  was dissolved in 100 mL of ethanol and stirred vigorously for 30 min. Then poured into an autoclave and thermally treated at 150 °C for 12 h. The finished product was collected, vacuum-filtered washed, and then calcined at 500 °C for 2 h, similar to the method conducted by [78]. Figure A4 (a) shows XRD analysis of CuO, the diffraction peaks located at 32.5°, 35.5°, 38.7°, 48.8°, 53.4°, 58.3°, 61.5°, 65.8°, 66.2° and 68° corresponding to (110), (-111), (111), (-202), (020), (202), (-113), (022), (-311) and (220) refer to copper oxide (JCPDS card number 45-0937), which agree with [132]. A Transmission Electron Microscopy TEM technique is used for investigations of the surface morphology of CuO, which is shown as nanoparticles, as shown in Figure A4 (b).

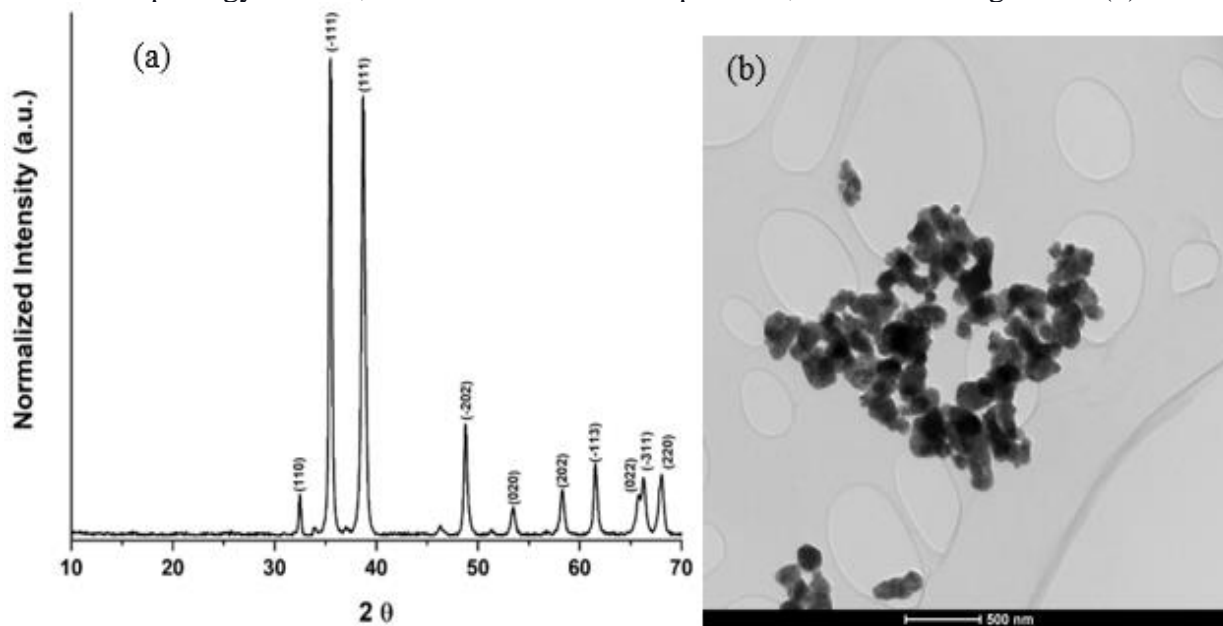


Figure A4. The XRD pattern of the synthesized CuO (a) and (b) TEM image of CuO nanoparticles

#### A.4 Iron oxide nanorods ( $\text{Fe}_2\text{O}_3$ )

Iron oxide nanorod production by a similar method used by [78],  $\text{FeCl}_3 \cdot 6\text{H}_2\text{O}$  precursor was dissolved in 100 mL of distilled water to gain a homogeneous solution. NaOH solution was added dropwise under stirring until the solution became base and then transferred to the autoclave at 90 °C for 9 h. To neutral pH, the product was washed with distilled water, dried and calcinated at 500 °C for 2 h. XRD analysis was performed to identify crystal structure, as shown in Figure A5 (a), the peaks located at 24.1°, 33.1°, 35.6°, 40.8°, 49.4°, 54°, 57.6°, 62.4°, 64° and 67.4° index to (012), (104), (110), (113), (024), (116), (018), (214), (300) and (442) originating to Hematite iron oxide ( $\alpha\text{-Fe}_2\text{O}_3$ ) (JCPDS 33-0664). This results in good agreement with [133]. A scanning electron microscopy SEM technique is used to investigate the surface morphology of  $\text{Fe}_2\text{O}_3$ , which is shown as nanorods, as shown in Figure A5 (b).

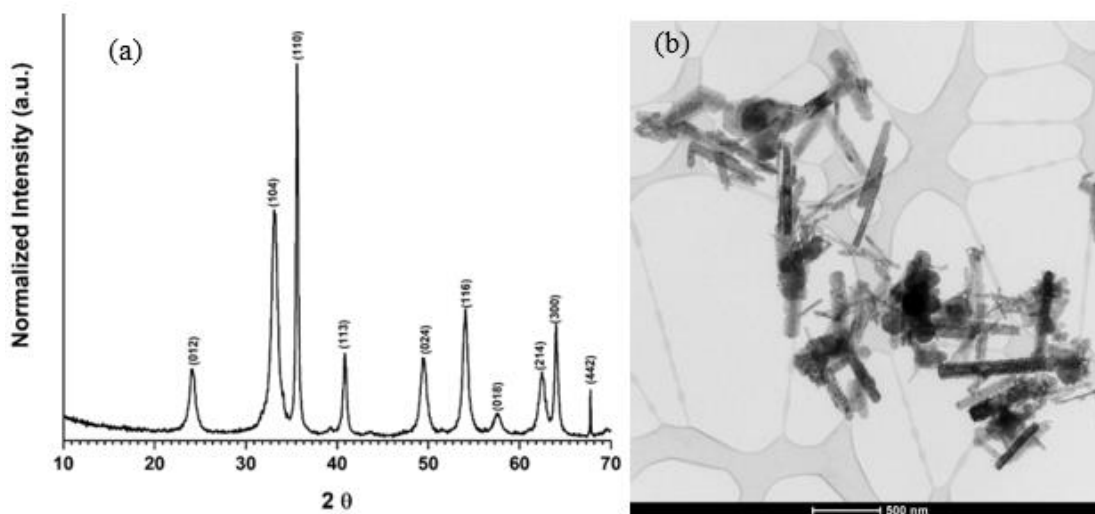


Figure A5. The XRD pattern of the synthesized  $\text{Fe}_2\text{O}_3$  (a) and (b) TEM image of  $\text{Fe}_2\text{O}_3$  nanorods

#### A.5 Zirconium Oxide nanoparticles ( $\text{ZrO}_2$ NPs)

The  $\text{ZrO}_2$  nanoparticles were supplied by (Research Nanomaterials, Inc., Houston, TX, USA) with a particle size of 20 nm, white colour, with 99.95% purity, and the SEM image in Figure A6 shows the morphology of the  $\text{ZrO}_2$  according to provided by the vendor.

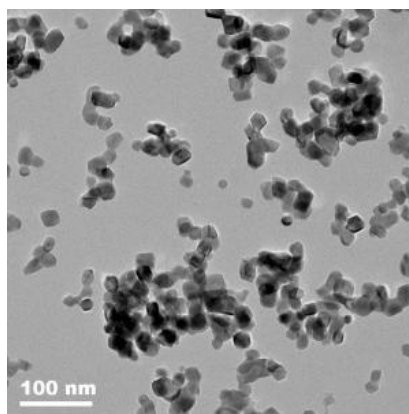


Figure A6. TEM image of the  $\text{ZrO}_2$  nanoparticles

## Appendix B

### Effect of passive and active cooling on the efficiency of the PVT system

The present study investigates the effects of passive and active cooling on the PV module performance using different configurations (namely cotton wicks integrated with rectangular aluminium fins (CWIRAFs)) and photovoltaic thermal PVT collectors under hot conditions. Few studies on this method have been conducted with different techniques and operating conditions than the present research. Integrated aluminium fins by cotton wicks immersed in water from the top to the bottom help to increase the heat transfer area and the effective evaporative cooling at the back surface of the PV module, leading to temperature dissipation of the PV module into the surrounding air, then, improve its performance. The experimental results of each cooling technique applied are compared with other studies according to thermal behaviour, efficiency, and power yield to identify the appropriate cooling technique.

#### B.1 Effect of evaporative cooling on photovoltaic module performance

##### B.1.1 Cooling techniques used and experiment procedure

Cotton wicks (CWs) were attached with rectangular aluminium fins (RAFs) by thermal silicon and attached at the rear of the PV module by thermal silicon adhesive. Fins are used as a partial rectangle (i.e. 52 cm long, 3 cm wide, and 1.5 mm thick) and uniform distance between RAFs. CWs were arranged in serpentine on the backside of the PV module, and fins formed contiguously without space between them. Table B1 shows the specifications of the CWIRAF components [107,140]. The CWs are characterized by a suitable heat transfer coefficient, lower thermal conductivity, and high absorbent capacity, which helps to distribute water to all CWs attached behind the PV module without using extra power. In addition, it's locally available, cost-effective and does not require maintenance. A total of 11 CW ends were submerged at the bottom of three plastic bottles full of water to supply water to CWIRAFs during the experiment, as shown in Figure B1 (a). The CW ends placed in the water tank have continuously provided water from the top to the bottom of the PV module. Therefore, four thermocouples were placed on each of the surfaces of the PV modules at different places, three were placed on the backside, and one was used to measure ambient temperature.

Table B1. Material specifications used for passive cooling

	Rectangular fins		Cotton wick
Material	Aluminum	Cotton wick diameter	8 mm
Number of fins	20	Cotton wick length	50 m
Thermal conductivity	237 W/m·K	Thermal conductivity	0.048 W/m·K
Specific heat	903 J/kg·K	Heat transfer coefficient	36 W/m °C
Density	2702 kg/m <sup>3</sup>	-	-

PVT solar collector consists of a PV module with a 9.5-mm diameter copper pipe arranged in serpentine and attached to an absorbent copper plate with 1.5-mm thickness placed on the rear side of the PV module. Copper pipes are covered by a layer of thermal wool insulation and aluminium cover, as shown in Figure 1B (a). PVT collector uses water as a medium that enters and exits from an inlet and outlet of the collector. The outlet water passes via two copper pipes with small holes to re-cool the water before being collected in an insulated storage tank with 0.75 kg of ice added in the storage tank every 30 min. The storage tank cover is partially opened to enable air to circulate. The flow rate was 1.4 L/min, pumped by a tiny pump placed inside the

storage tank. After that, two thermocouples were placed at the inlet and outlet of the PVT collector to measure water temperature.

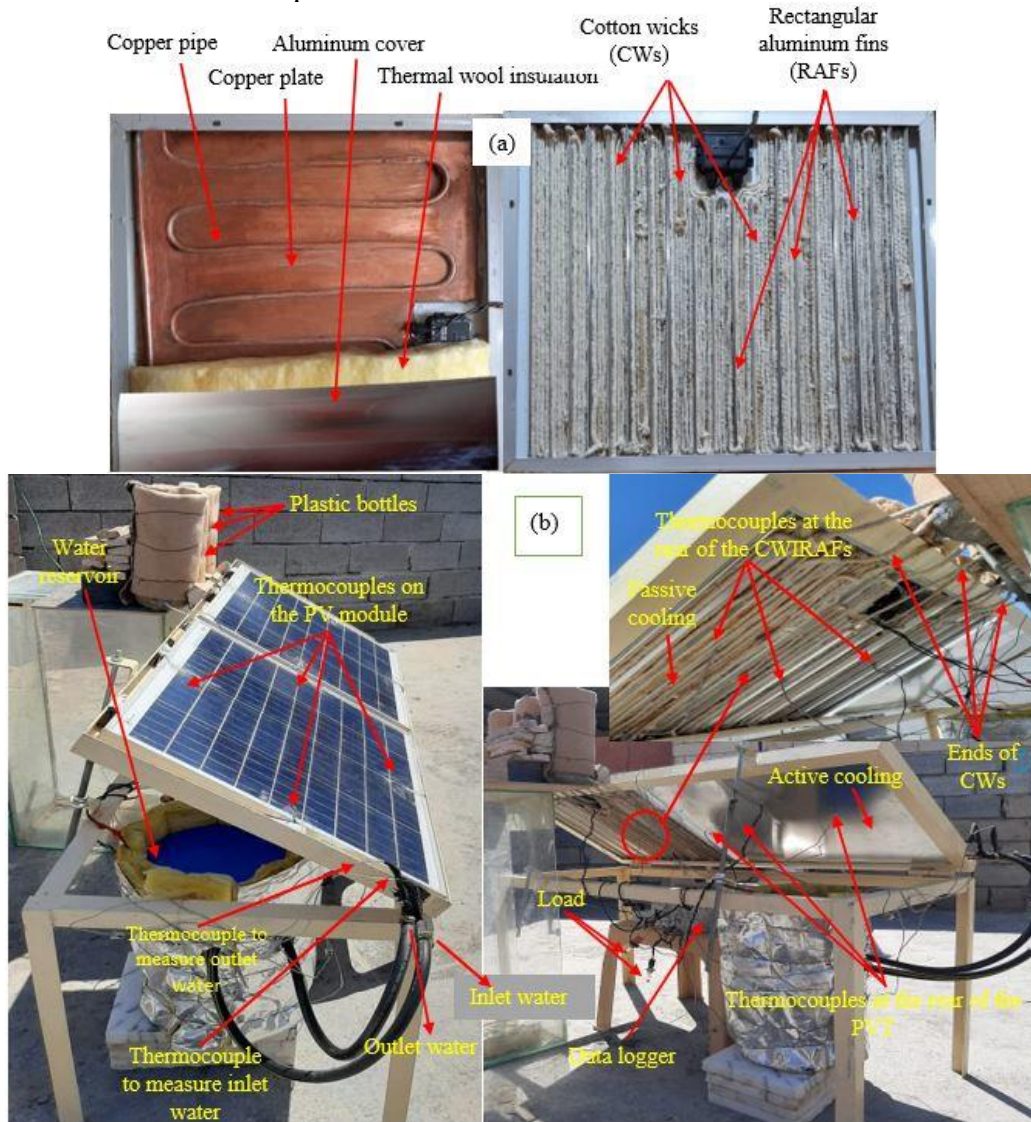


Figure B1. Configurations of PV with CWIRAFs and PVT collector (a) and (b) using passive and active cooling with PV modules

Figure B1 (b) shows additional details of the system. The CWIRAF module and PVT collector performance is compared with conventional PV modules without cooling installed individually under the same operating conditions. The experiments were conducted from 25 June to 15 July 2021 in Iraq (latitude:  $30.5^\circ$ ; longitude:  $48.14^\circ$ ). The weather during the experiments was sunny with a clear sky, and there was no substantial variation in temperature during the experiment days. According to the Iraqi Agricultural Meteorological Center, the average wind speed was 1.9–6.6 m/s [113]. Solar radiation values increased gradually from the start of the experiment and decreased in the afternoon. Three 50-W polycrystalline PV modules were used with  $0.65 \text{ m} \times 0.55 \text{ m} \times 0.03 \text{ m}$  dimensions. The modules have a tilt angle of  $29^\circ$ . The distance between PV modules and the ground allows air to pass on the backside of PV modules, which boosts the rate of evaporative cooling because of a convection mass transfer. The output power ( $P_{out}$ ) of the PV

modules with CWIRAFs and PVTC is calculated by using Eq. (1) [36], depending on the output voltage ( $V_{out}$ ) and current ( $C_{out}$ ) of the modules obtained every 10 min.

### B.1.2 Results and discussion

PV module with CWIRAFs was supplied with water for two hours to ensure that all CWs were wet before the experiment began. The start of the experiment was simultaneous with the beginning of sunrise when the value of solar radiation is low but increases with an increase in sunlight intensity. Figure B2 (a) presents the average solar radiation during the experiment, which gradually increases with operation hours until 12:30 PM. The maximum solar radiation recorded was  $1157 \text{ W/m}^2$  but reduced progressively. Increasing the ambient temperature is associated with increased solar radiation intensity, in which the average ambient temperatures are variable along the experiment period. At the beginning of the experiment, the ambient temperature increased gradually, and the maximum ambient temperature reached  $48.4 \text{ }^\circ\text{C}$  at 12:20 PM. After that, it decreased to  $40.8 \text{ }^\circ\text{C}$  when the experiment was over. In July, most days are sunny with rising temperatures and dropping humidity with moderate winds, as shown in Figure B2 (b).

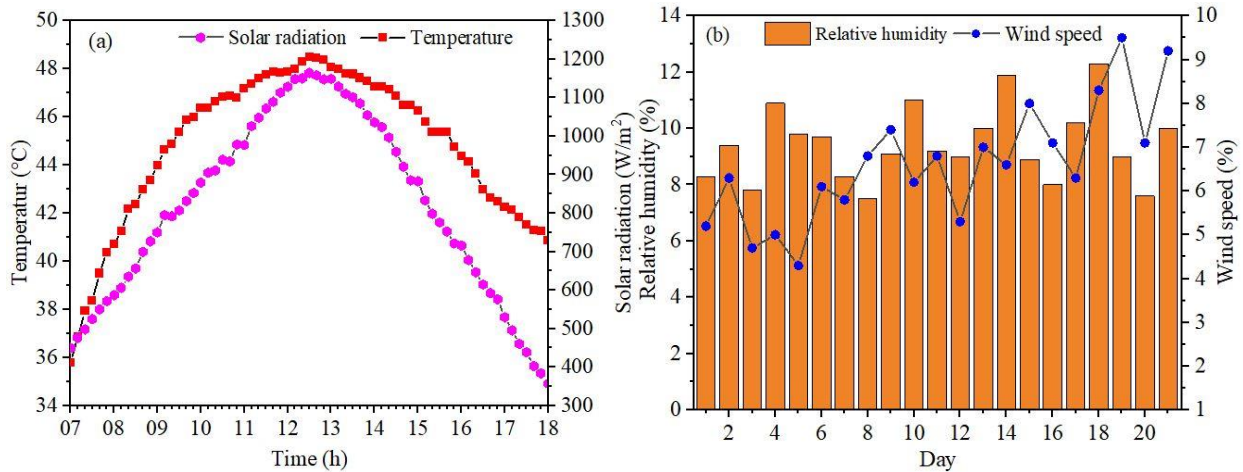


Figure B2. The operational parameters (a) ambient temperature and solar radiation, (b) wind speed and humidity throughout the experiments

#### B.1.2.1 Performance of PV module with CWIRAFs

Figures B3 (a) and (b) show the temperature distribution on the surface and backside of the PV module with used CWIRAFs and without cooling, respectively, throughout the experiment period. Temperature distribution on the sides of the PV module gives significant convergence, and this reason is logical to depend on the average temperature of the PV module in calculations. The maximum temperature was recorded from 12:00 PM to 12:50 PM before decreasing until the end of the day. Figure B3 (c) shows the average temperature of the surface, backside and PV module that used CWIRAFs. By contrast, the PV module temperature without cooling was recorded at  $80.2 \text{ }^\circ\text{C}$  and  $72 \text{ }^\circ\text{C}$  for both sides, and  $76.1 \text{ }^\circ\text{C}$  was the average temperature of the PV module. The evaporative cooling and increased heat dissipation area represented by integrating the rectangular aluminium fins with WC wicks have increased the heat transfer area of the PV module's backside and reduced the PV module temperature. Maximum temperatures for both sides of the PV module with CWIRAFs recorded at 12:30 PM were  $54.2 \text{ }^\circ\text{C}$  and  $49.8 \text{ }^\circ\text{C}$ , the maximum ambient temperature was  $48.4 \text{ }^\circ\text{C}$ , and the average temperature of the PV module was

52 °C. The evaporative cooling in CW provides an appropriate cooling environment that lowers approximately 47.97% of the surface PV module temperatures compared with the PV module without cooling. Thus, evaporative cooling in CW has provided an appropriate cooling environment, leading to lowers of approximately 46.34% of the PV module temperatures compared with the PV module without cooling.

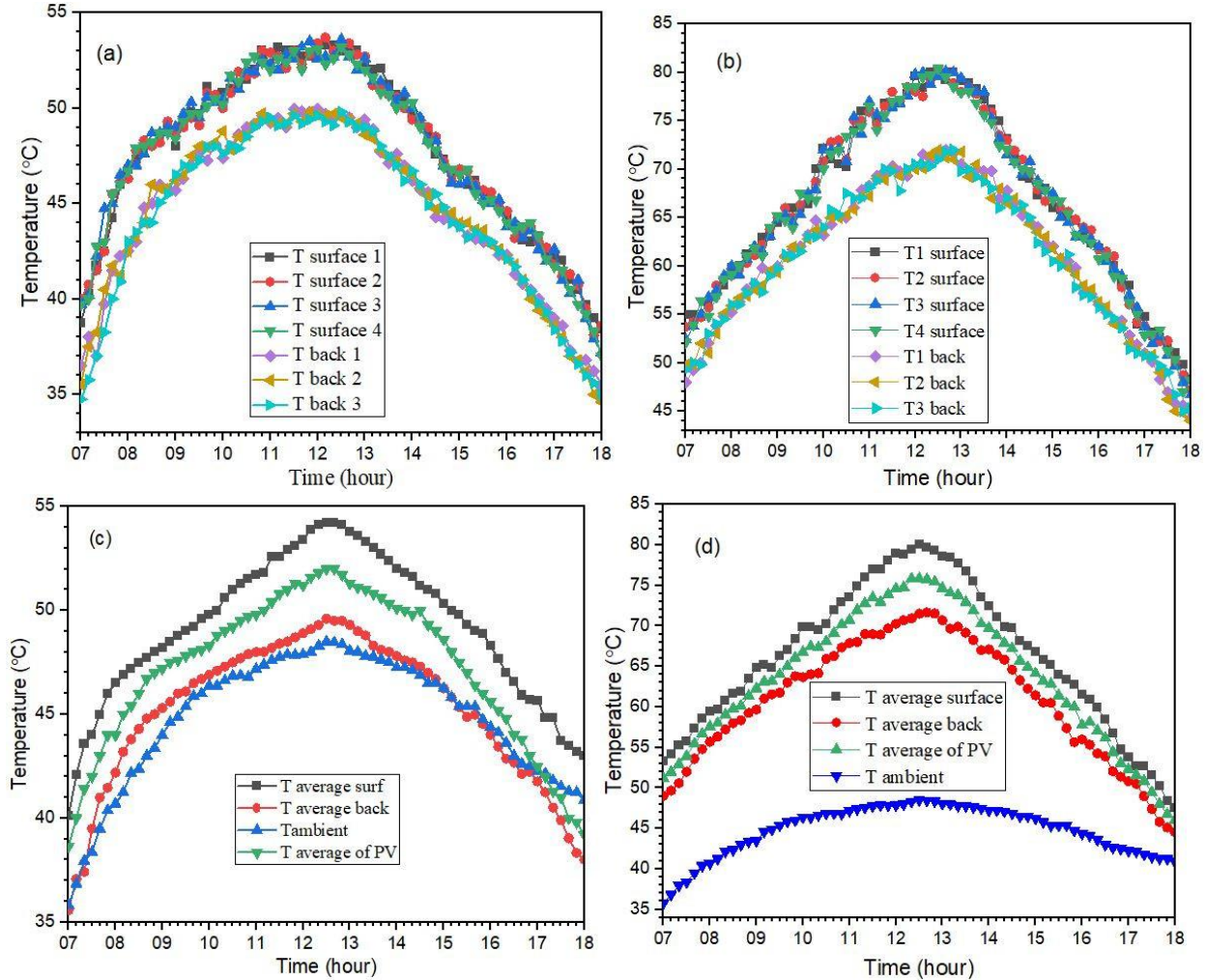


Figure B3. Temperature distribution on PV modules (a) with cooling, (b) without cooling, Average temperature of PV module (c) with cooling and (d) without cooling

Figure B3 (d) presents the temperature variation of the PV module without cooling that increases to a critical scale, causing degradation of the PV module. The effectiveness of active cooling causes the backside of the PV module temperature to decrease below the ambient temperature at 2:50 PM, as shown in Figure B3 (c), owing to reduced ambient temperature and increased wind speed. The decrease in the backside temperature was attributed to using CWIRAFs because of the effects of using evaporative cooling. PV module's power and efficiency values vary due to solar radiation and ambient temperature variables, and PV module temperature significantly affects its production, output voltage variation and current PV module. The CWIRAFs have enhanced the PV module's performance by reducing the temperature, which can be noticed in the increased output power shown in Figure B4 (a). Compared with the PV module without cooling,

the output voltage and current with CWIRAFs increased by approximately 55.4% and 25%, respectively. Therefore, the used passive cooling represented by CWIRAFs has achieved an impressive performance that increased the PV module's output power. Maximum output power was recorded at 34.75 W at 12:10 PM, an increase of 23.16 W compared with the PV module without cooling, and efficiency up to 8.6%. Figure B4 (b) shows the degradation of the PV module without cooling that affects its performance, which is evident by significantly dropping both its voltage and current. Increasing the PV module temperature to 76.1°C without cooling caused a significantly low output power of 11.59 W, representing maximum output power. The maximum efficiency of the PV module without cooling was recorded at 3.12%, attributed to the significant deterioration of the PV module performance. Note the fluctuation and decrease of the PV module productivity and efficiency between 12:10 and 1:00 PM. After that, it slightly increased but declined again until the experiment ended owing to increasing temperature and direct solar radiation on the PV modules.

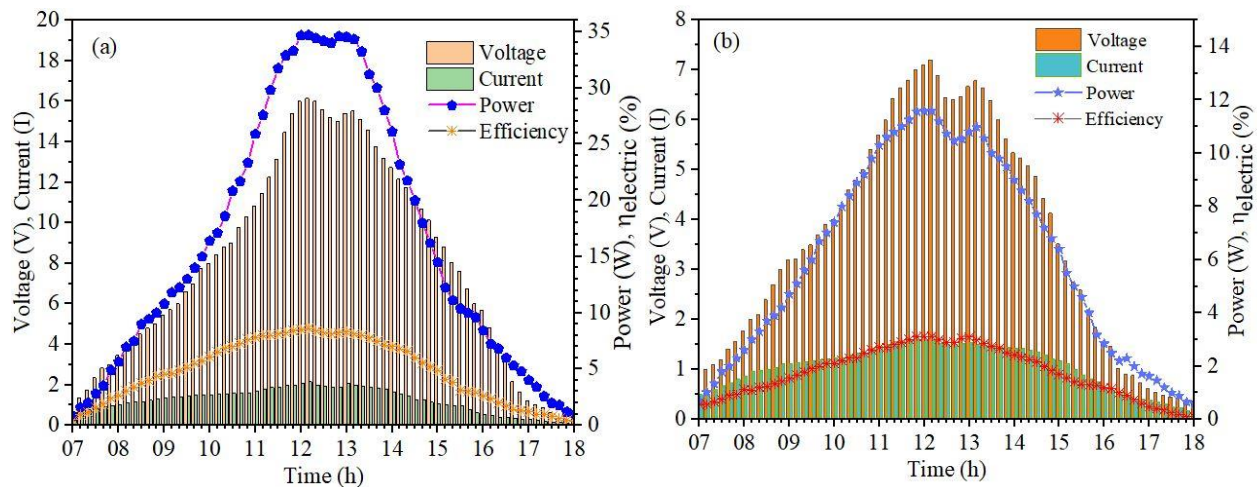


Figure B4. Performance of PV module with CWIRAFs (a) and (b) without cooling

### B.1.2.2 Performance of the PVT system

Heat flows from the hot surface that is directly exposed to the intensity of solar radiation to the cold surface resulting in a higher backside temperature of the PV module than the ambient temperature. At the beginning of the experiment, the PVT system surface temperature was 41.4 °C, and the back side (absorb plate) of the PVT collector was 38.2 °C, but it gradually increased. The maximum temperature of the PVT surface was 67.2 °C at 12:20 PM. The backside was 55.4 °C, as shown in Figure B5 (a). The used absorbing plate with water circulates into copper pipes attached to the backside of the PV module as active cooling has reduced the module temperature. Based on the average temperature, the surface and backside temperatures of the PVT collector were lower by approximately 19.3 % and 29.7 %, respectively, compared with the PV module without cooling. Decreased PV module temperature is attributed to conduction heat transfer from the copper plate directly attached to the backside of the PV module to copper pipes. After that, heat convection is transferred to water circulation into the pipes to reduce the PVT collector temperature. Figure B5 (b) shows the water temperature difference between the inlet and outlet water, in which the PVT collector recorded an average temperature reached 60 °C. Inlet water temperature slightly approached ambient temperature until 12:40 PM but decreased afterwards, affecting the thermal energy gained.

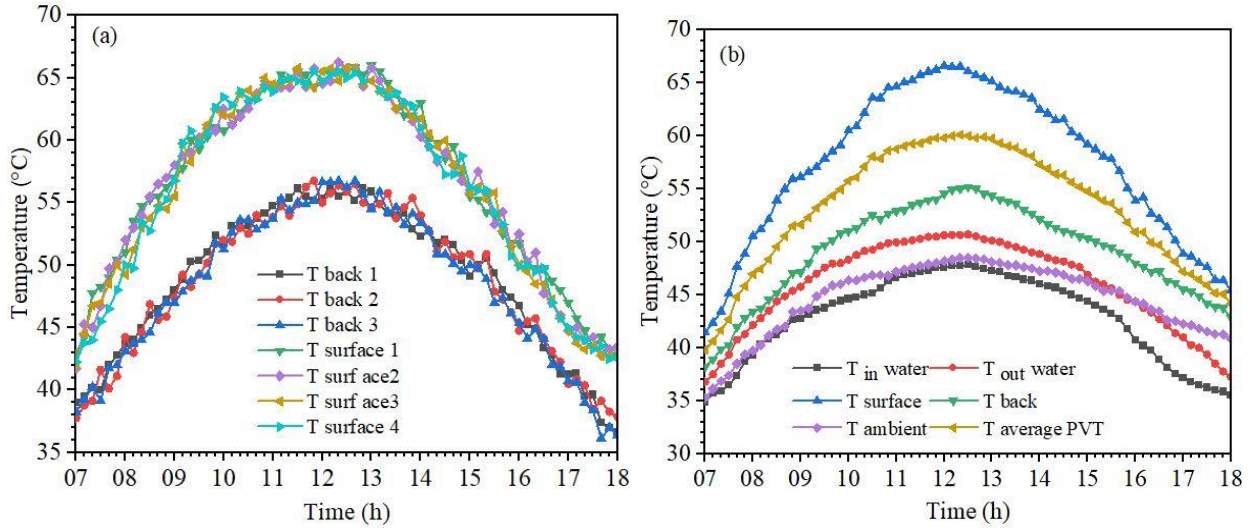


Figure B5. The temperature profile of the PVT collector (a) surface, backside temperature (b) average temperature of the PVT collector.

It can be noticed in the difference between inlet and outlet water temperatures. Using aluminium fins helps to increase the heat transfer area at the back surface of the PV module; integrating aluminium fins with cotton wicks immersed in water and exposed to the wind provides evaporative cooling that helps to reduce the temperature of the PV module. Thus, absorbing the temperature of the PV module and dissipating it into the surrounding air. Circulating the water into copper pipes attached to the absorbing plate removes the PV modules' excess heat. Thus, the temperature of PV cells was reduced because of increased heat transfer by conduction between the absorbing plate and the PV module backside.

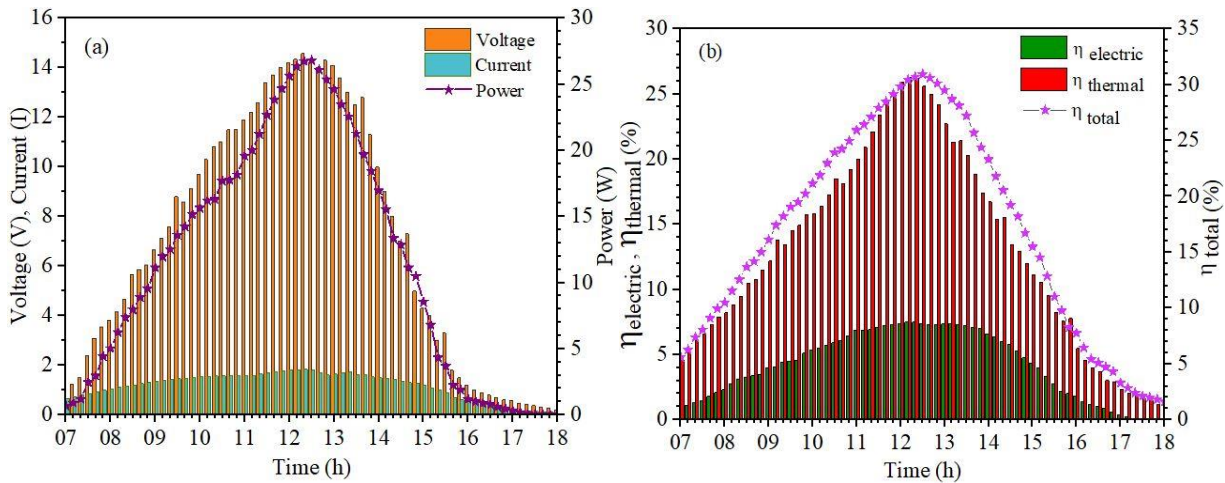


Figure B6. Performance of PVT collector: (a) energy yield and (b) efficiencies

The yield energy of the PVT system improved compared with another PV module without cooling owing to the thermal conductivity of water that circulated, thereby facilitating the removal of a portion of excess heat from the PV module's backside. A reduction in the temperature of PV cells achieved increased productivity output voltage, current and power yield of the PVT collector, where the maximum output voltage and current were 14.5 V and 1.85 A, respectively, at 12:20 PM, with an output power of 26.8 W, as shown in Figure B6 (a). However, reducing the PVT collector temperature has positively increased the electric efficiency by

approximately 7.9 %. The absorbed plate with pipes and water helps transfer the heat and achieve thermal efficiency, reaching 26.3 %, as shown in Figure B6 (b), thereby enhancing the PVT system performance by increasing the overall efficiency to 34.2%.

### B.1.2.3 Comparison of performance under different cooling techniques

Increasing the PV cell temperature throughout the experiment affected the performance, particularly without cooling. The PV module output power and efficiency recorded lower values than active and passive cooling. The immersion of CWIRAFs in water with variable wind speed created a cooling environment during the experiment. It contributed to lowering the average temperature of the PV module by 46.34 %, while active cooling reduced the PVT system temperature to 19.44 % compared PV module without cooling, respectively, at maximum temperature. The CWIRAFs, as passive cooling, achieved better performance than active cooling due to the evaporative cooling with increased heat dissipation area by aluminium fins.

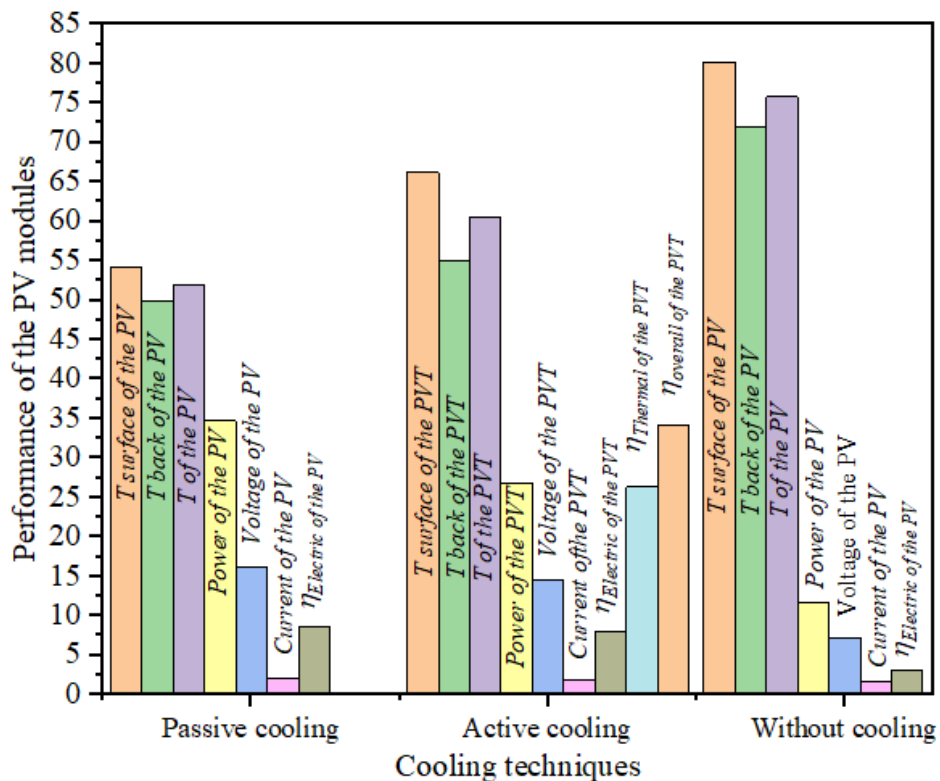


Figure B7. Comparison of PV module's performance under different cooling techniques

Therefore, output power increased by 199.8% and using active cooling increased the output power by 133% compared with PV modules without cooling. The electric efficiency of the passive cooling was enhanced by 175%, compared with active cooling, which recorded an enhancement of 153.2% compared to the PV module without cooling at maximum temperature. Active cooling, represented by water circulation into copper pipes attached to the absorbing plate, facilitates heat removal from the PV module backside and converts to heat energy gained. The maximum thermal energy recorded by the PVT collector was 26.3%, which caused an increase in the overall efficiency of the PVT collector to 34.2%. Figure B7 above shows the performance of the PV module under different cooling techniques. The PV module without

cooling deteriorated its performance due to the increasing PV cell temperature. The results obtained in the current study are compared with previous studies, considering some factors, such as the size of the PV/PVT system, type of cooling media applied, cooling configurations used, and measurement conditions, as shown in Tables B2 and B3. In the current study, passive cooling by CWIRAF shows better performance than active cooling concerning the reduced PV module temperature and enhanced performance, confirming the effectiveness of passive cooling.

Table B2. Comparing the PV module's performance with other passive previous studies

Ref.	Cooling techniques	Power increment %	Temperature reduction %	Electrical efficiency increment %
[110]	Passive cooling	5	10 °C	6.7
[28]	Passive cooling	32.7	16	31.7
[141]	Passive cooling	14	27.2	14.5
Current study	Passive cooling	66.6	31.4	63.7

Table B3. Comparing the PV module's performance with other active previous studies

Ref.	Cooling techniques	Thermal efficiency %	Electrical efficiency %	Temperature reduction %
[140]	Active cooling	25	8	16
[47]	Active cooling	52	13	9.8
Current study	Active cooling	26.3	8.1	20.8

#### B.1.2.4 Economic analysis of the passive cooling techniques

The purpose of economic analysis and the payback period is to give an effective cost estimation for the cooling techniques proposed [123]. The economic analysis and payback period of the conventional PV module with CWIRAF and conventional PV module have been calculated depending on maintenance, operation, CWIRAFs initial cost, and water supply cost. The net profit is calculated from Eq. (68) considering the cost of each element shown in Table B3. It can observe that the payback period of the PV module with CWIRAFs cooling technique was less than the conventional PV module by 77. This is a reasonable reason that makes the cooling technique proposed economically effective.

Table B3. Economic analysis of PV modules with CWWs and RAFs passive cooling

Element cost	CWWs cost in (IQD)	Conventional PV
Configuration	110000 IQD	90000
Maintenance	250 IQD/ day	115 IQD/day
Water supply	300 IQD /day	-----
Operation	280	0
CWIRAFs	20000 IQD	-----
Energy productivity	1592 IQD/day	522 IQD/day
Net profit	762	407
Payback period	144 days	221 Day

## B.2 Energy and exergy assessment of PVT system using tungsten trioxide nanofluid (WO<sub>3</sub>)

This work aims to experimentally study the effects of a new metal-oxide WO<sub>3</sub>/DI water nanofluid as a cooling fluid for a PVT system on electrical power generation and overall efficiency at different volume concentrations and constant flow rates. Moreover, exergy analysis of the PVT system and the effects of using WO<sub>3</sub>/DI water nanofluid on the entropy generation and exergy losses have been evaluated and discussed. Therefore, Serpentine pipes and a thermal absorber plate has proposed with fluid circulation to reduce the PV cell temperature and improve their efficiency. The current work experimentally investigates the effect of using tungsten trioxide (WO<sub>3</sub>) nanofluids on a PVT system's energy and exergy efficiency at different volume concentrations 0.5 vol%, 0.75 vol%, and 1 vol%.

### B.2.1 Results and discussions

Figure B8 presents the average daily weather data measured during the experiments for every 10 mins, where the average ambient temperature was 43.3 °C, and the maximum incident solar radiation was 1014 W/m<sup>2</sup>. The variation of the ambient temperature and solar radiation can be observed with a maximum ambient temperature and solar radiation recorded at 12:20 PM, which gradually dropped until the end of the experiment.

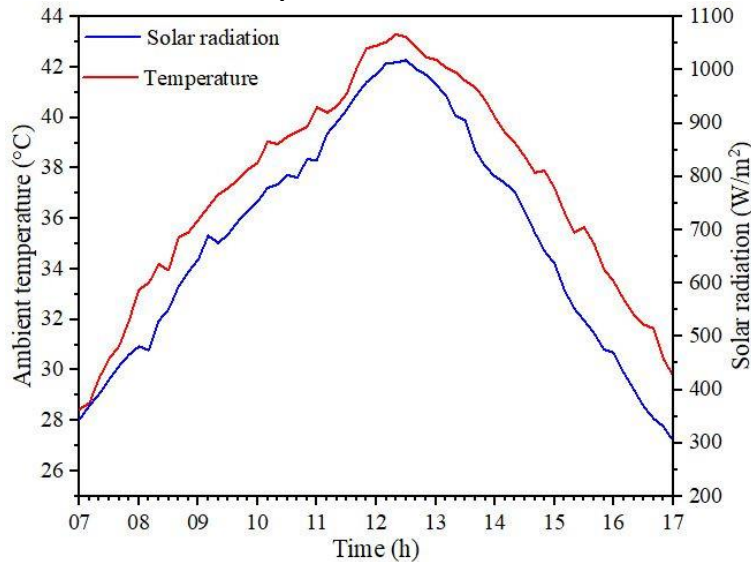


Figure B8. Average daily ambient temperature and incident solar radiation during the test period.

#### B.2.1.1 Energy analysis

The surface temperature increment of the reference PV module is noticeable due to direct exposure to solar radiation and the ambient temperature, reaching 58.8 °C. Figure B9 (a) shows the thermal behaviour of the PVT system under different volume concentrations of nanoparticles in the base fluid. The difference in the PVT system temperature can be noticed when cooling by DI water and WO<sub>3</sub> nanofluid. The temperature of the PVT system module is high with the base fluid and reduced more with the rising concentration of nanoparticles in the base fluid. Increasing the volume concentrations of nanoparticles in base fluid causes an increase in its thermal conductivity and then increases the nanofluid heat transfer coefficient. Thus, removing more heat from the PVT system through fluid circulation. The PVT system temperature was reduced using the DI water and WO<sub>3</sub> nanofluid at different volume concentrations (0.5 vol%,

0.75 vol%, and 1 vol%) by 9.9%, 13%, 18%, and 21%, respectively. The electrical power output is directly influenced by the operating temperature of the PV cells. Therefore, reducing the PVT system temperature reflects on the electrical power generation. Figure B9 (b) shows the effect of cooling by water and nanofluid at a different vol% on the electrical power output of the PVT system with time. The electric power was increased with the rise in the solar radiation intensity and reached a peak at 12:00 due to the absorption of many photons by the PV cells. The results indicated that using  $\text{WO}_3$  nanofluid enhanced electrical power by decreasing the temperature of the PVT system. The maximum electrical power of the reference PV module was recorded at 17.84 W, which shows that the rise in the PV module temperature has lowered the generated electrical power by the PV module. On the other hand, using  $\text{WO}_3$  nanofluid at different concentrations (0.5 vol%, 0.75 vol%, 1 vol%) gradually increased the electrical power by 7.87, 9.95, and 11.15 W, respectively, compared to the reference PV module. The electrical power generation increment of the PVT system was attributed to the increased volume concentration of nanoparticles in the base fluid by 44%, 55.7%, and 62%, respectively, and with DI water by 35.9% compared to the reference PV module.

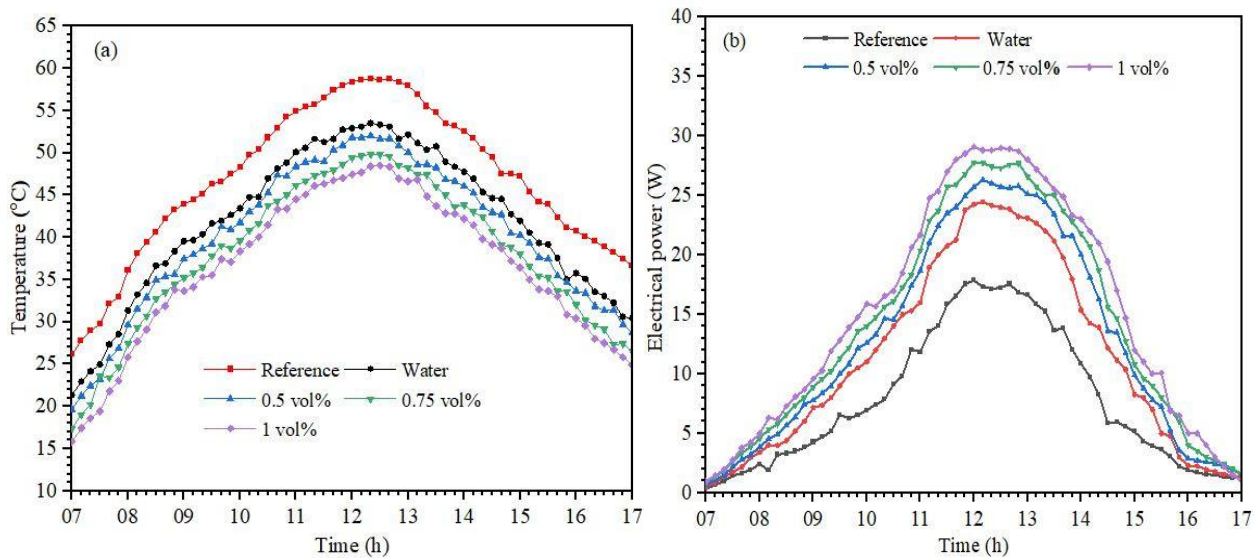


Figure B9. The average temperature of the PVT systems (a), (b)The electrical power output of the PVT modules.

The use of  $\text{WO}_3$  nanofluid has enhanced the heat removal capacity due to the increased convection heat transfer coefficient of the  $\text{WO}_3$  nanofluid. The temperature reduction of the PV module impacts noticeably on the electrical efficiency, which is improved by cooling it with water and nanofluid. Increasing the volume concentration of  $\text{WO}_3$  nanoparticles in the base fluid (0.5 vol%, 0.75 vol%, 1 vol%) caused an increment in the electrical efficiency by 31.6%, 48.3% and 52.3%, respectively, compared to DI water cooling. Figure B10 shows the gradual increment in the thermal efficiency of the PVT system at different volume concentrations. The maximum thermal efficiency was 30.1% at 1 vol% compared with the cooling by DI water. This boosts the overall efficiency of the PVT system by up to 39.29% at 1 vol% compared with cooling by DI water. The increase of Reynolds number and volume concentration of  $\text{WO}_3$  nanoparticles in the base fluid has been investigated to show the influence on the Nusselt number, heat transfer coefficient, friction factor and pressure drop. Figure B11 (a) shows the Nusselt number as a function of Reynold's number, and it can observe an increase in the Nusselt number with an

increase in the value of Reynold's number at a gradual increase in the volume concentration. Adding  $WO_3$  nanoparticles in the base fluid has enhanced the Nusselt number in which the maximum enhancement was about 51.2% at 1 vol% compared to the DI water. Dispersion of  $WO_3$  nanoparticles in the base fluid leads to an enhancement of the thermal properties of the cooling fluid. Moreover, the  $WO_3$  nanofluid has high Nusselt numbers than the base fluid, which positively increases the heat transfer efficiency. Figure B11 (b) indicates the variation of heat transfer coefficient values with Reynold's number at increased volume concentrations due to an increase in the thermal conductivity of the nanofluid. The increment of Reynolds number significantly increased the heat transfer coefficient of the nanofluid. In this regard, the heat transfer coefficient is enhanced by 5.3% compared to DI water at 1 vol %, consequently, nanofluids can increase the heat transfer coefficient and contributes to lower PV temperature more than DI water. Increasing the volume concentration of nanoparticles in the base fluid increases the nanofluid's density and thermal conductivity, which affects the pressure drop.

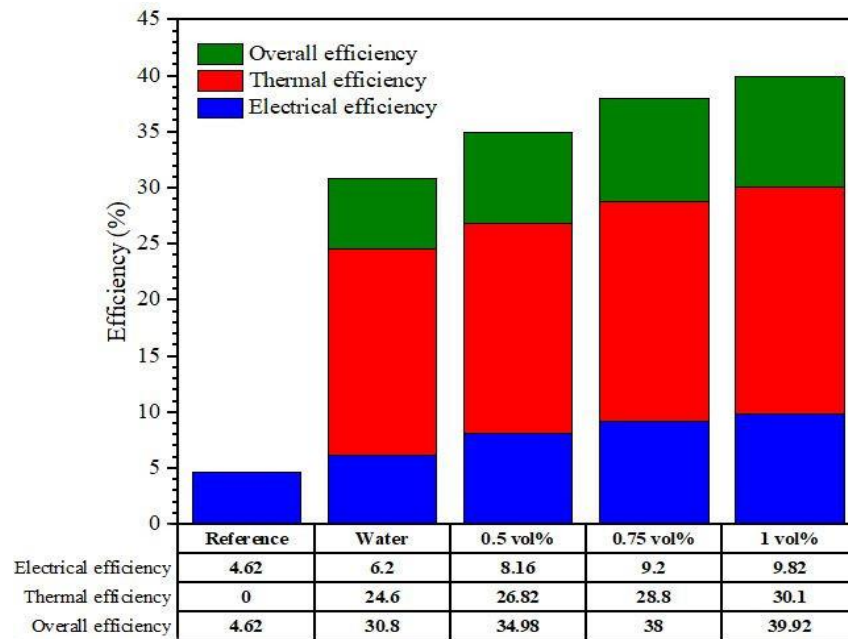


Figure B10. The overall efficiency of the PVT systems against the reference PV module

Figure B12 (a) shows the decrease of friction factor with the increase of Reynolds number and volume concentration of  $WO_3$  nanofluid. The friction factor of  $WO_3$  nanofluids was high due to the increased viscosity of nanofluids, more than that of the DI water. The friction factor decreases with the increased Reynolds number by 4.5%, 9% and 13.6%, respectively, at volume concentrations of 0.5 vol%, 0.75 vol% and 1 vol%. The concentration of nanoparticles in the base fluid increased the nanofluid's density and thermal conductivity, which impacted the pressure drop. Figure B12 (b) shows the pressure drop increment with the increased Reynolds number at different volume concentrations. On the other hand, the increase in both density and viscosity has increased the pressure drop in the nanofluid compared with the base fluid. Besides, increasing the pressure drop of the nanofluid resulted from the flow resistance of nanoparticles compared to the case of the base fluid. Thus, the increased volume concentration and Reynolds number increased the pressure drop to 49.2 % at 1 vol%, compared with the DI water.

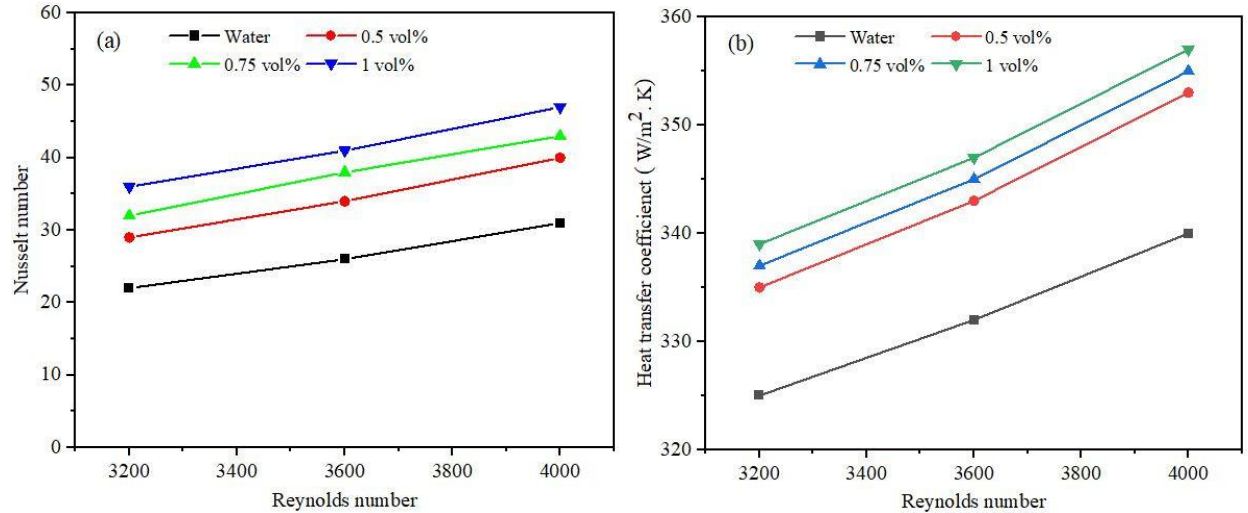


Figure B11. Effect of Reynolds number and volume concentration on (a) Nusselt number and (b) heat transfer coefficient

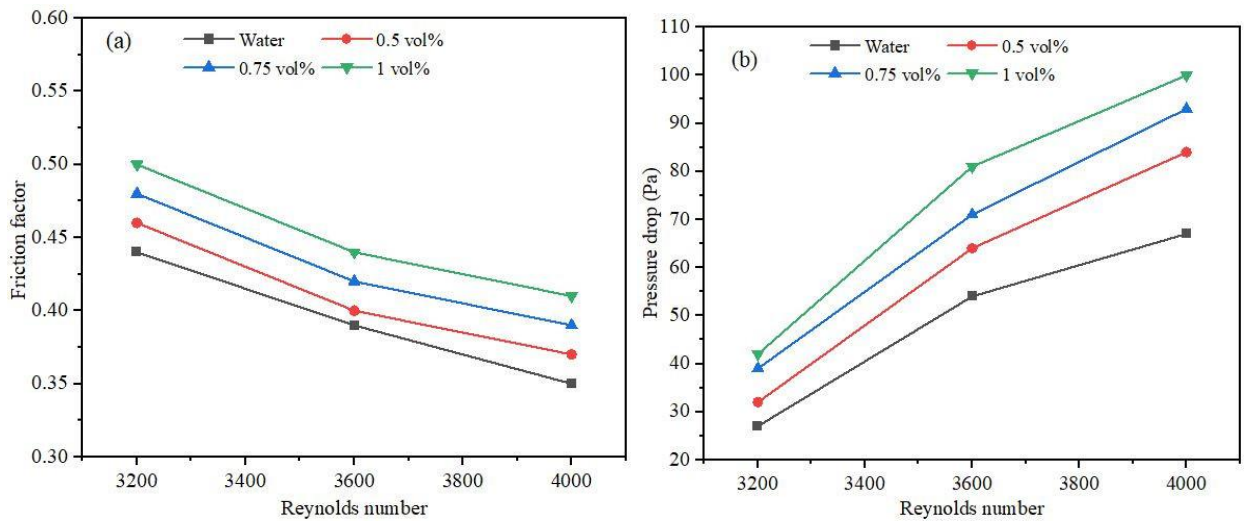


Figure B12. Effect of Reynolds number and volume concentration on (a) friction factor and (b) pressure drop

### B.2.1.2 Exergy and entropy generation results

This section assesses the effect of  $\text{WO}_3$  nanofluid and water on the exergy efficiencies, losses and entropy generation of the PVT system. According to Eq. (40), the input exergy of the solar radiation to the PVT system is calculated during experimental days wherein the maximum, average and minimum solar exergies were 947, 672.33 and 336.13  $\text{W/m}^2$ , respectively. Figure B13 (a) shows the thermal exergy of the PVT system, which recorded a lower value than the electrical exergy, attributed to the close fluid outlet temperature to the ambient temperature. Furthermore, the thermal exergy is impacted by the thermophysical properties of the nanofluid, such as the specific heat and the high thermal conductivity. Figure B13 (b) above shows the effect of  $\text{WO}_3$  nanofluid and DI water on the PVT system's thermal and electrical exergy efficiencies. The thermal exergy efficiency was remarkably low compared to the electrical exergy efficiency. This is attributed to the low quality of the thermal exergy. Circulating the

WO<sub>3</sub> nanofluid into the serpentine tube enhances the electrical exergy by reducing the PV module temperature and positively enhancing the electrical exergy efficiency. Increasing the vol% of WO<sub>3</sub> nanoparticles (0.5 vol%, 0.75 vol%, 1 vol%) in the base fluid has raised the electrical exergy efficiency by 26.9%, 42%, and 50%, respectively, to the DI water cooling. The evaluation of exergy loss and entropy generation is an important parameter in the PVT system for specifying their losses and irreversibilities.

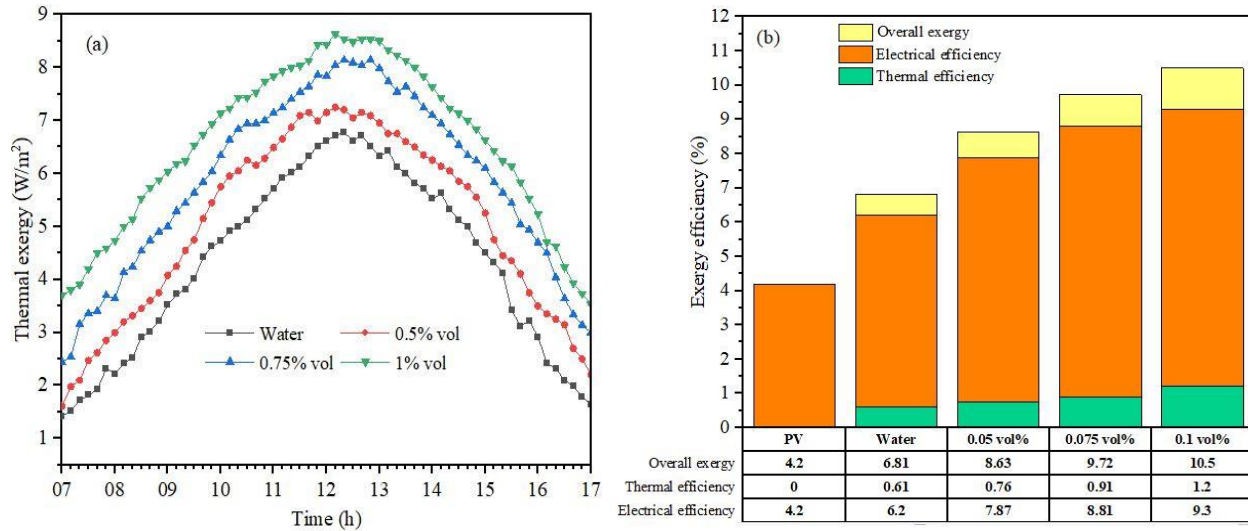


Figure B13. Average thermal exergy of the PVT system (a), (b) Average electrical and thermal efficiency of the PVT system

According to Figure B14, the exergy loss in the reference PV module was high compared to the PVT system due to the cooling technique used in the PVT system. Moreover, using WO<sub>3</sub> nanofluids has effectively reduced the exergy loss due to enhancing the heat transfer coefficient. Compared to the reference PV module, a gradual increase in WO<sub>3</sub> nanoparticles vol% has reduced the exergy loss by 15.32% at 1 vol% due to the heat transfer enhancement. Minimizing the entropy generation rate is significant for determining the system's operating conditions and reducing the lost work. Increasing the temperature of the PV module increases the heat transfer between the system and the environment, thus, increasing the entropy generation. In the PVT system, entropy generation is affected by heat transfer and fluid friction into the PVT system. Figure B14 shows a substantial drop in the entropy generation value compared to the reference PV module due to the enhanced thermal properties of the WO<sub>3</sub> nanofluid. The gradual reduction of the entropy generation when using WO<sub>3</sub> nanofluid reached 53.5% compared to the reference PV module.

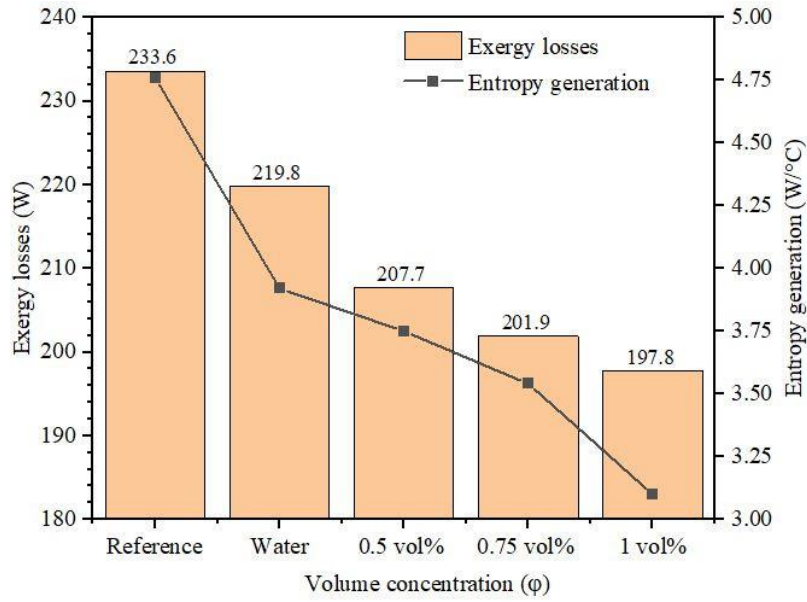


Figure B14. Exergy losses and entropy generation of the PVT system at different concentrations against the PV module

### B.3 New contributions results

#### Contribution 8

The current study compares passive (CWIRAF) and active cooling (circulated water) techniques to enhance the PV module's performance. Increasing the heat dissipation area of the back surface of the PV module by aluminium fins integrated with wet cotton bristles and exposed to air contributed to creating a cooling environment during the experiment period. Thereby contributing to lowering the PV module's average temperature more than the active cooling technique. The cooling techniques applied showed sustained performance of the PV modules under hot conditions. The following conclusions are derived from the present work, as follows:

- The CWIRAFs passive cooling technique shows improved behaviour and significantly enhances the PV module performance by lowering its temperature under hot conditions using minimal equipment.
- Increasing the heat dissipation area of the back surface of the PV module by aluminium fins integrated with wet cotton bristles and exposed to the air created a cooling environment during the experiment period. Thereby contributing to lowering the PV module's average temperature by 137.7% than the active cooling technique.
- A reduction in PV module temperature using the CWIRAF technique increased the power yield and efficiency by 13.78% and 8.86%, respectively, compared with the PVT collector.
- The passive cooling applied in this work effectively reduces the PV module temperature and improves its performance better than in other studies, which makes it more reliable.
- The active cooling technique showed lower performance than passive cooling under similar conditions. This result is attributed to heat transfer across different PVT collector layers, not directly, such as CWIRAFs cooling.
- The PVT collector enhances thermal energy by removing excess heat from the PV module's backside by circulating water inside pipes, improving the overall efficiency of the PVT collector.

- PV modules used without cooling in hot climate conditions significantly deteriorated their performance.
- The economic analysis of the PVT system has achieved a good payback period within a short period compared with the conventional reference PV module, which confirms the feasibility of the cooling approach used.

The cooling technique applied may be feasible for small installations of PV modules, such as a family house system. In future work, the research domain will consider more extended experimental periods with the help of numerical tools and suggest improvements for reducing water consumption.

### **Contribution 9**

The increased volume concentration of  $WO_3$  nanoparticles in the base fluid reduced the PV module temperature due to enhanced  $WO_3$  nanofluid thermal conductivity compared to DI water. Thus, the reduced PV module temperature has positively improved electrical power generation. According to the results obtained, the following conclusions are summarized:

- The increased volume concentration of  $WO_3$  nanoparticles in DI water reduced the temperature of the PV cells by 21% has enhanced the electrical power by 62% due to improved heat transfer coefficient compared with DI water, which increased the electrical efficiency of the PVT system by 52%. The increase in volume concentration gradually increased the thermal efficiency of the PVT system by 30.1%.
- Nusselt number and the heat transfer coefficient of the  $WO_3$  nanofluid were improved by 51.2% and 5.3% with the increase of the volume concentration and Reynolds number due to the increased nanofluid density and viscosity. Increasing volume concentration and Reynolds number has increased the pressure drop by 49.2% compared to DI water.
- The thermal exergy of the PVT system was lower than the electrical exergy due to the convergence of the fluid outlet temperature of the PVT system to the ambient temperature. Increasing the volume concentrations of  $WO_3$  nanofluid achieved a relative increment of the thermal exergy compared to the cooling by DI water.
- The thermal exergy efficiency of the PVT system was low due to the drop in the quality of the thermal exergy. Thus, an increased volume concentration has positively influenced the thermal and electrical exergy efficiencies due to the enhanced nanofluid heat transfer coefficient. Using  $WO_3$  nanofluids effectively reduced the exergy loss and entropy generation by 15.32% and 53.5% because of their heat transfer enhancement and reduced fluid friction in PVT systems.